A NOVEL 2kWe BIOMASS-ORGANIC RANKINE CYCLE MICRO COGENERATION SYSTEM

Ferdinand F. O. Daminabo

(B.Tech; MSc.Arch.)

Thesis submitted to the University of Nottingham

for the degree of Doctor of Philosophy

April, 2009

Contents

ABSTRACT

Energy is potentially at the hub of modern civilization and right from Industrial Revolution, technology has refined and redefined the way we use energy; but technological advancement in all spheres will continue to depend and use energy to progress. However, fossil fuels (coal, gas, oil) have remained the dominant energy resource accounting for a larger proportion of world energy consumption when compared to nuclear energy and renewable energy resources. There are mounting fears of both the climate and our environment reaching a characteristic tipping point due to global warming. This is associated with the relentless use of fossil fuels and uncontrolled emissions of greenhouse gases. The persistent trend has triggered the need for alternative and renewable energy options which are now being considered and pursued globally to avert the possibility of climate change attaining a state of irreversibility.

This research describes the development of a novel 2kWe biomass fired Organic Rankine Cycle (ORC) system intended for remote off-grid locations, employing a multi-vane expander as the prime mover. The expander is a four vane model 6AM-FRV-5A 3kW Gast Air motor manufactured by Gast Manufacturing Inc. The prime mover will harness power produced by high pressure vapour to generate torque and rotational motion on the shaft and the mechanical energy generated is converted to electricity by means of an automotive alternator. The conversion of low and medium temperature heat from biomass to electricity by using low cost, lightweight and low maintenance expander as well organic substances or hydrofluoroether, HFE 7100 and HFE 7000 is the subject of

this research. In order to assess and predict the performance of the system an EES simulation of a basic cycle is carried out in order to compare the the outcome with the actual cycle. A preliminary air test of the system was also carried out to have a perspective on actual performance using compressed air. However, the organic substance, hydrofluoroether (HFE) to be used in further tests is selected because of its thermodynamic properties of having a lower specific volume and higher molecular weight than steam allowing for smaller, less complex, less costly energy applications like expanders and smaller diameter tubes to be employed for low temperature micro system. This is achieved through a phase change transformation in a Rankine cycle process between specified temperature limits when compared to turbines which operate at higher temperature and pressure.

An experimental study and initial testing is carried out using a Chromalox-Model CES-12, 9 kW boiler providing temperatures between 100°C and 115°C and test measurements collated and analysed to predict performance and assess outputs and possibly fluctuations in the system. A test involving the use of the biomass boiler is carried out later and analysed results compared with that of the electric boiler. The process will involve the supply of heat from the biomass boiler and the high pressured vapour generated in the ORC cycle is expanded through the prime mover with a fall in temperature and pressure at the exhaust and exiting as saturated vapour or a mixture of vapour and liquid. The energy stored in the working fluid in the vapour state is converted to electricity by work on the shaft while the exhaust heat can be tapped for domestic uses as the

vapour is expanded down to low pressure in the condenser and the saturated liquid is pumped to a high pressure in the evaporator to resume the cycle.

ACKNOWLEDGEMENTS

My sincere gratitude to my supervisor Professor S. B. Riffat, whose deep insight and vast knowledge made this research work possible and as also to thank and appreciate Dr. Xudong Zhao who is my second supervisor.

I would like to also appreciate Dr. Hao Liu and Dr. Guoquan Qiu for their invaluable assistance at the later part of my research work and not forgetting Dr. Prince Doherty who inspired me and was a source of encouragement. The team of laboratory technicians, Dave Oliver, Dave Taylor, Jonathan Moss and Bob Clarke are appreciated for being available despite their excruciating schedules.

I want to finally thank and appreciate my wife, Nimi for the support she offered and the children, David, Esther and Luke for their resilience and their charming virtue and am very proud of them.

Nomenclature

Cp Isobaric specific heat capacity at each stage [J/kg·K]

D   diameter of cylinder bore

e   eccentricity

f   thickness of oil film (0.1- 0.2 mm)

F_1,   leakage fraction of the working fluid

F_f total frictional loss

h specific enthalpy at each stage [J/kg]

h_1 specific enthalpy of saturated vapour entering the expander (J/kg)

h_2 specific enthalpy of saturated vapour leaving the expander (J/kg)

h_3 specific enthalpy of saturated fluid leaving the pump (J/kg)

h_4 specific enthalpy of saturated fluid entering the pump (J/kg)

h_f specific enthalpy of saturated liquid leaving the expander (J/Kg)

h_g specific enthalpy saturated vapour leaving the expander (J/Kg)

h_{fg} specific enthalpy of saturated mixture leaving the expander (J/kg)

$\dot{I}$ exergy destruction (irreversibility)

L   length of rotor (vane) in mm

$\dot{m}$ Mass flow rate [kg/s]

m_v the mass of the vane

n   number of vanes

P_{in} Turbine inlet pressure [Pa]

P_sat pressure of saturated vapour at the expander inlet [^{o}C]

X

P_{out} Turbine outlet pressure [Pa]

Q_{in} Evaporator input [W]

Q_{out} Condenser output [W]

R   radius of cylinder bore

r   radius of rotor

s   thickness of vane

s_g specific entropy of saturated vapour leaving the expander (J/kg.K)

s_f specific entropy of saturated liquid leaving the leaving (J/kg.K)

s_{gf} specific entropy of saturated mixture leaving the expander (J/kg.K)

s_{gen} entropy generation due to internal irreversiblities (J/kg.K)

s_0 entropy at the dead state (J/kg.K)

Sr   the radial clearance between the rotor and the cylinder

T torque [Nm]

t_{ad} adiabatic compression temperature

T_H the arithmetic mean temperature of the heat carrier

T_{in} turbine inlet temperature [^{o}C]

T_{out} turbine outlet temperature [^{o}C]

T_0 temperature at the dead state [^{o}C]

T_sat temperature of saturated vapour at the expander inlet [^{o}C]

v_f specific volume of saturated liquid entering the pump (kg/m^3)

v_g specific volume of saturated vapour entering the expander (kg/m^3)

W_p Pump work [W]

W_t Turbine output [W]

General subscripts

ad   adiabatic compression

in   inlet

o   dead state

out   outlet (exit)

t   turbine

v   vane

Greek symbols

α   coefficient of thermal expansion

η_{eff} Total efficiency of turbine [%]

η_{pump} Pump efficiency [%]

η_t Turbine efficiency [%]

$\eta_{transmission}$ the belt transmission efficiency given as 0.95.

η_{th} thermal efficiency, [%];

$\eta_{th,carnot}$ Carnot efficiency

π   Pressure ratio, P_{in}/P_{out} [-]

μ_e the vane/stator coefficient of friction

ψ exergy involving fluid stream (J/kg)

LIST OF TABLES

Chapter 6:

Chapter 7:

LIST OF FIGURES

Chapter 1:

Chapter 2:

Chapter 3:

Chapter 4:

Chapter 5:

Chapter 6:

Chapter 7:

Chapter 8:

CHAPTER 1: INTRODUCTION

1.1 Background

The most fundamental processes in nature are solar driven, and the Sun's energy positively drives and catalysis most natural processes; for instance photosynthesis in plants yielding biomass, heat energy and light, and thus various life forms and cycles are sustained in nature. Energy is required for virtually every industrial, transport and commercial activity and also needed to meet our household needs of heating, lighting and cooking. At the global level, consumption of energy is growing steadily by around 2% a year in the decade 1990 - 2000 and probably more in 2000-2020 [1]. Figure 1.1 [2], shows the escalating prices of oil in recent times, and Figure 1.2 [3], show world energy demand. Both are galloping upwards and have not been helped by the global crisis on terror and different arms conflict in the Middle East and the Nigerian oil crisis in the Niger delta

Figure 1.1: Statistics of Sharp oil price increases.

region of that country, with its highest intensity building up from May, 2007. However, these uncertainties are cyclic and mostly unpredictable with many turns in the way and this is evident in the spikes of oil prices having a negative impact on global economies.
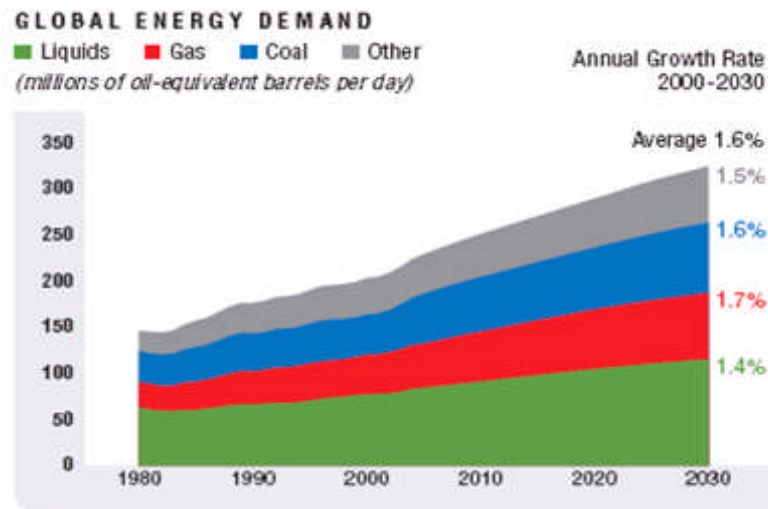
Figure 1.2: Global Energy Demand

In the EU, a scenario is also observed where large scale power plants are situated far from population centres. This prevents efficient utilization when viewed against the maximum efficiencies of power stations at 40%. Grid depreciation returns only about 35% of the original energy for final consumption [4]. The huge implication is for more fossil fuel consumption to keep up with demand. However, the steep increases in atmospheric carbon and other greenhouse gases and the effect on the global climate have brought the issues of global warming and climate change to a sharp focus. Against the fears of severe climate change, the need for new and sustainable energy technologies including renewable forms of energy are

urgently required for power and heat production in the most environmentally friendly way. Significant interest in this form of power production has developed progressively in recent times spurred by the need for low carbon emissions and decentralized smaller power systems from low temperature applications that are sourced from renewable energy options. The EU in its directive 2004/8/EC of the European Paliament and of the Council of the EU of 11 of Februarry 2004 emphasised the promotion of micro cogeneration technologies based on useful heat demand in the internal energy market [5]. However, Cogeneration technologies which refers to an array of small and medium generators focuses on combined local production instead of separate production of heat and power from renewable sources of energy and this also reduces energy transmission and network losses, reduce network congestion and saving primary energy as well as emission reduction.

The renewable energy options; geothermal, wind energy, hydropower,
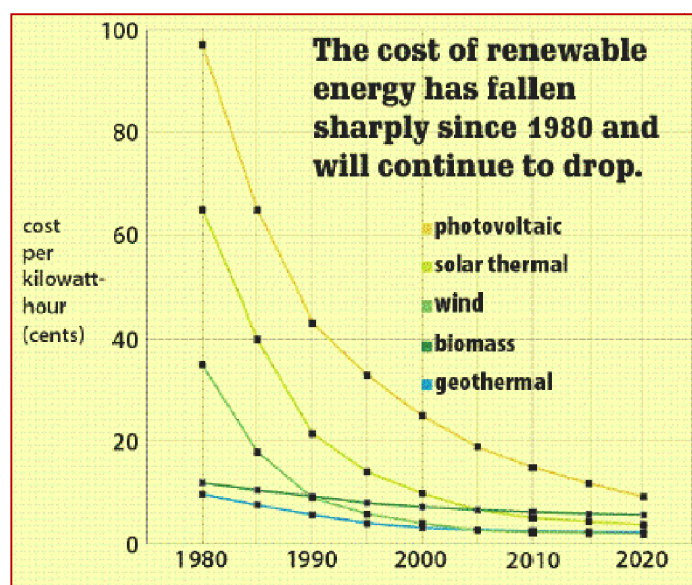
Figure 1.3: The falling trend in the cost of Renewable energy

photovoltaic and solar thermal energy as well as biomass apart from their green and clean credentials are also sustainable forms of energy. These forms of energy are beginning to prominently feature and gaining reception in the energy market.

There are also positive indicators that the cost of renewable energy has shown a downward trend in the last four decades [6]. Figure 1.3 [7], also indicate future projections of the downward trend up to 2020 from the 1980's dealing with five renewable energy options, photovoltaic, solar, wind, geothermal and biomass. The purpose of this work is to explore and harness biomass energy for combined power and heat production. The biomass driven Organic Rankine cycle will be a low temperature application employing a prime mover for a micro-CHP system. The choice of working fluid will be very crucial as it must comply with an environmentally friendly option in terms of toxicity, fouling characteristics and low flammability [8]. The anticipated system output is 2kWe with electrical efficiency of 6 - 7.8% and the expected boiler efficiency of 85 - 90% is for a 25kW biomass boiler. The implementation will focus in ensuring that various configuration parameters are considered in keeping the system simple and low cost. The prime mover which is a Gast air motor is employed as the expander; the cheap low maintenance and lightweight air compressor will serve to do the work of a conventional turbine. Multi-vane expanders are better than conventional turbines in low temperature Rankine cycles [9]. Organic Rankine processes are usually employed in low temperature heat sources as it is not thermodynamically

feasible to employ low-grade heat for conventional Rankine cycle which operates at very high temperature [10]. Biomass, solar collectors, exhausts heat from power plants and geothermal are considered as low grade heat sources and organic fluids (hydrocarbons) are the prefered working fluid. Hydrocarbons are better than water in low-grade heat power applications because of their low specific volume and higher molecular weight when compared to water [11]. The use of organic fluids for better efficiency in small turbo machinery is a well known feature of organic Rankine engines (ORC), [12].

1.2 Global Warming and Energy Demand

Energy is the pivot for the advancement of modern civilization and the ever increasing demand for energy to both industrialize and accelerate economic growth appears to be at the centre of the causes of global warming and climate change. The unmitigated burning of fossil fuels and land use changes have accelerated and will continue to emit increasing quantities of greenhouse gases into the earths atmosphere chief among these being carbon dioxide (CO_2), nitrogen dioxide (N_2O) and methane (CH_4). The pre-industrial carbon dioxide emission indicated in Figure 1.4 [13], shows pre-industrial concentration and that of methane Figure 1.5 [13], a trend that is sure to continue into the near future with no assurances that this post industrial period will be any different from the experiences in the past.
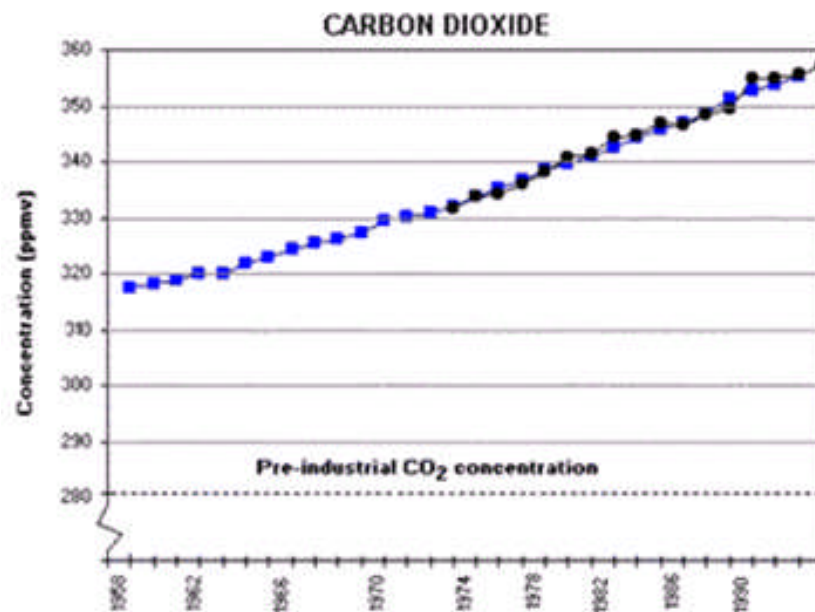
Figure 1.4: Carbon dioxide concentration in (pppmv)
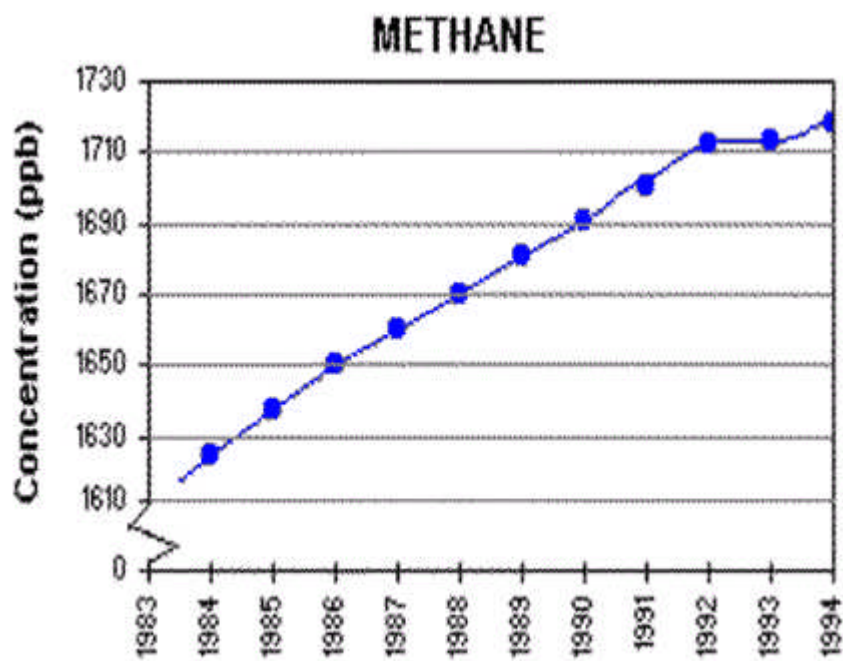
Figure 1.5 Methane concentration in (ppb)

However, this has remained fairly progressive and emission continues to have an upward trend with no indication that there will be any quick fixes to the trend. In his state of union address in 2006, the then United States president George W. Bush inferred to America's addiction to oil. However, oil addiction is a global trend that is not going away in the near future except something serious is done in reducing the carbon footprint of individual nations in global terms. China and India appear to be suffering severe addiction to oil due to their emerging economies nearly over taking the United States of America because of their rapidly growing industrial sector. The industrialised nations must seriously consider alternatives to fossil fuel if a global catastrophe as a result of global warming and climate change must be averted or slowed down. The impact of which is clearly seen in the region of the arctic cycle and on most of the global landscapes and environment. This might reach a characteristic tipping point not only with the environment and various ecosystems but also the economics of things and with the possibilities of a major global food crisis. New evidence abound from the scientific world strengthening the argument on climate change with a consensus among opinion leaders and well informed individuals including the environmental scientists that there appears to be a discernable human influence on the climate. This notion further suggests a link between the concentrations of carbon dioxide and the surge in global temperatures. On the economics of climate change Sir, Nicholas Stern [14] provides a major review of the economics of climate change and to understand more comprehensively the nature of the

economic challenges in the future for both the UK and globally. As head of the Government Economic Service and adviser to the Government on economics of climate change and development and commissioned on the 19th of July 2005 by the Chancellor Exchequer, Gordon Brown now British Prime Minister, he did come out with some strong but grave appraisals on the effects of climate on the economy thus;

- ❖ Melting glaciers will initially increase flood risk and then strongly reduce water supplies, eventually threatening one-sixth of the world's population, predominantly in the Indian sub-continent, parts of China, and the Andes in South America.

- ❖ Declining crop yields, especially in Africa, could leave hundreds of millions without the ability to produce or purchase sufficient food. At mid to high latitudes, crop yields may increase for moderate temperature rises (2 - 3°C), but then decline with greater amounts of warming. At 4°C and above, global food production is likely to be seriously affected.

- ❖ In higher latitudes, cold-related deaths will decrease. But climate change will increase worldwide deaths from malnutrition and heat stress. Vector-borne diseases such as malaria and dengue fever could become more widespread if effective control measures are not in place.

- ❖ Rising sea levels will result in tens to hundreds of millions more people flooded each year with warming of (3 or 4°C). There will be serious risks and increasing pressures for coastal protection in

South East Asia (Bangladesh and Vietnam), small islands in the Caribbean and the Pacific, and large coastal cities, such as Tokyo, New York, Cairo and London. According to one estimate, by the middle of the century, 200 million people may become permanently displaced due to rising sea levels, heavier floods, and more intense droughts.

❖ Ecosystems will be particularly vulnerable to climate change, with around 15 - 40% of species potentially facing extinction after only 2°C of warming. And ocean acidification, a direct result of rising carbon dioxide levels, will have major effects on marine ecosystems, with possible adverse consequences on fish stocks.

The long term implication of this global trend is that heat trapping gases generated by the current consumption of fossils retains more of the suns' warming energy in the earth's atmosphere causing the greenhouse effect or global warming due to entrapped heat and re-radiation. Over the last century, atmospheric concentration of CO_2 increased from a pre-industrial value of 278 parts per million (ppm) to 379 parts per million in 2005, and the average global temperature rose by $0.7^{o}C$. According to scientists, this is the largest and fastest warming trend in the history of the earth. It is on record that 11 out of 12 warmest years have occurred in the past 12 years, [15], even as Figure 1.6 [16] mirrors global temperature trends.
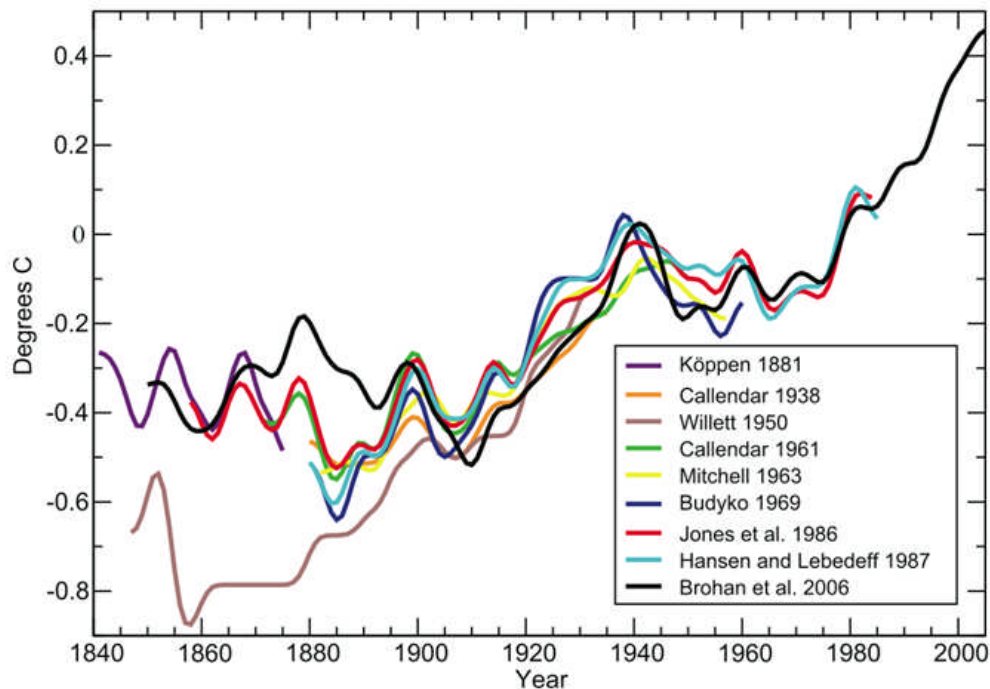
Figure 1.6 Global Temperature Series 1840-2000(IPCC, 2007)

The increasing emissions could be said to result from massive industrial activities of the most industrialized nations, a case in point being the recent climatic malaise experienced at the 2008 Beijing Olympic Games with massive smog cover shown in Figure1.7, which is as a result of massive industrial activities and uncontrolled emissions of GHG, an earmark for the future of the global climate, though emissions from developing nations are also in the upsurge but the Beijing episode only emphasises the need for a change.

Figure 1.7: Graphic images of Smog cover over Beijing Bird's nest Stadium and a man crossing a bridge in Beijing [Reuters; 2008]

The seriousness of the surge in climate change can be visualized from the recent climate submit in Bali, 15 December, 2007 where 187 countries met to strengthen the international climate change deal. In tandem with the global search for solutions to curb further carbon dioxide emissions, this research is a novel effort in assessing and contributing to the many options that might be available in the future to address the issues of global warming as every little contribution counts based on the very grim prospects of doing nothing to mitigate the danger to the environment.

This is on the heels of the Kyoto protocol which is expiring in 2012. Some of the deals include mitigating measures to further reduce CO2 emissions including issues like emission trading in Figure 1.8 [17] showing 2005 contract price and spot price as well as 2008 contract price in euros per tonne CO_2 equivalent.

Euros per tonne of CO$_2$ equivalent

Figure 1.8: BP Statistical Review of World Energy 2007

Early in the 2005, the EU developed The EU Emission Trading Scheme (EU ETS), the largest multi-national greenhouse gas emissions trading scheme in the world [18]. One of the key policies introduced by the European Union to help meet the EU's greenhouse gas emissions reduction target of 8% below the 1990 levels under the Kyoto Protocol specifies that states must develop National Allocation Plan (NAP) approved by the EU setting an overall 'cap' on total amount of emissions allowed from all installations covered by the scheme [19] which is converted to allowances with 1 - allowance equals 1 tonne CO_2. On the global scale, highly polluting countries can buy credits from those which are allowed to emit more than they actually do while some are allowed to gain credits for activities which boost the environment's capacity to absorb carbon such as tree planting and soil conservation. Global warming has wide ranging effects on the environment with many indicators; these
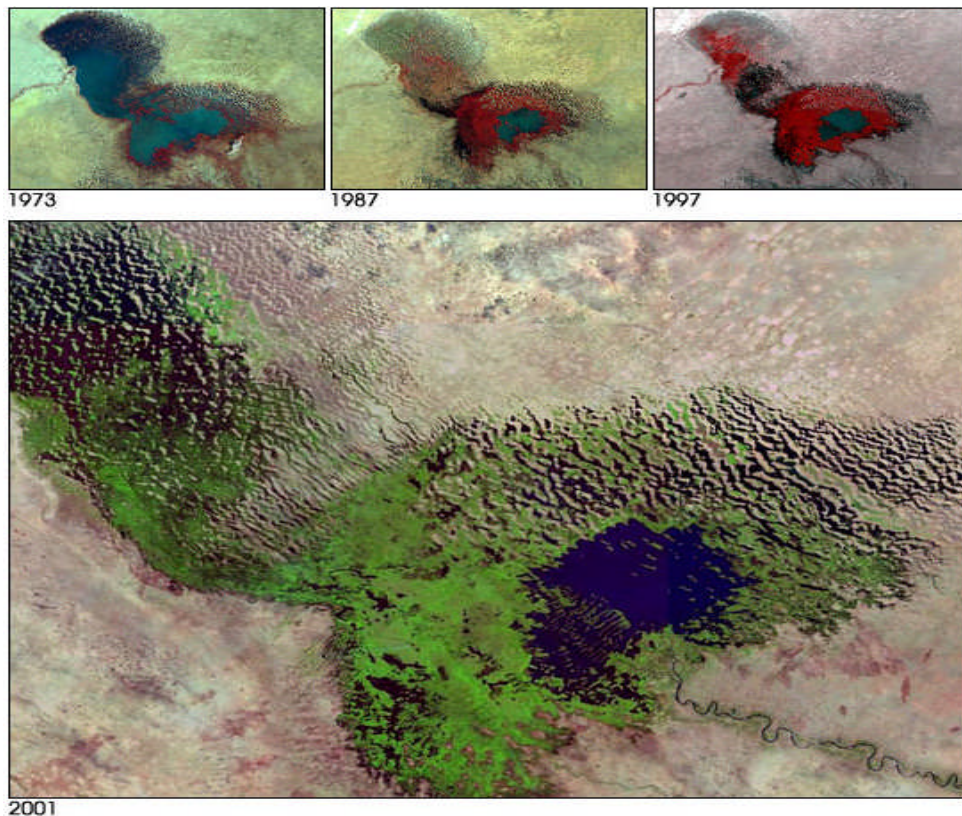
Figure 1.9: Satellite images of Lake Chad shrinking.

include increases in the average air and ocean temperature, melting snow and ice, terrestrial ecosystem and biodiversity.

However the frequency and intensity of extreme weather conditions; droughts, floods and heavy precipitations are regular headline features in major national news and print media. These events are predicted to rise even with small average temperature rise [20]. Figure 1.9 [21] is a graphical example of the grievousness of climate change on the environment and under the business as usual scenario, greenhouse gas emissions could raise by 25-90 percent by 2030 relative to 2000 and the earth could warm by $3^{o}C$ this century [16].

This research will involve the investigation of a novel biomass organic Rankine cycle which will allow for a sustainable micro - power and heat generation using environmentally friendly organic fluid as the working fluid. The biomass organic Rankine cycle will be a low temperature application using a multi-vane expander as prime mover. Organic Rankine process is usually employed in low temperature heat sources as it is not thermodynamically feasible to employ low-grade heat for conventional Rankine cycle. However, biomass in terms of carbon footprint is regarded as carbon neutral as the same amount of carbon taken in by plants through photosynthesis equates to the carbon released when it is allowed to decay naturally or efficiently burnt.

The research objectives are;

1. To evaluate the performance of the ORC system and identify the operating parameters using an electric boiler as the heat source to the working fluid.

2. To monitor the thermodynamic performance of the system using the working fluid, HFE 7100.

3. The evaluation of the difference in performance of a second working fluid, HFE 7000.

4. Study system performance with the introduction of a recuperator into the exhaust stream of the expander.

5. To substitute the electric boiler with a biomass generator and gauge the thermodynamic performance of the cycle.

To realise these objectives;

a. EES software is used to simulate the reversible or ideal Rankine cycle along the same heat source and heat sink temperature bands and to determine the efficiencies.

b. Adaptation and modification have been made to the basic system to extract the most energy from the heat source.

c. Optimization of the system based on the governing parameters and choice of the novel working fluid.

d. Theoretical studies have been carried out with respect to the system and components making up the system.

e. To experimentally identify the conditions key to system improvement thus providing an experimental proof that demonstrates the possibilities of the novel concept

However, this work is not an attempt to design and construct the prime mover but to discover and adopt a suitable alternative to conventional turbines and the work is not also aimed at producing mega power output but to demonstrate the possibilities of generating micro outputs of a few watts to anticipated 2kW of electricity and heat. This can be used in isolated and off grid locations very common in most third world rural centres, farms and in most developing economies. Nigeria is one scenario where only about 17 percent of the rural population have access to grid connected electricity [22]. However the United Nations Environment Programme report indicates that grid connections generally do not exceed 25 percent of village households [23]. The reality of the Nigerian situation is that a greater proportion of the population, about 70 percent live in rural

areas [22], and this concept could become the most vital process of providing a few kilowatts of electricity in an affordable and sustainable manner for use in these areas. This will be adequate for very low energy appliances and charging of cell phones and batteries of laptops. An array of this novel device can also be integrated into a heat recovery system from the exhaust heat of most power plants in a low temperature ORC power generation system. This is predicated on the potential demand for an alternative source of energy other than the grid system which is considered a preference in most developing economies. This will be governed by a set of factors and defined by current energy developments and future consumption benefits including climate protection and the reduction in the emission of greenhouse gases.

1.3 Novelty and Creativity of the System

In this work, a combined system of a biomass boiler, the prime mover, and an automotive alternator will be used for a micro cogeneration system with an anticipated output of 2kWe and heat production. The major innovation is that of using a 3kW Gast air motor as the expander instead of a conventional turbine while a 140A automotive alternator will serve as the micro-electric generator. The use of alternators will benefit the environment as every year, approximately 2 million new vehicles are registered and a similar number are scrapped in the UK [24]. The expected electrical efficiency will be based on the expander to alternator conversion efficiency of between 50-65% [112]. At maximum turbine output of 3kW, the electrical output at 50% conversion ratio will be 1.5kWe

and 1.95kWe at 65% respectively. The 65% alternator conversion ratio is for heavy duty alternator intended to achieve the 2kWe output. The electrical efficiency based on the assumed output using the biomass boiler with boiler efficiency of 85 - 90% is 6 - 7.8%. This is compared to the value in literature for ORC process which is between 6 and 17% [25]. This novel system is intended to address the energy needs of remote locations and rural areas in developing countries [22, 23] that do not have grid connections and just need enough outputs to charge their cell phones, laptops and some form of indoor lighting of a few watts for reading.

1.4 Thesis Structure

This research focuses on the use of biomass as energy source for a micro combined heat and power production system. The biomass organic Rankine system is predicated on a novel MVE, a non conventional micro turbine that integrates specially selected components to implement the thermodynamic Rankine cycle involving two cycles. In the two cycles involved, first a biomass generator will harness energy from biomass fuel to raise hot water between temperatures of about $100^{o}C$ – $115^{o}C$ in the water loop circulated through a compact heat exchanger. The hot water is used to heat a secondary fluid HFE 7100 into high pressure vapour. The vapour will be expanded through the MVE to provide rotational motion at the shaft resulting in mechanical power which will be converted to electricity. The vapour is condensed to liquid state with the rejected heat used for domestic purposes or discharged to the ambient. The working fluid is an environmentally friendly organic fluid with low boiling point of

$61^{o}C$ for HFE 7100 and $34^{o}C$ for HFE 7000 both with low specific volume and high molecular weight than water. This property makes it preferred to water in low temperature thermodynamic processes as it is not thermodynamically feasible to use low grade heat for conventional turbines.

The second chapter covers literature reviews and important summaries of baselines that inform on the modus operandi and overviews about this research. This chapter provides a brief review of the various studies and the state of art technologies relevant to this work. Others include a background on biomass, its composition, the process of photosynthesis and various biomass conversion technologies. Reviews are also made on the Rankine process which is a thermodynamic cycle and in this case will convert heat energy from biomass to mechanical work. Some existing technologies are also summarised.

In chapter 3, is the description of components making up the cycle including a detailed glimpse at the properties of the working fluid, its chemical and physical characteristics as well as the health and environmental impact assessment. A perspective of the individual components in the cycle is described and including their functional disposition and parameters. Peripheral devices for data acquisition thermocouples and gauges have been also summarised for a better understanding of their functions.

The fourth chapter describes the basic considerations and analysis of vane expander and motivation for the choice of the Gast air motor for this

application which will implement a low temperature Organic Rankine-cycle. A Rotorvane compressor had been made available at the beginning of this research but discarded and or replaced because of functional difficulties discussed later in this work. This also considers the necessary parameters for configuring the expander to work with other components in the system as well as the some modifications required to achieve performance. The geometrical characteristics of the expander are also assessed in this chapter in order to broaden and better understand the characteristics of the prime mover.

The fifth chapter consists in the theoretical study of the thermodynamic cycle and analysis relevant to the novel micro–power biomass system that will implement the Rankine cycle process. The elements that make up the cycle are analysed. Although specific cycle designs differ, three basic elements of the power cycle which are of significance are discussed.

The sixth chapter describes key considerations and various parameters involved in the experimental methodology and testing. The evaluation and analysis of variation of test results and data at each stage of progression is proposed. System optimization and various improvements on the test rig are described.

In the seventh chapter experiments involving the use of a second working fluid HFE 7000 is described and subsequently the introduction of biomass boiler used also in a series of experiments. The test results are analysed and compared with previous tests involving the use of the electric boiler.

Discussions and the deductions from the various tests are also included in this chapter with the summary of the findings.

The eighth chapter embodies the conclusions, further work, and recommendations. This chapter examines the critical aspects of the research work and outcomes. The prospects of this novel concept in micro power and heat generation using biomass as energy resource is weighed with respect to its benefits and contributions to curbing the effects of global warming and climate change. The economic impact of the development of biomass technologies in job creation is also discussed in this chapter.

CHAPTER 2: Literature Review

This chapter provides a brief review of the various studies and the state of art technologies relevant to this research. A background on biomass and various conversion technologies are considered. A review on the Rankine process as well as its significance in this research is highlighted.

2.1 Background on Biomass

Biomass is composed of organic matter derived from plants because of photosynthesis, which is a process that enables trees and plants store up solar energy in the chemical bonds of their structural components. Carbon dioxide from the atmosphere vigorously combines with water from the earth in the process of photosynthesis to produce carbohydrates (sugar) and this constitutes the building block of biomass, shown in Figures 2.1 [26] and expressed in the chemical equation.

$$6H_2O + 6CO_2 \xrightarrow{\text{SUNLIGHT}} C_6H_{12}O_6 + 6O_2$$
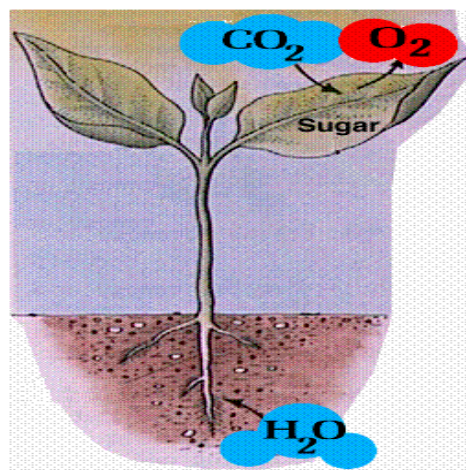
Figure 2.1: Photosynthesis process
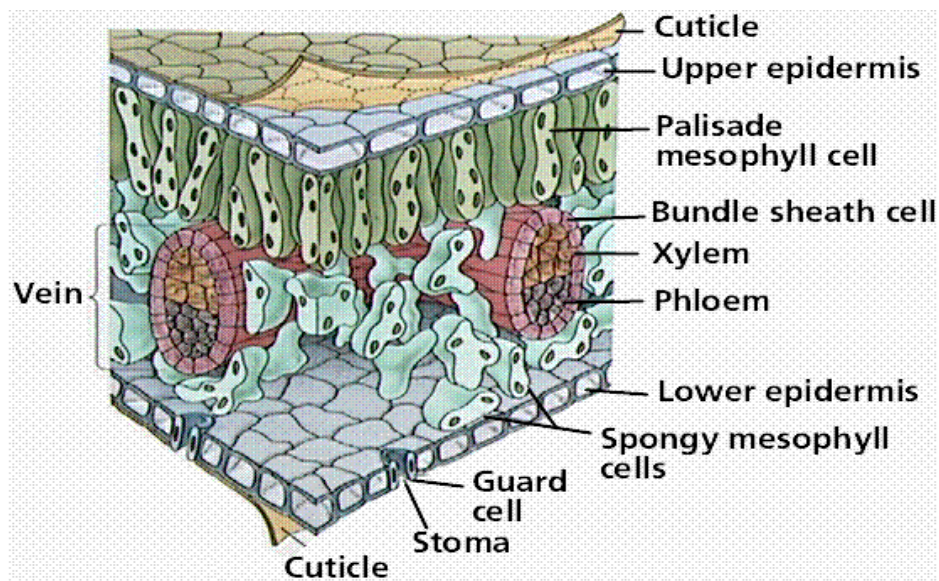
Figure 2.2: Anatomical section of leaf vital in photosynthesis process

The essential raw materials of photosynthesis, water and carbon dioxide enter the cells of the leaf shown in Figure 2.2 [26] producing sugar and oxygen. The earth's biomass exists in the thin layer called biosphere, an enormous energy store constantly replenished by energy flow from the sun through photosynthesis.

Biomass has two categories; "virgin biomass" which encompasses forestry and energy crops and "waste biomass" from forest thinning, wood residues, recycles, sewage and municipal wastes as well as food and animal wastes. Biomass still remains mans vital source of energy despite the advent of new and modern fossil energy technologies especially in the developing world. It is estimated that biomass production is about eight times the total annual world consumption of energy from all sources. At present the world population uses only 7% of the estimated annual production of biomass [27, 28]. Biomass also constitutes around 5% of EU's energy supply, and 65% of renewable energy production [29].

Essentially, the use of biomass for energy is the reversal of photosynthesis process;
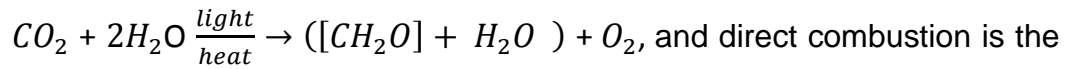
$CO_2 + 2H_2O \xrightarrow[heat]{light} ([CH_2O] + H_2O) + O_2$, and direct combustion is the simplest and most common method of capturing the energy contained within biomass. Combustion devices are commercially available as well as proven technology for converting biomass to energy. However improvements are continuously being made in fuel preparation, combustion and flue gas cleaning technologies, as a result of demand to utilize new or uncommon fuels, improve efficiencies, minimize costs and reduce emissions [30].

The energy from biomass combustion is used as the primary heat source for this work and the heat is used to vaporise the working fluid. The vapour is expanded down in the turbine to produce mechanical work which is converted into electricity. However an electric boiler is employed for the preliminary investigation of the system. The net energy available in the biomass when combusted ranges between 8 MJ/kg for greenwood, to 55 MJ/kg for oven dry plant matter and 55MJ/kg for methane compared to 23-30MJ/kg for coal [31]. Biomass is considered carbon neutral in terms of energy production and emissions as the same amount of carbon taken up by plants during growth is also released when combusted ,resulting in no net gain of carbon dioxide into the atmosphere. If forestry and agricultural residues or wastes were allowed to decay naturally, the same amount of carbon will be liberated into the atmosphere as they would if used as fuel.

2.2 Chemical and Physical Composition of Biomass

There are various chemical compositions that make up biomass and these vary among species consisting of about 25% lignin and 75% carbohydrates or sugar; most of the species contain around 5% of smaller molecular fragments called extractives [32]. The carbohydrates fraction consists of many sugar molecules linked together in small chains or polymers. The cellulose and hemi-cellulose are two large categories of carbohydrates that possess significant values of sugar molecules. However, the lignin fraction has non-sugar type molecules linked together in large two dimensional mesh structures. The long cellulose polymers are used to build the fibres that guarantees the plant its strength. Water is always present in biomass fuels known as moisture content and expressed in percentage of weight; 20 - 30% moisture content is considered tolerable in wood combustion. Water content lowers the calorific value of the fuel as water must be evaporated, a process which requires energy if not solar dried. High moisture content of biomass decreases the potential energy input for steam generation, and consequently decreases the efficiency of power generation (both in combustion and gasification systems) [33].

The calorific value is often express as higher heating value (HHV) or Lower heating value (LHV).This equates to the maximum or minimum potential energy released during oxidation of a unit of fuel [32]. Figure 2.3

[34], shows the evolution of lower heating value (LHV, in MJ/kg) of wood

as a function of moisture content. Moisture content of biomass is always
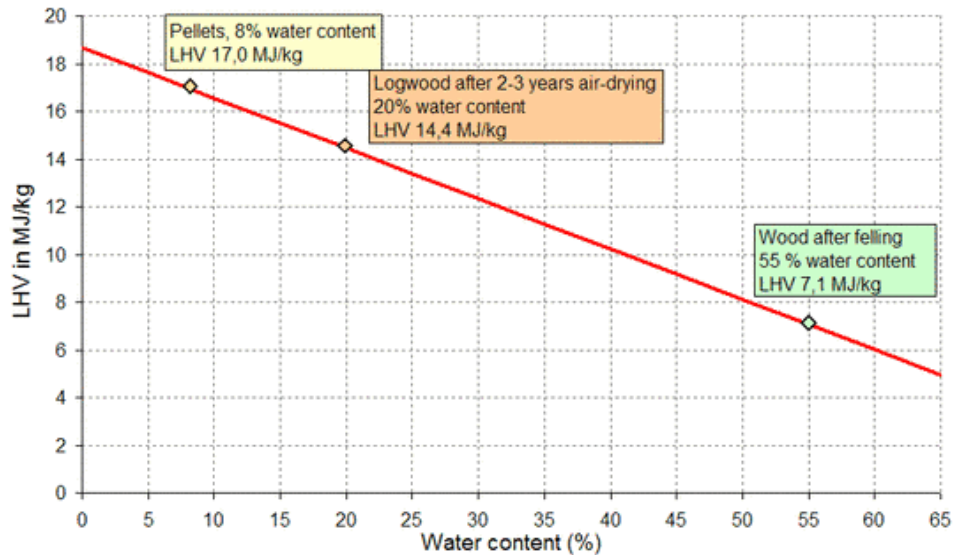
Figure 2.3: Moisture content of Biomass.

Source: www.eubia.org

considered with respect to combustion and other thermochemical

processes and since this research will involve combustion, it will be a

significant issue to consider during the experiments. In addition, many

ranges of biomass fuels can be utilised, and these include forestry and

agricultural residues, woodchips, wood pellets/granules all possessing

different calorific values as shown in Table 2.1 [35] and Figure 2.4 [36].

Other examples of common agricultural residues are crop residues (wheat

straw, corn stalks, nut shells, orchard prunings, vineyard stakes, sugar

cane bagasse, etc.), forest residues (slash, forest thinning), urban wood

waste (construction residues, grass clippings and backyard prunings), and

several energy crops (Miscanthus, SRC, etc.) [37]. Figure 2.5 shows

different modes of packaging straw as square or rolled bales.

Figure 2.4: Wood pellets. Source; http://www.mo.nrcs.usda.gov

A

B

Figure 2.5: Different forms of straw bales.

Source; http://www.irishphotonews.com

Table 2.1: Table of Calorific Value of Biomass and other Fuels

FUEL	GCV IN MJ/Kg
Paper	14.6
Rags	16.3
Wood	17.6
Straw	18.0
Animal waste	18.0
Rubber	34.7
Plastic	37.0
Coal	24.4
Oil	44.0
Natural Gas	52.4

Thermal Energy Q = Mass (M) x Calorific value of fuel (CV)

Source: EUR-21350

Further research and extensive studies [38] have been performed over a period that deals with the physical characteristics and the chemical composition of biofuels and are indicated in the Table 2.1 [38] which is an overview of the typical values associated with the physical parameters of biomass fuels. The knowledge of these physical parameters is very vital in this research as it makes for easy setting of experimental boundaries and to properly adjust the system to operate more smoothly for instance moisture content can significantly influence the performance of biomass fuel during combustion in terms of temperature of combustion and heat generated per unit mass of fuel.

Table 2.2: Gross calorific value, water content, net calorific value, bulk density and energy density of different bio-fuels

	Water content [wt %(w.b)]	GCV [kWh.kg (d.b)]	NCV [kWh.kg (w.b)]	Bulk density [kg (w.b) m^3	Energy density [kWh.m^3]
Wood pellets	10.0	5.5	4.6	600	2756
Woodchips, hardwood, pre-dried	30.0	5.5	3.4	320	1094
Wood chips, Hardwood	50.0	5.5	2.2	450	1009
Wood chips, softwood, pre-dried	30.0	5.5	3.4	250	855
Wood chips, Softwood	50.0	5.5	2.2	350	785
Grass high pressure Bales	18.0	5.1	3.8	200	760
Bark	50.0	5.6	2.3	320	727
Triticale (cereals), high pressure bales	15.0	5.2	4.0	175	703
Sawdust	50.0	5.5	2.2	240	538
Straw (winter wheat); high pressure bales	15.0	5.2	4.2	720	482

Abriviations; GCV, gross calorific value; ncv, calorific value; d.b dry basis; w.b wet basis

2.3 Biomass Conversion Technologies and state of art

Biomass energy presents an enormous energy portfolio of the future as it can be converted to thermal, solid, liquid and gaseous fuels and other chemical products through a variety of conversion processes. On average in the industrialized countries, biomass contributes some 9-13% to the total energy supplies, but in developing countries the proportion is as high as a fifth or one third [39]. In quite a number of countries, biomass covers even over 50 to 90% of the total energy demand. A large part of this biomass use is however non-commercial and are used for cooking and space heating, and generally by the poorer section of the population. This also explains why the contribution of biomass to the energy supply is not exactly known; non-commercial use is poorly mapped [40]. Biomass is basically an organic matter that can be processed into energy for power generation, liquid fuels and heat. The use of biomass in energy production remains an important strategy for reducing our carbon footprints by investment in low carbon technologies. At present, the world population uses only about 7% of the estimated annual production of biomass, which is 8 times the total annual world consumption of energy from all sources, and this makes it sensible to consider technologies for capturing this huge energy store for the future. In Sweden in particular, a significant market has developed for biomass pellets, which are fired in automated firing systems [41]. It is one of the objectives of this thesis to take advantage of this huge energy resource, a process that is likely to have a positive effect by not creating a scenario that impacts on the global carbon balance.

The conversion processes are; direct combustion, co-firing, pyrolysis, gasification, anaerobic digestion (landfill gas), fermentation and hydrolysis. Some of these conversion technologies are examined as part of this study to further understand the benefits in energy production from biomass. However, a sub-classification of biomass into two main categories can be deduced; "Wet biomass" (organic waste fluids, manures and marine algae), "Dry biomass"; (waste from lumber industry and forest waste, wood), agricultural and forest biomass; (nutshells, olive baggasse, rice husks). Two other conversion routes are; biochemical routes (microbial digestion, acid digestion and anaerobic digestion) applied to convert wet biomass. Thermochemical routes are gasification, combustion, pyrolysis and liquefaction applied to convert dry biomass involving the use of heat to decompose organic matter through chemical reaction. With the knowledge that biomass is composed of cellulose ($C_6H_{10}O_5$), gasification and combustion can be depicted by a global chemical equations;

$C_6H_{10}O_5 + 0.5O_2 \rightarrow 6CO + 5H_2$ - gasification

$C_6H1_0O_5 + 6O_2 \rightarrow 6CO_2 + 5H_2O$ - combustion

However literature shows that combustive reactions release more heat - 17.5MJ/kg than gasification reaction - 1.85MJ/kg [20] exclusive of gas production factor, and heat from biomass combustion will be used as external heat carrier for the operation of the ORC. This study will also consider a brief overview of a few other biomass strategies that are applicable to small scale CHP or micro electricity production.

2.3.1 Landfill gas

A similar technology to anaerobic digestion and occurs as a by-product of the decomposition of solid waste in Figure 2.6 [42] consisting of 50% methane, 45% CO_2 and 4% nitrogen. The Trans-Jordan landfill in West Jordan is an example where natural gas is captured from the decomposing landfill than allowing it escape into the atmosphere and causing atmospheric pollution. The gas can be collected after a 3-D mapping of the landfill to locate the gas and a conventional drill collection or the push-in collection process is usually adopted to retrieve the gas. The former uses normal gas drilling techniques while the "push-in" uses the 3-D mapping mentioned earlier to find the gas well before pushing to exploit the gas.
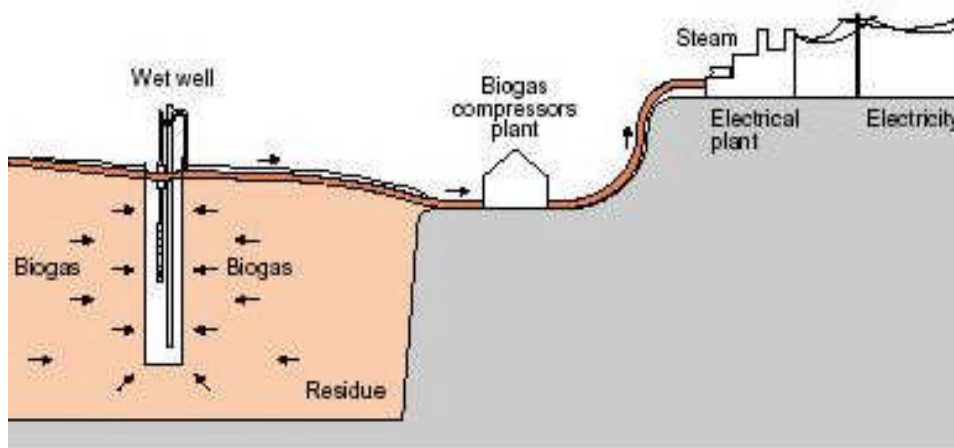
Figure 2.6: Landfill gas. Source; www.reuk.co.uk

Countries like Denmark and Germany have a strong position with advanced digestion systems used for processing various wet waste streams [43].

2.3.2 Pyrolysis

This is a process where biomass is combusted at high temperature and decomposed in the absence of oxygen to liquid (bio-oil), gaseous (syngas) and solid fractions (char) and tar, as indicated in Figure 2.7a [44]. The oil can also be upgraded (e.g. via hydrogenation) but pyrolysis and upgrading technology is largely in the demonstration phase [45]. Liquefaction (conversion under high pressure) and HTU, or Hydro Thermal Upgrading (a process originally developed by Shell and in pre-pilot phase, that converts biomass at a high pressure in water and moderate temperatures to bio-crude [46], are other ways of producing 'raw intermediate' liquids from biomass. When the by-product, brown liquid pyrolysis oil in Figure 2.7b [44] is cooled, it can be used in a gasifier.

When sped up, a process known as fast Pyrolysis, up to 75% more bio-oil is generated. The European Biomass Technology group has created bio-oil using the fast pyrolysis technique by combining wood residue with hot sand in a rotating cone. On a small scale, the rotating cone technology uses 250 tons of wood/day and generates 50 tons of oil (the equivalent of 0.314 barrels of oil).
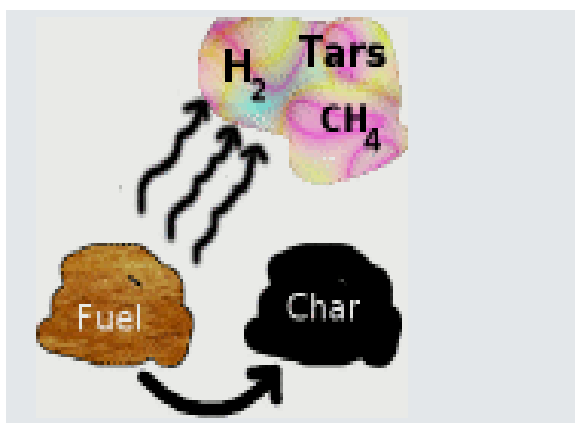
(a)   (b)

Figure 2.7: The by-product from Pyrolysis process

2.3.3 Gasification

Biomass gasification involves the conversion of solid biomass into gaseous form normally referred as syngas, which can be run through a power conversion technology such as a combined-cycle gas turbine or a coal power plant. Experts believe that the process can yield more efficient biomass power plants. The basic operational mode of a gasifier in Figure 2.8 [47], is the heating of biomass in an enclosure where solid biomass breaks down into flammable gas which has obvious advantages over direct combustion in that the biogas can be treated to remove particulates and problematic chemical compounds. The gas can be used for more efficient power generating systems or combined cycles to generate electricity. The conversion strategy involves biomass fuel being placed in the gasifier to be turned into a hot pressurised combustion gas that is subsequently passed through a gas cleaner to precipitate elements that can affect the system. The energy from the combustion is used to produce work in a turbine or a scroll expander described in appendix III, and the mechanical energy is converted to electricity. The exhaust heat can be recovered and used for domestic hot water. The by-product, which is a non-toxic ash, could be composted to help grow more biomass.
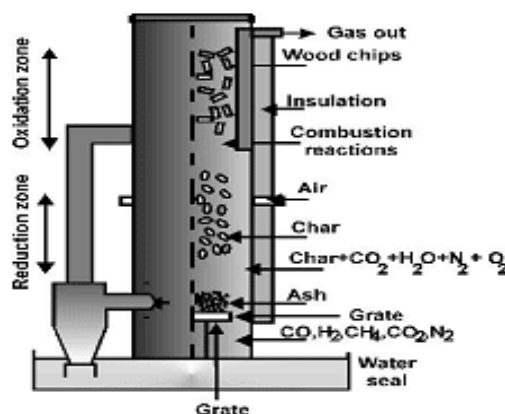
Figure 2.8: Schematic diagram of a Biomass gasifier

2.3.4: Benefits of Biomass

1. Reduction in Air Pollution:

Biomass is regarded as carbon neutral, as plants take in carbon dioxide during growth and release equal amount if allowed to naturally decay or burnt efficiently. A biomass resource produces less emission than fossil fuel and contains less contaminants and this varies with the conversion technologies as more advanced systems can deal with particulates.

2. Improvement of watershed quality:

The agglomeration of water bodies channelled into a single water course is known as watershed. These include rivers, lakes and other water bodies that collect and direct water from a land mass which a significant habitat for plants, animals and the human community offering recreation and makes irrigation possible and for drinking. Converting waste through anaerobic digestion of waste flow from sanitation services, food processing and livestock flows will immensely contribute to improved water quality.

3. Forest *Thinning*

This is a forest management technique that enhances the forest ability to cope or survive wildfires. It involves cutting small diameter trees which act as fuel for flames. This also allows space for the trees left to increase growth. The small diameter trees which would have made the trees incendiary now becomes a source of biomass fuel thus generating some form of market for biomass fuel. This becomes a win - win situation;

reducing fire hazards and generating biomass fuel as jobs are also created in the process.

4. Economic and social benefits:

The need to address issues of global warming and the long term effect on the environment has brought biomass fuel to a sharp focus globally as a major alternative resource. Though the technology is sill developing, biomass is set to positively impact on job creation not only in rural economy but open new areas for farmers who might grow energy crops which are relatively inexpensive to grow and are resistant to disease. It is claimed that more than 66,000 jobs are supported by biomass in the U.S [48], and It is predicted that by the year 2010, over 13,000 megawatts of biomass power could be installed, with over 40 percent of the fuel supplied from 4 million acres of energy crops and the remainder from biomass residues (DOE, NREL, 1998) supporting over 170,000 U.S. jobs and could significantly benefit rural economies.

2.4 Micro cogeneration technologies

Microgeneraton as defined by the UK government applies to a mix of heat and power technologies with thermal output that is below $45kW_t$ or an electrical output of $50kW_e$ [49]. It is comprised of three basic types of technology among which are, heat producing, electricity producing and heat and power production the later known as micro-cogeneration systems. The basic types of micro-cogeneration systems considered in this section include fuel cells technology, gas turbine cycles and solar thermal/ PV collectors.

❖ **Gas Turbine cycles**

Micro gas turbines can be defined as small high-speed turbo-alternators that operate as a Brayton cycle in a thermodynamic cycle where air is compressed isentropically, combustion occurs at constant pressure and expansion occurs isentropically back to the starting pressure as shown in Figure 2.9. The gas turbine comprises a centrifugal compressor, a regenerator, a combustion chamber and a radial turbine connected to a permanent magnet alternator rotor indicated in Figure 2.10 and Figure 2 .11 [54], (Pilavachi, 2002; [50]. There are a number of recent references in the literature on the performance of microturbines as indicated by Fairchild et al. (2001), [51] Gomes et al. (2004) [52] and Bruno et al. (2004) [53]. Other research on micro gas turbines has focused on miniature gas turbine and J.M.Peirs et al is developing a micro power generator based on a micro gas turbine expected to offer the highest power density combining an axial turbine with a centrifugal compressor and tested with

hot compressed airupto 130,000 rpm at 330°C [54]. It generates upto 50W mechanical power with efficiency between 20% and 24% also generates about 36W of electrical power. However, the production and advancement of micro gas turbines have steadily advanced and will most
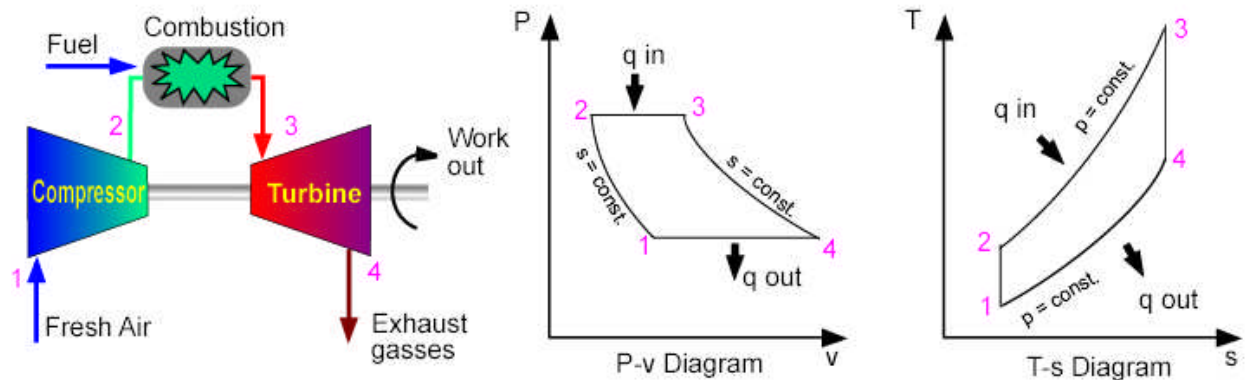
Figure 2.9: Idealized Brayton cycle

1-2. Connector

3. Stationary nozzle

4. Bearing

5. Turbine rotor

6. Outlet disc
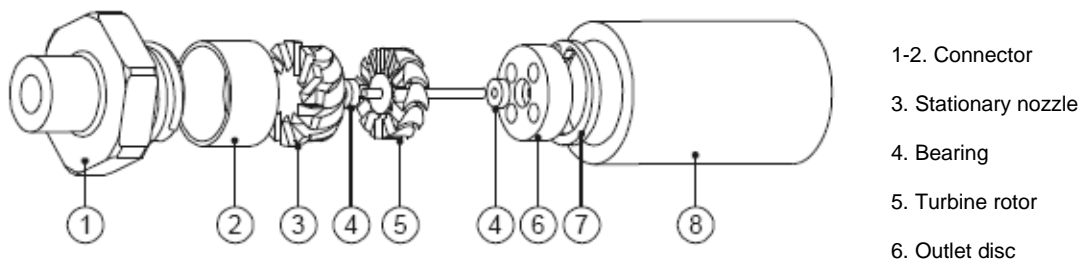
Figure 2.10: Exploded view of Gas Turbine design
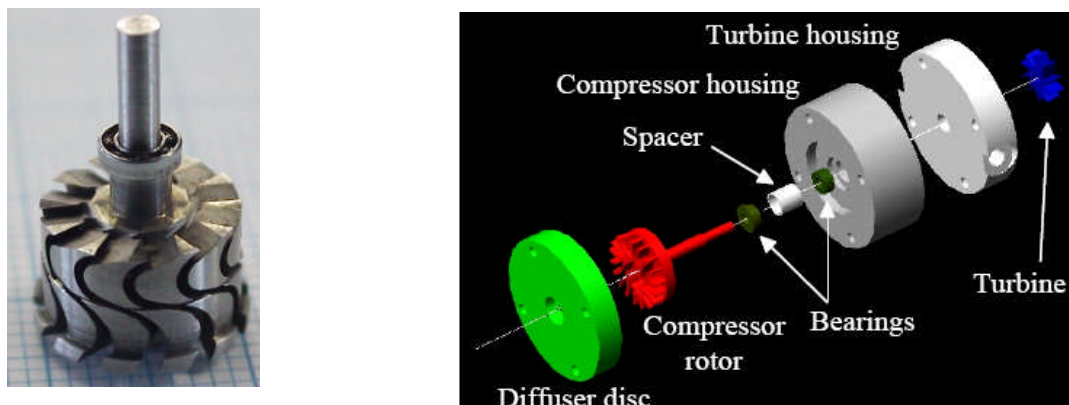
Figure 2.11: Turbine rotor and exploded view of compressor

36

certainly continue to evolve especially when viewed against the background of progress in computer sciences and finite element analysis along with material advances allowing for more compression ratios and combustion capabilities to be achieved. Micro gas turbines have a perspective to achievemuch higer efficiency as 40% by introducing higher turbine inlet temperature and higher recuperative effectiveness [55].

❖ Fuel cells

Fuel cells are devices that produce power electrochemically converting chemical energy of hydrogen into water and electricity; $2H_2$ (gas) + O_2 (gas) = $2H_2O$ (vapour) + Energy and are currently in the early stages of development. The system is shown in (Figure 2.12 and Figure 2.13) [56]. A fuel cell has two electrodes, the node and the cathode which are the negative and positive polarities respectively. The reactions that produce electricity takes place at the electrodes with the electrolyte carrying electrically charged particles from one electrode to the other as well as a catalyst which speeds the reactions at the electrodes. Fuel cells are normally stacked, as a single fuel cell generates a very little amount of direct current (DC) electricity and they are not subject to thermodynamic laws that limit majority of power plants. Electricity is generated electrochemically and not by combustion. The basic fuel used is hydrogen but also require oxygen and together oxygen and hydrogen form water as a by - product which normally drains from the cells. Some of the chemical potential energy is transformed into heat.

To produce electricity, hydrogen atoms enter the fuel cell at the anode where they are striped of their electrons by chemical reaction as the hydrogen atoms becomes ionized carrying a positive electrical charge.The negatively charged electrons provides the current true the wires to do work just as oxygen enters the fuel cell at the cathode and combines with the electrons returning from the electrical circuit and hydrogen ions travelling through the electrolyte from the anode. However, the electrolyte must permit only the appropriate ions between the anode and cathode to
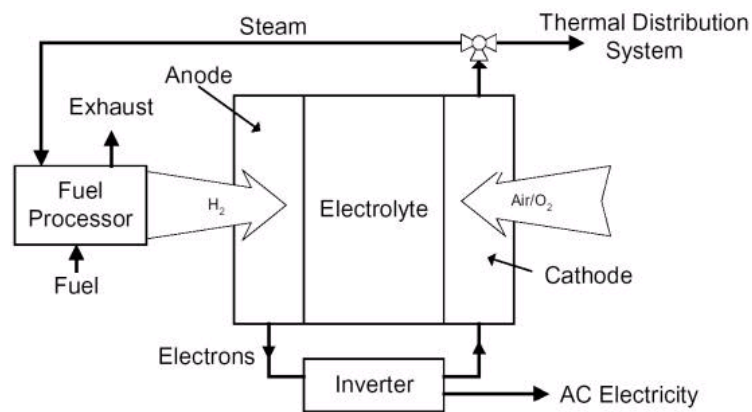
Figure 2.12: Fuel cell system
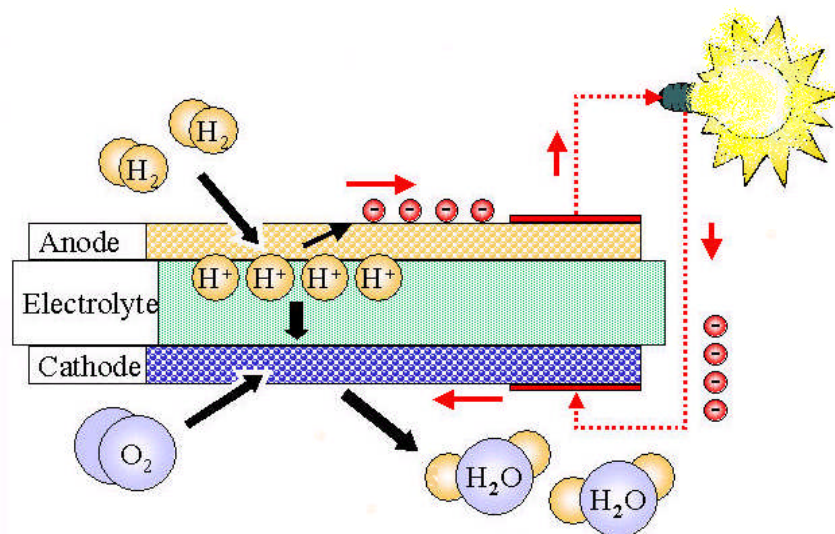
Figure 2.13: Fuel cell electrochemical process

avoid disruption in the chemical reaction. An inverter is required to convert the DC output to an alternating current (AC). Fuel cells operations depends on the electrolyte, some requiring pure hydrogen while some can tolerate some impuities but requiring higher temperatures to operate and waste heat from some cells can be harnessed boosting the system efficiency as chemical potential energy is converted into heat.
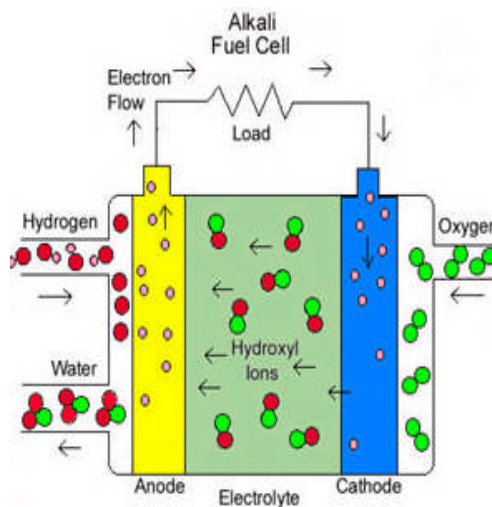
A. Schematic drawing of Alkali cell
Uses compressed hydrogen and oxygen with a solution of pottassium hydroxide as electrolyte. Has about 70% efficiency. Operating temperature is 150-200°C. Cell output is 300W-5kW.
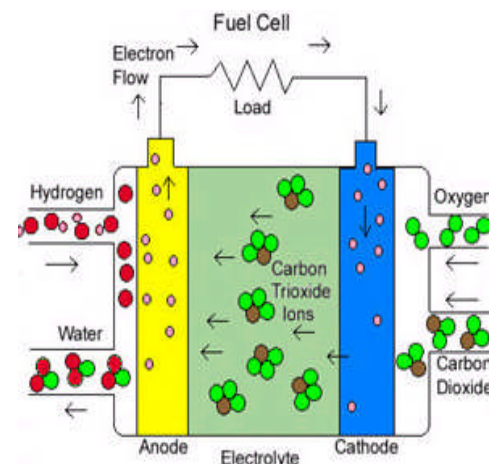
B. Molten carbonate cell
Uses high temperature compound salts, sodium Or magnesium carbonates as electrolyte. Efficiency is 60-80%, operating temperature Is 650°C and units with upto 2MW exist.
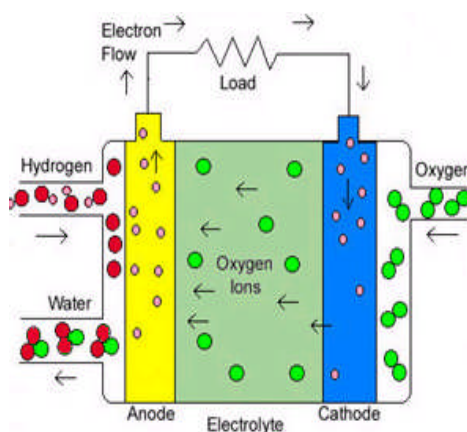
C. Solid oxide fuel cell
Uses ceramic compounds like calcium or Zirconium oxides as electrolyte. Efficiency is about 60%, operating temperature is 1000°C and cell output is upto 100kW
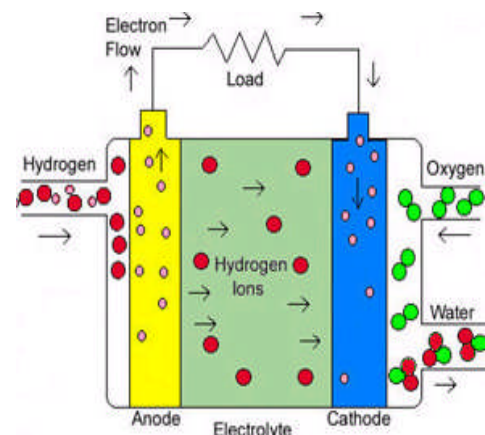
D. Phosphoric acid and PCM Fuel cells
Uses phosphoric acid for phosphoric fuel cells as eletro -lyte or a polymer electrolyte, a thin permeable sheet for Proton exchange membrane(PCM) The former has operating 150-200°C and the later has 80°C. Efficiency is 40-80% or 40-50%; Cell output is upto 200Kw or 50-250kW respectively..

Figure 2.14: Types of electrolytes for fuel cells

The various electrolytes used for fuel cells are indicated and described in Figure 2.14 [57] from A – D. A typical area of fuel cell depending on the power requirements could range between 100cm^2 to 1000cm^2.

❖ **PV/Thermal solar system**

The PV/T is an integrated system involving the combination of Photovoltaic cell and solar thermal collector resulting in a device that simultenously converts solar radiation into heat and power. Their high efficiency per unit area makes it suitable for heat and power generation compared to either a separate photovoltaic panel or solar thermal collector. The earliest examination of PVT technologies was reported by Florschuetz et al, 1979 [58]. Zondag et al, 2003 [59] examined the various concepts of combined PV-thermal collector. Huang et al, 2001 [60] have developed a PV/T system using a polycrystalline solar PV module combined with a solar plate employing a thermal greese inbetween for beter contact. He et al, 2006 [61] studied the hybrid PVT system which used natural convection to circulate hot water with a combined efficiency of 50% with 40% attributed to thermal efficiency. However most PVT development uses silicon technologies though crystalline and armorphous silicon or thin films are also in the mix.

PV panels have about 10-15% average efficiency with 85% of solar heat rejected and by integrating solar collector which can use upto 70% of the heat resulting in hybrid system efficiency of 50%. The various types of PV/T collectors are; PV/T liquid collector, PV/T air collector, PV/T concentrator and the ventilated PV with heat recovery. Figure 2.15 [62]

and Figure 2.16 [63] shows the BIPVT which is a liquid collector and PVT Concentator respectively and these are selected examples of the PVT system.
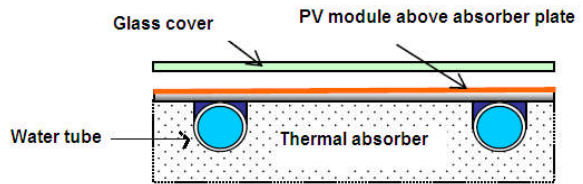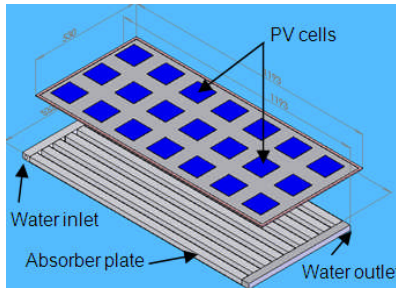
A. BIPVT Collector **B. Sectional detail of BIPVT collector**
Figure 2.15: BIPVT collector with sectional details.

Figure 2.16: PV/T concentrator

A. PVT air collector

Hot
exhaust
vent
(in Summer)

Fan   Air filter

Hot air
for water
heating

Healthy
warm air
to home
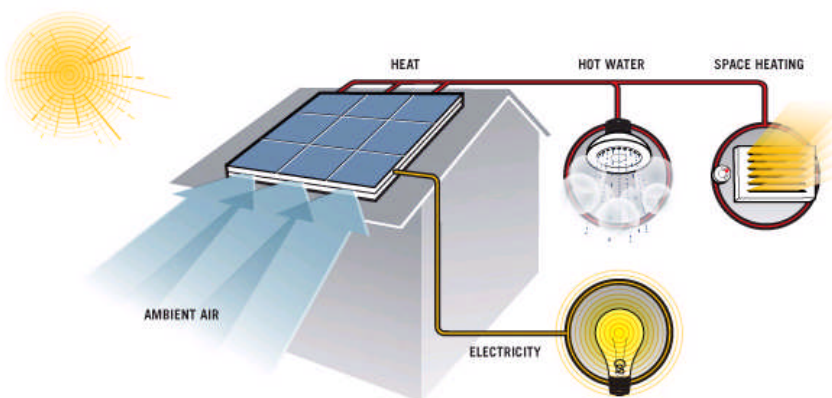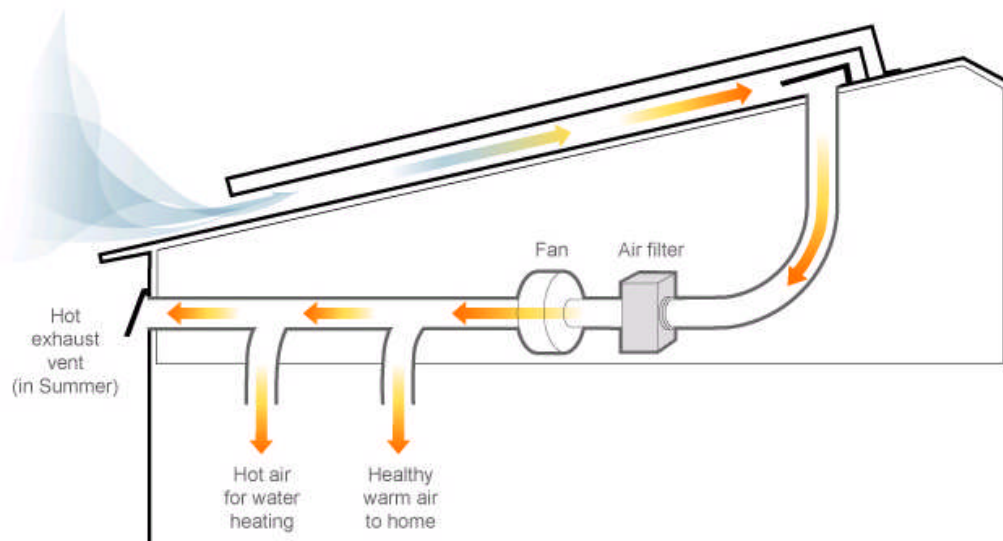
B. Working principles of PVT air collector

Figure 2.17: PVT air collector and the operational sequence

Waste heat is absorbed due to cooling effect of incoming ambient air on PV. Absorbed heat is further heated up passing through the thermal modules thus increasing the energy produced by the array. The controls and vents are used in the management of the high temperature air for hot and space heating

Figure 2.17 [64] shows a PVT air collector which absorbs heat from the

PV module cooled by incoming ambient air that is further heated by the

thermal modules thus increasing the resultant energy used for heating hot

water and space heating.

2.5 Early work on micro Rankine cycle systems

Some of the biomass technologies existing at the moment are still not commercially available but are maturing technologically. There are some research efforts to produce micro-CHP systems that use steam, but this study will use biomass to generate energy for the Organic Rankine cycle. The process will convert mechanical energy to micro electricity power outputs by means of an expander and a generator. Other technologies employed in micro power generation involves dynamic machines and Badr et al, have evaluated rotary machines such as the vane expanders which is also a subject of this research, the screw expander, and the Wankel, with isentropic efficiencies in steam operations published as; 65-80%, 25 - 40%, 13 - 25% respectively [65]. ORC has a significant showing in biomass utilization, geothermal and industrial heat recovery utilization. Expander implementation has been the focus in literature [66, 67]. These are cheap displacement compressors employed as expanders and are considered to be reasonably efficient [68, 69 and 70].

In terms of biomass mini power generation there has been some effort by the U.S. Department of Energy on Small Modular Biomass Initiative in conjunction with some industries to develop small modular biomass systems that are efficient and clean. One of these initiatives in 1998 was between the National Renewable Energy Laboratory in Golden, Colorado and Sandia National Laboratories in Albuquerque, New Mexico, who began work on the Small Modular Biomass Initiative shown in Figure 2.18 [71] which is a 15kW unit. These units are designed to be stand alone and

for use in remote areas but uses biomass fuel. Most biomass plants in

literature working with ORC

.

Figure 2.18 15kW modular biomass systems

Source ;(http://www.eren.doe.gov/biopower)

 process producing heat and/ or power have installed capacity of between

700 kWe and 1500 kWe [72]. The development of ORC combined heat

and power (CHP) plants based on biomass combustion were reviewed by

Obernberger [73] indicating the first demonstration of biomass fired Stirling

engine in Oberlech, Austria with 1MWel output ,18% electricity efficiency

and 80% thermal efficiency. An ORC biomass turbo-generator with

installed capacity of 400 kWel operated in Admont - Austria in 1999 with

electricity efficiency of 18% and using thermal oil as heating medium [74].

However, this work targets a micro - ORC biomass CHP system for output

of 0.1 – 2kWe different from the large scale productions that will address

the needs of remote off grid and rural locations or centers in developing

countries without any form of electricity. Two organic working fluid, known

as hydrofluoroether (HFE) HFE 7100 and HFE 7000 is used in this

research because of their lower boiling points. The later is to improve

upon the performance of HFE 7100 taking advantage of the lower boiling point of HFE 7000 so that the expansion of the saturated vapour will lead to dry vapour at the expander inlet. HFE 7100 has a boiling point of 61°C while HFE 7000 has a boiling point of 34°C removing the possibility of a non-homogenous mixture at the expander's inlet port.

Review of some prior work suggest the viability of micro CHP applications that range from 500 watts electricity to 1kWe for single households in the UK which is synonymous and within range of the predicted power output in this research. Auckland et al [75], first reported an analysis of individual house domestic CHP (DCHP) requirements. This was from average measurements of gas and electricity demands of about seven houses in winter and their conclusion is that the anticipated optimum output would be about 500W electricity. Information from government statistical service [76] also suggests that houses in the UK have an average electrical demand of 1kW. The argument is that since British Homes consume about 40% of the national demand of electricity and 30% of the total UK demand for energy and more especially seventeen million, or 80% [76] of these
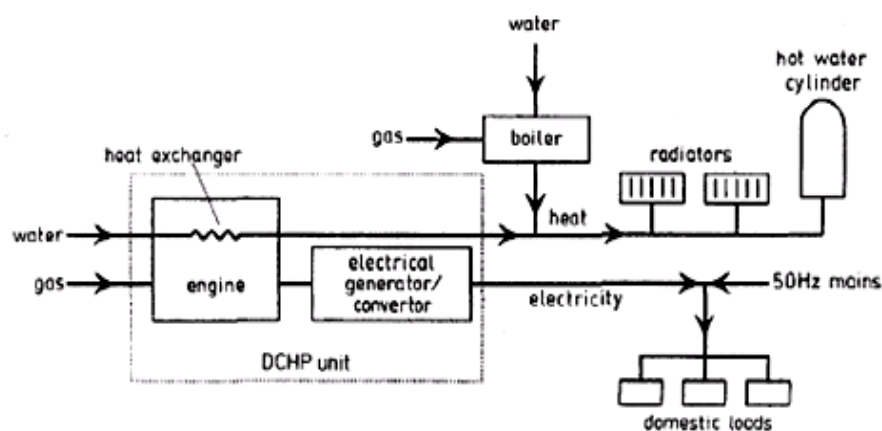
Figure 2.19: Proposed domestic combined heat and power system

homes already have gas central heating, there is a definite potential for electricity generated from gas within the home and the resulting heat utilised for water and space heating. This however is within the predicted range of 1kW as proposed by J. M. Pearce et al [77] and with the schematic diagram in Figure 2.19. [77] Everett *et al.* [78] measured energy use at sixty houses in Milton Keynes, Buckinghamshire. In each of three houses, numbers 33, 35 and 36, they measured the gas and electricity consumption in fifteen-minute periods over a six-month period in 1982 reinforcing the findings of 1kW national average electrical demand for houses in the UK. . As the aforementioned review suggests, Domestic CHP generators for individual homes greater than 1kW will be underutilised. Another interesting fact is the possibility of an enormous potential market for electricity generated within this range and format.

This finding justifies further research within this range of electrical outputs and specifically focused on the use of non fossil and renewable sources of energy such as biomass in an organic Rankine process. This is an aspect of this research in targeting outputs of 0.1 - 2kWe electricity. However several researches on Rankine or Organic Rankine systems dealing with low grade heat and the use of positive displacement machines have been performed. V. M. Nguyen et al [79] developed a prototype low temperature Rankine cycle electricity generating system with n-pentane as working fluid. The heat source is from a gas fired 60kW propane boiler; (Hamworthy heating, model P60). The result showed a thermal efficiency of 4.3%, a turbine inlet temperature of $390^{\circ}C$, an rpm of 65,000 and power output of 1,5kW$_e$. An air-cooled 120kW fan condenser NRS, model

MDF133-40 was used and the boiler was pressurised to 1.5 bar to allow operations above 100°C. Takahisa Yamamoto et al have already carried out design and testing of an ORC system indicated in Figure 2.20 [80], using low heat source and their findings indicate a cycle efficiency of 1.25%, a turbine output of 0.15kW, using HCFC123 and a 20kW boiler.
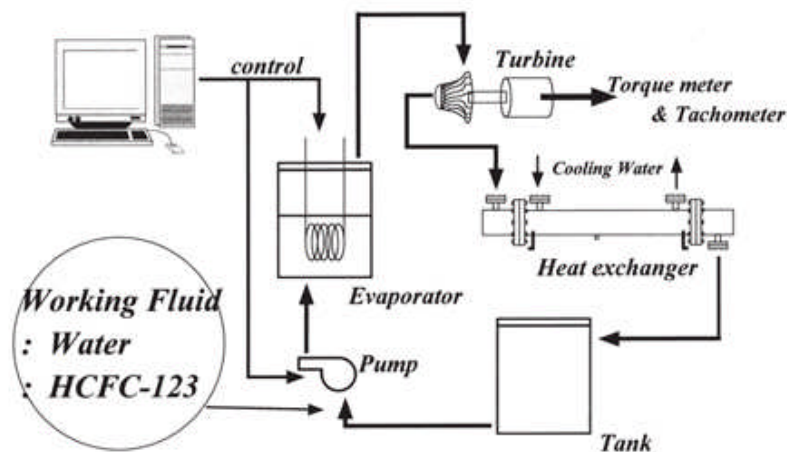
Figure 2.20: Schematic drawing of the experimental apparatus

Badr O et al [81], have investigated the behaviour of expanders in a Rankine engine using R113 as working fluid and the boiler output used in the experiment is an 85kW boiler at 180°C temperature output range. The expander output range is about (1.49 - 2.30) kW and (2.03 - 5.48) kW for the basic and optimized system respectively with an expander rpm of between 2820 - 3280. The small efficiencies are based on the fact that Organic Rankine systems are characterised by low efficiencies that range between 8% and 12% [82].

2.4 Organic Rankine Cycle (ORC)

Organic Rankine Cycle is a Rankine process where organic compounds are substituted for water as working fluid because of their higher molecular

weight, low boiling point as well as enthalpy which is lower than that of water. There are also suitable for single stage expanders but steam turbines will require superheating or multi-staging to improve the quality of the vapour. Organic Rankine Cycle is very similar to Rankine Cycle; however the use of organic substances instead of water makes for better cycle efficiency especially where low grade heat is involved. The ORC working fluid undergoes liquid to vapour and vapour to liquid transformation in order to execute the Rankine cycle between specified temperature limits. Badr et al, have investigated ORC heat engines studying the characteristics of working fluids and multivane expanders in low temperature applications [83 - 87].

2.4.1 The Rankine Cycle

For most traditional power plants and small-scale CHP production, the Rankine Cycle continues to be the main technology that is mostly adopted. L. G. Fréchette et al, 2003, developed a MEMS-based micro turbine device that implements a steam Rankine power cycle for portable power generation shown in Figure 2.21A, [88]. The system configuration consists of a heat source, a cooling mechanism (cooling fan or other heat removal approach). The Rankine device consists of a steam-driven turbine
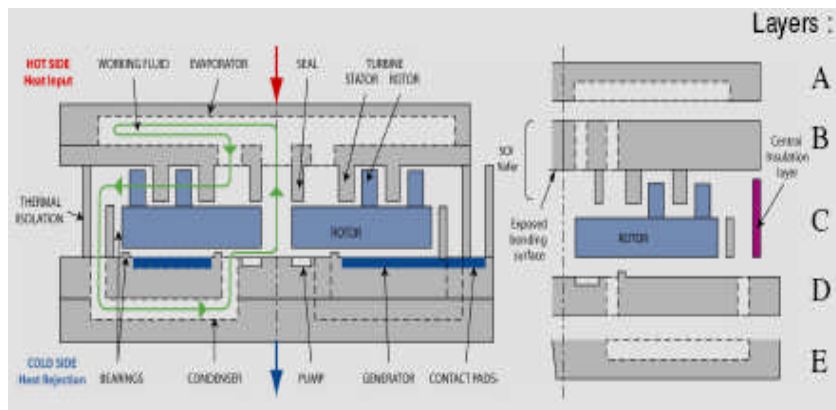
[A]-Details
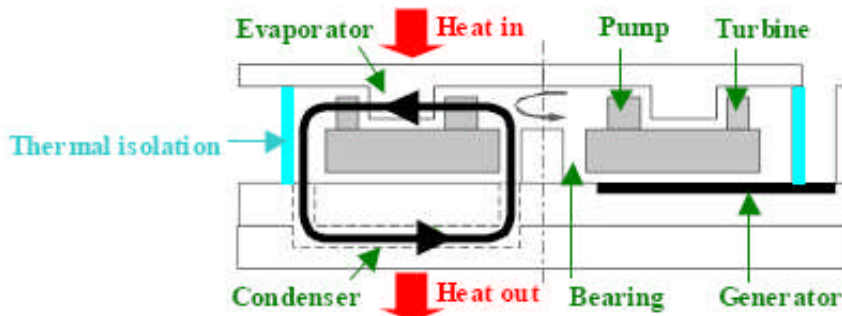
[B]-Process and external parts

Figure 2.21 [A and B]: Schematic cross-section of the Rankine steam Turbine device formed of five micro machined layers.

with a liquid pump and an integrated generator, along with a compact evaporator and a condenser seen in Figure 2.21B [88].

Takeo Saitoh et al 2002 [89], have proposed a solar Rankine cycle system with phase change steam accumulator and cpc solar collector shown in Figure 2.22 [89]. The system operates under a low temperature range of below 250°C with electricity generation efficiency of 16% and the working fluid used is R113 and has a combined cogeneration system efficiency of 60%.
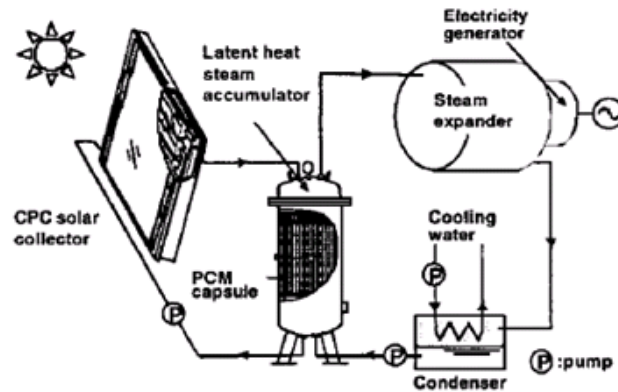
Figure 2.22: Solar Rankine cycle system

Cheng et al, 2005 developed solar thermal driven Organic Rankine cycle system using R123 and isobutene with cycle efficiency ranging between 18.5 and 25.90% and operating at temperatures between 80°C and 180° C [90]. Peterson et al, 2007 [91] investigated the performance of a small – scale regenerative Rankine power cycle employing scroll expanderwith efficiency of 7.2% and power output of between 187 and 256W and the operating temperature from a waste heat source is $150 – 400^{o}$C.

However, a standard vapour cycle that excludes internal irreversibilities is the ideal Rankine cyle. The expansion and compression process is isentropic (constant entropy) and the heat transfer in the evaporator and the condenser is isobaric (constant pressure, $\nabla_p = 0$). In the real cycle, irreversibility lowers the cycle efficiency. This mainly occurs during the expansion where only a part of the energy recoverable from the pressure difference is transformed into useful work. The other part is converted into heat and is lost. The efficiency of the expander is usually compared with an isentropic expansion. In Figure 2.23(a and b) [92]; the entropy of the
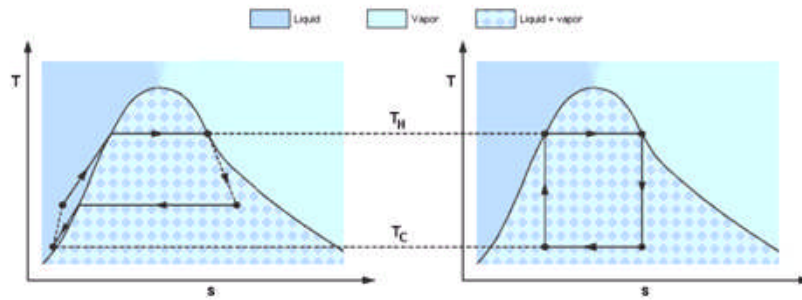
Figure 2.23a Real Cycle   **Figure 2.23b The Carnot cycle**

real cycle changes with temperature as shown in the curve under the T-S diagram but in the Carnot cycle irreversibilities and heat losses prevents the ideal from taking place in every step. The real cycle is non-adiabatic and irreversible, the consequence of irreversibility being a reduction in cycle efficiency and useful work output. The irreversibility can be categorised;

- Inefficencies in the heat exchangers

- Pressure drop in the heat exchangers

- Losses in the pump and expander (friction, leakage, etc)

However, the efficiency of a Rankine process can be increased by altering two main properties, the pressure or temperature of the boiler. The dark green area is decreased and the light green area increased in Figure 2.24a [93], and when the boiler pressure is increased, the Rankine efficiency is increased comparing the two scenarios. This also leads to cavitations on the turbine blades and decreased quality of steam or vapour at the exhaust of the turbine which should not be less than 90% in quality.
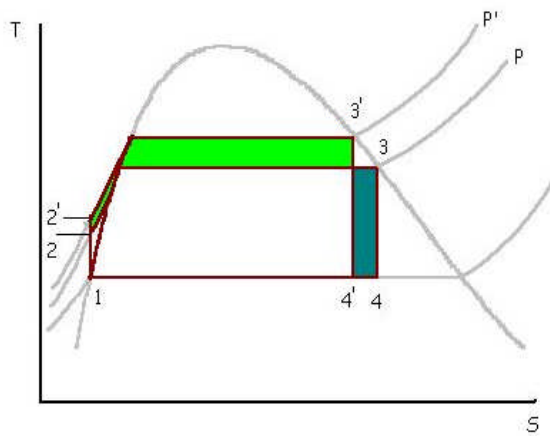
Figure 2.24a Pressure Increase   Figure 2.24b Temperatur   increase
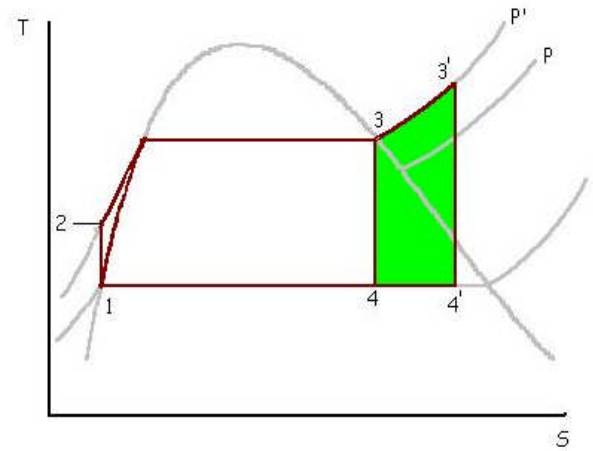
Conversely, in Figure 2.24b [93], increasing the temperature can also increase efficiency as vapour will be at the superheated region increasing the area and thus quality of the vapour exiting the turbine.

Four processes are identifiable with Rankine cycle that duly affect the state of the working fluid and usually specified in numerical terms as shown in the Figure 2,25 [93]. From 1 to 4 indicate transformation undergone by the working fluid due to change of state.
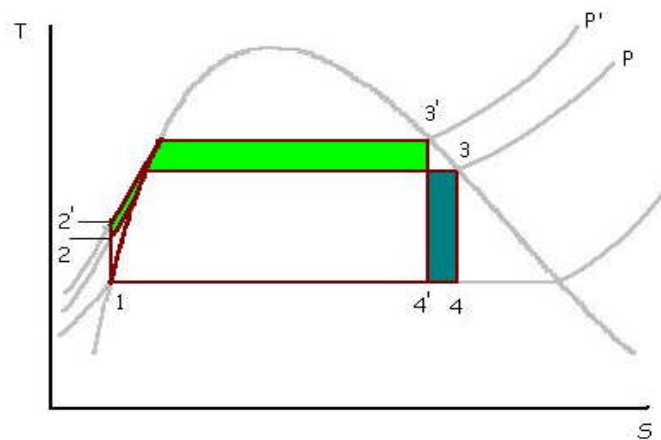
Figure 2.25: The four states in the Rankine cycle

However (1 - 4^1) applies when boiler pressure is increased and therefore state;

1-2 The working fluid is pumped from low pressure to high pressure saturated liquid in the boiler.(Isentropic compression).

2-3 High pressured liquid enters the boiler for heat addition at constant pressure.

3-4 The dry saturated vapour or superheated vapour expands through the prime mover generating power and causing a fall in temperature and pressure at the exhaust of the prime mover. (isentropic expansion).

4-1 The saturated vapour or a mixture of vapour and liquid enters the condenser where it is cooled at constant pressure and temperature to become saturated liquid.
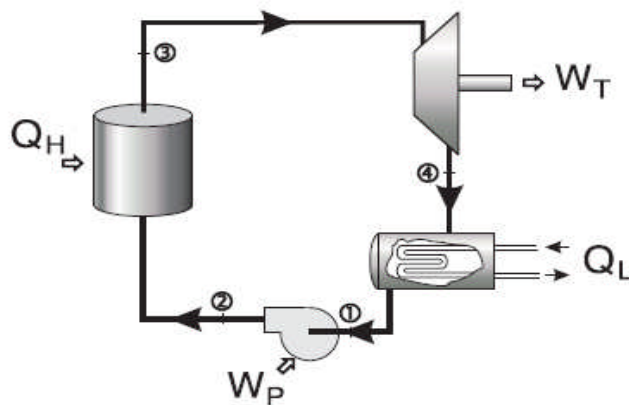
Figure 2.26 Typical Rankine power cycle

In analysing the process and assuming steady flow, and the first law of balance; energy in = energy out, various components involved in the

process can be summarised from the schematic diagram in Figure 2.26

[94]. The net work output is given as;

Boiler $Q_H = m\ (h_3 - h_2)$ (in)   (2.1)

Turbine $W_T = m\ (h3 - h_4)$ (out)   (2.2)

Condenser $Q_L = m\ (h_4 - h_1)$ (out)   (2.3)

Pump $W_P = m\ (h_2 - h_1)$ (in)   (2.4)

$W_{net} =$ $W_T - W_p$ (2.5)

The Rankine efficiency is

$$\eta_R = \frac{net\ work\ output}{heat\ supplied\ to\ the\ boiler}$$

$$= \frac{W_{net}}{Q_H}$$ (2.6)

2.4.2 Applications for Low temperature Organic Rankine cycle

The significant aspects of low temperature ORC is the use of low grade

heat to generate high grade energy in terms of outputs. There is also the

possibility of harnessing waste heat from either power plants or industrial

processes by integrating an ORC system. It is known that exhaust heat

from industrial processes and power plants are less than $370^{\circ}C$,

Donghong et al, [95]. This form of heat will not only be a waste but will be

a constant source of heat pollution to the environment if exhausted into

the atmosphere and further contributing to global warming.

The ORC integration will consume virtually no additional fuel but will

improve system efficiency.

Badr et al, 1990 [67], K. M. Lee and M. L Chien et al, 1998 [96], have made series of researches on ORC low temperature systems as well as the choice of proper working fluid employing a multi-vane expander. Researchers such as Hung et al [97], Yamamoto et al [66], Larjola et al [98], and Somayaji et al [99] have investigated the application and performance the Organic Rankine concept to demonstrate that organic fluids can be used to generate power from low temperature sources. Some of the viable low temperature sources for ORC are described;

● **Geothermal plants**

Geothermic heat source vary in temperature from 50 to 350°C. For low temperature geothermal sources (typically less than 100°C), S.Quoilin, 2007 [100], had suggested that the ambient temperature affects the power plant efficiency and thus the temperature of the heat sink. ORC systems can use this quality of heat for power generation depending on the evaporation temperature of the working fluid.

● **Solar thermal**

Solar energy, a result of extensive radiation from the sun can be converted to useful energy and when absorbed in solar collectors can be useful for domestic hot water supply or space heating and when parabolic concentrators are employed can provide high temperature heat for electricity generation or photovoltaic for direct conversion to electricity. Others are line focus collectors and heat tubes. The line focus can produce a temperature between 200°C - 400°C while a dish system can produce over 1500°C Figure 2.27 [101].

Figure 2.27: Radial arrays of Solar parabolic dish

Source: Status Report on Solar Thermal Power Plants. Pilkington Solar International GmbH: Cologne, Germany, 1996.]
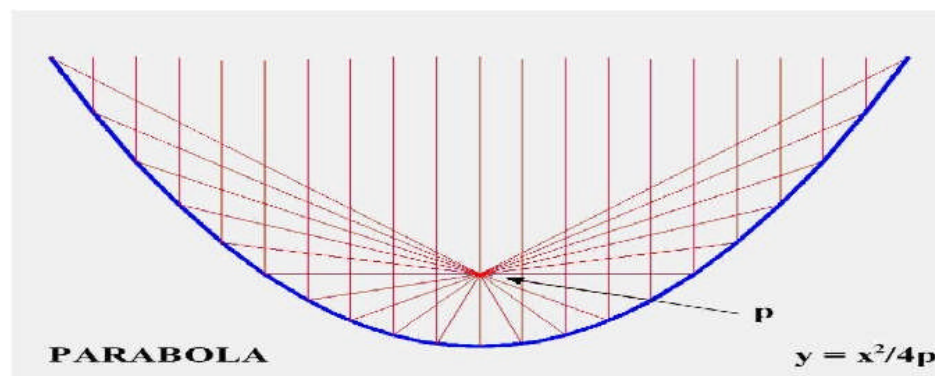
Figure 2.18: Parallel rays' convergence at a point or line.

The solar parabolic trough technology in Figure 2.18 can be adapted to Organic Rankine cycles rather than the usual steam Rankine cycle. Examples of low temperature parabolic trough technology have been studied by S. Canada, 2005 [102], and E.H. Malick Kane, 2002 [67]. The ORC allows reduced ambient losses and therefore better collecting efficiencies as well as the possibilities of reducing the size of the solar fields.

2.5 Summary

Based on the reviews and knowledge gained as a result, preliminary tests are conducted using an electric boiler to investigate the conditions and to analyse the system as well as demonstrating that the system can convert fuel energy to mechanical energy and to produce heat and power. An environmentally friendly organic working fluid, HFE 7100 and HFE 7000 are used because of their low boiling points making it suitable for the intended low temperature system and having a molecular weight and heat of vaporization that is better than water as an option. This work focuses on the use of biomass as the primary energy source to raise heat energy for the ORC process but in this chapter other potential sources have been reviewed as possible alternative sources of energy.

The review of early work brings to a focus previous research that establishes facts justifying further research in this area as well as the viability of such research endeavour. A background on the building block of biomass which occurs through the process of photosynthesis has been examined. The chemical composition and the calorific value of biomass are considered. The various biomass conversion technologies and state of art are included in this chapter. However, this research is focused on the use of energy from biomass to convert mechanical energy to electricity by driving an automotive alternator as the electric generator. Another aspect is the production of hot water though at a very small scale due to low exhaust heat. The low temperature sink at condenser of ORC systems makes it unlikely to operate a robust CHP system though sink temperature can attain about 40°C which can be of some domestic use.

CHAPTER 3: Theoretical analysis

The theoretical investigation of the characteristic thermal performance and thermodynamic cycle analysis of a novel micro–power biomass system that implements the Rankine cycle process is described in this chapter. The elements that make up the cycle will be analysed. Although specific cycle designs may defer, three basic elements of the power cycle, the turbine, boiler and the pump are of significance with efficiency being dependent on average heat flow and transfer in the heat exchangers, the expansion process in the turbine as well as the operating pressures.

3.1 Theoretical Investigation of the Thermal Performance

The schematic system layout and the thermodynamic cycle indicated on the T (temperature) - S (entropy) chart are shown in Figure 3.1 and Figure 3.4 respectively but of significance is the fact that the boilers and prime
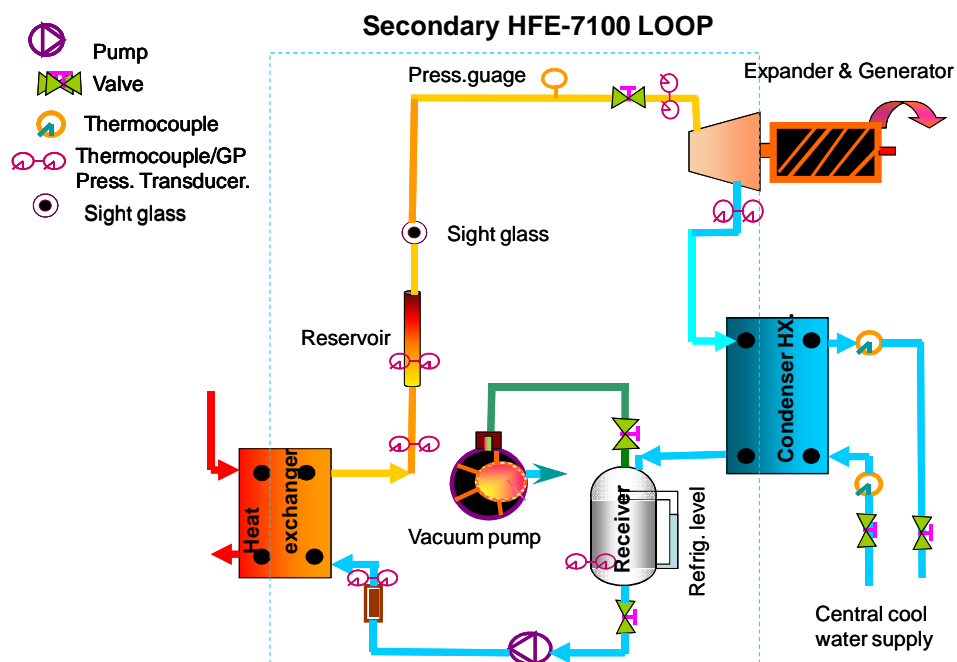
Figure 3.1: ORC Cycle with HFE7100 as working fluid

mover are existing or available so that the system setup had to respond to that very fact. An improvement on the system incorporating a regenerator is proposed in Figure 3.2 where the exhaust heat from the expander exit is used to preheat the working fluid being pumped into the boiler. The regenerator (recuperator) is a heat exchanger indicated in a detail diagram showing a more inclusive configuration in Figure 3.3. This will have an optimal effect on the thermodynamic properties of the working fluid and thus reduce the energy required in the boiler to vaporise the working fluid as well as improving the cycle efficiency though the work output remains the same.

System improvement using a Regenerator
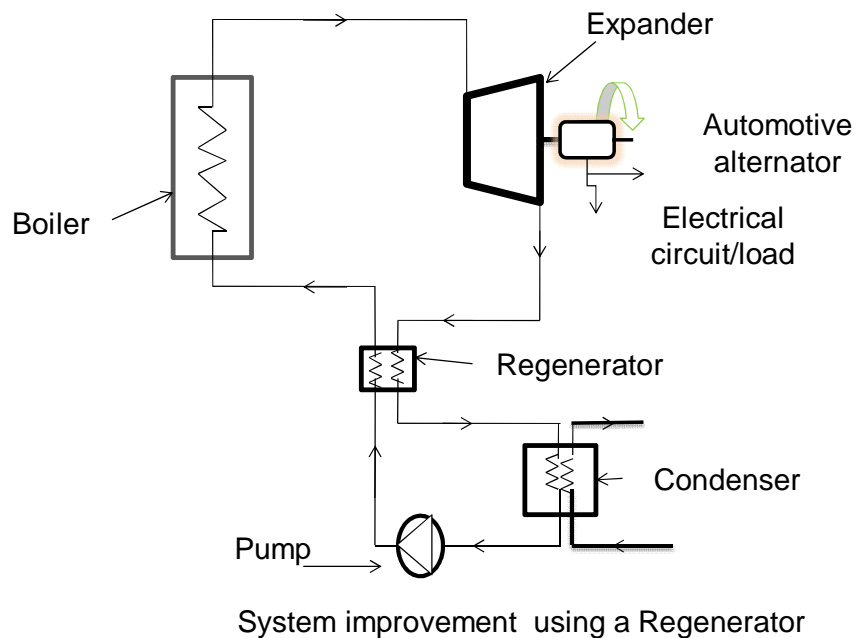
Figure 3.2: Schematic diagram of system improvement using a regenerator
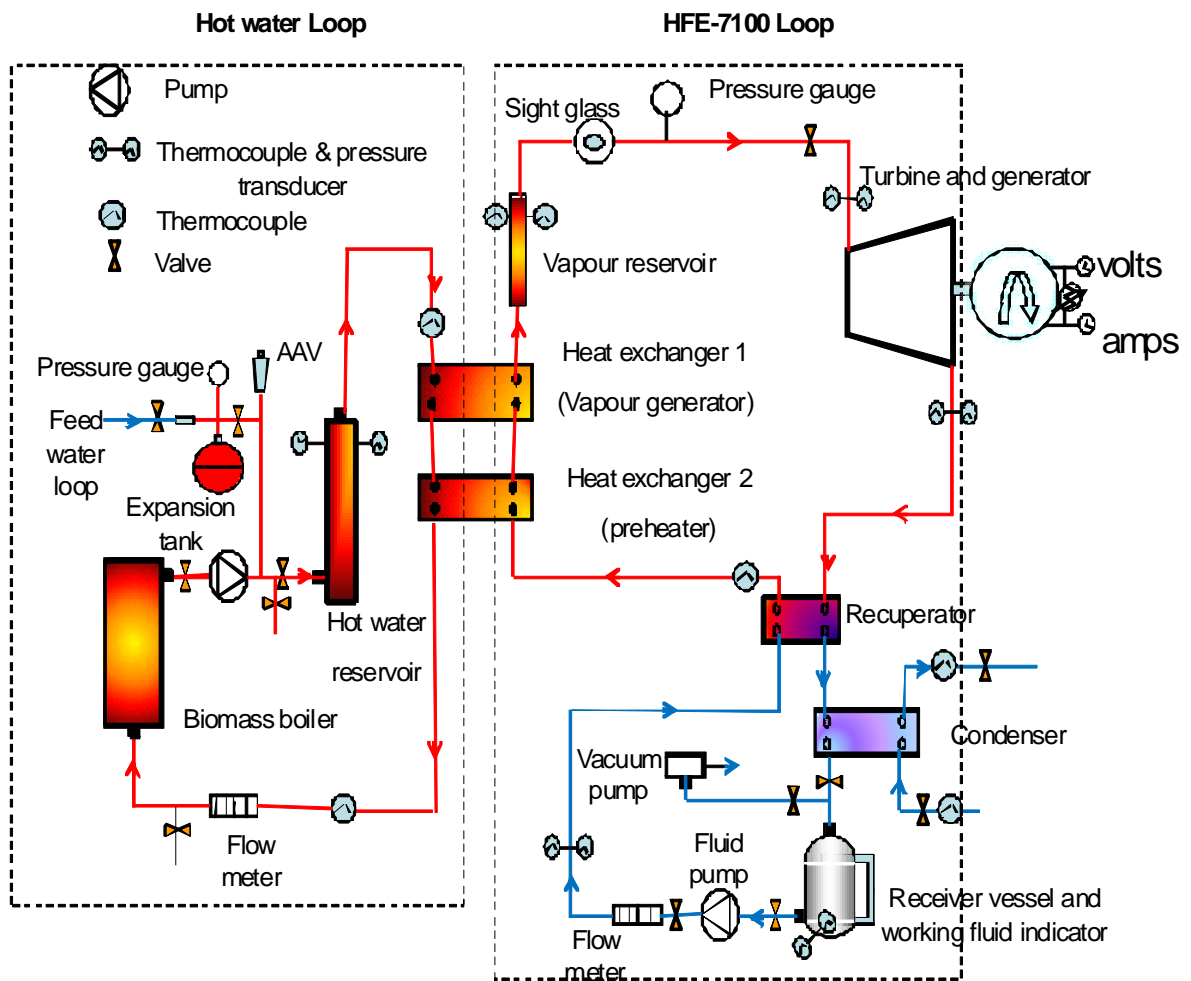
Figure 3.3: Schematic diagram showing more details of system improvement.

The System configuration incorporates an HFE 7100 loop in the Organic

Rankine cycle, with the corresponding schematics of the T-S chart. There

is however the hot water loop that supplies the heat to the system

discussed in chapter 2. The process involve a 115°C hot water loop

generated in the boiler and used to vaporise the working fluid, HFE 7100

resulting in change of state 1(under saturated liquid) to 2 (heat addition at constant pressure) in the boiler.
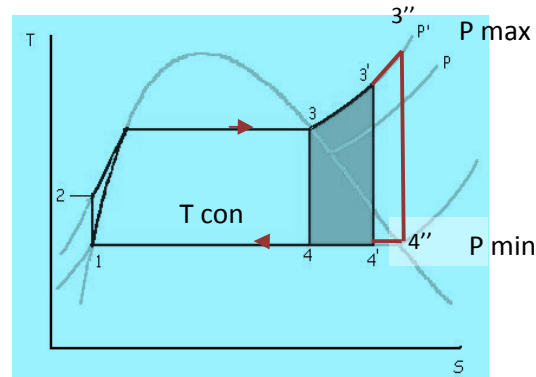
Figure 3.4: Schematic diagram of T-S Chart

And in state 3, 3' or 3" high pressured vapour is fed into the expander to generate work on the vanes and the resultant rotary motion in the shaft is then converted to electricity in the electric generator. However, 3, 3'and 3" indicate different temperature bands and the corresponding quality at 4, 4' and 4" with best quality at 4" in the supper heated region. As shown in Figure 3.4 [103], 1 to 4 indicates transformation undergone by the working fluid due to change of state. However (4, 4', and 4") indicates varying qualities of the state of the working fluid as the boiler temperature is increased and therefore state;

1-2 The working fluid is pumped from low pressure to high pressure saturated liquid in the boiler. (Isentropic compression).

2-3 High pressured liquid enters the boiler for heat addition at constant pressure.

3- 4 The dry saturated vapour or superheated vapour expands through the prime mover generating power and causing a fall in temperature and pressure at the exhaust of the prime mover. (Isentropic expansion).

4-1 The saturated vapour or a mixture of vapour and liquid enters the condenser where it is cooled at constant pressure and temperature to become saturated liquid.

The condensed working fluid at state 4 is then pumped to a higher pressure in the boiler to pressurised liquid state to repeat the cycle. The boiler mentioned here refers to the working fluid evaporator or vapour generator, a compact heat exchanger that facilitates heat transfer between two mediums from the electric boiler as source of heat and the working fluid in the evaporator. The condensation process could produce some degree of hot water with temperature between $35^{o}C$ and $40^{o}C$ for domestic use than being discharged to the environment contributing to heat pollution. Though the water temperature is not that high, it is adequate for simple domestic washing in winter months or just adequate for an early morning bath in the tropics.

3.2 Analysis of the Thermodynamic Cycle

As with most power plant steam cycle, three basic components which make up the plant cycle becomes crucial for closer examination and in this case the; expander, the pump and the heat exchanger. Despite variations in designs, these key elements form the plank for efficient performance and implementation of the Rankine Cycle process which in most steam cycles operate under the best theoretical conditions for the most efficient

outcome. Associated with these three key elements is the characteristic change in the properties of the working fluid where system efficiency can be determined knowing the temperature of the heat source (heat input) and heat sink (heat rejection) mechanism of the cycle. Based on the work that would have been produced by an ideal component operating in entropy between the inlet and outlet conditions, efficiencies of individual element can be calculated. However, the specific work output of thermodynamic cycles is fundamentally not a function of scale but of fluid properties at each point in the cycle. For consistent performance the output must be proportional to the mass flow rate of the working fluid through the device.

3.2.1 The Expander

The general equation under steady flow conditions with respect to the application of the first law of thermodynamics indicates that decrease in the enthalpy of the working fluid (h_5–h_6), which is the energy entering the expander as saturated or superheated vapour h_5 and the energy leaving the expander h_6 after perfect expansion and being isentropic (reversible adiabatic) is equal to work done by the working fluid on the expander vanes causing rotation on the shaft. The energy supplied by the boiler through heat transfer in the generator is indicated by the difference in enthalpy of the steam leaving the boiler and the saturated or condensed liquid entering the boiler (h_4-h_1) as indicated in Figure 3.5.

Figure 3.6 is a graphical description of the cycle using a typical T- s chart. The chart describes the various change of state and boundary conditions of a closed system including heat addition in the boiler, evaporation, expansion and condensation and these can be deduced from the chart at various states both adiabatic and the real(actual) process.
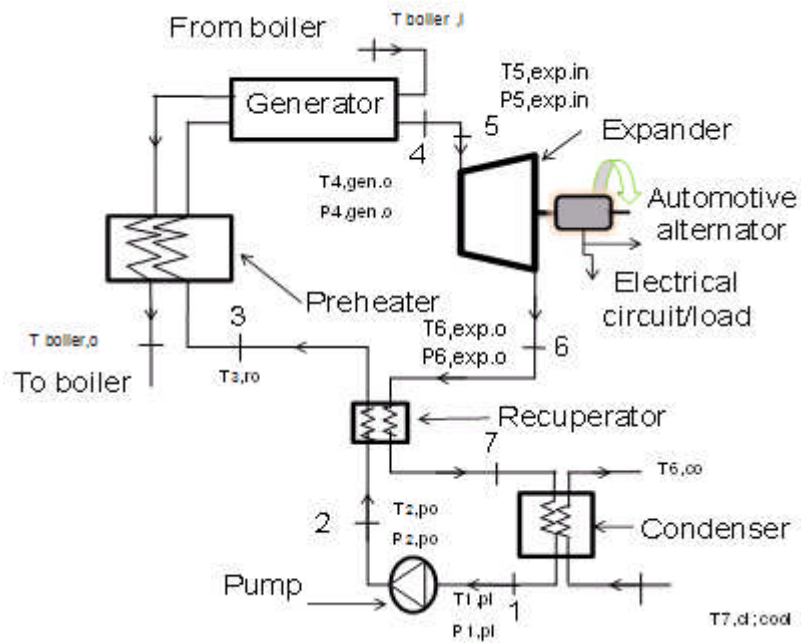
Figure 3.5: Schematics of the Rankine Cycle system
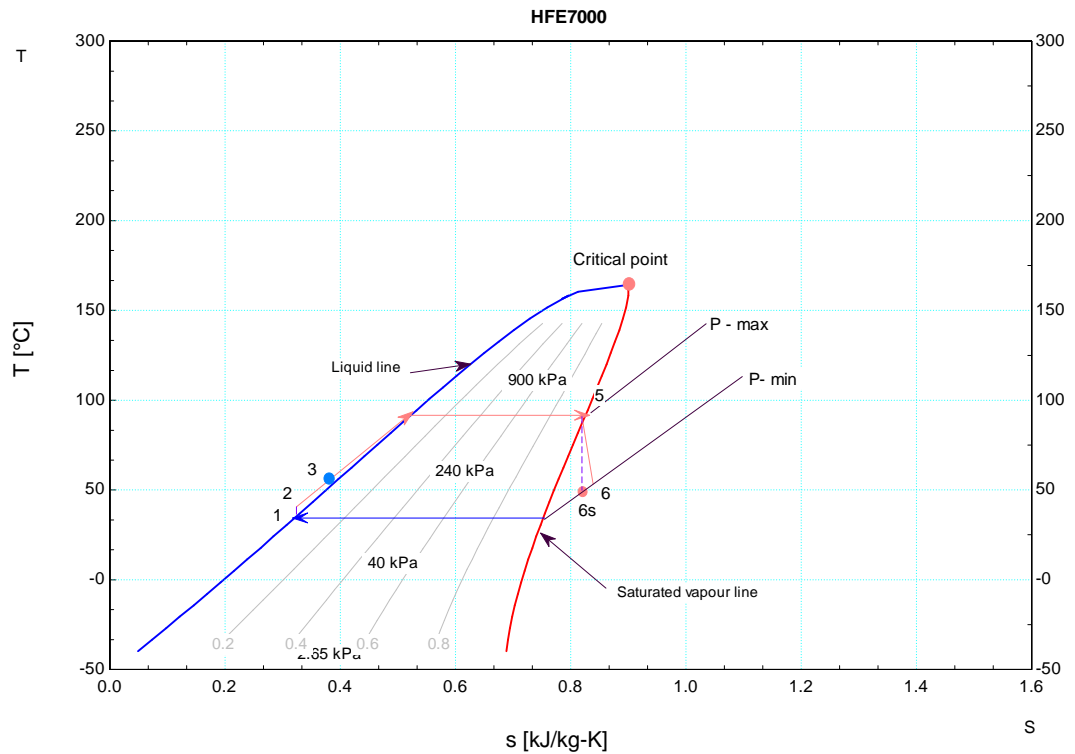
Figure 3.6 Typical T- s diagram of the biomass ORC cycle

The reduction in enthalpy in the expander can be determined from the graphical representations of an ideal or reversible isentropic (reversible adiabatic) process. However, the effect of irreversibility in the thermodynamic cycle produces a reduction of the useful work done and the cycle efficiency. The factors contributing to these and which constitutes the main irreversibility are; expander leakage fraction and frictional losses, pressure drops in heat exchanger including inefficiencies in the heat exchanger and pump losses. The converted expander work can be determined by knowing the enthalpy change and the mass flow rate of the working fluid in the Organic Rankine cycle;

$$W_t = m \ (h_5 - h_6) \tag{3.1}$$

This relationship occurs when both the kinetic and potential energy changes as well as heat losses of the working fluid are negligible. These are regarded as valid assumption for most practical applications and by assuming an ideal case the working fluid does work reversibly by expanding at constant entropy defining the so called ideal turbine. An actual turbine does less work because of friction losses in the blades, leakage past the blades and to some degree mechanical friction. Turbine efficiency or turbine isentropic efficiency at constant entropy is defined as a ratio of work done by the turbine, and actual work to the work that would have been done by the turbine as an ideal turbine.

$$\eta_t = \frac{W_{t\,actual}}{W_{t\,ideal}} \tag{3.2}$$

$$\eta_t = \frac{h_5 - h_{6_{actual}}}{h_5 - h_{6_s}} \tag{3.3}$$

3.2.2 Pump

The primary function of the pump is to move the working fluid by doing work on it causing change in enthalpy of the working fluid. Under the general energy equation and by implication the application first law of thermodynamics to simple pump under steady flow conditions; it is found that the change in enthalpy of the working fluid equals the work done by the pump;

$$W_p = m\,(h_2 - h_1) \tag{3.4}$$

This relationship occur when both the kinetic and potential energy changes as well as heat losses of the working fluid are negligible; a valid

assumption for most practical applications and another assumption being that the working fluid is incompressible. For the ideal;

$$W_{p\,ideal} = m\,(h_{2'} - h_1)_{ideal} \tag{3.5}$$

The basis of analysing the performance of an actual pump is to have a full understanding of the concept of an ideal pump and a clear definition of it. The actual pump for instance requires more work because of fluid turbulence and friction which constitutes unavoidable losses in the pump. The work done by the pump;

$$W_{p\,actual} = m\,(h_2 - h_1)_{actual} \tag{3.6}$$

$$\text{Pump efficiency, } \eta_p = \frac{W_{p\,ideal}}{W_{p\,actual}} \tag{3.7}$$

3.2.3 Heat Exchanger

Heat exchangers play significant role in steam cycles and are designed to transfer heat between two bodies or medium of differential temperature gradient, either for heat addition or heat sink. A number of heat exchangers can be integrated into a single cycle as vapour generator (evaporator) or condenser with the possibility of combining heat exchangers of varying sizes. In considering the first law of energy equation under the steady flow condition with respect to a simple heat exchanger, the mass flow rate and enthalpies of two fluid can be represented in the relation,

$$m_4 \ (h_{4out} - h_{2in}) = m_2 \ (h_{2out} - h_{2in}) \tag{3.11}$$

However the energy balance due to heat addition and heat rejection can also be indicated by the relationship;

$$Q_{supply} = C_p \ m \ (\Delta t) \tag{3.12}$$

$$Q_{cond.} = C_p \ m \ (\Delta t) \tag{3.13}$$

Therefore energy balance of the system under a steady flow condition can also be expressed as; Q supply equal to $Q_{cond.}$ The heat exchanger efficiency is up to 85% for the evaporator and 80% recuperator effectiveness.

3.2.4 EES Modelling

The engineering equation solver can be effective in modelling a thermodynamic cycle especially in deriving the thermodynamic properties at various state points or when comparing the ideal Rankine cycle to the actual cycle. A reversible thermodynamic cycle working within the temperature approximation as the experimental tests is used to model the example indicated in the appendix. The initial values indicate the known values from the test results and the unknown values can be calculated using the software for a completely reversible cycle. The cycle analysis is based on the various components making up the cycle and the phases of the working fluid is represented as either ($x = 0$), for liquid state or ($x = 1$) for saturated vapour. The implementation of the routines and procedures can be accessed from http://www.fchart.com/ees/eesgs.shtml

The modelled performance will later be compared with the actual performance to assess agreement. Biomass ORC systems in literature show low efficiency of between 8-12% range for major biomass plants. This model is based on the fact that Carnot cycles cannot be implemented in a real world approach but with a little modification to the Carnot cycle an Ideal Rankine system with the schemaics in Figure 3.7 and T-S chart in Figure 3.8b can mimic a practical cycle that can be implemented under a laboratory conditions. This is accomplished when the working fluid is allow to complete the condensation process at point 3, instead of point 3' as shown in Figure 3.9a which is a mixture of wet vapour and liquid. In a practical sense this makes compression of the working fluid difficult in the

pump. The most efficient ideal theoretical cycle conceivable is the Carnot cycle.
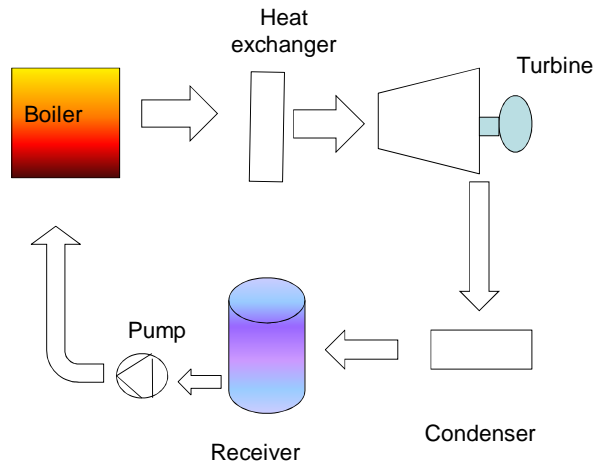
Figure 3.7: Schematics of a basic Rankine cycle
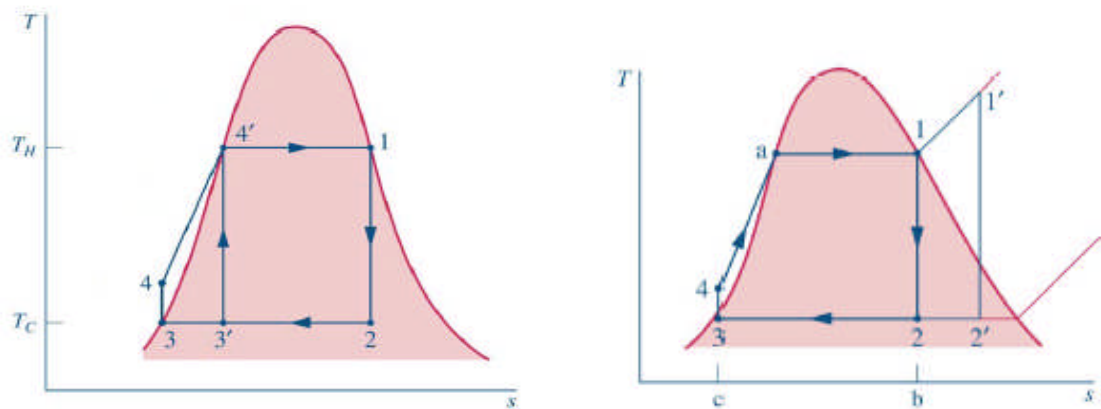
A/. Carnot cycle [1, 2, 3', 4'] modified   B/. Ideal Rankine cycle

Figure 3.8: Modification of the Carnot Cycle to an Ideal Rankine Cycle℃

Figure 3.9 and Figure 3.10 are modelled using the working fluid HFE 7100, the former without a recuperator and the later with a recuperator in the cycle. The inference indicate that an increase in condensation
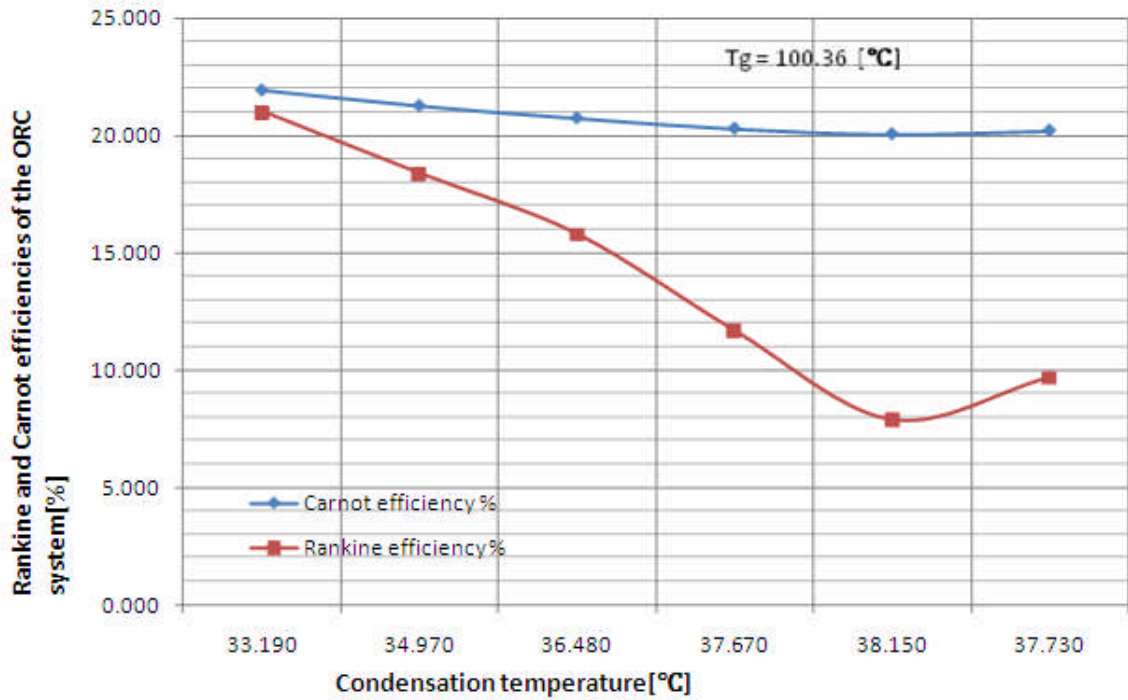
Figure 3.9: Modelled efficiencies of the ORC system with HFE7100 as working fluid with no recuperator vs. condensation temperature
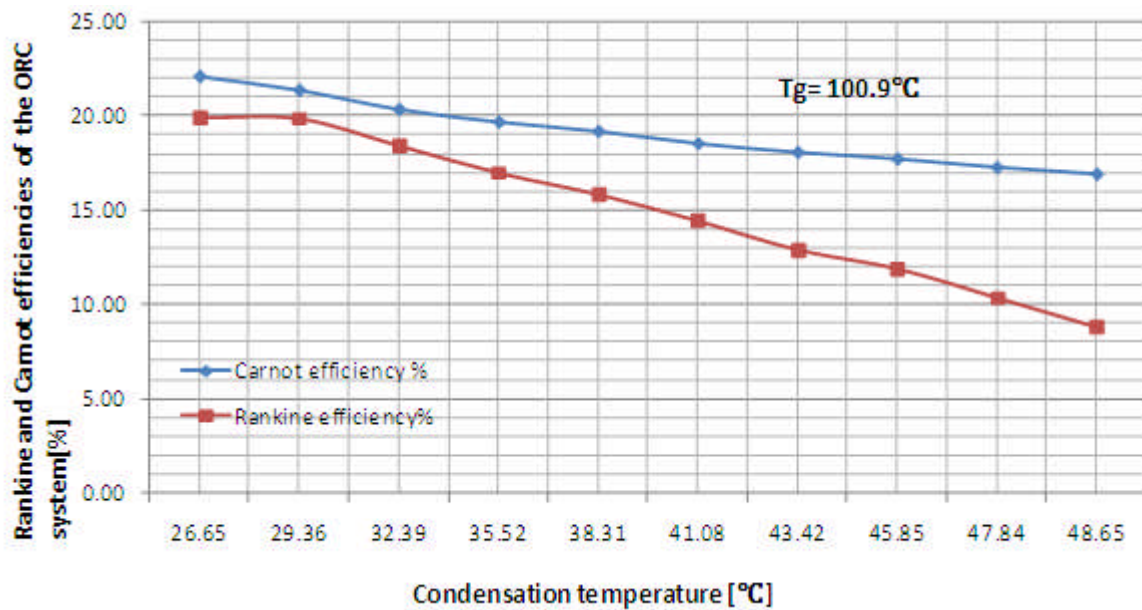
Figure 3.10 Modelled efficiencies of the ORC system with HFE7100 as working fluid with recuperator vs. condensation temperature

temperature in Figure 3.9 or Figure 3.10 will impact on the system efficiencies relative to the electric boiler output. Figure 3.9 also shows the effect of condensation temperature on system efficiency as efficiency starts to improve with again with lower temperature though at a point where the quality is a mixture. Figure 3.11 and Figure 3.12 model is performed with reference to the electric boiler and the biomass boiler ORC systems, with the recuperator in place and using the working fluid HFE 7000. The result in Figure 3.11 involving the electric boiler showed a progressive drop in efficiency with increase in condensation temperature but the biomass system indicate higher efficiency due to lower condenser temperature described earlier and having higher heat input than the electric boiler. The EES Modelling responds to the thermodynamic properties of the working fluid where two independent properties define the thermodynamic state of the working fluid.
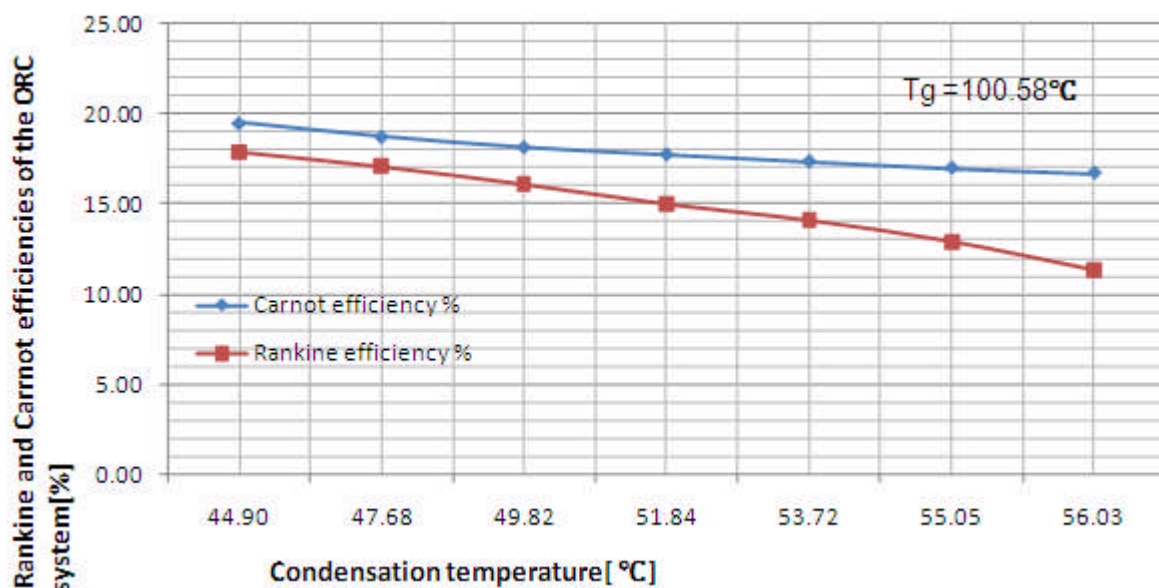
Figure 3.11 Modelled efficiencies of the ORC system with HFE7000 as working fluid vs. condensation temperature
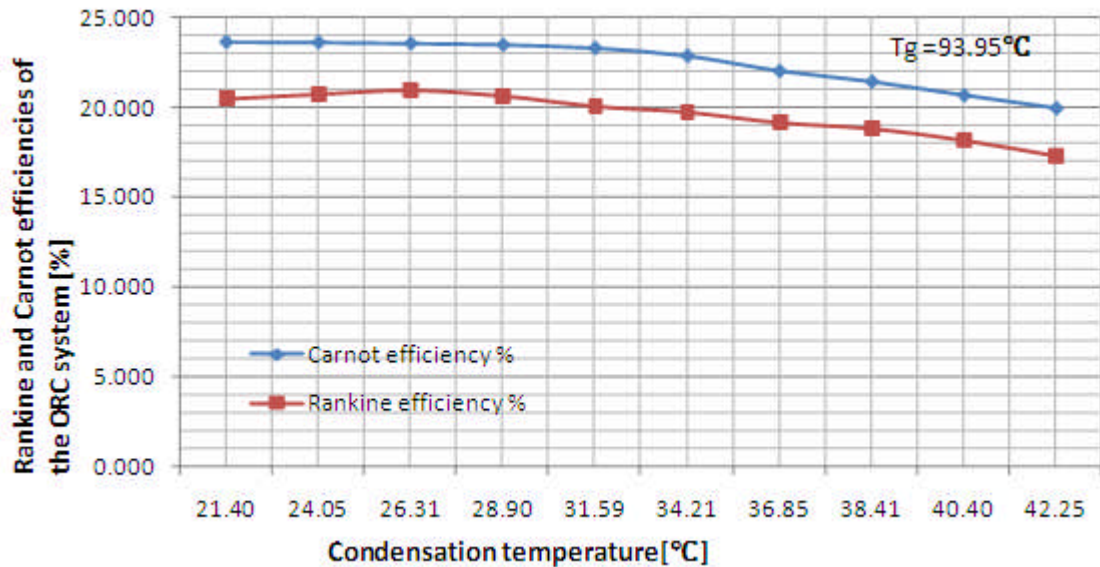
Figure 3.12: Modelled efficiencies vs. condensation temperature of the biomass ORC system

The basic operational and performance characteristic of the Rankine cycle is made possible by the use of the software considering a steady state conditions. The EES modelled assumptions are indicative that using HFE 7000 will produce an improvement in efficiency of the ORC system. The modelled performance will instructive in analysing the experimental results. Biomass system in literature shows low efficiency of between 8 - 12 % predicted range for major biomass plants. The micro turbine power output have been derived by estimation from the Gast manufacturing incorporated online resource which has the section covering the product manual at http://www.gastmfg.com/airmotor/6am%2B6AM%20Metric.pdf) showing output range of the air motor as an expander. The electrical power output of the alternator is predicted by expander to alternator conversion efficiency between 50-65% based on the size of the alternator.

The expander efficiency used for the EES modelling is 85% but the deviation based on the air motor actual efficiency will be calculated from the experimental data.
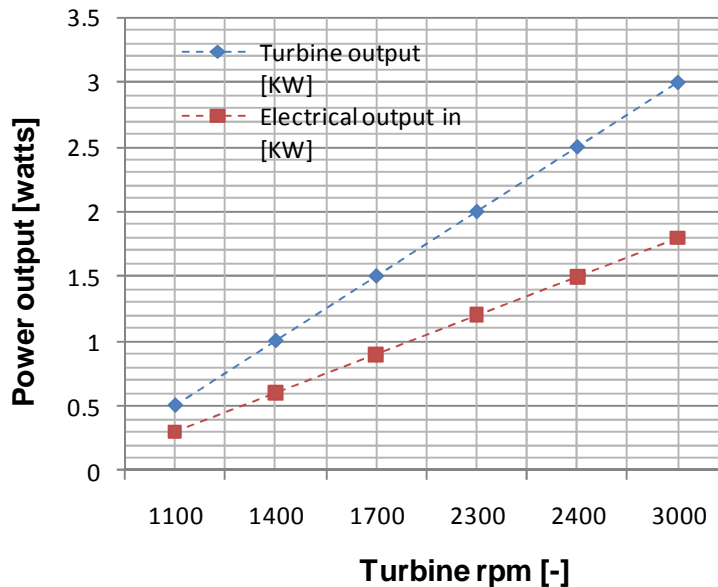
Figure 3.13: Predicted electrical output

The electrical output is based on the turbine to alternator conversion efficiency which is between 40% and 65% margin [112]. The conversion formula is;

(X / 100) * expander output.

The letter x represents the alternator conversion efficiency assumed at 50% for the 140A prestolite alternator. However, the predicted expander output remained small because of the low turbine rpm and low system output. The predicted electrical efficiency is 20% for the electric boiler and 13.9% for the biomass boiler respectively and derived by dividing the predicted electrical output by the known energy input from the boilers.

3.3 Summary

This chapter comprises a study of the basic characteristics and thermodynamic cycle analyses of an ORC system that will run with energy supplied by a biomass fired boiler though initial tests will be performed using an electric boiler. The various components that will guarantee performance of the system have been discussed; the three basic components being the turbine (expander), the pump and the heat exchanger, the later will be used as evaporator and condenser respectively. The EES Software analysis and modelling have been performed to predict the efficiencies of the system involving the Carnot and Rankine efficiencies which will be useful when the actual test are performed to evaluate performance. The various charts in this chapter depict predicted performance by following procedures in the EES software. The procedure is executed in close approximation to assumptions in the practical test. One of the basic deduction is the relationship between increasing pressure of the working fluid and the temperature at which boiling occurs. The increase in pressure will result in a simultaneous increase in temperature. There are indications that the the condenser heat sink temperature affects the cycle efficiency and the governing parameters can be optimized for a better performance of the cycle. The experimental data will also show how the system performance measures with the theoretical assumptions an expected output range of from 0.1 - 2kW. However, the heat available for hot water will also be considered for the ORC system especially asit relates to the electric boiler and the biomass boiler as well as the resultant heat sink in the condenser.

Chapter 4: Design and construction of the ORC cycle

The crucial aspect of this chapter is the consideration of constituent parts that make up the test rig and the role each of these components will play in the design and configuration of the integrated system, though the boiler and initial prime mover are either existing or provided at the inception of this work which was a constraint during the experiments. The experiment will also involve the use of organic working fluid in a low temperature Organic Rankine cycle that will convert heat to work by means of these devices. There is the prospect of the system being adapted as a potential future heat recovery system apart from the intended micro power and heat generating system. Though this is not the subject of this research will encourage the use of waste heat sources from outlets like power plants, solar thermals and geothermal plants.

4.1 System Design

The Organic Rankine cycle concept involves the use of organic fluids in a low temperature micro CHP system with an assembly of different but vital components articulated into a test rig. The major components are the expander (Turbine), the pump, the vapour generator (evaporator), a recuperator and the condenser. Other components include a receiver, which acts as reservoir for condensing working fluid and data acquisition components and other peripherals. These include various sensors such as thermocouples, pressure transducers, dc current transducer and the tachometer. The components that make up the test rig are further

discussed in this chapter. The challenge is to develop a means of exploiting biomass energy for heat and power generation through a system that operates the organic Rankine cycle (ORC) concept. The initial testing is carried out using an electric boiler. The process emphasises the conversion of heat to work with the special devices already mentioned including the use of a novel working fluid known as hydroflouroether (HFE), a working fluid that is not only environmentally friendly but with a low latent heat and high density to increase mass flow rate at the inlet of the prime mover.

4.1.1 Working Fluid

The working fluid is an environmentally friendly chemical, HFE7100, a two inseparable mixture of isomeric chemicals: methoxynonafluoroisobutane, and methoxynonafluorobutane, assessed as a single chemical entity, due to their similar boiling points and inseparable nature listed in the Australian Inventory of Chemical Substances (AICS).

The choice of the working fluid hydrofouroether (HFE) is predicated on the thermodynamic characteristics of the fluid and properties including its lower boiling temperature than water which makes the fluid useful in low temperature applications and heat recovery just like some refrigerants and hydrocarbons. The high latent heat of vaporization, density and higher molecular weight than water gives an added advantage as the later allows for more absorbtion of energy from the source in the evaporator thus reducing flow rate, size and pump. It is non-corrosive, non-flammable, non toxic with little or no effect on the ozone layer as well as on the

environment. The introduction of HFE 7000 later in the experiment is to take advantage of its lower boiling temperature which is lower than HFE 7100 so as to improve system performance. Unlike steam, HFE7100 remains dry during the expansion from high to a low pressure because of its hydrocarbon thermodynamic properties. However, a non-homogenous mixture has been observed during the tests not because of the aforementioned properties but because of increase in pressure in the cycle not supported by corresponding increases in temperature from the heat source. The boiler heat source is limited to an output of 9kW which returns temperature of $115^{o}C$ at the hot water side of the generator (evaporator). Further improvement on the system have been performed since the boiler output is fixed to extract the maximum heat energy from the heat source which included further insulation and the introduction of a recuperator at the exhaust of the prime mover designed to extract the exhaust heat in order to preheat the working fluid being pumped back to the evaporator.

4.1.2 Chemical Identity and Composition

Table 4.1 and Table 4.2 [104] describe the chemical and physical properties of HFE7100. The details of the second working fluid used in this research is discussed in chapter seven as both fluids share some similar properties but with different boiling points and both are hydrofluoroether(HFE).

Table 4.1 HFE 7100 chemical identity and composition

Chemical Name:	Mixture of methoxynonafluoroisobutane & methoxynonafluorobutane
Marketing or Other Names:	3M Cosmetic Fluid CF–61 HFE-7100 3M Brand Speciality Liquid T-6334
Molecular Weight:	250
Molecular Formula	$(C_5H_3F_9O)$ $(C_5H_3F_9O)$
Degree of purity	>99%

However, HFE7000 has a boiling point of 34^oC and will be used later in this work because of its lower boiling point than the HFE7100. This measure is to take advantage of its lower boiling point to improve system performance as the temperature of the heat carrier is limited which was a major laboratory constraint. This measure is designed to improve the average temperature of heat addition to the working fluid as well as the expander average inlet temperature.

4.1.3 Physical and Chemical Properties

HFE7100 is manufactured as a mixture of two inseparable isomers with essentially identical properties. The mixture is a clear and colourless liquid and the essential properties are indicated in Table 3.2.

Table 4.2: HFE7100 physical and chemical properties

Appearance @20ºC and 101.3 ka	clear colourless liquid
Boiling point:	58.34-58.59°C
Density:	1.5305 g/cm^3 at 20°C
Particle size:	Not applicable
Vapour pressure:	27.736 kPa at 25°C
Water solubility:	8.47 mg/L at 20°C
Partition co-efficient (n-octanol/water):	Log P_{ow} = 3.54 at 20°C
Hydrolysis as a function of pH:	$T_{1/2}$ 1 day to 1 year, at pH 4.0, 7.9, 9.9
Adsorption/desorption:	log K_{oc} 2.56 at 20°C
Dissociation constant:	Not provided
Flash point:	No flash point
Surface Tension	13.86 mN/m
Autoignition temperature:	397°C
Explosive properties:	Not explosive
Flammability limits:	Not flammable
Reactivity/stability:	Not reactive

4.1.4 Health effects

In terms of effects on health, HFE7100 is considered safe with low oral and inhalation toxicity and it is neither an eye nor skin irritant and does not sensitise the skin. It has no reproductive toxicity and does not inhibit development. HFE7100 is not classified as a hazardous chemical under the NOHSC Approved Criteria for Classifying Hazardous Substances (NOHSC, 2004) [105] and is not listed in the Australian Code for the Transport of Dangerous Goods by Road and Rail (FORS, 1998) [106].

The risk of inhalation exposure for consumers using room/air fresheners was determined from modelled data for cosmetic use, collected by the European Cosmetics and Toiletries Association (European Commission, 2003) [107]. No data were available for exposure during spraying of room/fresheners; therefore, exposure data from deodorant sprays was used in the model. The main route of exposure is inhalation, therefore, the inhalation NOAEL of 7500 ppm (76844 mg/m^3) determined from a 13-week repeat-dose inhalation toxicity study in rats exposed for 6 h per day, was chosen for the risk characterisation. Assuming 100% absorption, the average body weight of a rat as 0.35 kg and a rat respiratory rate of 0.29 m^3/day, (Derelanko, 2000) [108], the absorbed dose was determined by the equation from literature;

$$C_{inh} = \frac{Q_{prod} \times Fc_{prod}}{V_{room}}$$

where C_{inh} is the concentration in the room air, Q_{prod} the amount of product used per room, FC_{prod} the percentage of substance in the product, and V_{room} the room volume.

Inhalation exposure for the public using room air fresheners determined from modelled data was 0.1445mg/kg/d. Based on the NOAEL of 15918, the margin of exposure (MOE) was determined by the equation below;

$$I_{inh} = \frac{F_{resp} \times C_{inh} \times IH_{air} \times T_{contact} \times n}{BW}$$

where I_{inh} is the inhalatory uptake of substance, F_{resp} the respirable fraction of inhaled substance, C_{inh} is the concentration in the room air, IH_{air}, the

ventilation rate of the person, $T_{contact}$ duration of contact per event, n mean

number of events per day and BW the body weight.

Since the MOE for consumers was > 100 000, it is determined that there

is no risk of adverse health effects from this route of exposure.

4.1.5 Environmental effects

When used in specified manner in cosmetic products, the new compound

is not expected to be a risk to the aquatic or soil environmental

compartments, but will effectively contribute to a very small amount of

Australia's greenhouse gas emissions and contribute a similar range to

the global pool of short chain PFCAs. (National Industrial Chemicals

Notification and Assessment Scheme (NICNAS), July, 1990 [109].

4.2 The Boiler and Cycle setup

The heat is sourced from an existing electric boiler operating in a primary

thermodynamic hot water loop (Q_{in}) with a 9kW output capacity and

maximum operating pressure fixed at 6 bar, boiler efficiency is 85 - 90%

and the useful temperature is between 90 - 115°C hot water which is

pumped through an Alfa Laval plate heat exchanger as evaporator to

vaporise the working fluid in the secondary loop of the ORC cycle shown

in Figure 4.4. The useful temperature is however less than the critical

temperature of both working fluid of 195.3^{o}C for HFE 7100 and 165.3^{o}C

for HFE 7000. The system is comprised of a super heater in Figure 4.3

which later was discovered to be unnecessary as the boiler in Figure 4.2

could supply the required energy and then removed from the system.

Other components include an expansion vessel to check pressure surges

in the system, a hot water pump shown in Figure 4.1, thermocouples and pressure transducers to monitor the operating conditions and record data from the various tests for analysis.

Figure 4.1: Grundfos Selectric UPS 15/50 Central heating Pump photo from Test Rig.

Figure 4.2 Chromalox-Model CES-12 480V 9kW Boiler
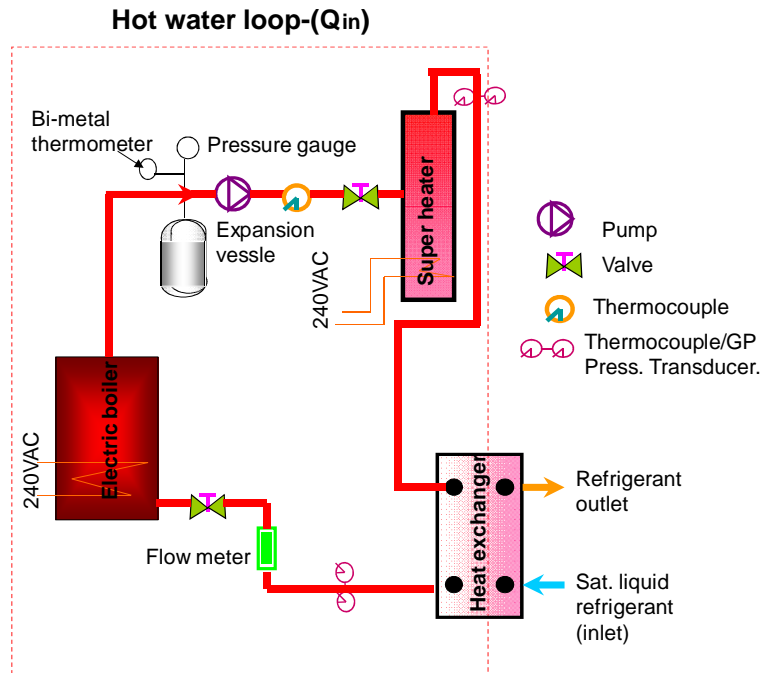
Figure 4.3: Schematics of the Primary hot water loops
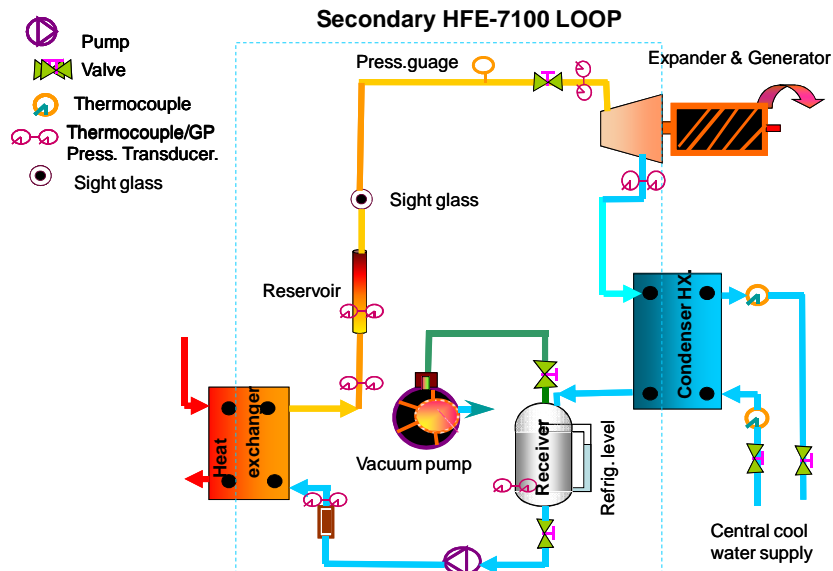
Figure 4.4: Schematics of the ORC Cycle with HFE7100 as fluid

Figure 4.4 is the configuration of the secondary loop showing the expander, heat exchanger and, reservoir which ensures that a steady supply of saturated vapour is available for the process to be continuous. Others are the sight glass, the vacuum pump to generate a vacuum condition in the cycle; the generator and the condenser are Alfa Laval brazen plate heat exchangers for generating high pressured vapour and condensing the working fluid. The combined cycle of the primary hot water loop and the secondary ORC cycle are shown in Figure 4.5. The heat energy is supplied to the secondary loop by a 9kW boiler through a compact plate heat exchanger as evaporator where the working fluid is completely vaporised by heat addition. The saturated liquid is pumped to a high pressure in the evaporator via a separate working fluid pump.

However, Figure 4.6 shows the cycle without the super heater which was removed from the system. This will as well reduce power consumption to the system.
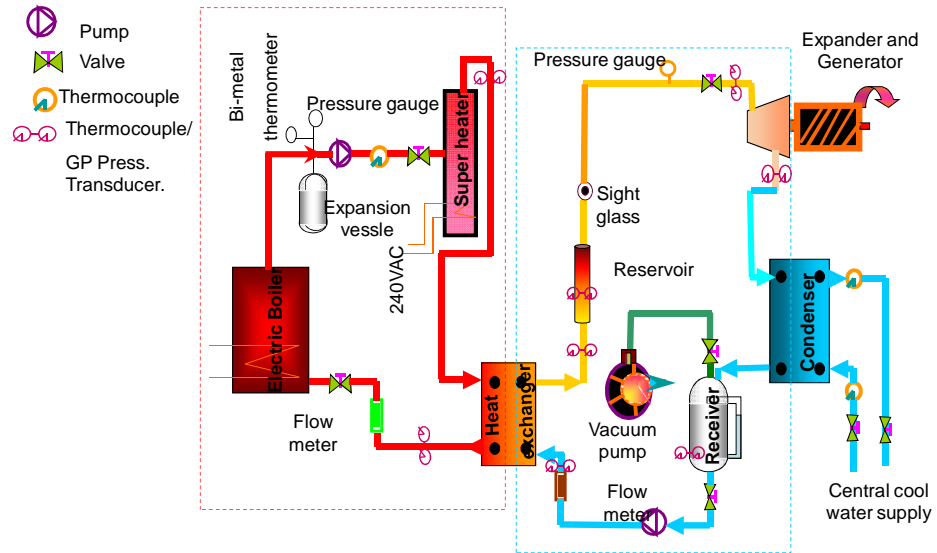
Figure 4.5: Schematic of ORC showing a combined loop
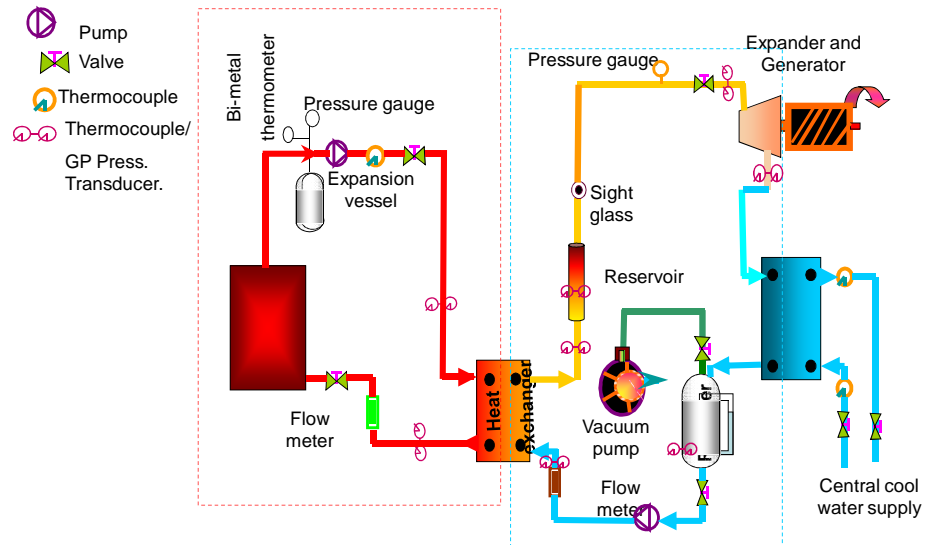
Figure 4.6 ORC Cycle showing combined loop without super heater

The cooling cycle is supplied by an existing laboratory central cooling water system and test are normally carried out when it is certain that it would not have dual usage throughout the duration of the test. The cooling
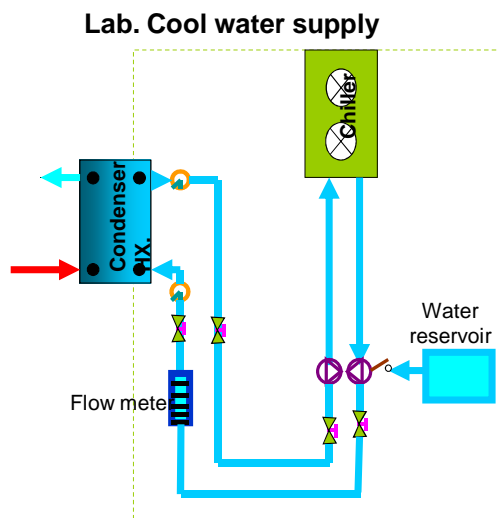
Figure 4.7; Laboratory cool water supply to Test Rig

system was later replaced by using water from the mains to allow for operational flexibility and mains fluctuations was overcome by the use of a water reservoir from where cooling water was pumped through the condenser. However, the biomass option will be employed for the next band of experimental testing to assess performance and to check various layers of the system output and system efficiencies. The experiment will use a second working fluid HFE 7000 because of its lower boiling point and latent heat of vaporisation. The system will be flushed of any residual HFE 7100 and be replaced with the HFE 7000.

4.3 The Expander

The expander is a new prototype 3kW Gast air motor, Model 6AM-FRV-5A; a sliding four-vane air compressor Figure 4.9 [110] but used here to test its resilience at higher temperatures with an environmentally friendly refrigerant HFE 7100 and HFE 7000 in an ORC CHP system that runs in an expander mode. The expander speed range is between 0 - 3000 rpm.

A low cost 650 series AC drive Eurothem 3-phase induction motor controls the gear pump speed in percentage speed incremental or reduction and allows various flow rates to be tested. The expander is fed with saturated vapour from the evaporator through the suction port and exhausted through the exit port. The closed cycle is completed when the condensed fluid is pumped to a higher pressure in the evaporator.

Figure 4.8: Eurotherm 650 Series speed control
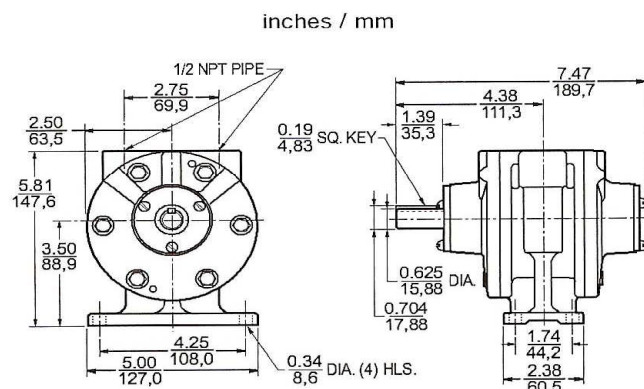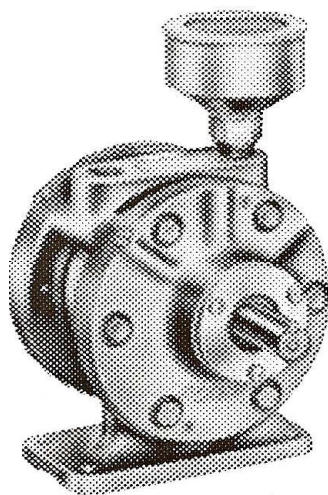
Figure 1Figure 4.9: Model 6AM-FRV-5A Gast air motor

Later, the eight vane version of the Gast expander will be used with some significant changes in the rpm but showing little difference under load conditions. The eight vane version also has a higher starting torque.

4.4 The Alternator (Electric Generator)

The alternator is the most common device that produces power in cars and various automobiles. In this study alternator will be used as power generator in the micro-power system implementing the Organic Rankine cycle. Some of the alternators shown in Figure 4.10 were liberated from auto scrap yard a suggestion that a ready supply could be harvested from this source in abundance as several automobiles are dumped each year.
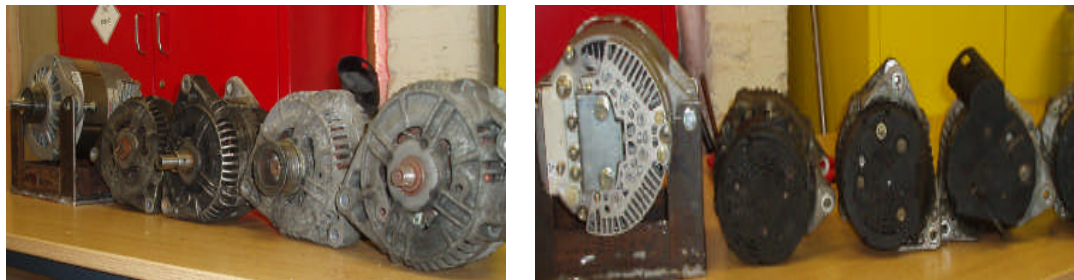
Figure 4.10: Bank of Alternators

It is however necessary to have an overview of the working principles of an alternator as to understand its use in this research. Figure 4.11, [111] shows an exploded view of a typical alternator with various components that make up the whole unit. The basic components are the housing, the stator assembly, the rotor assembly and the pulley. The rotor assembly is comprised of the shaft, the electromagnetic field coil, the slip rings concentrically mounted on the shaft which makes contact with the carbon brushes.
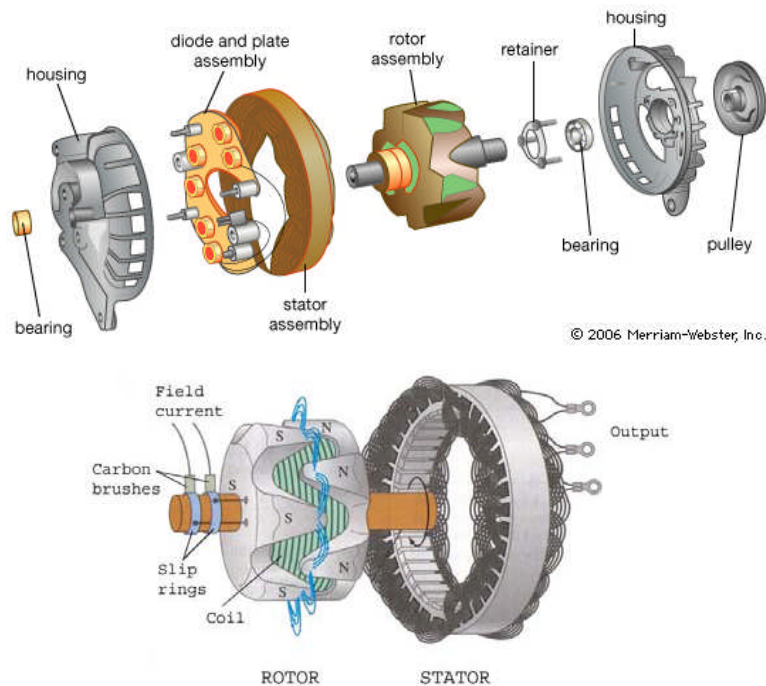
Figure 4.11: Exploded view of the Basic anatomy of an alternator

4.4.1 Working Principles

Automotive alternators are considered as three-phase generator with a built in rectifier circuit consisting of six diodes. The process involves a rotating pulley spun by the engines' crankshaft which turns a magnet past a stationary set of three-phase windings (stator) connected in a Y-configuration shown in Figure 4.12.
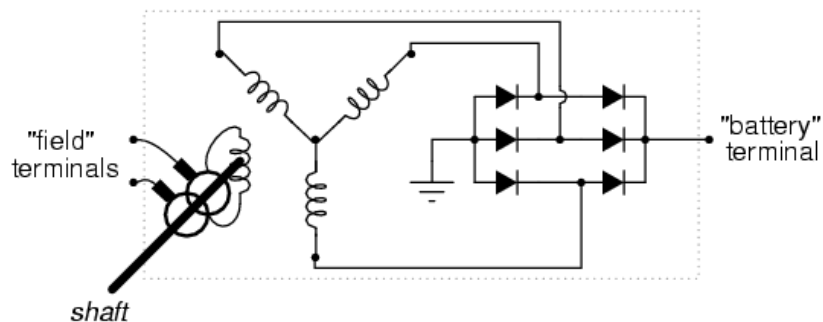
Figure 4.12: Alternator circuit diagram.

The magnet is electromagnetic and the field coil (rotor magnet coil) is energised by the battery with a small amount of electrical power input to let the alternator generate a lot of output power. A pair of slip rings conducts the power generated to the rotating field coil and the copper slip rings are concentrically mounted on the shaft and makes contact with stationary carbon brushes. Most modern alternators are equipped with in-built regulators that regulate output voltage.

D.M.Whaley et al, 2004 [112], have studied the performance of Lundell alternators using a dc machine dynamometer. The study catalogues strides aimed at improving alternator performance and over the years to improve upon the average automotive electrical requirements as indicated in Figure 4.13 [113].
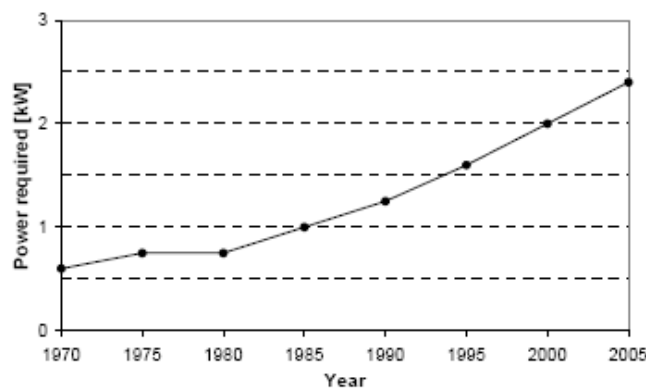
Figure 4.13: Automotive power requirements

The various test results from the study show alternator performance curves indicating dc output power with respect to the rpm in Figure 4.14 [112]. The output power and alternator efficiency as well as a summary table of alternator efficiencies in terms of output voltages are shown in both Figure 4.15 and Table 4.3 [112]. Maximum efficiency increased from

56% with internal regulators to 65% giving a significant improvement with a regulator by-pass.
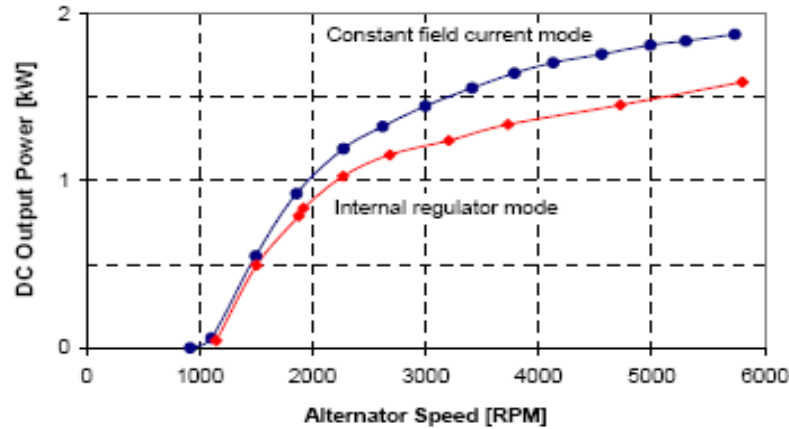
Figure 4.14: DC output power and RPM

The impact of heavy electrical load on the system causes a corresponding mechanical load on the alternator as mechanical energy is converted to electrical energy. This is usually overcome by increased rpm or torque. For low speeds or idle speeds, the output power remained unchanged about 600watts [112]. (D.M.Whaley et al).
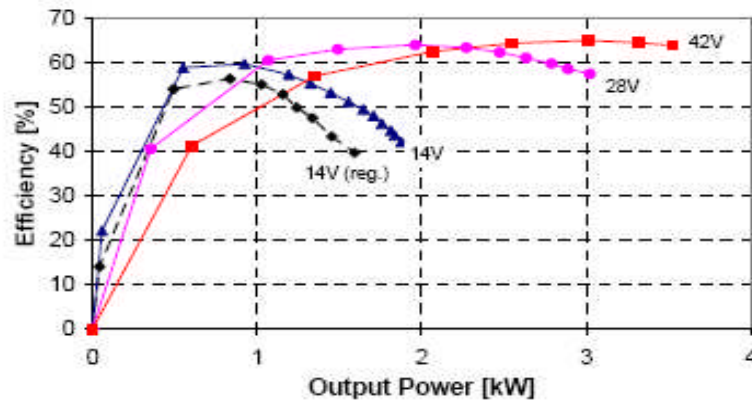
Figure 4.15: Output Power and efficiency curve

Table 4.3: Summary of alternator output voltage   and efficiencies

Output voltage [V]	Field current mode	Peak efficiency [%]
14	inbuilt regulator	56
14	constant current	60
28	constant current	64
42	constant current	65

92

The evaluatory study of the prestolite 140A alternator in Figure 4.16 [114] among some of the alternators employed in the experiment shows compliance with the aforementioned examples already discussed and will be critical in subsequent analysis of the results in this experiment.
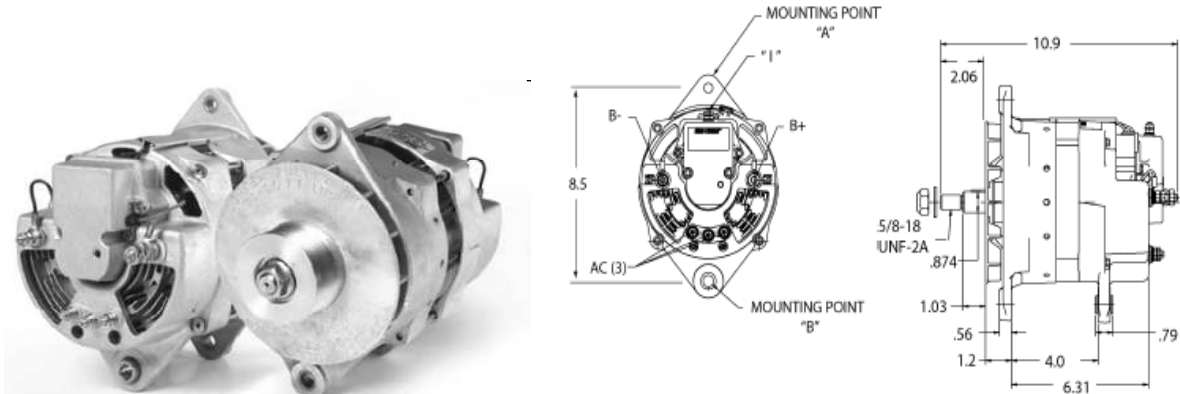
a. 140A Alternator   b. Back and side views
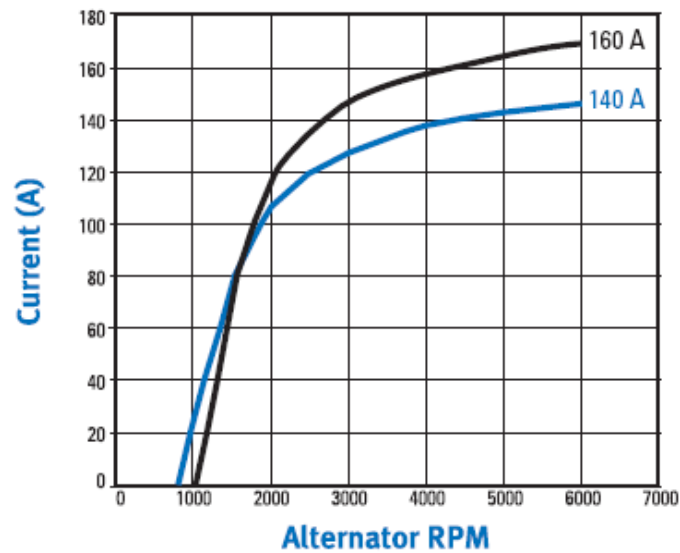
c. Alternator performance curve

Figure 4.16: Prestolite 140A alternator

Figure 4.16 also shows the various end views of the alternator and graph indicating current output based on the rpm. The graph also shows a minimum cut-in at about 800rpm for the 140A alternator. However various alternators were used in this study involving different sizes ranging in amperage between 90-200A and without much difference in their performances except for 200A size which did not perform. It should be noted that the various load tests indicate that the electrical load imposed a mechanical load on the alternator which usually results in a significant drop in the rpm of the expander. The expander rpm at this point only improves with increase in inlet pressure at the expander inlet and the electrical output significantly depends on this factor. At lower rpm the electrical output remained very small as read off the ammeter and voltmeter in Figure 4.17 and increases as the rpm increases to overcome the imposed load on the system. The rpm is usually measured with the hand held tachometer which optically measures the output rpm.
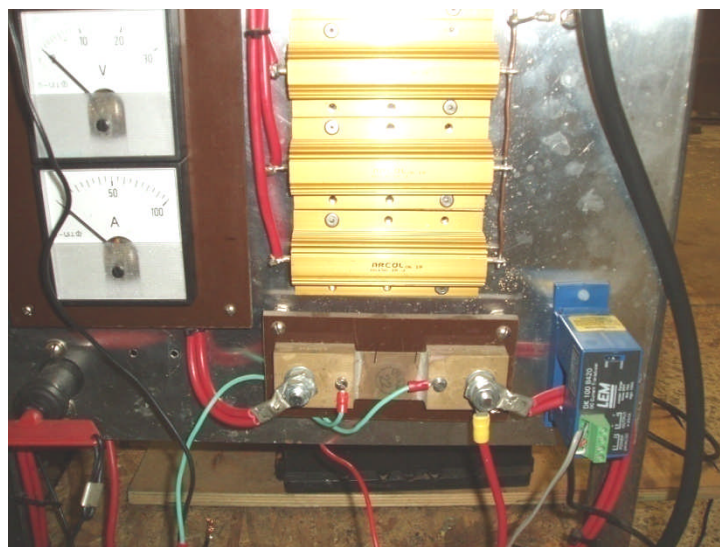
Figure 4.17: Electrical measurement devices

4.5 Pulley Configuration and Sizing

The pulley sizing is considered on the basic pulley calculation which by simple ratio increases the rpm of the secondary gear shown in Figure 4.18a and Figure 4.18b. This is simply achieved by increasing the diameter of the primary gear. The expander to alternator pulley ratios is 2:1 and 3:1. The ratios were assumed on the premise that automotive alternators do not produce much at idle speed but produce their maximum output when engine speeds are well above 2500 - 3000 rpm on average passenger vehicle and that cut-in speeds could be from 820 rpm minimum depending on the type of alternator whether heavy duty or passenger vehicle. This principle is indicated in the relations;

Ns x ds = Np x dp , Ns – rpm of secondary gear

dp – diameter of primary gear

ds – diameter of secondary gear

Np – diameter of the primary gear

when Np > Ns – the speed of the secondary will be faster than that of the primary;

when Ns > Np- the speed of the secondary will be slower than the speed of the primary and the relations can further be expressed as;

a/b = c/d,

also   ad = bc,

hence   a = bc/d, thus any of the unknown values can be calculated from the known, therefore;

Ns = Np*dp/ds
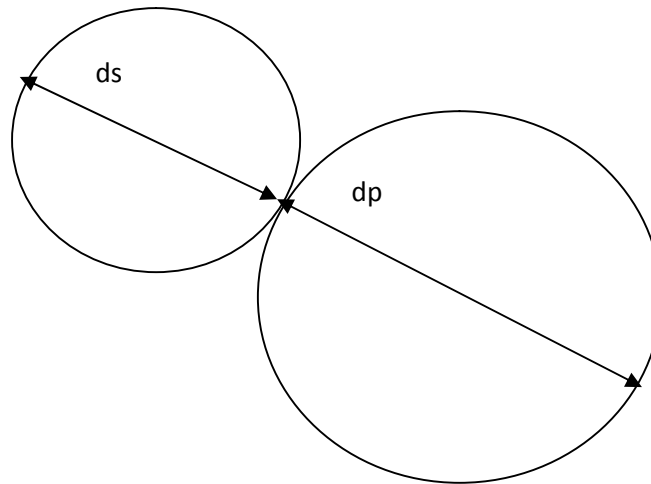
Figure 4.18a: Schematics of the Primary and secondary pulley

Figure 4.18b: Photograph of the Primary and Secondary Pulleys

4.6 Measurement Devices

The measurement devices simply enable data acquisition from different state points and sensors strategically positioned to capture useful operational data. This offers the opportunity to determine system performance and to understand the workings of the system with respect to predictions.

4.6.1 Data Taker

The data taker used is the DT500 series shown in Figure 4.19 [115] and data acquisition is normally defined as the regular collection of data which by implication involves the scanning of sensors, making of instantaneous measurements and transferring such to a recorder or a computer.
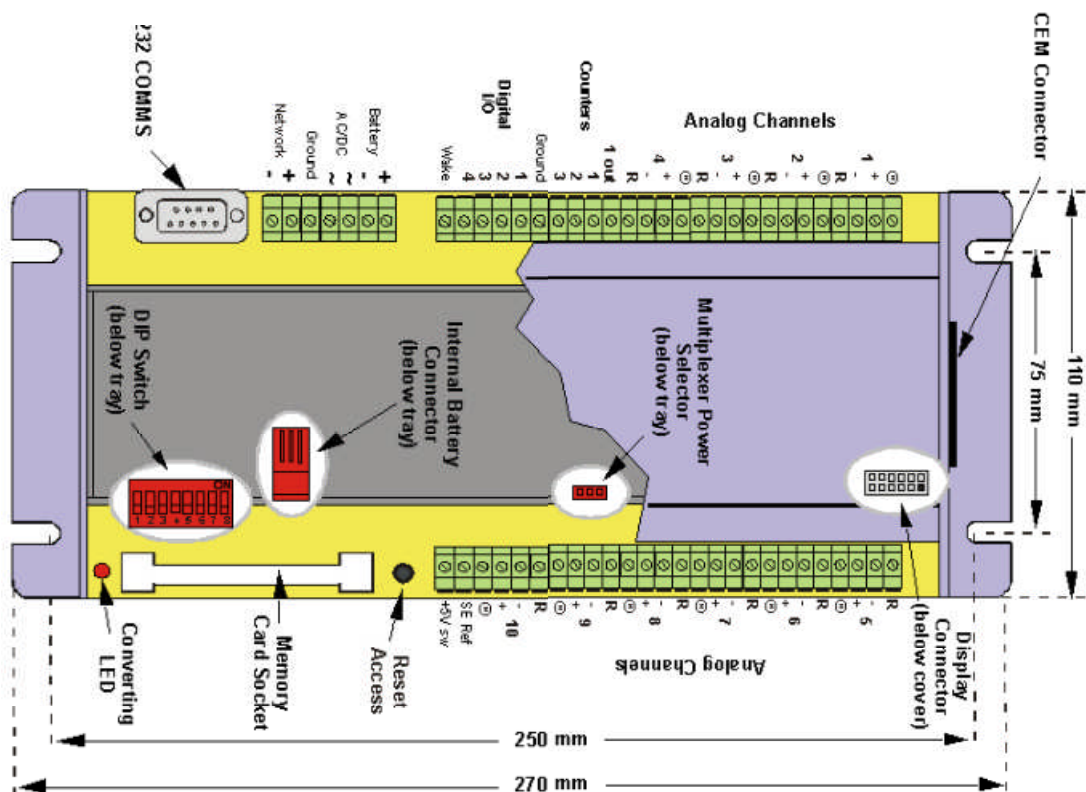
Figure 4.19: Basic diagram of DT500 series data taker

This data acquisition device combines data acquisition and data logging, the later involving the total operation of getting data and making a permanent record of it on a computer's hard disk or in electronic memory as well as acquiring data from sensors connected to it indicated as in Figure 4.20. Measurements are converted according to requirements i.e. voltage to ^{o}C or ^{o}F or carry out calculations on measurements, averages, standard deviation and also determines maximum or minimum values of measurements. These are usually displayed on the computer screen and data are returned in real time.

Figure 4.20: Data taker and Computer monitoring system

The data taker supports many types of inputs among which are;

Voltage

Resistance

Current (4-20Ma loops)

Thermocouples (Temperature)

Thermistors

Frequencies

Pressure sensors

Flow sensors

Time and Counts

The essential data are collated based on the relevant choice input which in this instance will cover voltage, temperature current and pressure.

4.6.2 One Memory Optical Tachometer

This single memory tachometer shown in Figure 4.21 is composed of an integrated optical transmitter and receiver at the top of the unit and a mechanical contact assembly at the base of the unit. The optical window is normally beamed at the rotating or spun object to read the rpm of the spinning object. A flashy strip that is normal to the optical rays helps to a great degree in registering accurate readings as the projected ray is reflected backwards.

Figure 4.21: Single memory optical tachometer

The 5-digit LCD automatically inverts when switched from optical to contact mode so that the display is always the right way up when viewed. The table of specifications and accuracy range are given in Table 4.4.

Table 4.4: Technical specification of optical tachometer

Technical specification of optical tachometer	
Measurement range	5 to 99999rpm (optical)
	0.5 to 19999rpm (contact)
Resolution	0.1rpm
Accuracy	$\pm$0.05% +1 digit (dependent on ambient light conditions)
Sensing range	50 to 150mm
Overall dimensions	215 x 65 x38mm (H x W x D)
Battery	4 x AA Cells (not supplied)

Battery must be changed after a prolonged use

4.6.3 DK current transducer

The current transducer used is a DK current transducer, a 100A,

4-20mA output range shown in Figure 4.22 (A & B) and this enables the

reading of the alternator output current which is transmitted through the

data acquisition device, the Data logger 500 series.
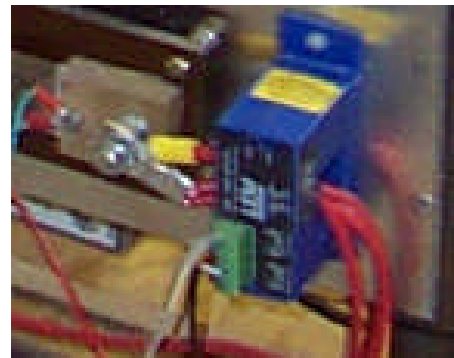
A. DK Current Transducer   B. DK transducer as Installed on Rig

Figure 4.22: 100A, 4-20mA DK Current Transducer

The current transducer is normally employed to measure current passing

through the split core as shown in Figure 4.2b and Figure 4.3 [116].
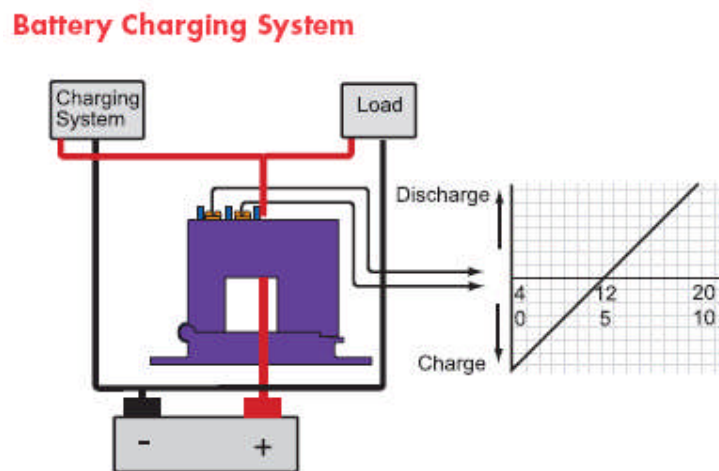
Figure 4.3: Sensor diagram and Battery charging loop

The current carrying cable is passed through the split core of the transducer to measure the value of current passing through it. Table 4.5 and Table 4.6 indicate the technical specification and attributes of the current transducer which has the capability of sensing dc current.

Table 4.5: Technical specification of DK current transducer.

Current type sensed	Isolation Test Voltage (Vac)	Max. Current Consumption (mA)	Linearity (%)
dc	3000	100	±0.75

Description: Transducer, 100 dc, 4-20Ma.

Table 4.6: Attributes of a DK Current Transducer

Attributes	
Category	Current Transducers
Supply Voltage	20 to 50 Vdc; 22 to 38Vac
Analogue Output Signal	4 to20mA
Load Resistance	650 Ω
Primary Nominal Current	100A
Accuracy of Reading	±1%
Current Type	dc
Depth	89.7mm
Height	57.2mm
Isolation Test Voltage	3000 Vac
Maximum Current Consumption	100mA
Operating Temperature Range	-20 to +50°C
Response Time	<100ms
Weight	120g
Width	30mm

4.6.4 GP pressure transmitter

The GP pressure transmitter is a multipurpose, high performance stainless steel 0-100Mv output transducer transmitting at 4-20mA output range. The pressure range is 0 - 10bar. It is a temperature compensated strain gauge technology with a +/- 0.25% accuracy full scale. Figure 4.24a and Figure 4.24b shows both GP pressure transducer and the mode of installation on the test rig with the extension output cable to the data logger.

(a). GP Pressure Transducer   (b). Photo of Installation on the Rig
Figure 4.24: Photo of Pressure Transducer installations on test rig.

Table 4.7: Attributes of the Pressure Transducer

Attributes	
Category	Pressure Sensors
Proof Pressure	2 x Range (x5 Burst Pressure)
Analogue Output	4 to 20mA
Supply Voltage	12 to 36Vdc • 0-5V output(Transducers) • -40 to +100/125°C transmitter/transducer range • 2x rated overpressure up to 250mbar

Description: General purpose pressure Transducer, 0-10 bar,4-20mA

4.6.5 Thermocouple Probe

The thermocouple probes used are the T- type coleparmer pipe plug probes 1/4"NPT male; 0.5"L, in Figure 4.25 and Figure 4.26 [117], which are composed of two dissimilar metals, joined to produce a voltage when the applied (measured) temperature differs from the reference temperature

Figure 2Figure 4.25: Pipe Plug probe

Table 4.8: Thermocouple specifications

Type	T
Temp range	-418 to 700°F (-250 to 371°C)
Probe length	1/4"
Diameter	0.25"
Cable length	5 ft
Sheath material	316 SS
Connections	miniconnector
Junction	grounded
Time constant	6 sec
Response time	30 sec

The T-type has the tolerance of class 1, which is a tolerance over the absolute temperature by thermocouple with $0^{o}C$ reference.

The $0^{o}C$ reference is given by an ice bath, where accuracy is evaluated to 0.05k (Ngendakumana et al, 2006) [110]. The wire material is made from copper and constantan with a sensitivity of $-43\mu V/^{o}C$.
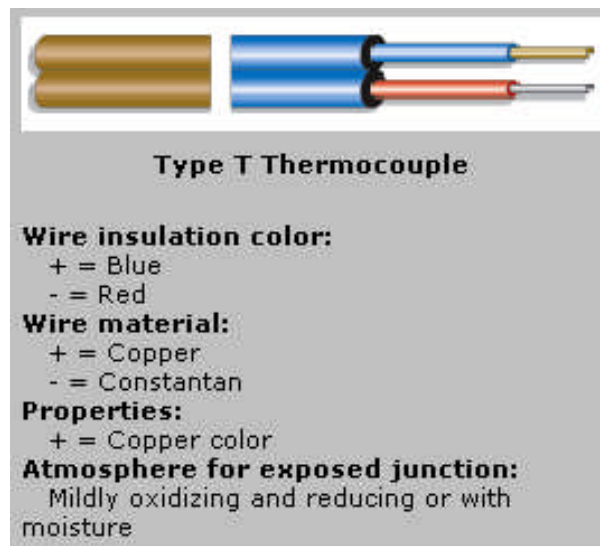
Figure 4.26: Physical Characteristics of Thermocouples

4.7 Heat Exchangers

Heat exchangers are designed to achieve better efficiencies by maximizing the surface area of the wall between the two fluids as resistance to fluid flow through the heat exchanger is minimized. Most heat exchangers are classified according to their flow pattern. The two flow arrangements are the parallel flow and the counter-flow heat exchangers shown in Figure 4.27 [118].
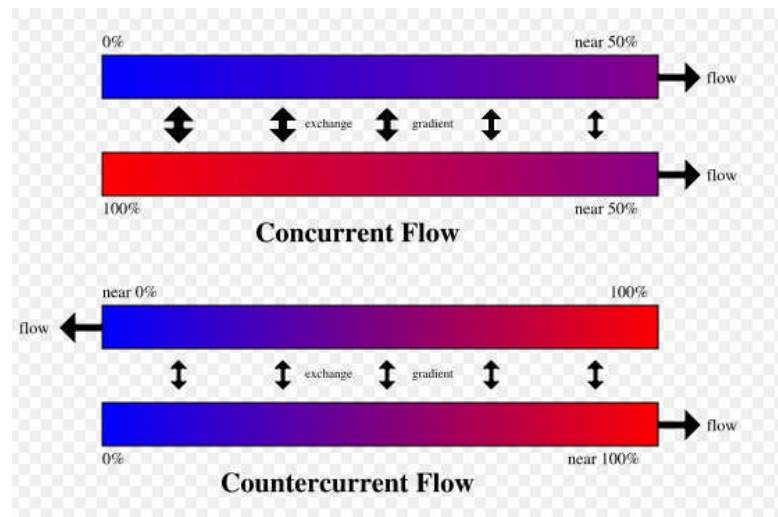
Figure 4.27: The schematic flow diagram of heat exchangers
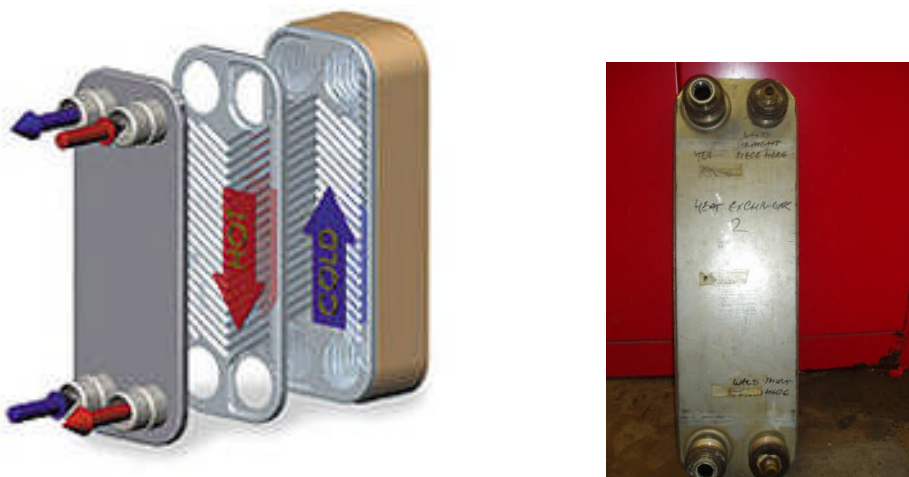
Figure 4.28: Counter flow flat plate heat exchanger

For the parallel flow heat exchangers, the two fluids enter at the same end and, while in counter flow heat exchangers the fluids enters from opposite directions as indicated in Figure 4.28 and is presumed to be the most efficient as it can transfer most of the heat. The performance of heat exchangers can be varied by addition of fins which increases the surface area thus channelling fluid flow or create turbulence. The mean temperature can be defined but driving temperature across the heat transfer surface varies with position.

The LMTD (log mean temperature difference) is used to determine the heat transfer in the flow system. This is translated to mean the logarithmic average temperature difference between the hot and cold streams at each end of the heat exchanger and the mathematical relations for the counter flow has been derived from literature [118];

the formula for counter flow is [118];

$$LMTD = \frac{(T_1 - t_2) - (T_2 - t_1)}{\ln \frac{(T_1 - t_2)}{(T_2 - t_1)}}$$

And parallel flow is;

$$LMTD = \frac{(T_1 - t_1) - (T_2 - t_2)}{\ln \frac{(T_1 - t_1)}{(T_2 - t_2)}}$$

T_1 = Hot stream inlet temperature

T_3 = Hot stream outlet temperature

t_1 = Cold stream inlet temperature

t_2 = Cold stream outlet temperature

Heat transfer is dependent on the value of LMTD, the larger the LMTD, the more heat is transferred. The materials used in making the plate heat exchangers are corrugated plate gasketed or brazed together and are very compact thus achieving larger surface areas, as indicated in Figure 4.29 [100] with some basic specifications shown in Table 4.9 [119]
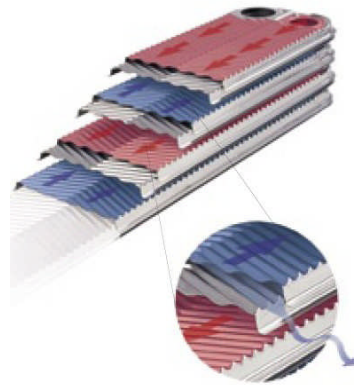
Figure 4.29: Brazed plate heat exchanger

The most important characteristics and the most significant parameter is the chevron angle which corresponds to the angle on the plate. The angle is associated with the heat exchange coefficient and pressure drop.

Two main heat exchangers were employed in this study all products of Alfa Laval and SWEP; one as an evaporator and the other as the condenser. The condenser was later substituted with another Alfa Laval
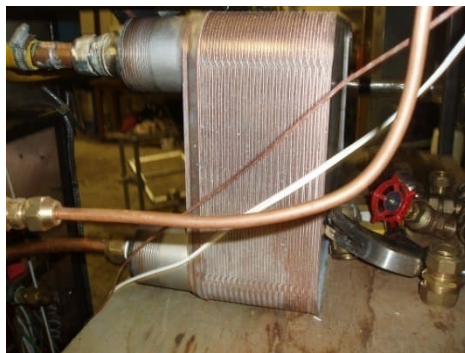
A. Photograph of the evaporator   **B. Photograph of condenser**
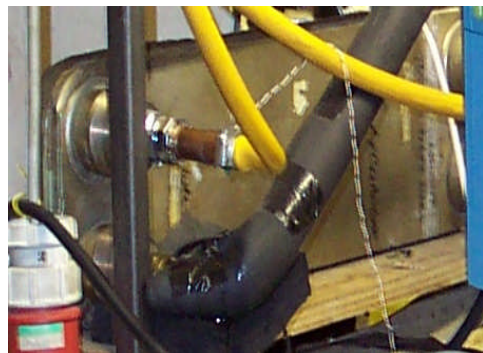
CB76   **CB26**

C. Photograph of substituted Condenser

Figure 4.31: Photograph of the heat exchangers

Table 4.9: The physical parameters of both heat exchangers; CB26 and CB76 used in the experiment.

	CB14	CB26	CB27	CB51	CB52	CB76	CB77
Min. working temperature **)	−160°C	−160°C	−160°C	−160°C	−160°C	−160°C	−160°C
Max. working temperature **)	175°C	175°C	175°C	175°C	175°C	175°C	175°C
Min. working pressure **)	Vacuum	Vacuum	Vacuum	Vacuum	Vacuum	Vacuum	Vacuum
Max. working pressure, S3S4/S1S2 **)	32 bar	32 bar	32 bar	32 bar	32 bar	A,E,H: 32 bar L,M: 25 bar	25/16 bar
Volume pr. channel, litres	0.02	0.05	0.05	0.095	0.095	A: 0.18/0.25 E: 0.18/0.18 C,M,H: 0.25/0.25	0.25
Max. flowrate, S3S4/S1S2. *)	3.6 m³/h	8.1 m³/h	8.1/12.7 m³/h	8.1 m³/h	8.1/12.7 m³/h	39 m³/h	39/63 m³/h
Standard number of plates H,M,L	14,20, 30,40	10,18,24, 34,50, 70,100	10,18,24, 34,50,70 100,120	10,20, 30,40, 50,60	10-100 (10,20,...)	20-150 (20,30,...)	20-150 (20,30,...)

*) Water at 5 m/s (connection velocity) **) According to European pressure vessel Directive (PED) (CE-Approval)

heat exchanger for want of improved heat sink because of larger heat transfer surface area. The heat exchanger operates by continual transfer of heat from one medium to another and by the natural law of physics allows the driving energy in a system to flow until equilibrium is achieved. This is sustained as long as there is temperature difference in the system as heat leaves the warmer body to the cold medium and as heat lost by

the former is equal to heat gained by the later. The heat load of a given system can be determined by;

$P = m \times c_p \times \Delta t$, and can also be determined by using the inlet and outlet enthalpies of the heat exchangers and multiplying the enthalpy difference by the mass flow rate with the unit in kW. This is represented as;

$P = m \times (h_i - h_e)$.

The specification of the compact heat exchangers is shown in Table 4.10;

Table 4.10: Compact heat exchanger Type and Specification

Model/Type	Alfa Laval (CB76)	SWEP (B120)	SWEP (B25)	SWEP (B15)
Description				
No. of plates	28	30	40	60
Dimension (mm)	93x120x190	80x115x525	106x240x520	155x240x520
Total volume (l)	3.5	1.55	4.5	6.989
Working Temp. [^{o}C]	225	185	225	225
" Pressure (bar)	30	30	27	27
Area (m^2)	0.64	1.81	4.99	7.49

The overall heat transfer coefficient of plate heat exchangers is between 6000 - 8000 W/m^2 ^{o}C. The flow rate is between 0.05 kg/s - 1000 kg/s. The heat transfer efficiency will depend on the thermodynamic properties of the working fluid and any given flow rate putting into account the pressure and temperature limits. The mean temperature efficiency is indicated by,

$$\eta_h = \frac{T_{h\,inlet} - T_{h\,outlet}}{T_{h\,inlet} - T_{c\,outlet}} \times 100 \qquad (3.1)$$

$$\eta_c = \frac{T_{c\,outlet} - T_{c\,inlet}}{T_{h\,inlet} - T_{c\,inlet}} \times 100 \qquad (3.2)$$

$$\eta_m = \frac{\eta_h + \eta_c}{2} \qquad\qquad\qquad (3.3)$$

3.8 Summary

The performance characteristics and technical attributes of each of the components that makeup the system is a very vital factor as to how each component relates to another and the target achievable by operating the system. The study of the components makes for a better understanding and visualization of how the system will perform as an integrated system. The specifications and assumptions of some of the major components is shown in Table 4.11. The area of specific interest is the selection and the

Table 4.11 Specifications and assumptions of key components

Components	output [kW]	T [C]	P [bar]	Efficiency [%]
Biomass boiler	25	95	3	85-90
Electric boiler	9	115	6	85-95
Turbine	3	120	7	20

properties of the working fluid HFE 7100 and HFE 7000 which are environmental friendly working fluid that does not pose any health hazards during use or to the environment. Their low boiling point at 61^oC and 34^oC respectively, molecular weight and latent heat of vaporization were considered an advantage. The critical temperature of the working fluids is also of significance at 195^oC for HFE 7100 and 165.3^oC for HFE 7000 meaning that heat transfer temperature can be brought close to the critical temperature and pressure without exceeding rated value and thus avoids

substance decomposition. The choice of the boiler which is the heat carrier was based on an existing electric boiler in the test laboratory which had some limitations because the experiment could not go beyond its output capacity and therefore had to be used by introducing measures that improves the process of heat addition. A biomass boiler will later replace the electric boiler in the main test involving biomass heat source.

The prime mover consideration was based on a low cost, light weight and maintenance free multivane Gast Air motor, used as expander or turbine and this is combined with the electricity generator which is an automotive alternator. This approach is a novel attempt in finding substitute micro Turbines as alternatives to conventional turbines. They can be acquired very cheaply and put into meaningful use in a manner that does not pollute the environment. Other major components and measurement devices including an evaluatory study of the heat exchanger have been undertaken in this chapter to further broaden the understanding of their operational modes and working parameters.

CHAPTER 5: Prime mover Consideration

A Rotorvane compressor was available at the beginning of this work and this chapter involves the study and consideration of vane expanders and the key motivation for the choice of the Gast air motor as the prime mover. One of the factors is ability to perform in a low temperature Organic Rankine-cycle as micro turbine instead of using conventional turbines. This study will consider among other things, the necessary parameters for configuring the expander to work with other components in the system as well as the modifications required to achieve performance. The geometrical characteristics of the expander will also be discussed in this chapter.

5.1 Background

Generally expanders do better than conventional turbines involving the use of low-grade heat or low temperature heat sources [6]. The key characteristic of vane expanders is that they are lightweight, cheap and requires little maintenance. Heat transfer losses in a multi-vane expander (MVE) or prime mover in a low temperature or low grade energy Rankine-cycle engine have minor effects on the expander's performance and moreover can be partially compensated by energy dissipated due to friction [123].

In the early 1800's, Lemielle exhauster, the very first types of vane machines was invented in France and widely used in Belgium to provide ventilation for Collieries. Rotating drums had the vanes hinged and mounted on their surfaces and the drums eccentrically mounted within a

casing. Modern day Sliding Vanes shown in, Figure 5.1 [120] dates back to the early 1900's when an American, Robert Blackmer invented the first rotary vane pump. The oil injected version came along in the late 1920's by an Italian, Pneumofore Spa and then followed a range of varieties and diverse models articulated by manufacturers across the globe. Towards the end of 1940's in the UK, Major P. C. Bird patented a new type of lubricated vane compressor "The Oil Vane"
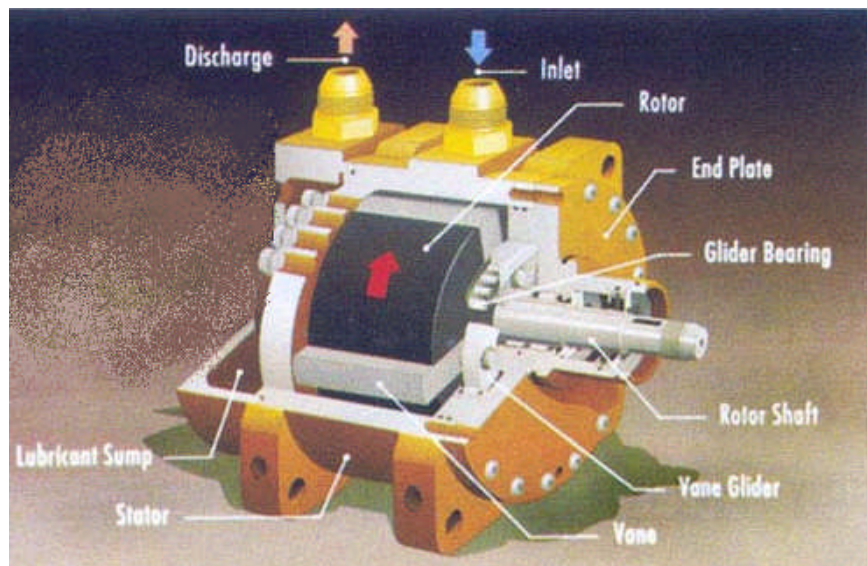
Figure 5.1: Isometric view of a typical Vane Compressor
Source: http://www.hvacindia.org.in/journal 2001.apr

Having acquired an exclusive right from Major Bird, Alfred Ballows came up with the first hydro vane compressor which was indicative of technological strides during that period. However, vane compressors are classified into two main categories;

- Dry type Vane Compressor
- Lubricated type Vane Compressor

These had distinctive characteristics, the former able to operate at low pressure because of extremely high temperature and the later is the drip type or oil flooded. The major attraction for vane compressors is that of being a viable alternative to conventional turbines in low grade heat applications as single stage expanders. Their mechanisms are simple coupled with the fact that they are easy to maintain and lightweight devices. The operational characteristics of compressors can further be classified into two broad operational spectrums; the intermittent flow compressors and the continuous flow compressors. The operational mode of the intermittent flow compressor is cyclic in nature in that specific quantity of gas is ingested by the compressor, thus producing work and then discharged before the repeat of the cycle. The compressors using intermittent flow mode are referred to as positive displacement compressors. There are also subdivided into two categories, the reciprocating and the rotary compressors in Figure 5.2 and Figure 5.5.

 The flow pattern in the continuous flow compressor will have the gas moved into the compressor acted upon and moved through the compressor and discharged without interrupting of the flow stream at any time in the process. They are marked by two main types; the dynamic machines and the ejector. The ejector does not involve mechanical action. Both classes of compressors have further subdivisions that are indicated in the chart shown in Figure 5.2. The example for the reciprocating machine is the mechanical piston, shown in Figure 5.3, while the rotary will include the liquid piston, the helical and straight lobe in Figure 5.4 and Figure 5.5 and the sliding vane compressor similar to

that used in this research is indicated in Figure 5.6. The dynamic machine is made up of the radial (centrifugal), the mixed and axial flow types as indicted in the chart in Figure 5.2.
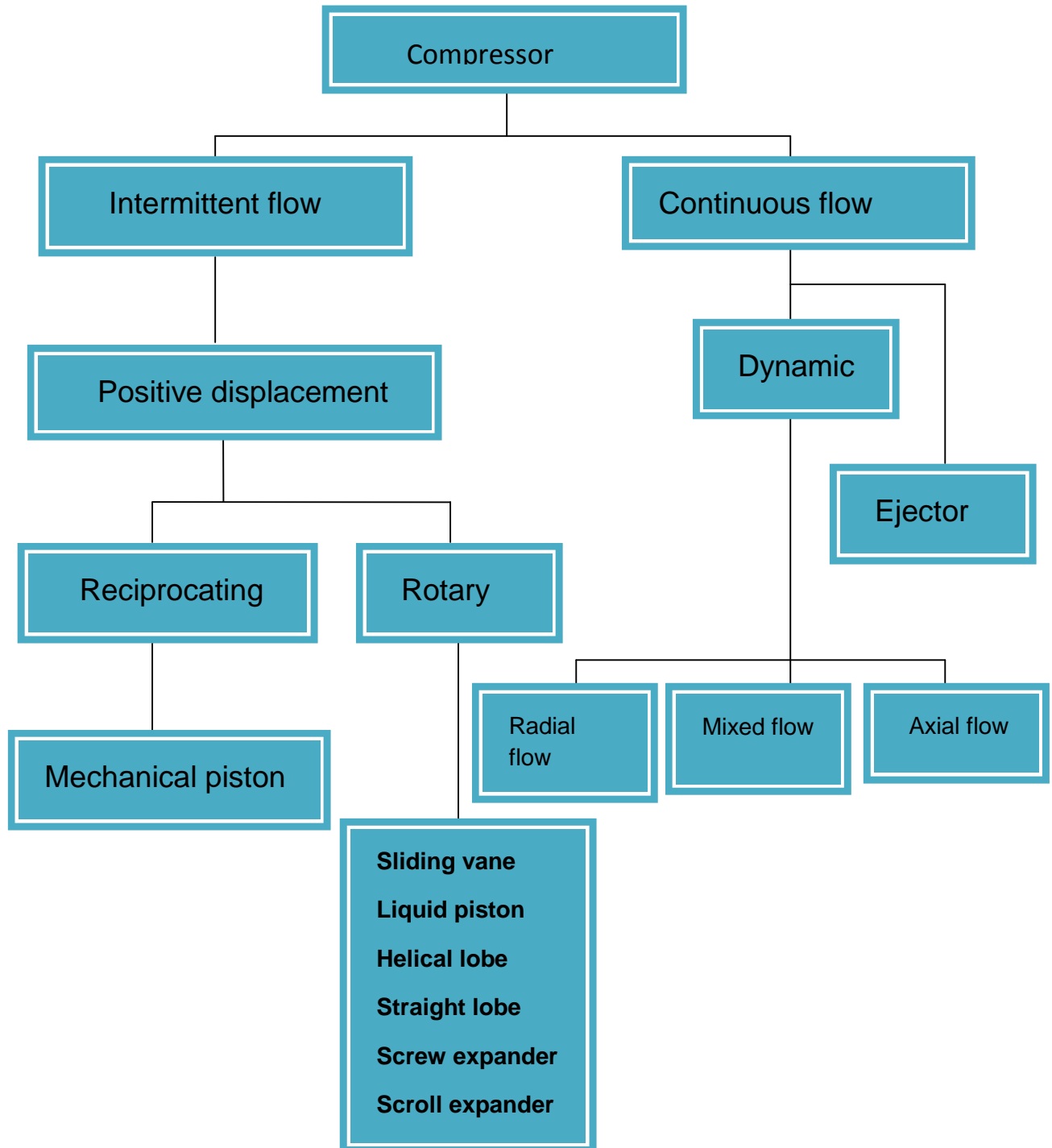
Figure 5.2: Types of Compressor
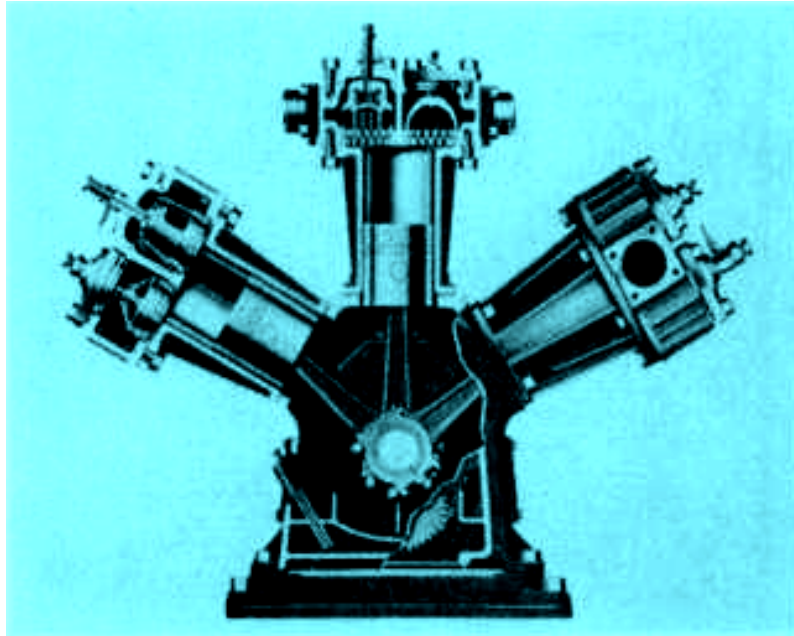
Figure 5.3: A three-stage-single acting reciprocating compressor (Courtesy of Ingersoll Rand)
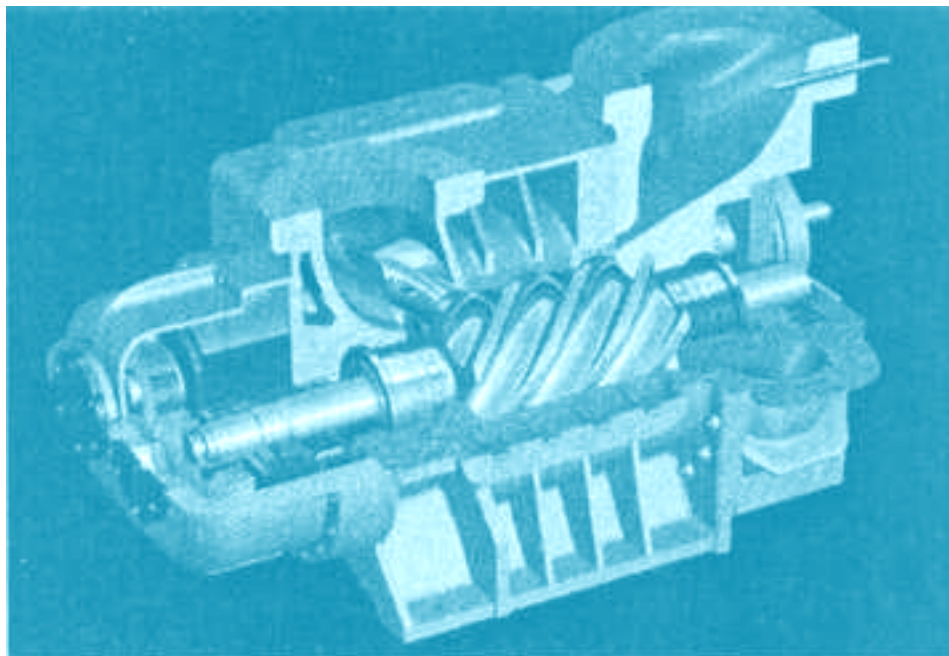
Figure 5.4: A section through an oil-free helical-lobe compressor

(Courtesy of A.C Compressor Corporation)
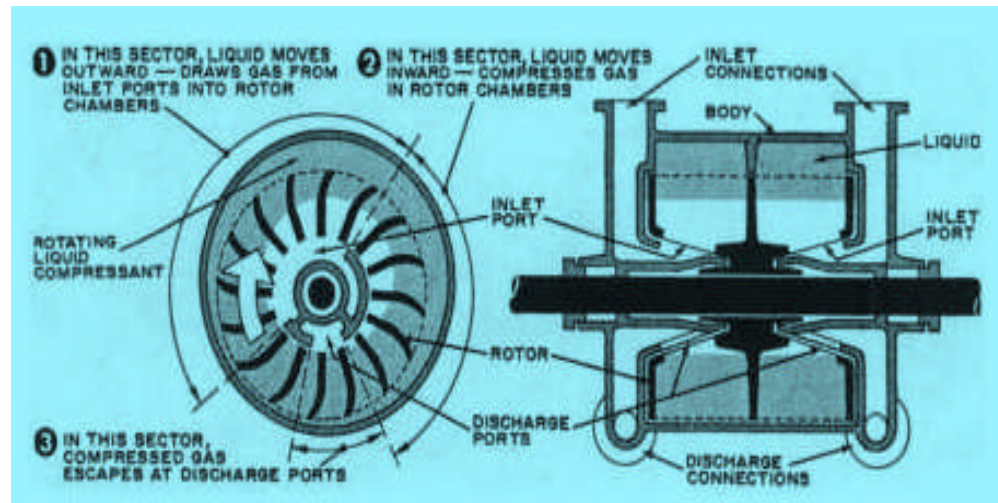
Figure 5.5: A sectional and end view of a liquid piston compressor. (Courtesy of Nash Engineering Co.)
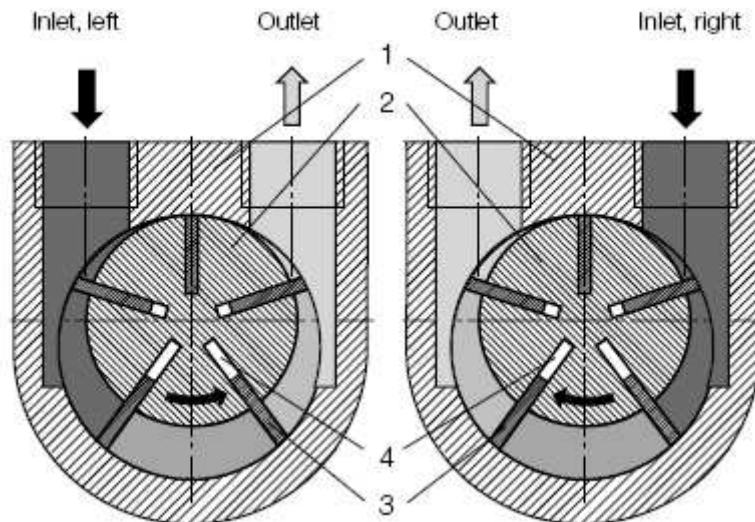
Figure 5.6: A cross section of a sliding vane compressor

1-Rotor cylinder, **2**-Rotor, **3**-vanes, **4**-Spring, **5**-End piece with bearing

 5.2 Geometry and Theoretical study of multi-vane expander

The geometry and basic description of the Vane expander is the key to understanding its operational mode and characteristic anatomy. Because of the simple design structure, it does not require electricity to operate when compared to an electric motor and the fact that it is low cost as well as being quite easy to maintain.

5.2.1 Geometric description

The sliding vane expander geometry consists of a singular rotor seated eccentrically in a cylinder or stationery housing with a cylindrical cavity slightly larger than the rotor in such a way that it almost makes contact with the cylinder wall. The rotor has series of radial slots milled into the rotor that hold a set of more than one vane or more which are free to move within the rotor slots. They are spun to make contact with the cylindrical wall by the centrifugal force generated by the spinning rotor. A crescent shaped cell is formed between the peripheral surface of the rotor and the internal cylinder wall thus describing the working chamber interspaced by pairs of vanes as shown in Figure 5.7 [126]. The crescent shape between two vanes constitutes a cell or cell volume allowing for the
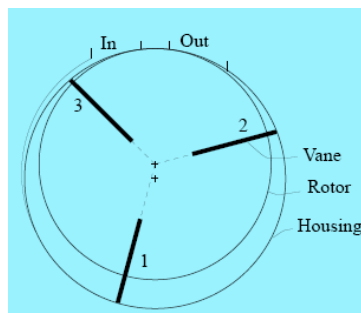
Figure 5.7: Simple geometry showing rotational sequence

working fluid to be moved and compressed circumferentially as the vane pair moves towards the discharge port. However pressure ratios and port location counts for efficient compression to occur. The compression cycle diagram Figure 5.8 [121], is indicative of the fact that if port optimized ratio is P_2/P_1 then the compression line from 1 - 2 will be a smooth curve. If the port cut pressure is lower than the external pressure ratio i.e. $P_0/P_1 > P_2/P_1$, or the port cut pressure is higher than the external pressure ratio so that $P_U/P_1 < P_2/P_1$ two things are likely to occur; when the port opens at point 2, the discharged gas in the former will return to the expander from the line requiring extra energy to do so as shown by shaded portion
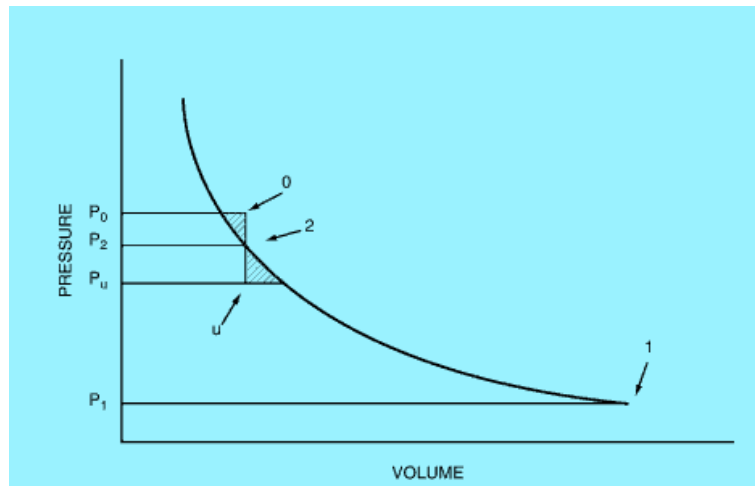
Figure 5.8: Pressure-Volume diagram of the compression cycle of sliding vane expander

left of line 0 - 2 assumed to be wasted energy, but if the later is the case, then gas over compression will occur at point 2 when the port opens to expand to point u and lost energy represented by shaded portion right of line u - 2 [121].

The displaced capacity per revolution or swept volume of a multivane expander can be determined if the geometric information is available such as the rotor diameter, the bore, the cylinder length and the vane thickness as well the number of vanes in each case. However geometric information and data does not unfortunately come with the vendor catalogue data or when it does, may be too scanty or insufficient to be reasonable for required measurements to be extracted. However measurements can be taken where reused or discarded units are available. The displaced volume per revolution Q_r, can be estimated by the equation [121],

$$Q_r = 2eL \ (\pi D - ms) \qquad\qquad (5.1\}$$
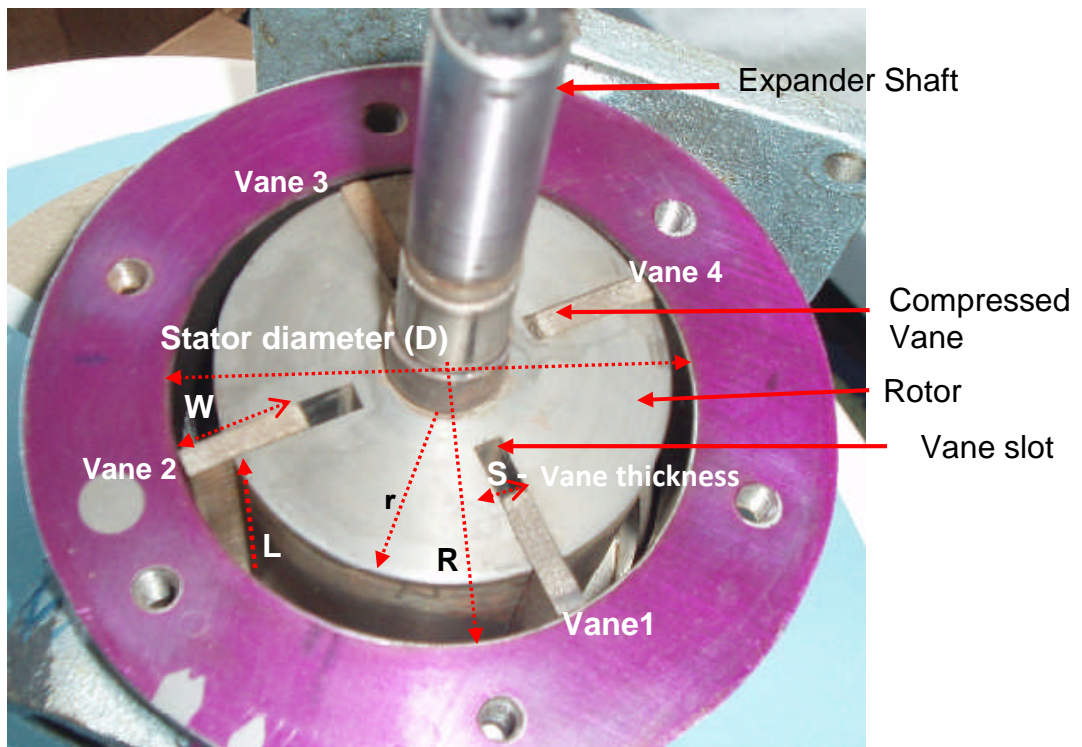
Figure 4.9: Photo of the structure of the Gast expander indicating Vane positions and actual measurements

Figure 5.9 indicates a close shot of the internal structure of the Gast expander used in this study which was dissembled and actual measurements taken showing all the vanes, the stator cylinder and the rotor. There are four basic vanes numbered 1- 4 positioned in their slots. The vanes 1 and 2 are shown in an extended position projected against the cylinder wall creating a cell or cell volume. There are other cells also generated between the vanes. Cells 2 and 3 as well as 2 and 4 joins to form a crescent shape diminished towards the compression zone between vanes 3 and 4. The six circular openings are for bolting the end plates. The purple colour membrane is a seal. The shaft diameter is 16mm (5/8'') and positioned at the centre of the rotor forming an offset with the centre of the stator cylinder.
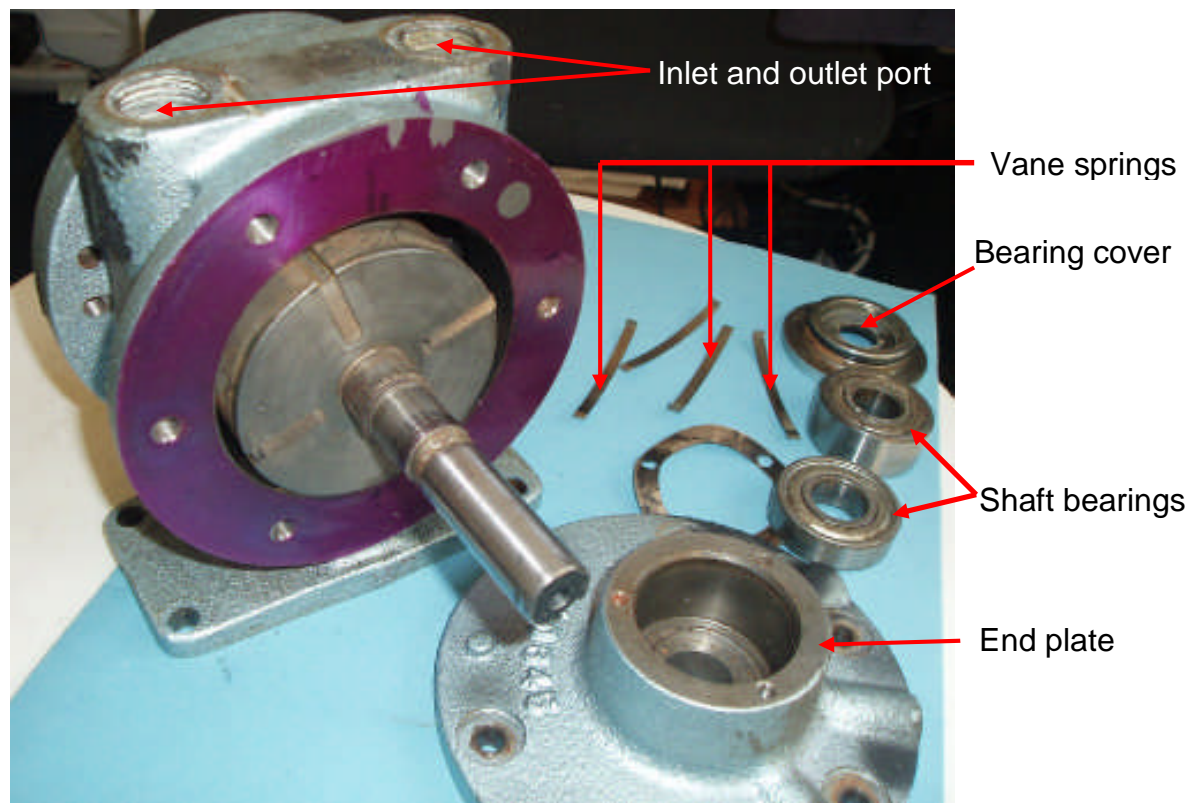
Figure 5.10: Photo of various components of the Gast expander

This offset is very crucial in the normal operation of the prime mover and a

critical factor in its operations. The measurements

from Figure 5.9, are represented by letters D, L, r, R, s, W and measured

in mm and Figure 5.10 show the various component parts;

The measured values from the dissembled Gast air motor are direct

measurements with the measured values indicated as follows;

L = 63mm

r = 36mm

D = 82mm

R = 41mm

s = 4mm

W = 20mm

e = 5mm

The eccentricity is given by the difference in distance between the stator

radius and that of the rotor, (R–r) as indicated in Figure 5.11. The shaded

portion indicates the largest volume between two vanes which can be

determined and known as the cell volume; the product of the length of the

cylinder and the hatched area. The spring groove at the base of the vane

that facilitates the positioning of the vanes in the vane slots is placed

60mm or 3mm from either ends of the vane base. The bent end of the

spring is inserted into the groove as a restraint so that the spring is held in

a fixed position and not to slide. The length of the vane, the rotor and the cylinder are the same and fit in-between the endplates.
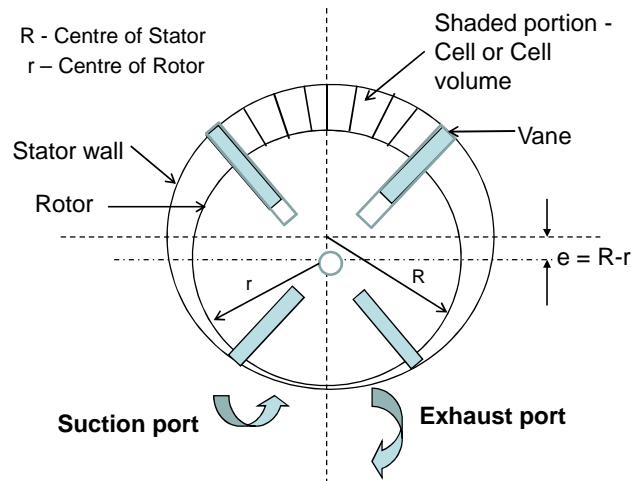
Figure 5.11: Schematic section through a multi-four vane expander

Figure 5.12 is the stator cylinder showing the groove leading to one of the external port which is an inlet or outlet port as the expander is completely reversible depending direction of flow of the working fluid. The diameters of the port are 16mm and are tangential to the circumference of the stator wall. Figure 5.13 shows the vanes of the expander that describe the circumference of the cylinder wall as they move in and out of the slots in a continuous radial motion. They are thrown out by centrifugal force and spurn thus generating shaft motion, a mechanical energy that is converted into electricity. The vanes play a key role in the effective operation of the prime mover by generating the necessary conditions that enables compression of the working fluid between cells of the expander. The vanes are embedded in the grooves of the rotor, just as the rotor

124

maintains an offset with the stator centre forming a crescent shape. The offset is indicated by the letter 'e' which is the eccentricity between the centre of the rotor and the stator.
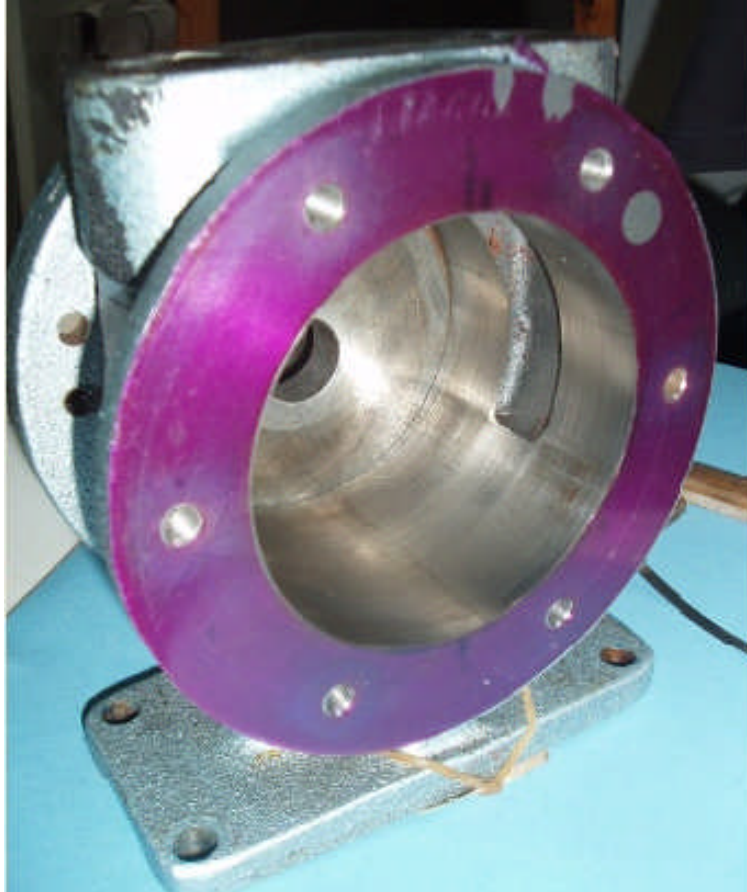
Figure 5.12: Stator Cylinder showing one of the ports grooves
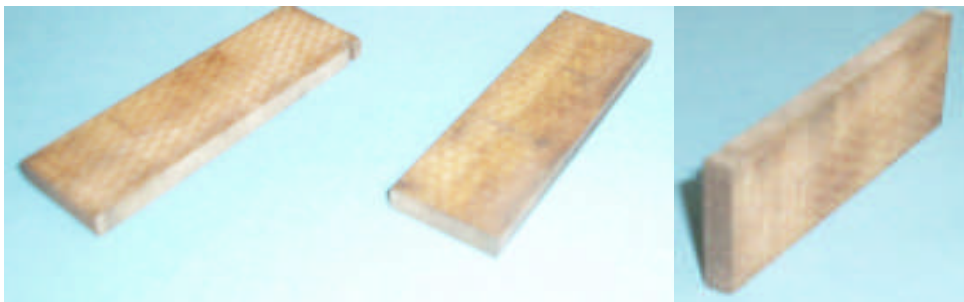
Figure 5.13: The Expander vanes

5.2.2 Theoretical study of sliding vane expander

The geometrical make up and general characteristics of multivane expander are very critical to the understanding of the prime mover in low temperature applications. The basic configuration consists of a single rotor seated eccentrically in a slightly larger cylinder than the rotor with the rotor having a series of radial slots that holds the vanes. The vanes move freely within the slots thrown out by centrifugal force in a radial motion describing the circumference of the cylinder.

Badr et al, 1985 [122], have made series of researches on geometry and vane kinematics as well as performances of multivane expanders in a Rankine engine especially involving low temperature applications or low grade heat simulations and low power outputs. The study also indicates that the prime mover possess many advantages as a device for organic Rankine cycle engines. S.E.Eckard, 1975 [9], had indicated the effect of leakage between the vanes and the stator wall which does affect expander performance and efficiency. Examining only leakage losses is given by Eckard as;

$$\eta_L = 1 - F_1, \tag{5.2}$$

where F_1, leakage fraction of the working fluid is defined as ,

$$F_1 = \frac{\text{(total measured inlet mass flow)-(theoretical mass flow)}}{\text{(total inlet mass flow)}}$$

Robertson, Gerald and Carl Wolgemuth, 1975 [123], have also investigated the effect of end clearance on the leakage fraction indicating

some drop in pressure of about 40% with 0.025mm clearance and 70% with 0.05m clearance. The study showed that drop in efficiency at a particular pressure, increases with increasing pressure because the pressure surge drives working fluid between the vanes and end plate. Similarly, the drop in efficiency at a given pressure decreases with increasing speed because the working fluid has less time to leak from one compartment to another. Frictional losses also contributes to the general loss mechanism of multi vane expanders and though the system of monitoring power loss due to friction is quite complicated as indicated by Thomas Davidson et al,1997 [124], Eckard has indicated that power loss due to friction can be estimated by the relation;

$$F_f \sim \mu_e \, m_v \, r \, v_r^3 \qquad\qquad (5.3)$$

The findings by Eckard suggest a low density vane material, low speed operation (1200 - 1800rpm maximum) and selective injection of liquid lubricant into the expander to minimize frictional losses. However issues of breathing losses also affect expander performance in that working fluid is prematurely expanded on entering the expander. Eckard claims that breathing losses can be reduced by proper design because the vane expander does not posses any dynamic inlet valve. Figure 5.14 and Figure 5.15 are two different models of expanders used during the experiment with varying performance characteristics even as the use of the Rotor vane expander was discontinued for performance reasons and.
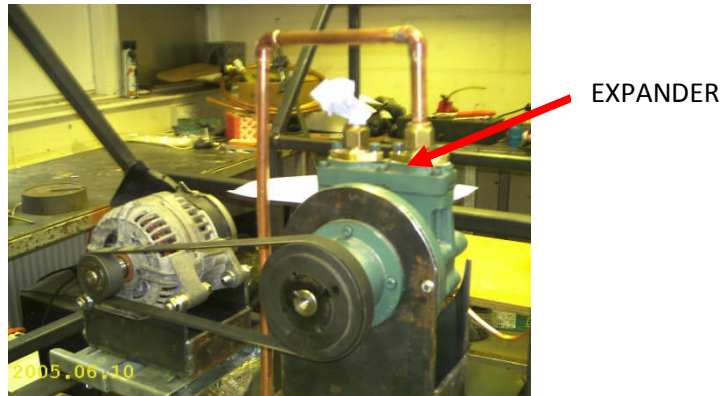
Figure 5.14: Photograph of Rotor Vane expander used in the preliminary tests
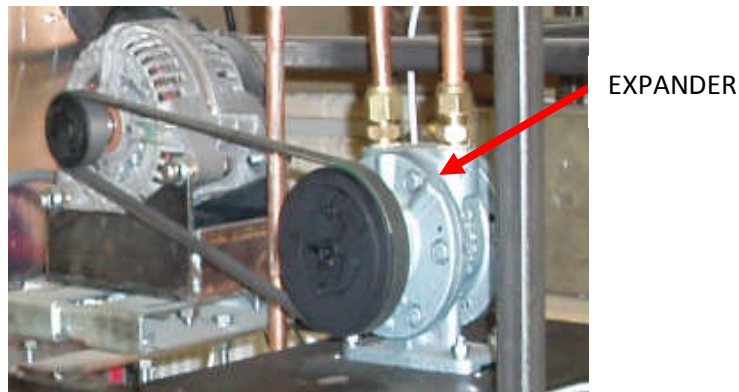
Figure 5.15: Photograph of Gast Expander used in the main test

replaced with the Gast Air-motor which has structural advantages over the former that guarantees performance. However some typical geometric and parametric values enunciated by Professor Vladmir Chlumsky of Technical University of Prague [125], in his book; Reciprocating and Rotary Compressors first published in 1965 had basic relative dimensions for vane–type low pressure compressors.

The length of clearance gap between the vane (rotor) and the stator (cover) is given as; 0.01 - 0.04 and can be estimated by the relation,

$$S_d = \frac{2}{3}\ \alpha\ L\ (t_{ad} - t_s) + f \quad mm, \tag{5.4}$$

The thickness is 1- 3 mm, and coefficient of friction is 0.10.
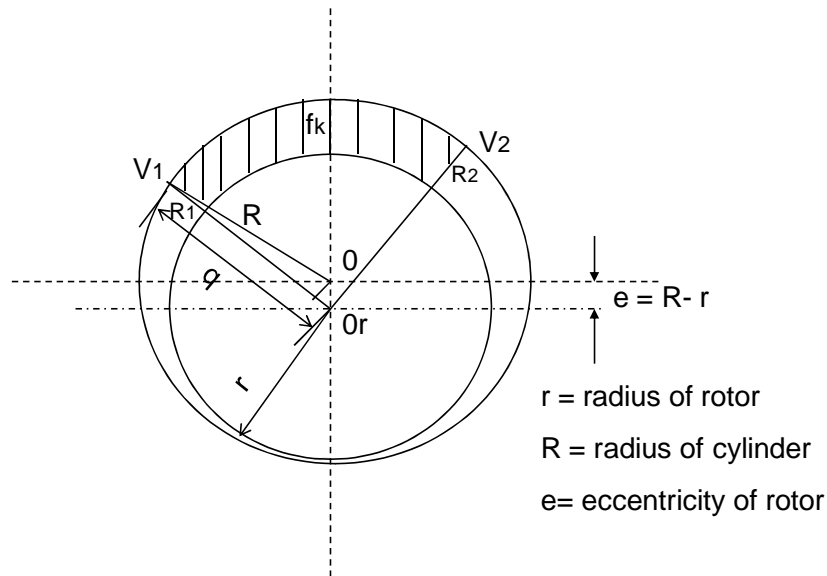
Figure 5.16: Schematic section through a rotary vane compressor

The overall volumetric efficiency of vane compressors is given as;

$\eta_{vo} = {}^{Vs}/_{V}$ between 0.6 and 0.9 and for large machines 0.95 with

compression ratio of 5.

α = coefficient of thermal expansion

t_{ad} = adiabatic compression temperature

L = length of rotor (vane) in mm

t_{s} = temperature of induced gas (working fluid)

f = thickness of oil film (0.1- 0.2 mm)

The radial clearance between the rotor and the cylinder is given in the

relation; $Sr = {}^{2}/_{3} \alpha L (t_{ad} - t_{s}) + f$ mm, (5.5)

substituting r for L. The largest volume between two vanes is given by Chlumsky as, the product of the length of the cylinder L, and the hatched area as shown in Figure 5.16.

$$f_k = R_1 V_1 V_2 R_2,$$ (5.6)

L = 3.2 - 4.2R and the radial width of the vane w $\cong$ 3.8e. However, it is also indicated that; r/R = 0.86 or e = 0.14R for low pressure and for high pressure units, r/R = 0.885 or e = 0.115R.
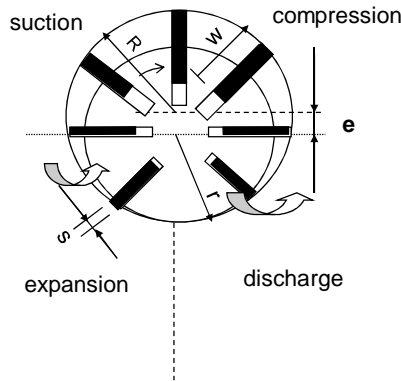
Figure 5.17: Working cycle of a multi vane expander

The working cycle of the vane expander is shwn in Figure 5.17 while coordinates in Figure 5.18 [126] indicates the peripheral radius of the stator as R_2, and the periphery of the rotor has a radius R1 with the offset between the two circles indicated by the distance d, and judging by the Cartesian and the polar coordinates the distance from the origin to the distance of the housing R_2 occurs as a function of the angular position θ. Therefore the gap between the rotor and the housing at any angle say θ is indicated by the relation [121];

130

S (θ) = R$_h$ (θ) - R$_1$, the housing and the rotor are tangential at $\theta = {}^{\pi}/_2$

however, if R$_2$ - R$_1$ is less than d, the circles will intersect and the function

s, will be less than zero at $\theta = {}^{\pi}/_2$
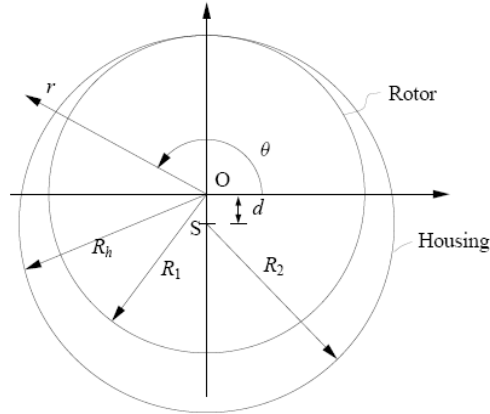
Figure 5.18: Coordinates and basic geometry of an expander

The geometric parameters of the multi-vane expander gives a general

overview and understanding of the basics design principles of an

expander which further broadens the knowledge of the basic performance

characteristics especially as it will relate to this research work.

5.3 Summary

The advent of Vane compressors dates back to the 1800s' when the first

type of vane machine was invented in France and widely used in Belgium

to provide ventilation for Collieries. However, Vane compressors have

since been put to various uses including being an alternative to

conventional turbines especially in low temperature applications where

exhaust heat could be utilized instead of being dumped into the

environment as heat contaminant. This chapter is a study of Vane

compressors to further broaden the basic knowledge of the design and

geometry of the vane device. Measurements of a dissembled Gast Air

motor, a vane compressor used in this research has been carried out to correlate some of the specifications resulting from the theoretical study covered in this chapter. This to a large extent is in agreement with the postulations in literature. Some of these are the vane thickness, the clearance gap between the vane and the stator, the largest volume between two vanes and the stator wall and the eccentricity between the rotor and the stator key to a perfect system operation. The use the prime mover as an expander in a Rankine engine is said to do better than conventional turbine when low grade heat sources are involved, however the system theoretical results are addressed in chapter 5.

CHAPTER 6: Experimental methodology and test results

This chapter describes key considerations and various parameters adopted before and during the system experimental testing. The evaluation and analysis of various test data and test results at each stage of progression is proposed. The determination of feasible operational range of heat flow and heat transfer is identified and system optimization and various improvements on the test rig are described.

6.1 Preliminary Tests

The first type of expander employed in the preliminary test is the RC140 RotoVane expander from Jotek Engineering Ltd., Canada. The initial test was performed using compressed air, but with some difficulties because the expander required initial motoring for the vanes to be thrown out of the vane slots, and this will require additional energy to achieve. The vanes also become sticky due to lubrication and not all the vanes dislodged from their slots shown in Figure 6.1 [127] and rendering normal operations difficult. The compressor was already available at inception of this work.

A-Sectional view of expander   B-Expander profile and cells
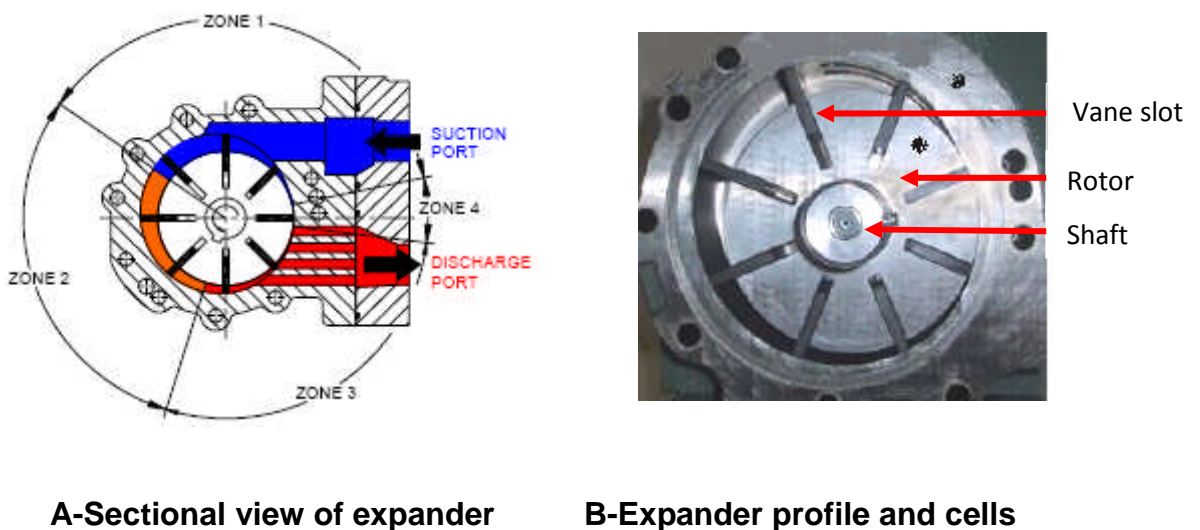
Figure 6.1: Rotovane expander

6.1.1 The Procedure

The experimental procedure involves the connection of the expander inlet port to an air supply source from the laboratory central air compressor. The main difficulty during test operations was the likelyhood that someone might use other supply outlets resulting in sudden drop in pressure at the expander inlet port. The next critical aspect encountered during the experiment is the proximity and location of the compressor to the test rig involving the use of lenghty hose in the air supply stream and thus contributing to further pressure drop. The air flowrate is read from an air flowmeter in liters per minute. Each test lasted a few minutes because of the noise level generated at the expanders exhaust port. Though a noise muffler is installed, it was still within the threshold of pain or above the safety levels allowed in the laboratory. A hose is later connected to the exhaust to further dampen the noise but this stalled the performance of the expander due to the lenghty hose resulting in further pressure drop.

6.1.2 Starting procedure

- Data logging devices are activated
- Data acquisition mode is selected and saved to a file ready for data logging
- Required air pressure is set by adjusting the regulator on the air supply line.
- A valve is turned on to to allow airflow at the set pressure as expander becomes operational. The valve is turned off to stop expander.

This procedure became successful only with the replacement of the RC140 expander which required initial motoring to become operational.

6.1.3 Expander test results

The RC140 expander in Figure 6.2A is replaced with Gast 6AM expander shown in Figure 6.2B, and described in chapter 3 which is a practical solution to the problem encountered with the RC140 when tested with compressed air. The vanes of the Gast expander have micro-springs at the base of the vanes within the slots. This positioned the vanes during rotation and then the vanes are sustained by centifugal force as the vanes move in and out of the slots in a continuous radial motion. The choice of the Gast expander was based on its geometrical advantage over the former which required some form of motoring to start functioning and this
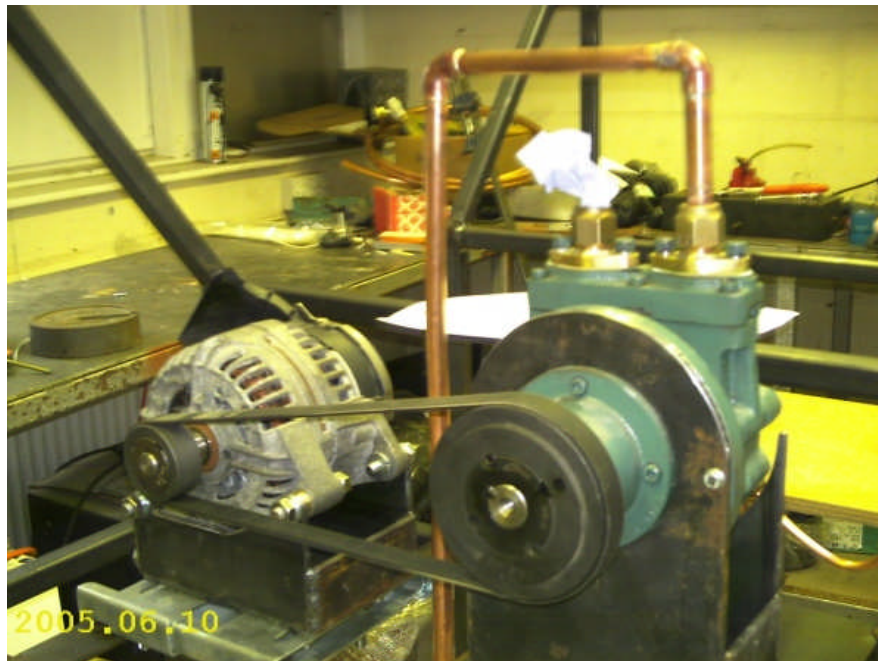
Figure 6.2A: RC140 Rotovane expander initially used for the air test

became a major hindrance during the exploratory tests. Having overcome the initial hitches, it became necessary to configured the data acquisition devices and to check that the data returned matched the programme set up and the outputs from the enabling sensor channels of the data logger.
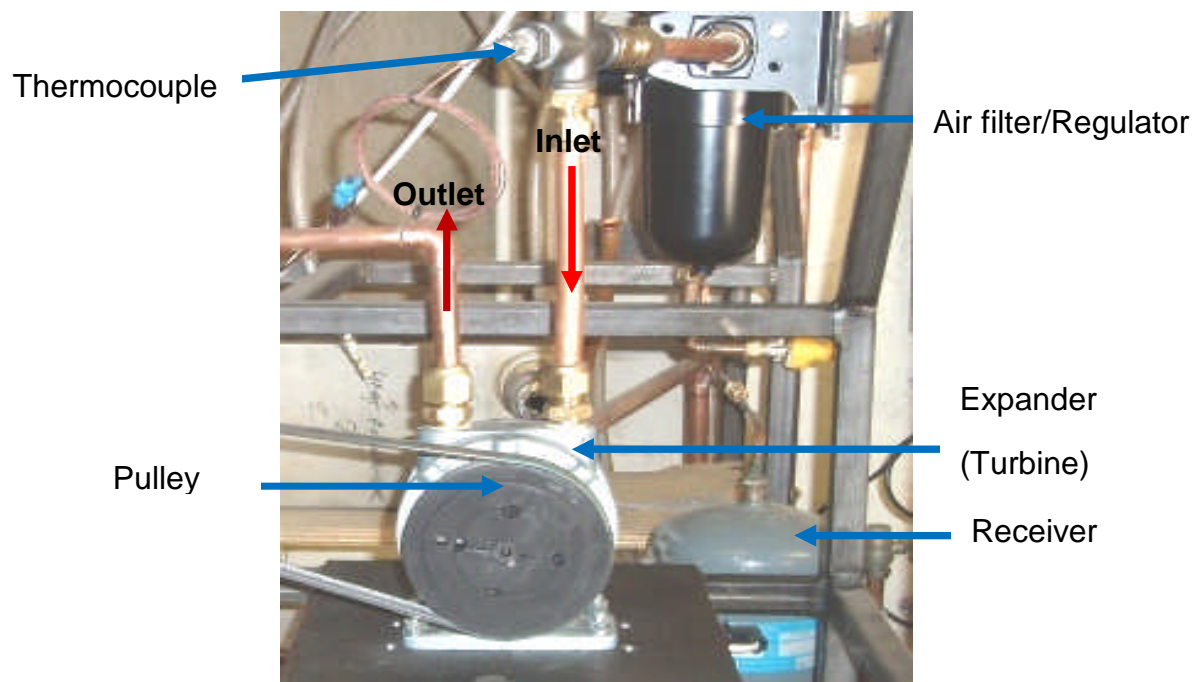
Figure 6.2B: Gast Expander showing other other components on Rig.

Table 6.1.1 Sample air test results recorded by data logger

Date/time	Sensors	Values	Units
29/05/2007 15:05	Pump outlet temp	15.625	^{o}C
29/05/2007 15:05	Reservoir Temp.	16.583	^{o}C
29/05/2007 15:05	Exp.inlet temp.	17.129	^{o}C
29/05/2007 15:05	Exp.outlet temp.	16.99	^{o}C
29/05/2007 15:05	Superheater Temp	15.85	^{o}C
29/05/2007 15:05	Exp. outlet Pr.	1.441	bar
29/05/2007 15:05	Exp. inlet Pr.	2.066	bar
29/05/2007 15:05	Pump outlet PR.	2.076	bar
29/05/2007 15:05	Superheater Pr.	2.114	bar
29/05/2007 15:05	Working fluid flowrate	1.64	l/m

The sensors returned real time data that is visible on the computer monitor and then saved to a file in the directory. The data can also be saved to a replay file and the data logger programming allows for units to be set for various outputs depending on the type of sensor. Units can be set for temperature in ^{o}C, pressure in bars or kilopascal (kPa) as well as current in amperes or voltage in volts. The data range is usually set by using the span-format specifying the range and how the output value will be displayed.

Table 6.1.2 *Sample air test results recorded by data logger*

Date/time	Sensors	Values	Units
29/05/2007 15:06	Pump outlet temp	15.63	^{o}C
29/05/2007 15:06	Reservoir Temp.	16.59	^{o}C
29/05/2007 15:06	Exp.inlet temp.	17.14	^{o}C
29/05/2007 15:06	Exp.outlet temp.	16.89	^{o}C
29/05/2007 15:06	Superheater Temp	15.86	^{o}C
29/05/2007 15:06	Exp. outlet Pr.	1.442	bar
29/05/2007 15:06	Exp. inlet Pr.	2.067	bar
29/05/2007 15:06	Pump outlet PR.	2.076	bar
29/05/2007 15:06	Superheater Pr.	2.114	bar
29/05/2007 15:06	Working fluid flowrate	1.6417	l/m

The sample test result shown on Table 6.1.1 and Table 6.1.2, indicate that both the data logger setup and the expander had become functional as the later showed both drop in temperature and pressure at the expanders inlet port and exhaust port. This is a strong indication that the expander can implement the thermodynamic Rankine cycle. Further tests also confirmed the drop in temperature and pressure as indicated in Figure 6.3 and Figure 6.4 respectively. These preliminary tests are crucial to the main test being carried out, as the expander is an air compressor and had not been tried in operations involving high temperatures.

Time (s)
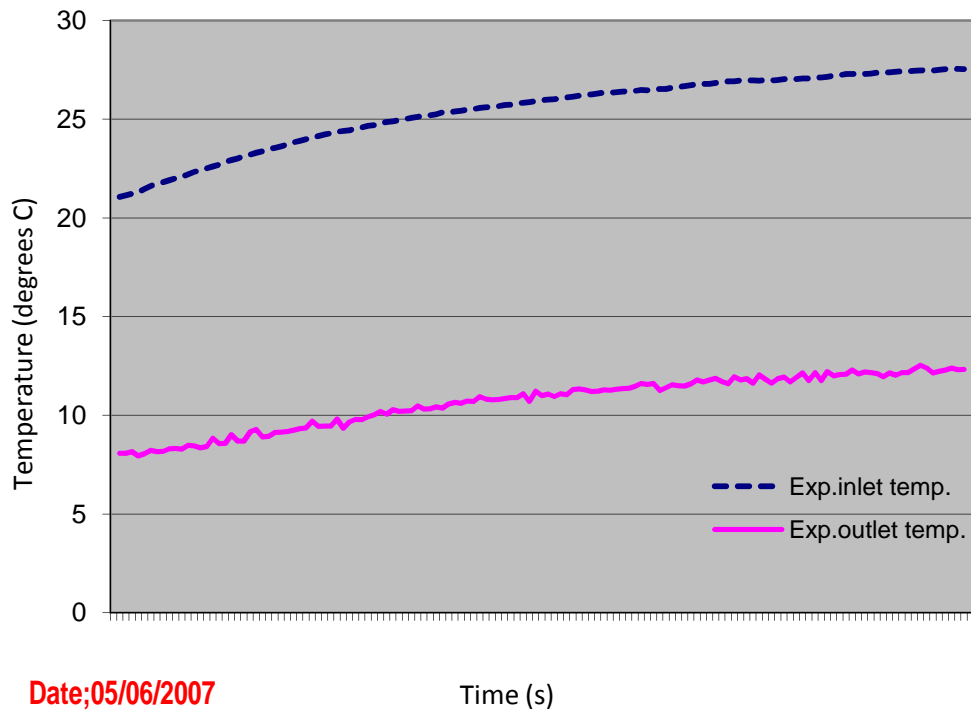
Figure 6.3: Expander inlet and outlet temperature vs.time

Time(s)
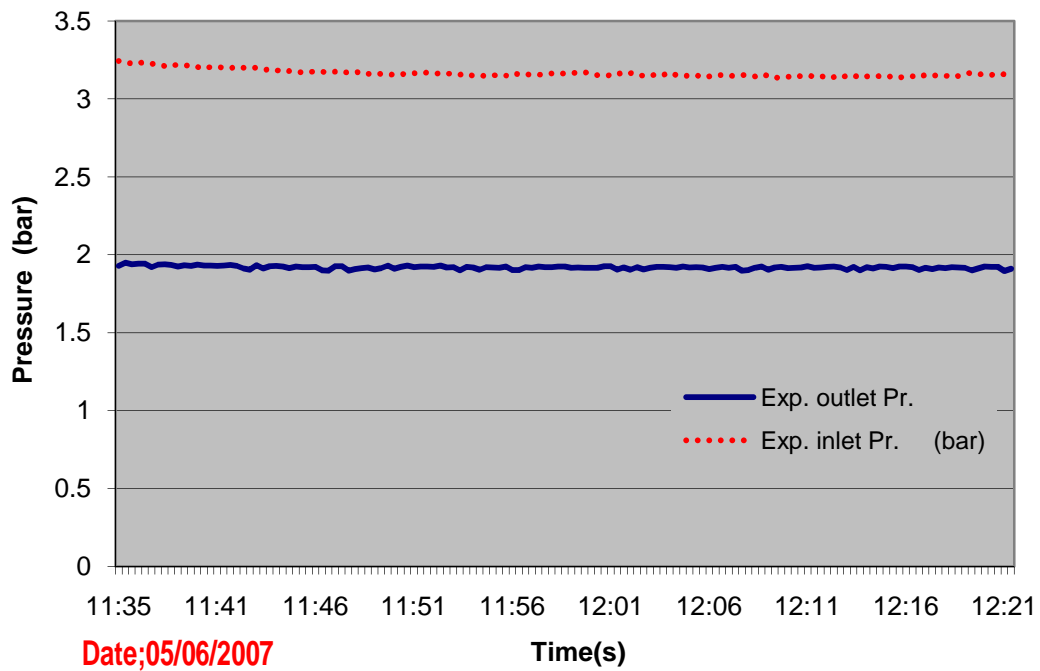
Figure 6.4: Expander inlet and outlet pressure vs.time

 This experiment will involve the use of a refrigerant as working fluid and the expander will be subjected to high temperature heat.
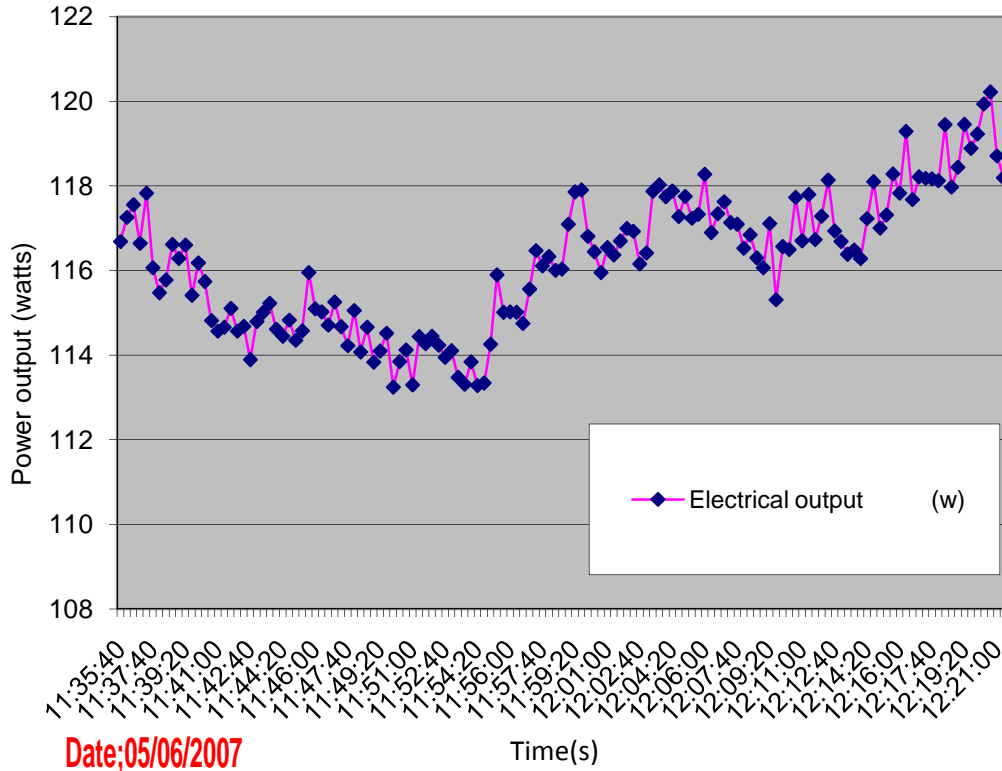
Figure 6.5: Graph showing sample power output vs. time

The power output configuration is also tested and recorded by the data logger as indicated in Figure 6.5. These preliminary tests allowed for a studied adjustments and initial modification to be made to the system prior to the vapour test using the working fluid HFE 7100. The modifications involved the removal of some components that were unsuitable for the vapour test. These include such components as the oil separator and the air filter/regulator as well as the lubricator installed close to the inlet port of the expander in Figure 6.2. The reason for the removal was the premature expansion and condensation that occur because of the volume of these vessels. The result is that working fluid at the vapour state condensed in

these vessels before reaching the inlet port of the expander due to sudden drop in temperature and pressure. These tests also afforded checks for leakage in the system and other peripheral leaks at joints and soldered areas between piping and vessels installed in the system. Other areas examined include the direction of rotation of the expander shaft since it has to drive the electric generator in a clockwise direction using a belt, as the expander is reversible. This involved pressurising each port and checking the direction of shaft rotation. The belt transmission efficiency has been given as 0.95 [100].

The shaft speed or shaft rpm increased with increase in pressure and flowrate at the inlet of the expander as indicated in Table 6.2 and Figure 6.6. The system also slows down as pressure is reduced. The shaft speed can be controlled by a valve at a location close to the inlet port of the expander using a sight glass to monitor that no moisture is in the air stream.

Table 6.2: Preliminary air test data

Air pressure (bar)	Air flowrate (l/min)	Expander (Rpm)
1.00	10	350
1.40	30	358
1.80	100	395
2.20	150	435
2.60	205	485
3.00	230	515
3.40	285	535
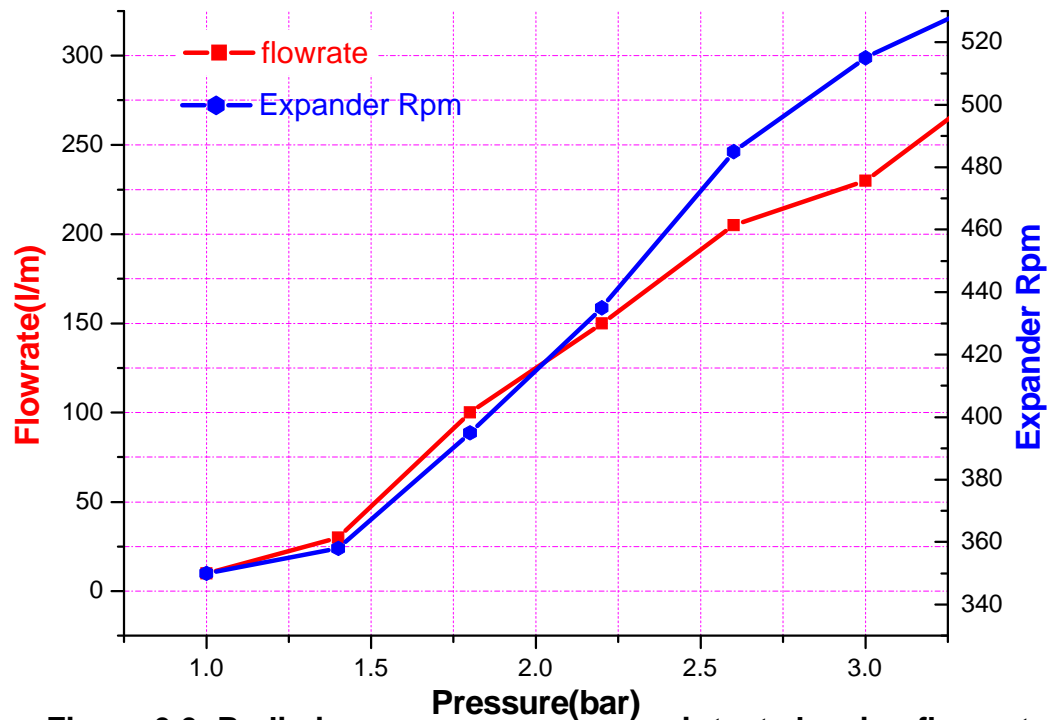
Figure 6.6: Preliminary air test showing flow rate
and expander shaft Rpm vs. pressure

This can occur at higher pressures requiring the integration of an air filter into the system though this had to be removed during the vapour test.The power test is not performed with the air test because the desired rpm was not reached due to laboratory limitation and air compressor performance. This caused pressure drops and the stream resistance, pulley and belt frictions lowered the expander rpm and the system will require higher air pressure for better performance. At the end of the air test, the rig is reconfigured and modified for the vapour phase of the experiment using a 9KW electric boiler. An environmentally friendly chemical, HFE 7100 is the working fluid employed in the tests. HFE 7100 is a mixture of two inseparable isomeric chemicals known as methoxynonafluoroisobutane and methoxynona-fluorobutane both considered as a single chemical entity, due to their similar boiling points and inseparable nature listed in

the Australian Inventory of Chemical substances (AICS). The thermo-physical properties are neither hazardous nor likely to cause any health defects and irritations. The boiling point and molecular weight is indicative of its suitability for the proposed experiments. A study in chapter three covers area of health and safety as well as the behaviour of HFE 7100 at critical temperature. Other areas of the study include the physical and chemical properties, the chemical identity and composition as well as the effects on the environment. However, a second working fluid, HFE 7000 also a hydrofuoroether (HFE) similar to HFE 7100 is employed in the next series of tests because of its lower boiling point. This option is dictated by the limitations imposed by the Electric Boiler output temperature at 115$^{\text{o}}$C and the fact that HFE 7100 has a boiling point of 61^{0}C when compared to 34$^{\text{o}}$C for HFE 7000 which offers some performance advantage in terms of vapour quality.

6.2 The ORC experiment employing the electric boiler as heat source

The electric boiler used in the experiment is the Chromalox-Model CES-12 480V 9kW Boiler, which supplies the heat required to vaporise the working fluid HFE 7100 and subsequently HFE 7000 in a real world thermodynamic cycle in contrast to the ideal Rankine cycle. The actual vapour power cycle differs from the ideal Rankine Cycle due to irreversibilities in various components as high quality vapour is expanded isentropically through the prime mover to produce shaft work. The common causes of irreversibility are;

    i.   Pressure drop due to fluid friction in the boiler, condenser and piping between various components.

    ii.   The prime mover inlet pressure is somewhat lower than the boiler exit because of pressure drop between connecting pipes.

    iii.   Heat loss from the system to the surroundings and electrical resistance.

To compensate for the pressure drops, the working fluid must be pumped to a sufficiently higher pressure than an ideal cycle by increasing pump output thus increasing work input.

6.2.1 Operational Checks

1 /. Pre-Start

A checklist of some precautionary measures before the commencement of any test will include checks on;

- Ventilation
- Leakage
- Overall system integrity
- Data acquisition devices
- Sensors
- Valves
- Boiler filling operation and bleeding
- Pressure and temperature operational limits
- General safety

Ventilation - The need to ensure that the laboratory space have some degree of ventilation is critically examined so that any form of emission due to leaks in the system will not pose the danger of inhalation or fouling of the laboratory airspace. However, the chemical and thermophysical properties of HFE is indicative of its non-hazardous nature but precautions must be taken as there might be exceptional cases of allergies and where very sensitive individuals become exposed to such an environment. For the biomass boiler sufficient air is required for combustion.

Leakage - Leak tests and critical examination of pipes and tubing had been carried out during pipe connections and assembly. This cover bends, couplings, joints and loops in the system. All vessels connected to the system also underwent systematic checks to ensure that their integrity is not in anyway compromised and that there is no leakage whatsoever. Normally, the use of foamy liquid substance is the most common way to check for leaks especially when the system is pressurised and leaks can be spotted through bubbles developing at the hotspot. This is usually a tasking and difficult exercise but it is a worthwhile exercise because of safety and ensuring overall system performance.

Overall system integrity - The need for wholesome visual inspection cannot be overstated to check the general system conditions. These will include boiler integrity, sight glasses, piping and different couplings and that they match functional specifications and range. Nuts at couplings are secured and properly tightened to avoid a blow-out in the system where

very high temperatures is involved as well as hot surfaces. The prime mover is constantly checked for leaks at the seals and end plates because some seals are found to have compromised after a lengthy period of use, ranging over 2000 hours considering the high operational temperatures.

Data acquisition devices - The data taker used is the DT500 series and involves the regular collection of data, which by implication include the scanning of sensors, making of instantaneous measurements and transferring such to a recorder or a computer as indicated in Figure 6.7. The measurements are then converted according to requirements i.e. voltage, ^{o}C or ^{o}F. There is also the possibility of carrying out calculations on measurements, averages, standard deviation as well as maximum or minimum values. These are displayed on the computer screen and data returned in real time.
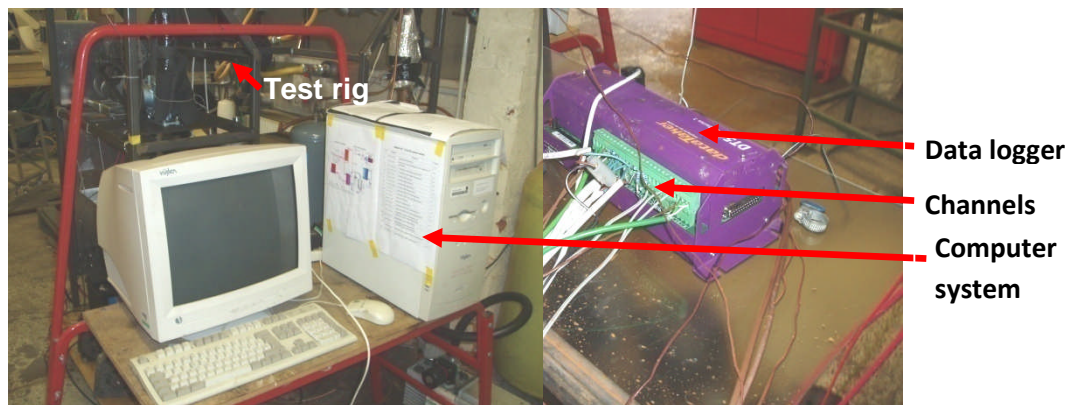
 Figure 6.7: Data Logger DT500 and Computer System

The sensors are connected to channels and the software makes it possible for data to be downloaded to the computer. The returned data is monitored through graphical window in real time on the monitor screen.

Sensors - These are devices capable of detecting and responding to physical stimuli such as movement, light, heat or pressures. Some sensors can measure voltage and current in an electrical circuit. The typical connection of various sensors is shown in appendix IV connected to different channels. Each channel can support three sensors and a ground. The negatives of the three sensors are connected to the ground (R) and their positive terminals connected to (*), (-) and (+) terminals to afford the relay of signals from the data taker. The description of each sensor outlet is either R*, R-ve, or R+ve. There are ten major channels and another dedicated to counters. There must be utmost care in handling of the data logger as any exposure to water or any other liquid could cause a crash of the system. The data range of the data logger must not be exceeded and resistors are used to bring higher outputs within the range of the data logger and spans are set in order to return actual values in real time.

Valves - These mechanical devices control liquid or gaseous flow through pipes, channels or other passages shown in Figure 6.8 and Figure 6.9 [129]. There are several types of valves; globe valve, gate valve, butterfly and needle valves. They exert control using movable and adjustable elements that shuts, opens or partially blocks an opening in a passageway. The globe valve and the ball valve are employed in this experiment. The valves are also useful when changing some components in the system as it affords isolation of the sections that changes need to be made thus preserving the working fluid. With the valves securely shut,

components can be replaced as well as allow for repairs and facilitating

system optimization.
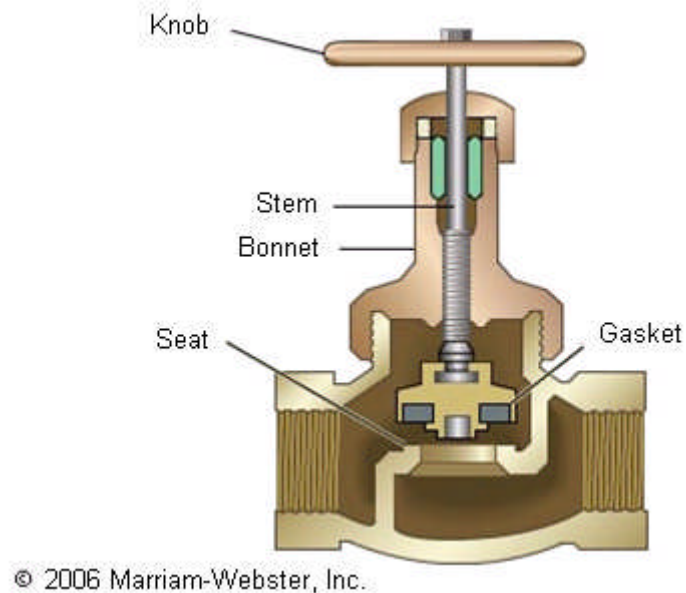
Figure 6.8: The Isometric view of a typical globe valve
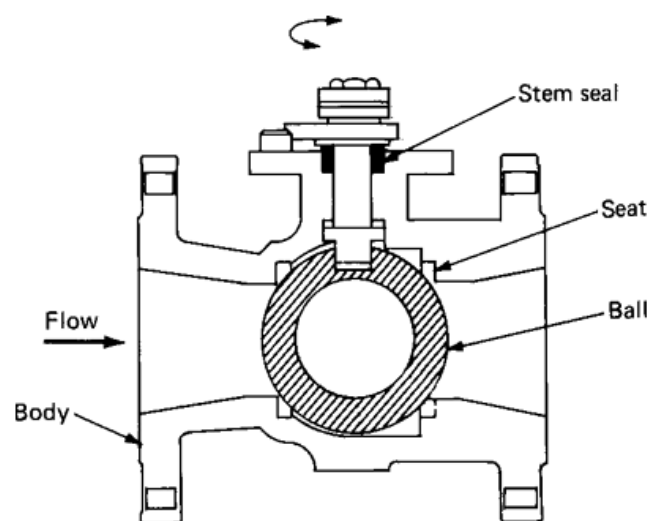
Figure 6.9: Across sectional area of a typical ball valve

Boiler filling operation and bleeding - The electric boiler is filled with clean tap water to specified pressure within the safety limits of the boiler. A water hose is connected to the mains supply and the boiler inlet through a control valve. The boiler is then bled through the bleeding valve of the hot water pump to remove any trapped air in the system. The boiler is ready for use after the conclusion of the process. The boiler integrity check is repeated at the beginning of every test to ensure that nothing is compromised and for safety reasons.

Pressure and temperature operational limits - The pressure and temperature limits indicated in the boiler operational manual is followed and observed throughout the test operations. The boiler pressure and temperature thermostats are set to the required range as a very tangible safety measure so that the boiler will not exceed the 6 bar maximum pressure limit. The boiler is allowed to cool after shutdown allowing some time-lag for the hot water pump to re-circulate the water in the closed loop and later switching it off after temperature and pressure attenuation.

General Safety – This involves general safety checks carried out before and after an experiment is concluded. The routine checks involves overall system shutdown including switches, valves where necessary and making safe the test bench to avoid any form of accidents after system shutdown. The cooling water system is normally allowed to run for sometime after the system shutdown to cool down the system and encourage condensation of the working fluid as well as lead to attenuation of hot surfaces.

2/.Start procedure for ORC experiment using the electric as heat source

The electric boiler has a primary hot water loop, which is configured to supply the required heat to vaporise the working fluid in an evaporator in a closed loop as shown in Figure 6.10.
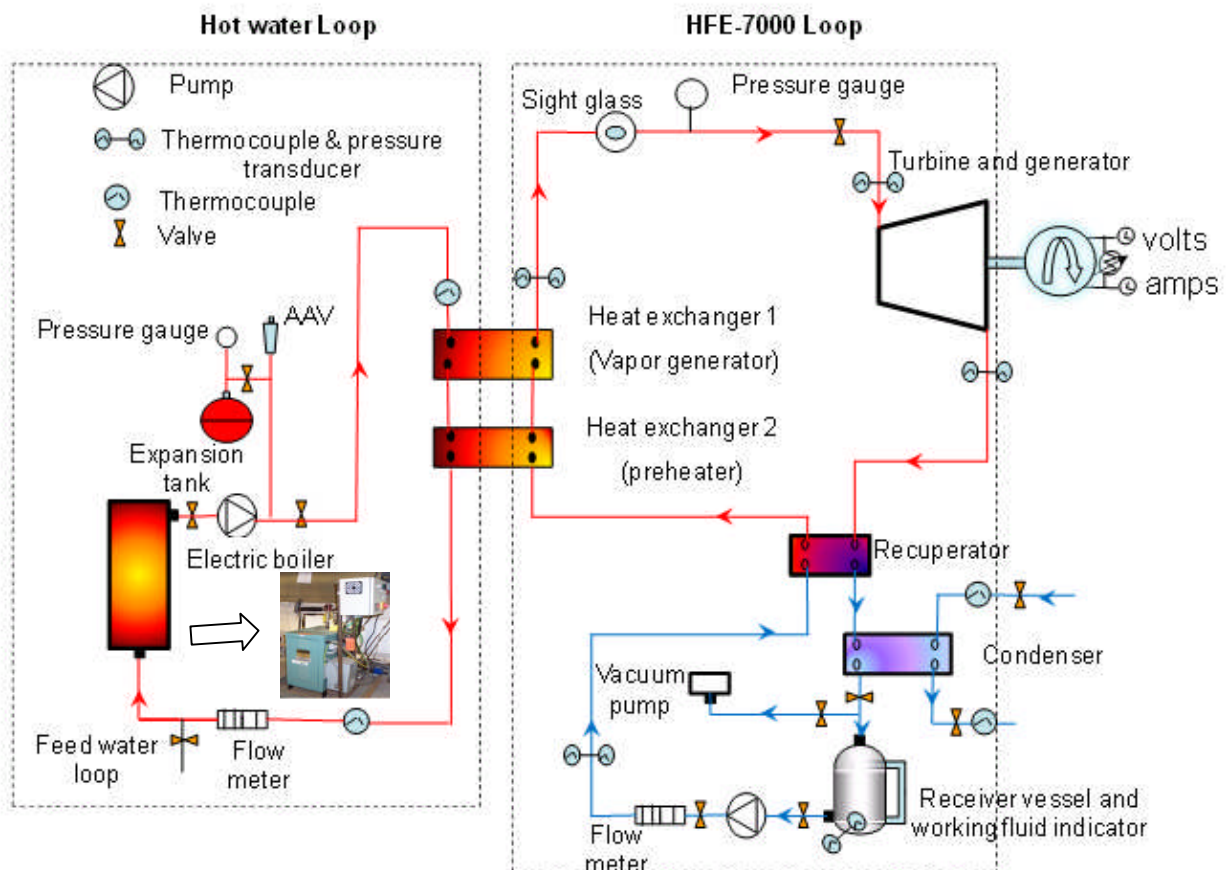
Figure 6.10: Schematic diagram of the Primary hot water loop and the Secondary loop of the ORC cycle.

The experimental start up procedure involves;

A/. The boiler is filled with clean tap water from the mains supply by means of a hose to a gauge pressure of 1.5 bars. This is to ensure that the optimal pressure of the boiler is not exceeded during the addition of heat

and any trapped air within the system is expelled by bleeding through the bleed valve of the hot water pump.

B/. Switch on the boiler and set the temperature at 115°C through a control panel attached to the boiler. This is also the maximum output temperature from the boiler.

C/. Switch on the central laboratory cooling water system after turning on the water supply pumps to the chiller. Set the chiller temperature at 17°C from the control panel. This temperature reduces the possibility of dumping sub-cooled liquid after condensation in the receiver thus requiring more energy to vaporise the working fluid. After the test, the shutdown sequence is to switch off the chiller before the pump and the reverse when switching on the system.

D/. Once the boiler is up and running and has attained the desired temperature of 115°C, the working fluid pump is turned on and set at an initial pumping rate of 10% with a 3% incremental. The pumping process is continued until the moisture is observed in the sight glass at the expander inlet, an indication of poor vapour quality. Since this can affect the vanes of the prime mover due to bombardment by liquid molecules incident on the vane surfaces, the test is suspended at that very moment. This happens when the pressure increase is not marched with corresponding increase in temperature.

E/. The data logging process is the next step where the computer system is turned on and the data taker is connected. A data file name is set and saved. The data logging operations follows some sort of convention; Window $\longrightarrow$ Text $\longrightarrow$ Display data $\longrightarrow$ Capture data in disk and then

choose a directory for the files. The saved file, which is in the (.txt) format, is converted to (.xls) file. The (.txt) file is opened as Microsoft excel; choose column A, ➔ choose "data" in the main menu, ➔ choose "Text" to columns, ➔choose "Delimited" ➔ choose "next"➔ choose "comma" next ➔ finish and it will be saved as data.xls.

F/. The test commences at this stage and the expander is operational, the expander rpm is recorded manually using a tachometer. The various pressure gauges are visually read and recorded.

They key issue in each test is the expander rpm and the parameters that produce the highest shaft speed. This is significant because the expander drives the alternator to produce electricity. The expander is fitted with a pulley, which is belt driven and is at a ratio of 2:1 for the small pulley and 3:1 for the big pulley shown in Figure 6.11.
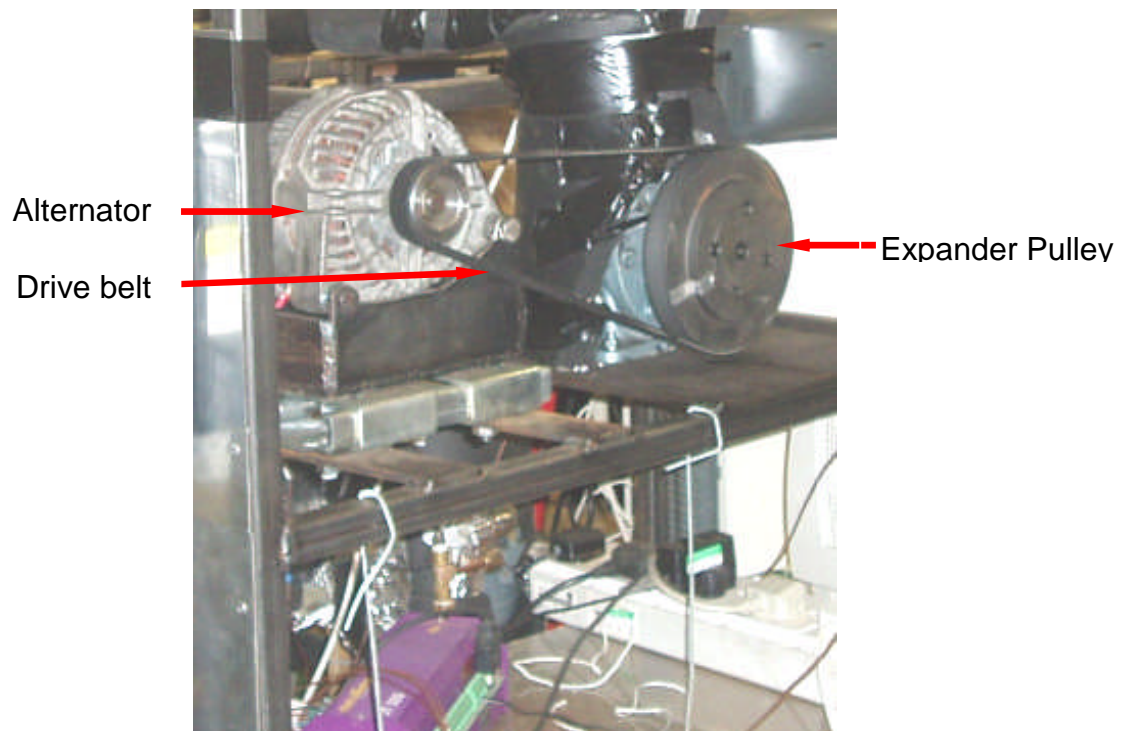
Figure 6.11: Photo of test rig showing Pulley arrangement

The power output from the alternator increases with increase in rpm. However, the expander rpm also increases with increase in pressure at the inlet port of the expander in a thermodynamic organic Rankine process. The overall performance of the expander is dependent on both temperature and pressure of the cycle, which is a product of different components in the system.

The main components are the electric boiler, the expander, the generator, the pump and condenser; and the later being a brazen compact Alfa Laval heat exchanger. The evaporator or vapour generator and the pre-heater are also compact heat exchangers. These components perform major roles in generating an output from the energy input. The pump for an example uses the work input to move the working fluid back through the cycle, while the saturated vapour passes through the prime mover to produce shaft work. The condenser extracts heat from the expanded vapour or mixture to a saturated liquid in the receiver. The investigation of this novel system will give an insight into how well a multi vane expander operates in a vapour power system and the viability and effectiveness when combined with an automotive alternator as the electric generator. Another interesting aspect is that of using a variety of alternators which can be acquired locally at very little cost and can as well be retrieved from auto-breakdown yards. The later will be a good recycling strategy, which is good and healthy for the environment instead of having them dumped in the landfills.

6.2.2 Experimental test of the ORC using HFE 7100 and test results

This covers a series of experimental tests performed by varying of test conditions and parameters having made some preliminary considerations.

6.2.2.1 Preliminary considerations

A series of tests are proposed by varying the pump flow rates through the pumps' control panel in percentage increments and determining the actual flow rates in lit/min. This is then converted to kg/min by multiplying the
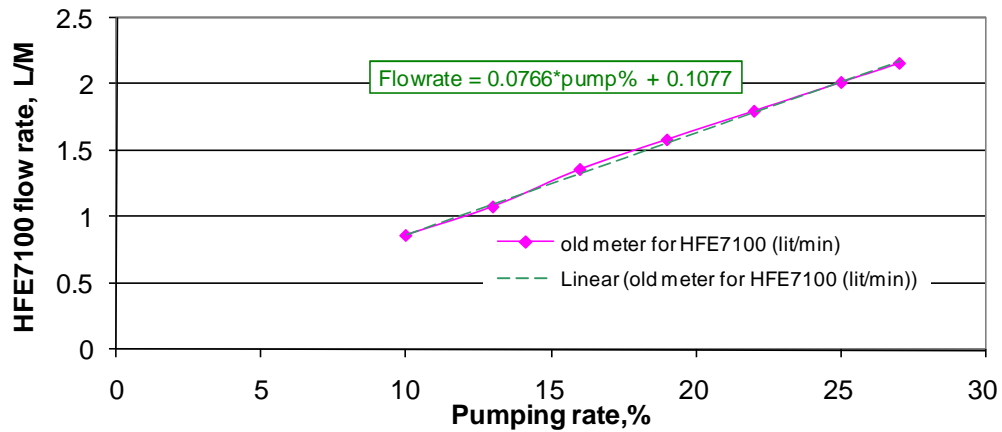
Figure 6.12a: Flow meter reading in lit/min
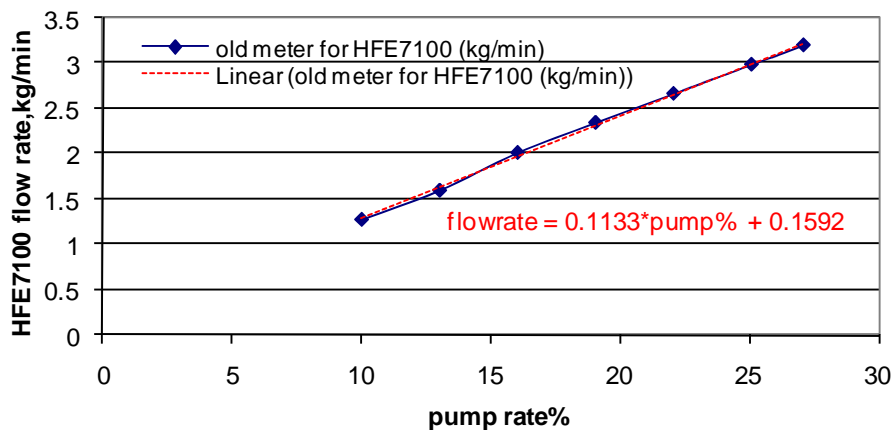
Figure 6.12b: Flow meter reading converted to kg/min
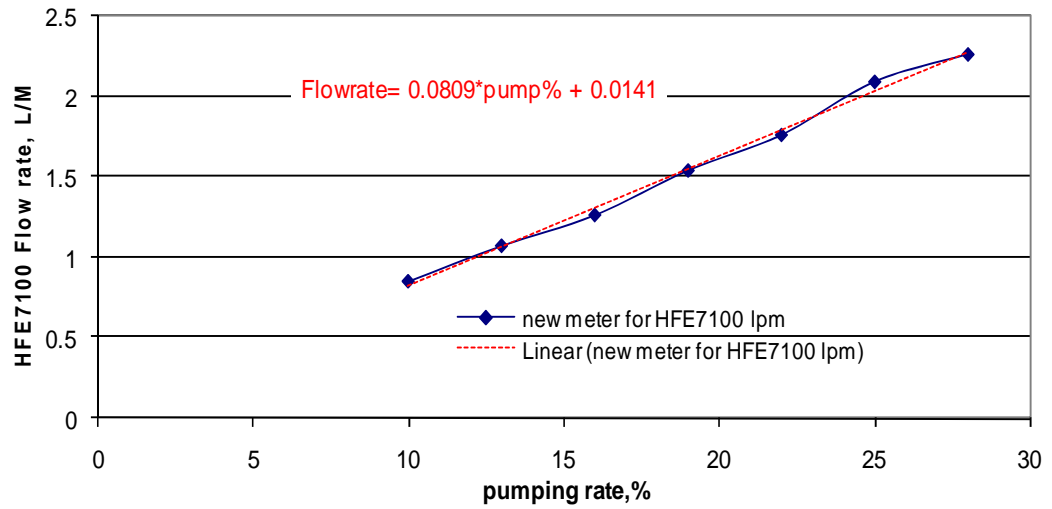
Figure 6.13a: New flow meter reading in lit/min
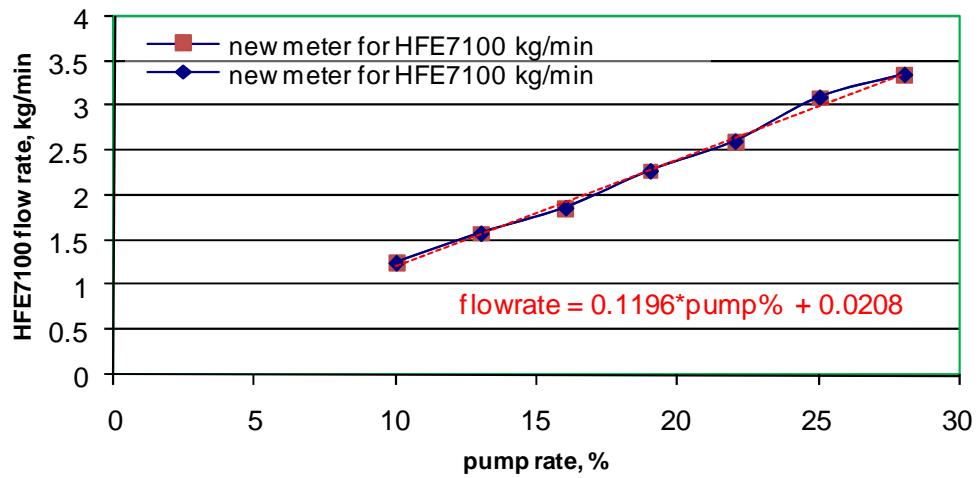
Figure 6.13b: New flow meter reading in kg/min

excel equation by the density of the working fluid as shown in Figure 6.12a

to Figure 6.13b and further dividing by 60 to convert to kg/s. Two flow

meters are used during the process described as old flow meter and new

flow meter the later being a replacement. The flow stream in the

condenser is counter flow and subsequently parallel flow, the later having

low heat transfer efficiency with higher temperature heat sink. This reduces the level of sub cooling at the condenser outlet.

The starting procedure is as described earlier in this chapter and the schematic diagram of the basic ORC system is shown in Figure 6.14, Figure 6.15 and Figure 6.16a. The basic process involved;

1 - 2 Pumping process.

2 - 3 Constant pressure heat addition.

3 - 4 Expansion process in the prime mover

4 - 1 Constant pressure heat rejection in condenser.
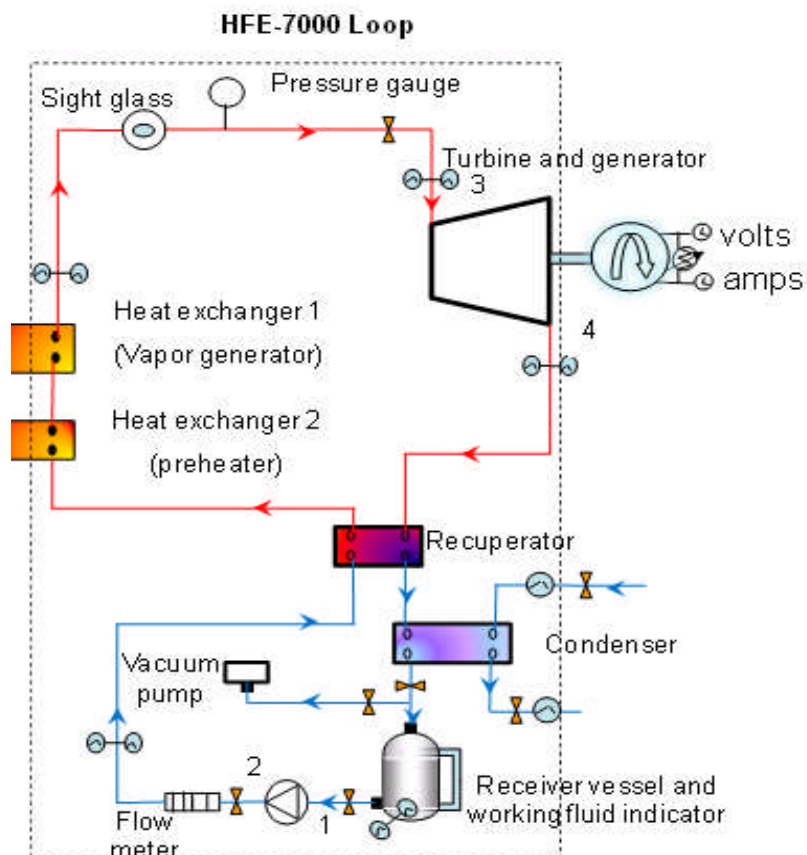
Figure 6.14: Basic ORC Rankine Cycle
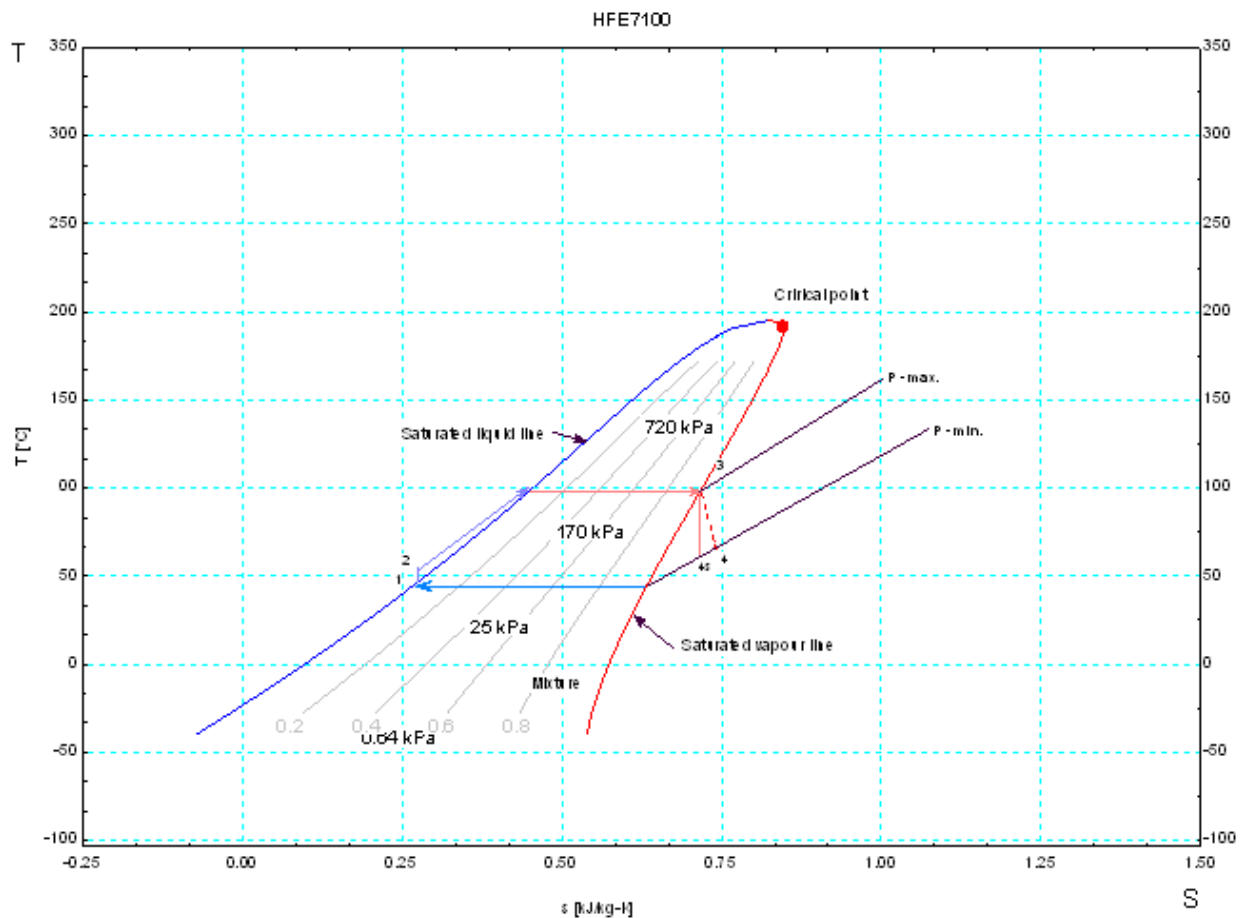
Figure 6.15: Schematic T, s-diagram for basic cycle generated from EES software for fluid with bell-shaped curve and saturated vapour line at the expander exit.

The processes described from 1- 4 is synonymous with heat engines which specifically convert heat in to work by;

I.   Capturing heat from a high temperature source

II.   Part of the heat energy captured is converted to work by means of rotating shaft.

III. The remaining waste heat is rejected to a low temperature heat sink.

IV.   The system operates a cycle.
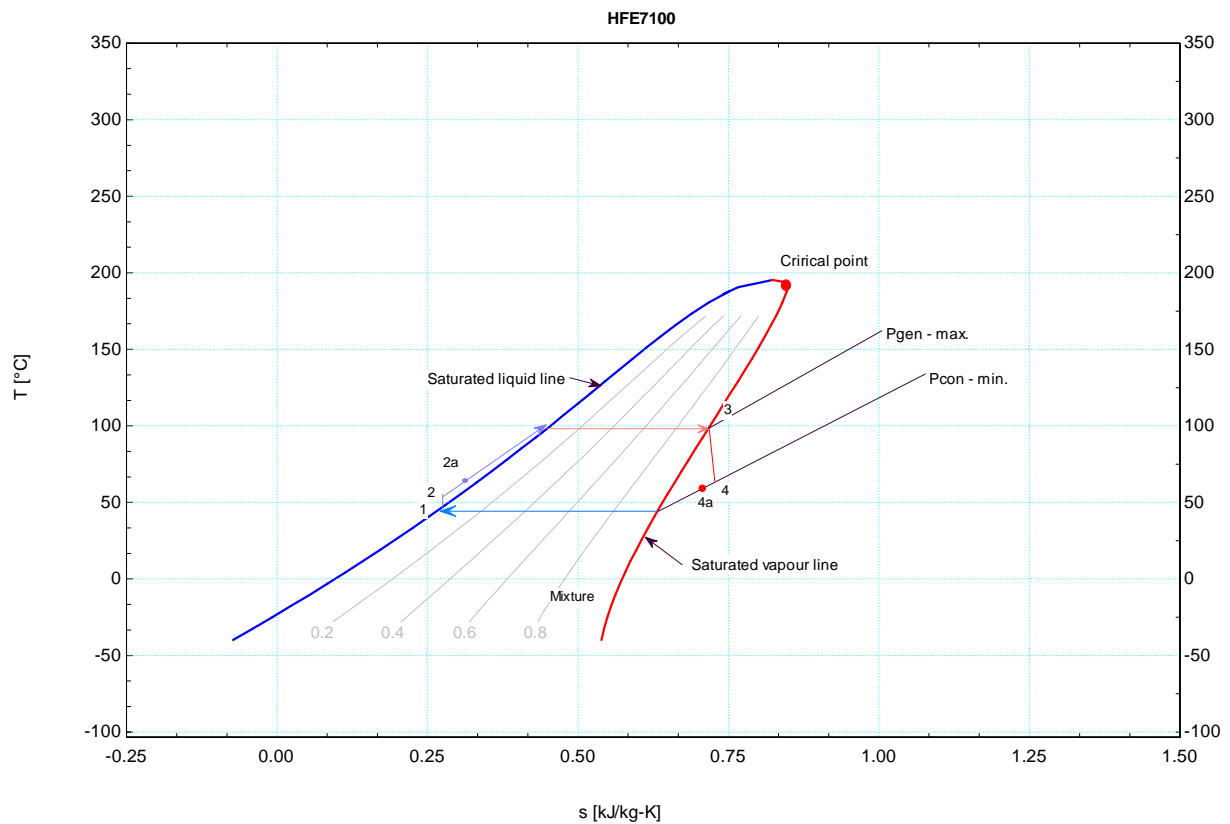
Figure 6.16a: Schematic T, s-diagram actual, generated from EES software for fluid with overhanging coexistence curve and saturated vapour line at the expander inlet and showing the effect of a recuperator in the cycle

The entire system had some improvement carried out as the experiment progressed by varying different components that make up the system. Some of the components include the heat exchangers and changing of some pipes of varying sizes as well as variation in the types of Gast expanders. The types used are based on the number of vane make-up, which are the 4-vane and the eight vane types. The aim is to optimize and improve system performance and reduce exergy loss to the system. The System improvement later involved some modifications to a regenerative

cycle by introducing a recuperator, as shown in Figure 6.16B, indicated by

points 4a and 2a on the T-S chart in Figure 6.18a at the outlet port of the
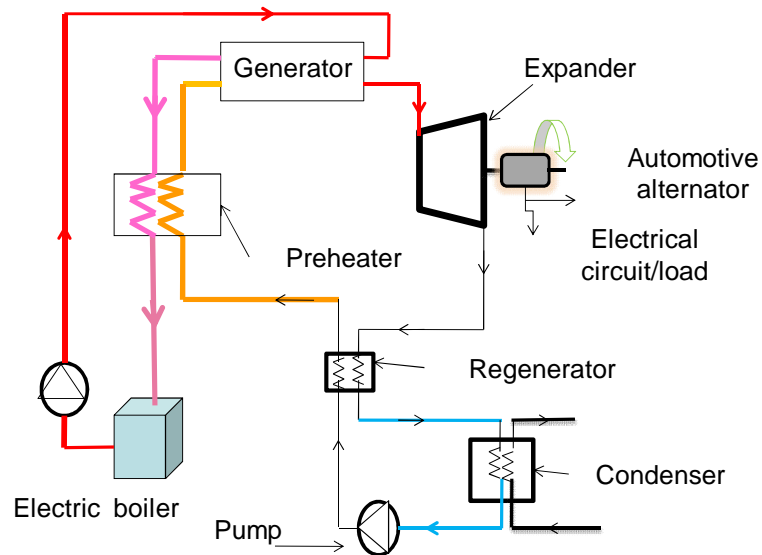
Figure 6.16B: System improvement using a Regenerator

expander and pump respectively. This is a heat recovery measure and

later a second refrigerant, HFE 7000 is used. The heat recovery measure

achieved by the introduction of a recuperator is specifically aimed at

improving the system. The process involves the use of expanding or

expanded vapour to preheat the working fluid before it enters the

evaporator so that heat transfer to the working fluid occurs at a higher

average temperature and to improve efficiency. Exergy destruction mainly

due to irreversiblties in the cycle or some of the systems components can

also be reduced by this means. The actual tests is carried out under

ambient conditions or dead state i.e. the temperature and pressure is at

the same state as the surrounding ambient conditions and subsequently

other tests are performed under a vacuum. The result is analysed and

compared with those performed under normal conditions. The process of lowering the operating pressure in the evaporator by pulling a vacuum automatically lowers the temperature at which boiling takes place in the evaporator. The working fluid in this respect is HFE 7100, which has a boiling point of 61°C. Using the EES software the effect of pressure on the saturation temperature, T_{sat} of the working fluid is determined. This is without considering pressure drops and stream resistance involved in the actual test indicated in Figure 6.17, using the equation; T_sat_1=T_sat (HFE7100, P=P_1), to derive values in Table 6.3,

Table 6.3: T_sat values of HFE 7100 from EES software

P (bar)	T_sat (^{0}C)
0.3	26.86
0.4	33.95
0.5	39.75
0.6	44.69
0.7	49.02
0.8	52.90
1.03	60.58
1.2	65.38
1.5	72.75
2.0	82.82
2.5	91.10
3.0	98.19
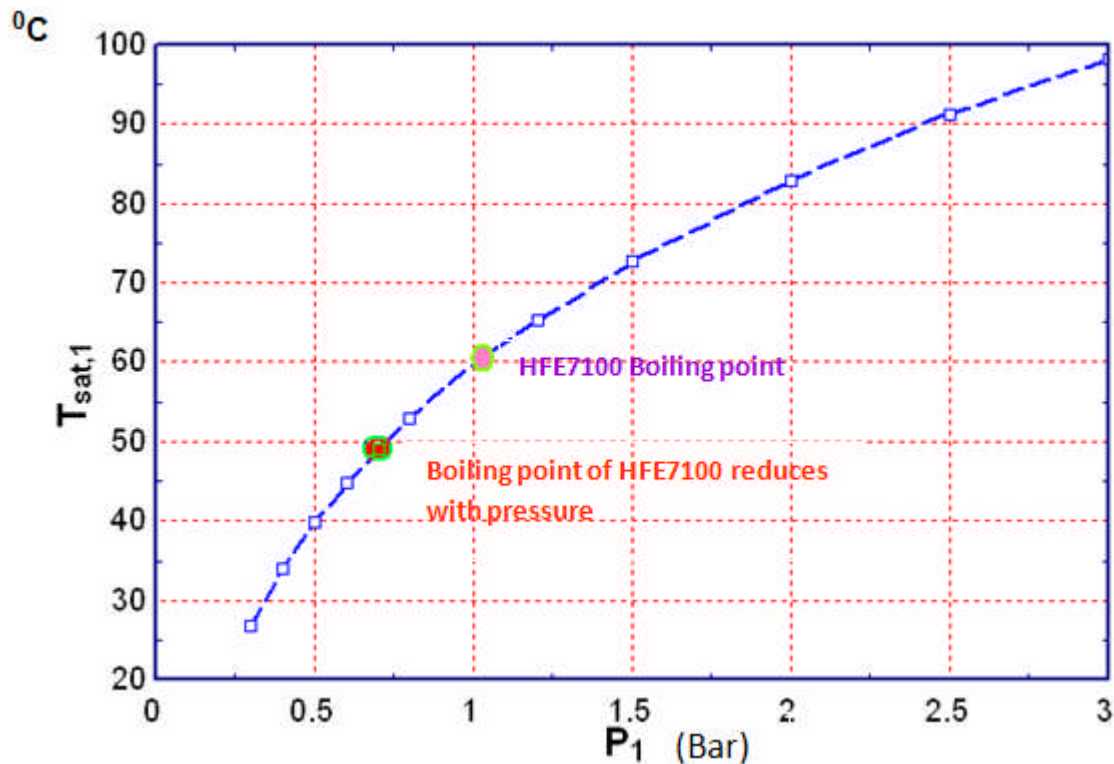
Figure 6.17: T_sat vs. P chart on effect of pressure on T-sat (HFE7100). The red and purple dots are values at 0.7 and 1.03 bar respectively. (EES software; 1992-2008).

The significance of this assumption is that the boiler imposes a limitation on the maximum attainable temperature of 115^oC, and this cannot be exceeded because the electric boiler output is only 9kW. Therefore, by lowering the pressure in the generator below atmospheric pressure more working fluid can be vaporised in the generator at the temperature of which heat is transfer from the boiler, the ratio $T_{gen,\ e}$ / $T_{boiler,\ i,}$ being about 0.89. The test results indicated that at higher flow rates the quality of working fluid deteriorates to a mixture or poor quality because of the temperature limitation associated with the boiler output, which is inadequate at higher turbine pressure. Both temperature and pressure are obviously dependent properties especially during the process of phase

161

change i.e., Tsat = f(Psat). The implication of this phenomenon is that Tsat increases with Psat. This means that a substance of higher pressure will boil at a higher temperature. However, poor quality vapour at the expander inlet could damage the vanes and reduce efficiency of the expander because of liquid molecule that will constantly bombard the vanes impeding effective overall performance of the expander. The expander shaft speed is a crucial and very important factor in electricity generation in the automotive alternator. The alternator, which is used as the electric generator, is a 140A Bosch alternator with a cut-in at about 800rpm.The cut-in is the ignition point of the alternator when it starts producing electrical power of a few watts at the 850-rpm mark. The maximum output is usually at higher rotational speed (rpm) between 1500 to 6000 rpm as indicated in Table 6.4 and Figure 6.18. The maximum output at 6000rpm is 1752W from the chart. Most of the alternators used are from automobile breakdown garages, which could be a positive way of recycling used alternators instead of dumping them in landfills constituting environmental degradation and pollution. The use of alternators for micro-power generation can become a novel way of providing electricity in rural areas and poor settlements in developing countries that are off grid and without any form of electricity supply. There is also the possibility of integrating the device into low temperature heat sources as a heat recovery device that implements the ORC Rankine process using low-grade heat to produce electricity and some form of domestic hot water though this in many instances have been found to be low.

Table 6.4 Computed alternator Rpm and output by comparing data from different manuals. The 140A alternator cut-in ranges from 800rpm. To achieve higher output the rpm must increase with the increasing output from the prime mover.

Alternator Rpm	Current (A)	Power(a*v) (W)
800	0	0
850	10	120
1000	20	240
1500	80	960
2000	107	1284
2500	120	1440
3000	128	1536
3500	135	1620
4000	139	1668
4500	141	1692
5000	144	1728
5500	145	1740
6000	146	1752
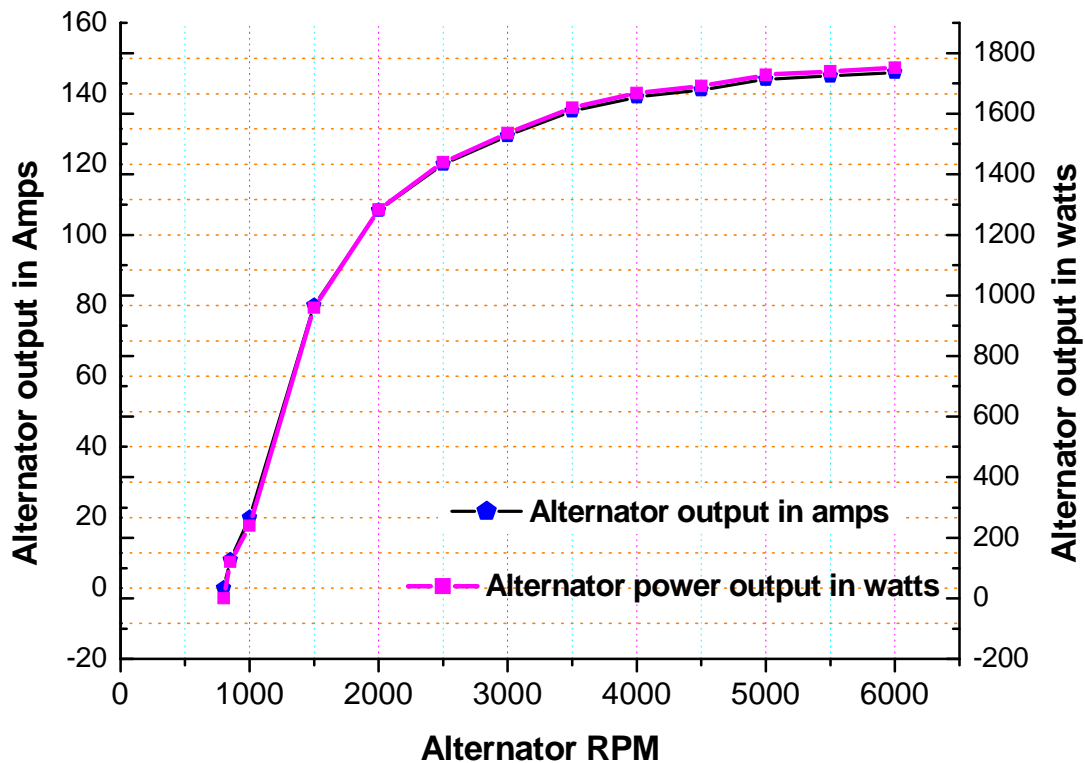
Figure 6.18: Alternator output is computed by comparing chart from manuals of different brands of 140A alternators. The power output is derived by multiplying the amperes and the battery output voltage at 12volts.

6.2.3 Test Categories and measured data

The test results are analysed based on test performed at steady state conditions, putting into consideration the flow pattern in the condenser. The initial test is counter flow in the condenser as contrasted with subsequent tests, which is configured as parallel flow in the condenser and later interchanged between the two processes. This is to regulate the temperature of the condenser heat sink, as this affects the working fluid temperature pumped back into the evaporator. If the working fluid temperature is sub cool, then more energy will be required to vaporise the working fluid in the evaporator thus increasing the amount of energy

required in the boiler. This however happened while testing with HFE7100 which has a higher boiling point compared to HFE7000.

6.2.4 Results of Experimental Test – 1

The first test involved system evacuation by applying a vacuum which is achieved by means of a vacuum pump that is connected to the system

Figure 6.19: Vacuum pump and connection arrangements

through a suction tube with a fitted valve. The valve serves two purposes one of which is retaining the vacuum and or enabling the introduction of the working fluid into the system, as shown in Figure 6.19. Once vacuum is established in the system as monitored from the readings of the pressure sensors captured and displayed in the monitor screen, the working fluid can then be drawn into the receiver to a desired quantity. The fluid injection process is enabled by the existence of a vacuum condition. This is however different from pulling a vacuum for the purposes of commencing an experimental test. The various components integrated to create the cycle have been carefully sealed to retain the vacuum condition using appropriate sealants and ensuring that joints and pipe couplings are properly brazed or welded. Compressed fittings are used and pipe threads

are properly secured to avoid leaks. These series of tests considered specific cycle parameters including the working fluid property, shown in Table 6.5, which is of great significance especially in predicting the performance of the cycle.

Table 6.5: Properties of HFE 7100

Properties of HFE7100						
Chemical Name	Molecular formula	Molecular weight	Critical pressure	Critical temp.	Critical density	**Heat of Vaporization
Methoxy-Nonafluorobutane	$C_4F_9OCH_3$	250g/mol	2.23MPa	195.3^{o}C	555kg/m^3	111.6kJ/kg

* HFE7100 liquid density@ 25°C–1475kg/m^3; Boiling point–61°C, **@ B.P

6.2.4.1 Test Conditions and measured data

Table 6.6: Test Parameters

HFE 7100 flow rate %	Time [h:m:s]	Turbine RPM	Gauge pressure @ turbine inlet(bar)	HFE 7100 flow rate(l/min)	Vapour quality in sight glass
10	11:08:40	880	- 0.12	30.0	Clear
13	11:13:10	1036	-0.01	37.5	Clear
16	11:30:00	1150	0.11	47.5	Clear
19	11:45:00	1225	0.20	55.0	Clear
22	12:00:10	1275	0.31	62.5	Clear
25	12:16:20	1309	0.41	70.0	Clear
27	12:33:30	1330	0.50	75.0	Clear
29	12:49:50	1355	0.55	80.0	Clear
30	14:22:00	1366	0.59	85.0	Moisture

Table 6.6 and Table 6.7 shows the experimental parameters, test conditions and measured data. The test condition shows the recorded experimental sequence and measured data include both the temperature and pressure at the inlet and outlet conditions as well as the calculated

values of the heat balance between the vapour generator and the condenser. Table 6.6 shows the experimental outlines during the test indicating working fluid flow rate in percentage increments. The percentage flow rate is adjusted through the pump setting by means of a regulator. The actual flow rate is read from the working fluid flow meter in litres per minute as recorded in the table. The expander rpm is measured with a tachometer in revolution per minute. The vapour quality as observed through the sight glass is either dry or a mixture of vapour and liquid is observed in course of the experimental test. This is usually an indication that the saturated vapour quality has deteriorated and the test will normally end once this occurred.

The reason is that the liquid molecules of the working fluid incident on the expander vanes could cause damage to the vanes and the expander compromised. The performance of the expander is also affected because of the poor quality of the vapour. The enthalpy and working fluid flow rate in kg/s are computed in Table 6.7 however, the value of the enthalpy in the same table is determined using the EES software, which calculates the values when both the temperature and pressure are entered as parameters.

Table 6.7: ORC Experimental Data from Test - 1

| Pump setting | Turbine | | | | | | | Generator | | | | | |
	inlet T [°C]	Outlet T [°C]	Inlet P [Bar]	Outlet P [Bar]	Inlet h (kJ/kg)	Outlet h (kJ/kg)	ΔH (kW)	rpm	Refr. Outlet T[°C]	Refr. inlet T[°C]	Heat Input Kw	Heat from Cond.[kW]	mass flowrate[Kg/s]
10	89.91	71.53	-0.01	-0.42	233.4	216.2	0.370	880	91.17	21.74	4.01	3.52	0.022
13	93.95	80.67	0.009	-0.35	237.1	224.9	0.332	1036	95.36	24.14	4.45	4.66	0.027
16	99.04	87.22	0.14	-0.27	241.9	231.1	0.355	1150	100.5	26.95	5.77	5.72	0.033
19	97.38	88.32	0.26	-0.19	240	232	0.308	1225	98.96	29.85	8.34	6.6	0.039
22	92.55	85.74	0.37	-0.13	235.1	229.4	0.252	1275	94.14	32.45	9.2	7.32	0.044
25	87.93	82.15	0.48	-0.07	230.3	225.8	0.224	1309	89.39	34.52	9.81	7.85	0.050
27	81.93	76.35	0.66	0.031	224.1	220	0.220	1330	83.2	36.27	9.89	8.21	0.054
29	76.9	72.12	0.73	0.112	220.3	215.8	0.258	1355	77.41	37.18	9.87	8.51	0.057
30	79.53	73.96	0.67	0.084	221.8	217.7	0.243	1366	80.95	36.61	9.58	8.51	0.059

168

Figure 6.20 and Figure 6.21 indicate the relationship between the flow rate and the expander rpm, as well as the temperature variation of the expander and the evaporator. The expander rpm in Figure 6.20 increases as the working fluid flow rate increases. At some instances during the experiment, the rpm did not increase with the flow rate especially when there is a mixture of liquid and vapour in the flow stream at the inlet of the expander. This phenomenon is usually due to the effect of the liquid molecules on the vanes of the expander as the droplets incident on the vane surface impede its rotational motion thus a slur in speed is noticed when measured with a hand held tachometer.

The flow rate is converted from percentage flow rate in litres per minute to kg/min by multiplying with the density of the working fluid as shown in Figure 6.12. However, the flow rate of the working fluid is controlled by means of a control panel that regulates the flow rate in percentage increments. The maximum flow rate at 30% is 3.553 kg/min and by dividing this value by 60 converts the value to 0.059 kg/s.
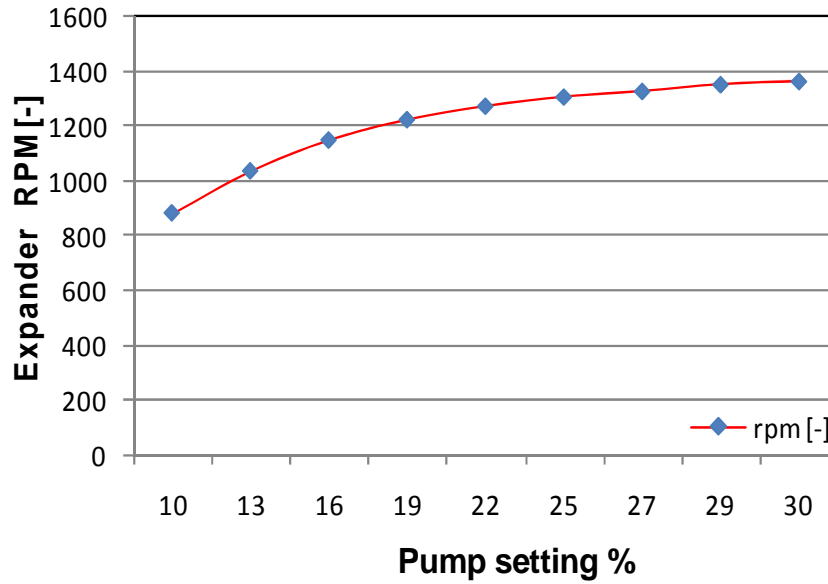
Figure 6.20: Turbine rpm increases with pump setting
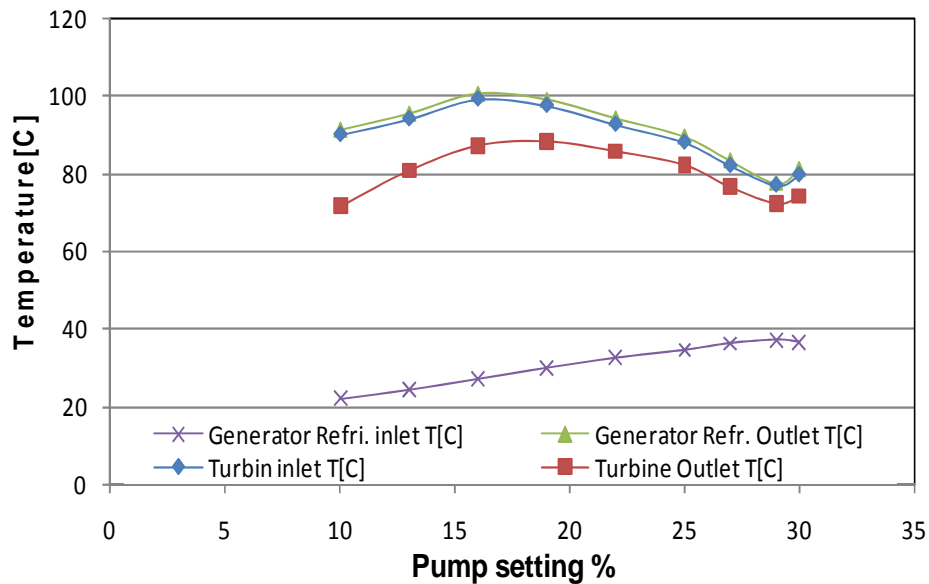
Figure 6.21: Inlet and outlet Temperature vs. pump setting
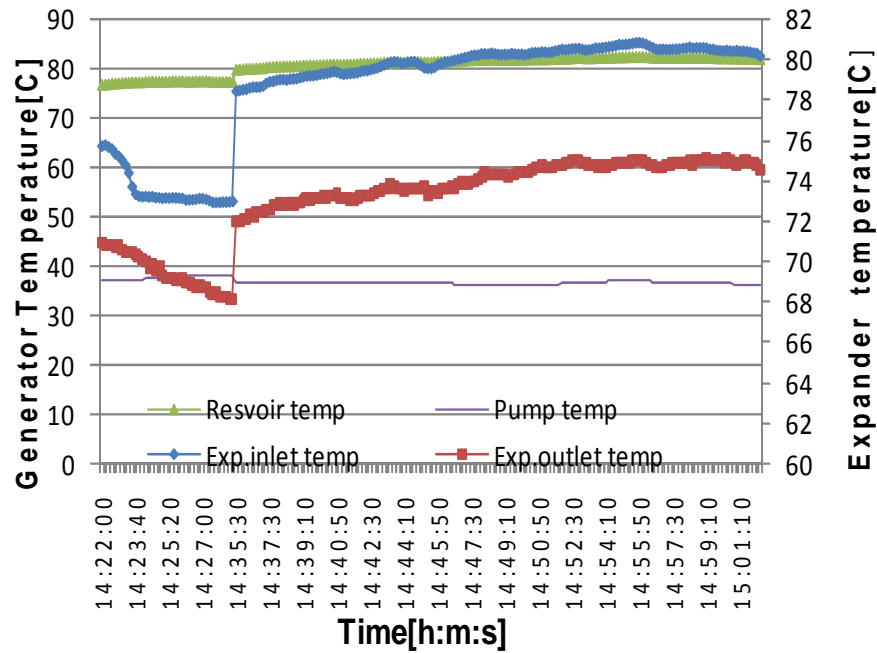
Figure 6.22: Inlet and outlet temperature of Expander, Pump and Reservoir vs.Time
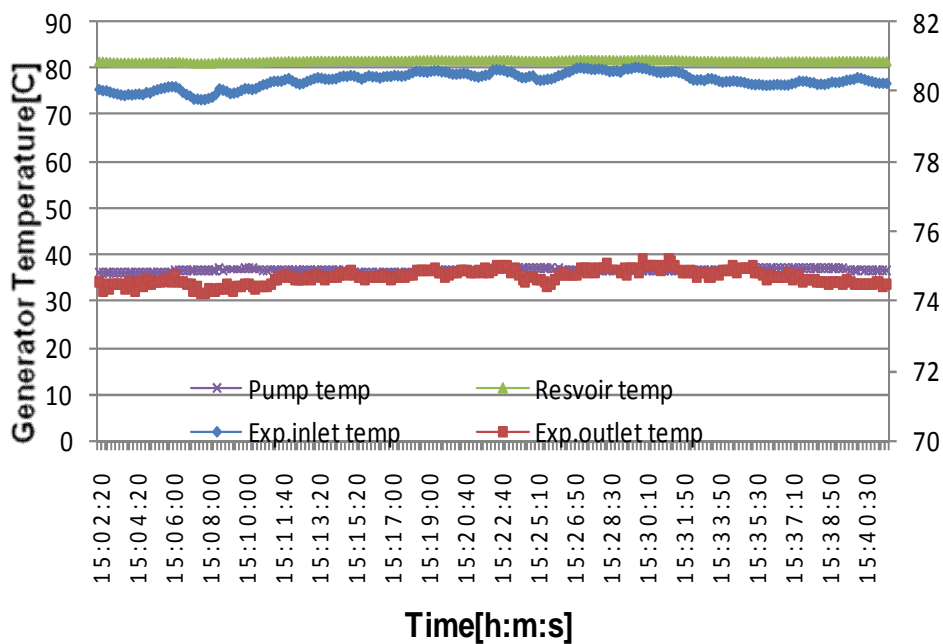
Figure 6.22: Inlet and outlet Temperature of Expander, Pump and Reservoir vs.Time (contd.)

Figure 6.22 is the time related temperature at the exit of the vapour

generator, i.e. before reservoir and exiting into it, the temperature of the

expander as well as the temperature of the pump. The reservoir is actually

a vapour accumulator that allows a continuous and unimpeded flow of

saturated vapour through the expander. The reservoir introduced early into

the cycle is to boost the volume of the space available for the evaporation

of the working fluid apart from that which occurs in the vapour
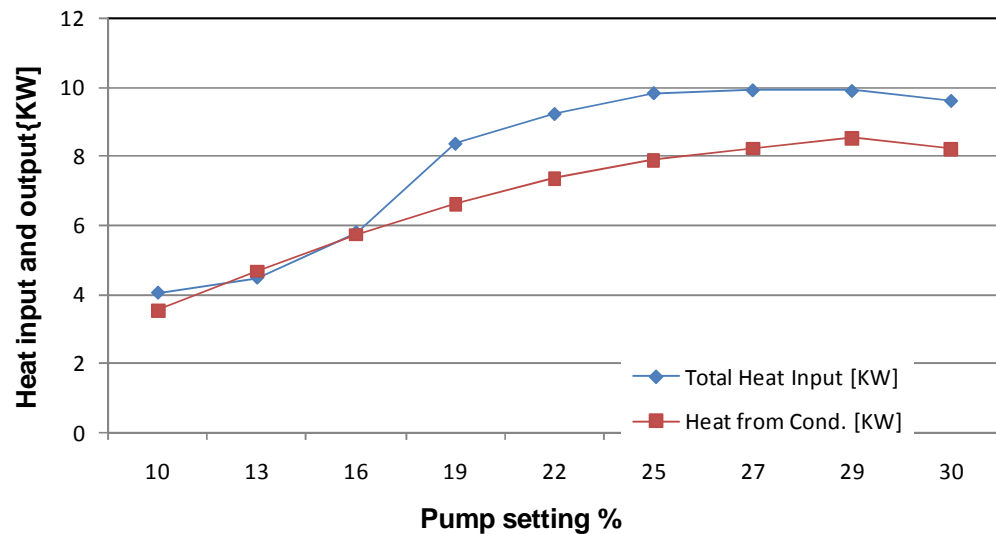
Figure 6.23 Energy balance of Vapour Generator and Condenser vs. Pump setting

generator. Thermocouple sensor and a GP pressure transducer fitted to

the reservoir transmits both temperature and pressure of the vapour

stream to the data logger and can be observed on the monitor and stored

in the computer. The accumulated data are later analysed after each

experiment. Figure 6.23 and Figure 6.24 are the energy balance of the

heat addition and heat rejection of the primary cycle. The primary cycle is

the heat source, from the waterside, and the secondary cycle is the

Organic Rankine cycle operating with an environmentally friendly working

fluid, HFE 7100.
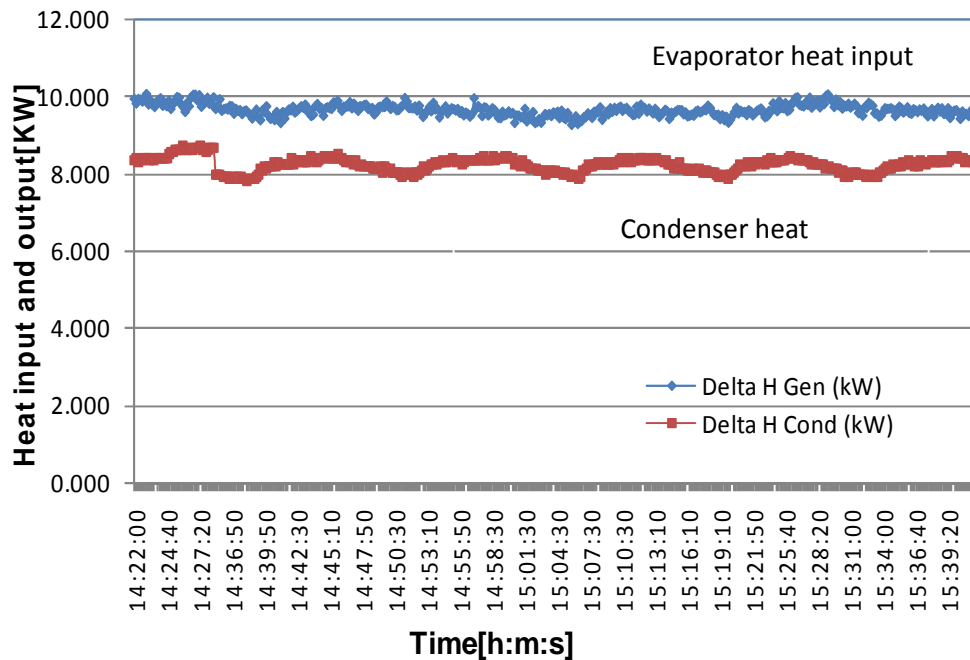
 Figure 6.24: Energy balance of Vapour Generator and Condenser vs. Time

The brazen compact heat exchangers manufactured by Alfa Laval CB76 and SWEP compact heat exchangers are used as both the evaporator for heat addition and the condenser for heat rejection respectively. Figure 6.23 shows the variation of heat input and heat rejection based on the pump flow rate. The heat addition and rejection appears similar between 10% and 16% flow rates but changes appear from the 16% point. This is due to the similarity in flow rate of the primary cycle flow rate and the pump flow rate at this range. The difference becomes apparent from 16% as the pump flow rate increases beyond that of the boiler as indicated in the graph. Figure 6.24 indicate the heat input from the boiler and output from the condenser based on a time scale. The cooling water temperature is fixed at 17°C and the flow rate is 5.9 litres per minute. The cooling water

is from the laboratory central supply. The central cooling system can be used without fluctuations if the experiment is at a time when there is no second user of the central cooling system.

Table 6.8 Ideal Performance parameters of system output (Test 2)

Parameter	Nomenclature	value	unit
Boiler heat rate	Q_{in}	9.269	kW
Condenser heat sink	Q_{out}	8.510	kW
Pump power output	W_p	0.0051	kW
Turbine power output	W_t	0.76	kW
Power required to operate pump	τ_p	0.00697	kW
Net power output	W_{net}	0.725	kW
Carnot efficiency	η_{Carnot}	21.35	%
Cycle efficiency	η_{ideal}	11.50	%
Working fluid mass flow rate	$\dot{m}_{HFE7100}$	0.05930	kg/s
Hot water flow rate	$\dot{m}_{water}$	0.166	kg/s

Table 6.9 Actual performance parameters against pump setting

Pump setting	W_t	W_{net}	Q_{in}	$\eta_{actual,thermal}$
%	(kW)	(kW)	(kW)	[%]
10	0.315	0.302	3.984	7.57
13	0.282	0.271	5.061	5.35
16	0.302	0.289	6.169	4.68
19	0.262	0.247	7.039	3.50
22	0.214	0.199	7.723	2.57
25	0.199	0.197	8.336	2.36
27	0.187	0.185	8.521	2.16
29	0.219	0.207	8.666	2.39
30	0.207	0.204	9.269	2.20

Table 6.8 is derived by modelling an ideal system at the 30% mark using data in close approximation to experimental data while Table 6.9 is derived

by calculating for the actual cycle performance, and involves some degree of irreversibility in the system. The thermal efficiency is far smaller in the actual cycle when compared to the ideal, which does not involve any exergy loss.

The thermal efficiency is set against the pump setting and progressively decreases with increase in the flow rate as shown in Table 6.9. The thermal efficiency is dependent on the difference between the expander output and the pump output ($W_{net)}$. However, the expander rpm in Figure 6.20 increases with the flow rate; a factor that has to do with the increase in pressure and temperature at the evaporator and expander inlet port.

(a)   **(b)**
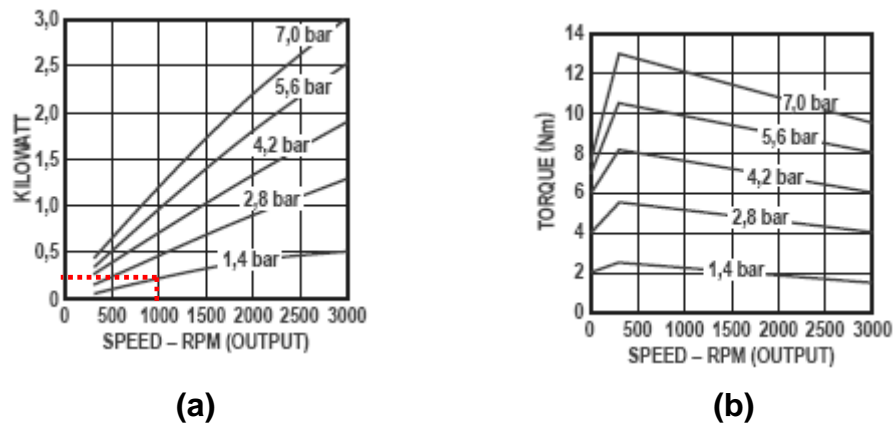
Figure 6.25: Performance chart showing output range of expander

The actual expander work output of 0.207kW at slightly above 1000rpm is similar to that specified in the product technical manual and specification Figure 6.25(a) with corresponding torque in Figure 6.25 (b) [130]. However, it must be noted the experimental result shows expander performance under load conditions at variance under a no load test shown in Figure 6.25. The dotted lines in Figure 6.25a shows output at 1000rpm at a lower pressure than the 1.4bar indicated in the chart. The model 6AM

Gast Air motor employed in this experiment has been selected from an array of different models indicated in Figure 6.26 [130] because it presents the best case scenario of maximizing the performance characteristics of the cycle. Except for leaks in the expander through the seals at higher pressure, its role as a substitute to a conventional turbine is promising as the leaks can be contained with proper sealing method and heat resistant seals which can be sourced from credible manufactures of such products. The known performance characteristics and that observed through the laboratory tests indicate that;

❖ The expander output power is relative to both expander speed and the stream pressure.

❖ The expander slows down with increase in load just as the torque increases to a point where it matches the load; however, the load is normally due to electrical load, which imposes a mechanical load on the prime mover to the stalled condition if there is no further increase in both the stream pressure and expander speed.

❖ Motor speed increases with reduction in load and the torque will normally decrease to match the reduced load
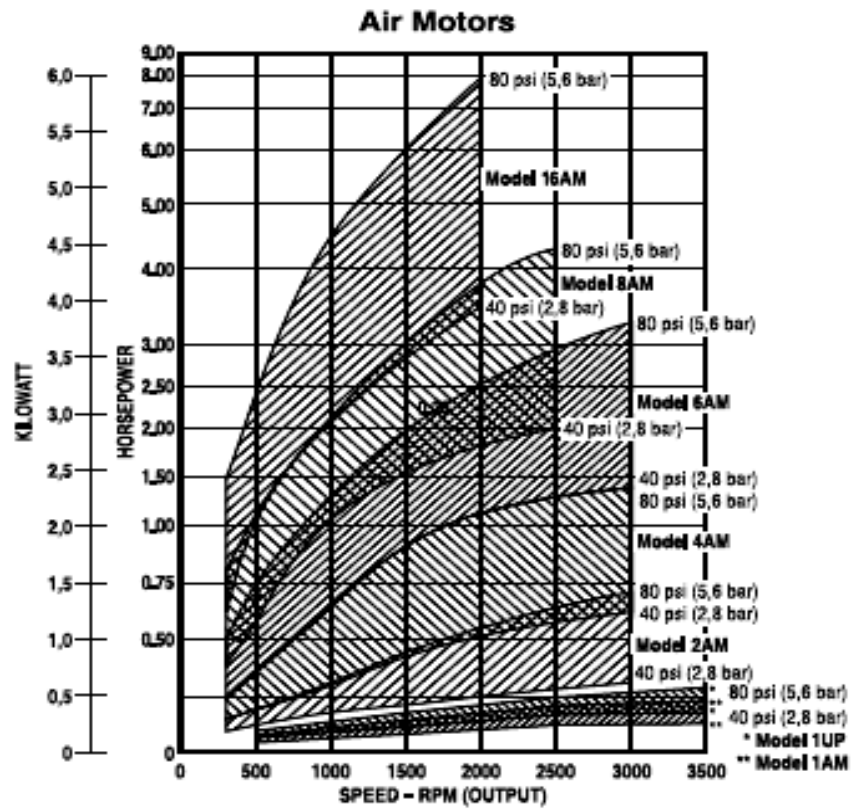
Figure 6.26: Performance ranges of various models of Air motors

6.2.5 Results of Experimental Test – 2

The introduction of a recuperator in the cycle in Test - 2 is an improvement strategy to Test - 1 and also a heat recovery measure to boost the heat transfer mechanism of the system. The recuperator in Figure 6.27 is introduced at the exhaust of the prime mover in order to extract heat and to preheat the working fluid being pumped into the vapour generator
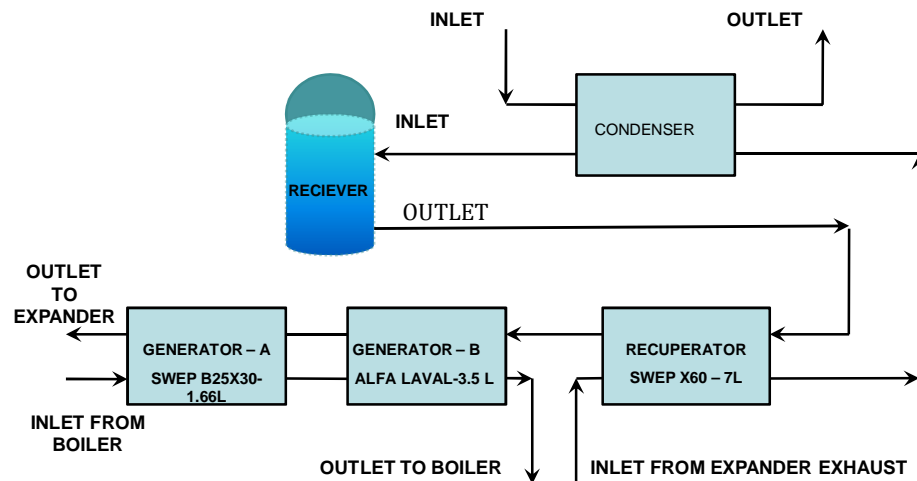
Figure 6.27: Compact heat exchanger configuration
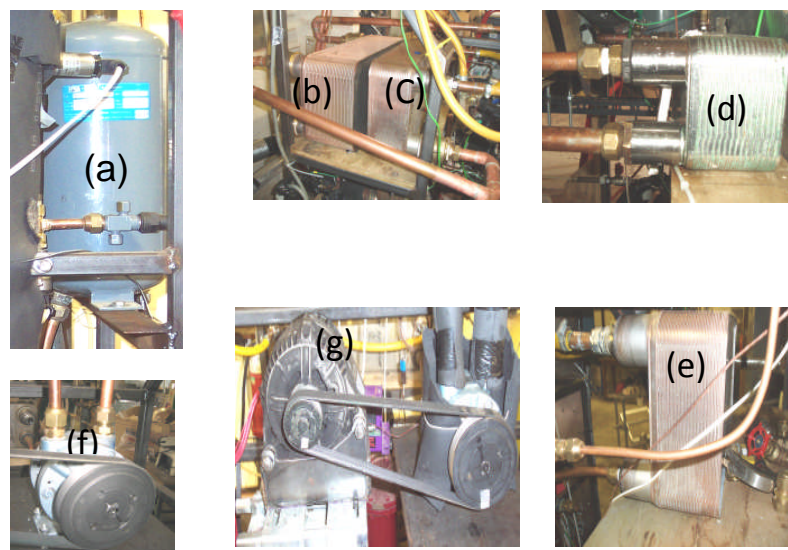
Figure 6.28: Photo of heat exchangers, receiver and prime mover.

from the receiver. This is realised by networking of a series of compact heat exchangers c, d, e linked to b, the recuperator. The receiver, prime mover and automotive alternator are represented by the alphabets; a, f, g respectively in Figure 6.28. The letter c represents the condenser; d and e is both the intermediate and main vapour generator. Figure 6.29 is the schematic diagram of the integrated cycle showing the heat exchangers, the primary hot water loop and the secondary HFE7100 loop and other components that make up the system.
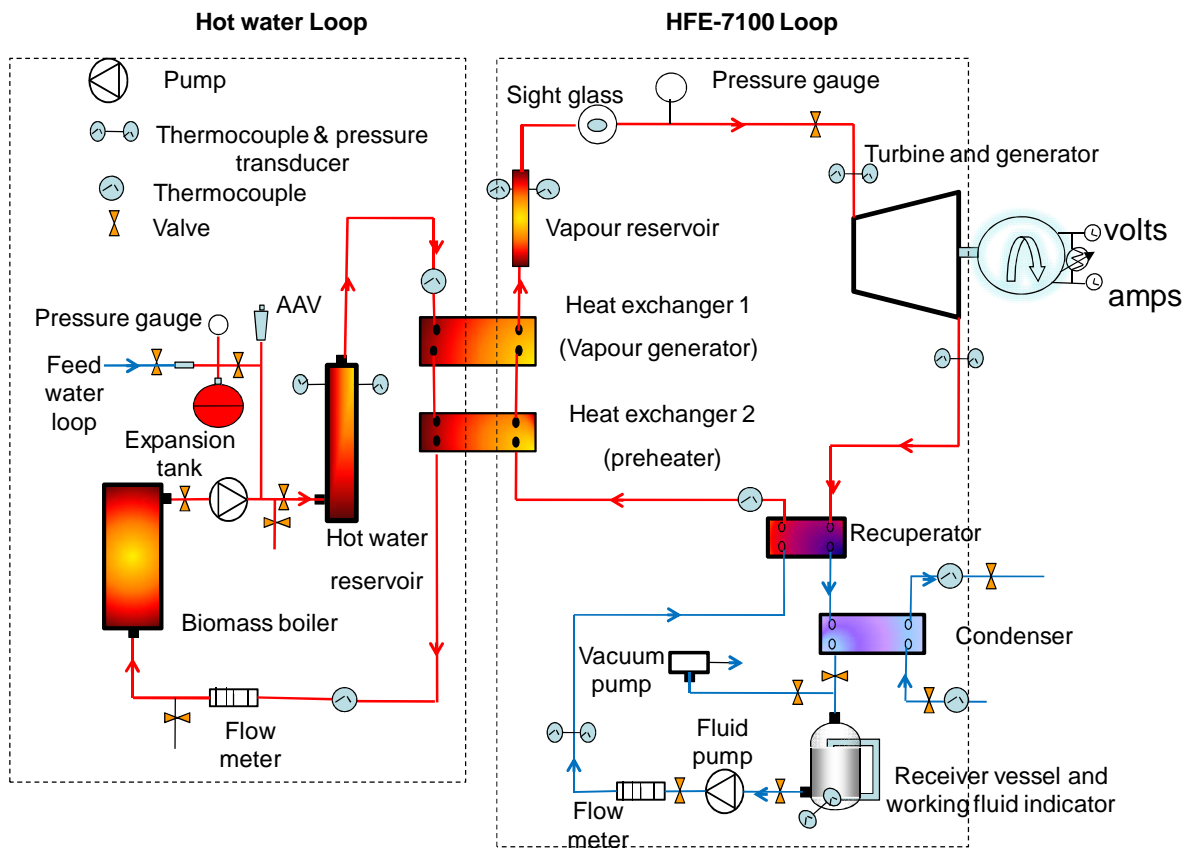
Figure 6.29: Improved Primary and Secondary loop with the introduction of a Recuperator and Pre-heater (Generator 2)

The specification of the compact heat exchangers is shown in Table 6.10;

Table 6.10: Compact heat exchanger Type and Specification

Model/Type	Alfa Laval (CB76)	SWEP (B120)	SWEP (B25)	SWEP (B15)
Description	Generator B	Generator A	Condenser	Recuperator
No. of plates	28	30	40	60
Dimension (mm)	93x120x190	80x115x525	106x240x520	155x240x520
Total volume (l)	3.5	1.55	4.5	6.989
Working Temp. [C]	225	185	225	225
" Pressure (bar)	30	30	27	27

This experiment involves the use of vacuum, a process that is already described in the second test. The use of the recuperator in the cycle also improves the nature of heat transfer so that heat transfer to the working fluid occurs at a higher average temperature and thus the system performance is increased. The flow stream in the condenser is counter flow. The results from this experiment are considered and analysed based on the test parameters in Table 6.11. This is also further indicated in

6.2.6 Test Conditions and measured data

Table 6.11: Test Parameters

HFE7100 flow rate %	Time [h:m:s]	Turbine RPM	Gauge pressure @ turbine inlet(bar)	HFE 7100 flow rate(l/min)	Vapour quality in sight glass
10	10:03:00	190	0.35	23	Clear
13	10:14:20	301	0.50	35	Clear
16	10:33:00	421	0.70	41	Clear
19	10:43:50	519	0.85	47	Clear
22	10:53:20	606	1.00	56	Clear
25	11:03:20	675	1.20	62	Clear
28	11:14:40	720	1.35	71	Clear
31	11:26:20	775	1.50	80	Clear
34	11:36:20	814	1.65	92	Clear
37	11:46:20	850	1.80	101	Clear
40	11:56:20	872	1.85	107	Clear
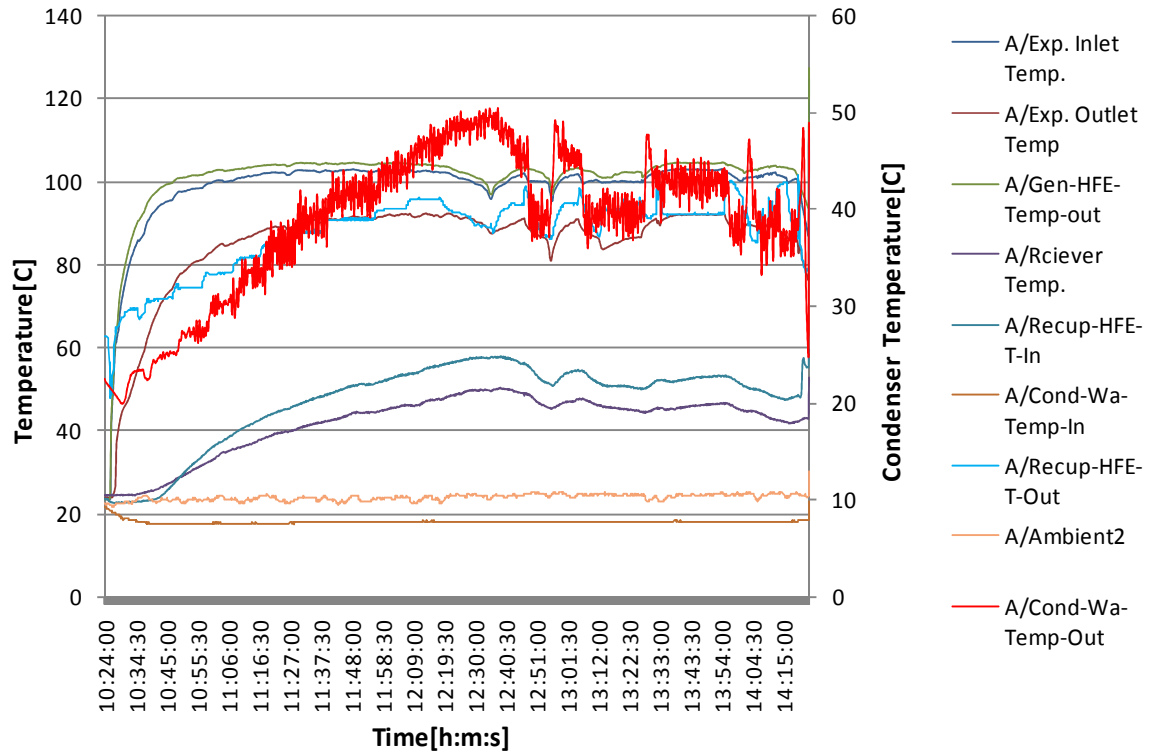
Figure 6.30: Inlet and outlet temperature versus Time
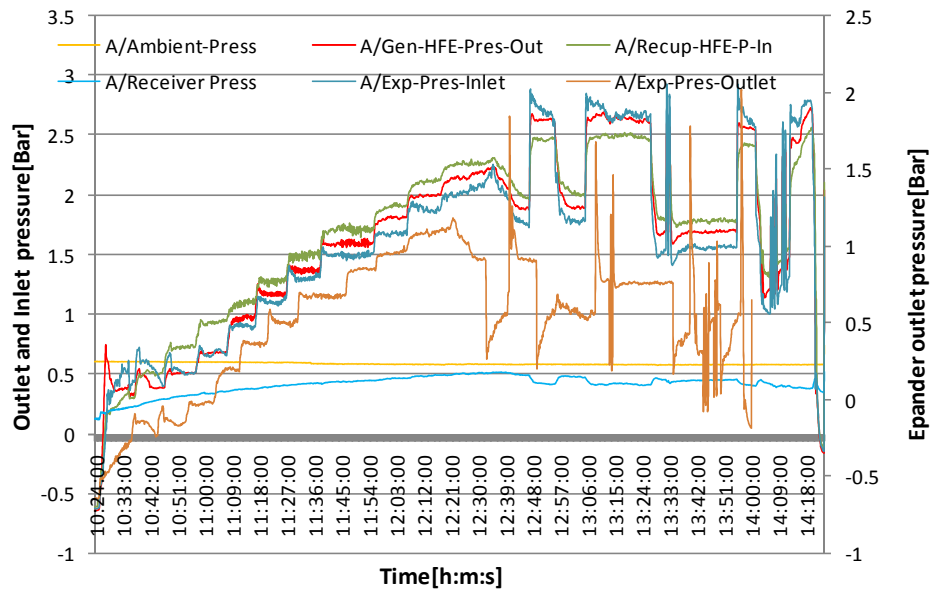
Figure 6.31: Inlet and outlet Pressure versus Time

charts and graphs depicting the various system Performances. Table 6.12

indicate the temperature variations at the inlet and outlet channels of the

expander, generator and the recuperator as well as the pressure and time related performance characteristics of the system. The results are also tabulated based on the system flow rate in percentage increments. The heat addition and rejection are also indicated. The expander rpm is relative to the flow rate, pressure and enthalpy differential at the expander inlet and outlet conditions. The expander and vapour generator pressure and enthalpies at the inlet and outlet conditions including the recuperator inlet and outlet conditions are indicated. Turbine and or expander in this work is used interchangeably.

The expander pressure and enthalpy drop are also a significant factor in the operation and performance of the expander as a higher pressure and enthalpy drop means a better expander performance, as demonstrated in Figure 6.32, Figure 6.33 and Figure 6.34. Aided by pressure and enthalpy drop at the exit port, the vapour stream will push the mechanism providing acceleration at the expander's shaft with increase in the average rpm. There is however some degree of laboratory limitations to the expander's performance imposed by the output of both heat source and supply temperature.

The 9kW electric boiler supplies heat at the temperature of about 115°C to the evaporator which remained the maximum output temperature in this electric boiler tests when compared to similar systems in literature operating at higher boiler output and temperature.

Table 6.12: ORC experimental data from Test - 2

Pump	Turbine									Working fluid	Generator		Recuperator		Total Heat Input	Heat from cond.
setting%	inlet T[C]	Outlet T[C]	Inlet P[bar]	Outlet P[bar]	Inlet h [kJ/kg]	Outlet h [kJ/kg]	ΔH turbine (kW)	rpm [-]	Flowrate [kg/min]	Ref. Outlet T[C]	Work. inlet T[C]	inlet T[C]	inlet T[C]	outlet T[C]	[kW]	[kW]
10	80.06	50.05	0.45	-0.354	222.7	195.5	3.88	252	7.77	84.68	24.33	22.72	68.22		3.01	3.01
13	92.54	67.69	0.55	-0.167	234.7	211.3	3.47	405	8.39	96.98	25.84	24.07	71.14		3.45	3.45
16	97.37	78.57	0.54	-0.13	239.5	222.5	2.76	493	8.79	100.82	29.39	30.24	74.19		3.99	3.99
19	99.45	83.53	0.660	-0.03	241.4	227	2.38	596	8.97	102.21	33.21	36.28	77.5		4.67	4.67
22	100.7	86.33	0.88	0.16	242.2	229.4	2.17	683	9.07	103.02	36.16	40.65	81.08		7.87	7.87
25	101.69	88.7	1.106	0.36	242.8	231.3	1.98	752	9.14	103.72	38.75	44.02	84.42		6.17	6.17
28	102.19	90.15	1.307	0.507	243.5	232.5	1.84	809	9.19	104.11	40.67	46.62	87.62		6.73	6.73
31	102.25	91	1.486	0.664	242.7	233	1.73	850	9.21	104.05	43.17	49.87	90.59		7.25	7.25
34	102.42	91.7	1.674	0.844	242.5	233.3	1.65	890	9.22	104.13	44.97	52.23	93.19		7.89	7.89
37	102	91.84	1.869	0.943	241.9	233.3	1.59	918	9.22	103.88	46.33	54.16	95.43		8.24	8.24
40	101	91.63	1.99	1.059	240.8	232.8	1.48	940	9.20	102.65	48.07	56.1	93.46		8.7	8.7
42	99	90.39	2.09	1.102	244	235.3	1.36	958	9.30	100.78	49.44	57.23	90.12		9.05	9.05

These are between 20 - 60kW output boilers and supplying heat with temperatures well above 350°C [95]. However the output of this system
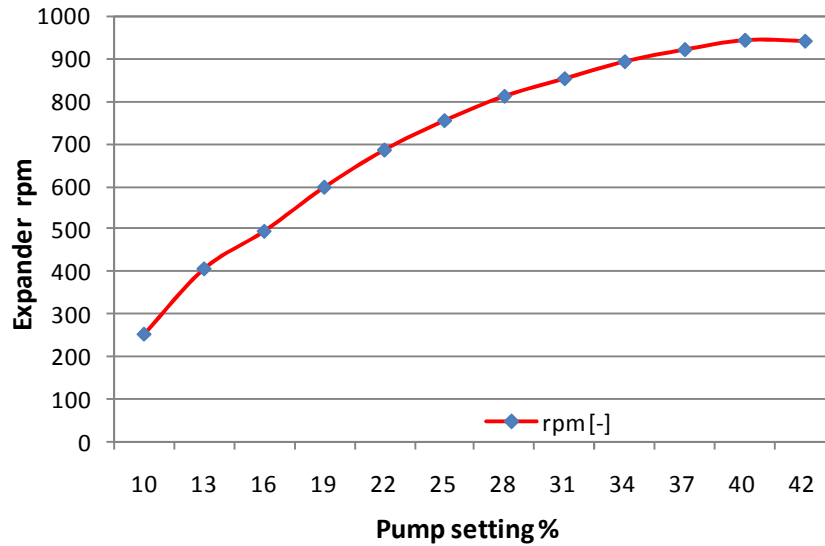
Figure 6.32 Expander rotational speed vs. pump setting
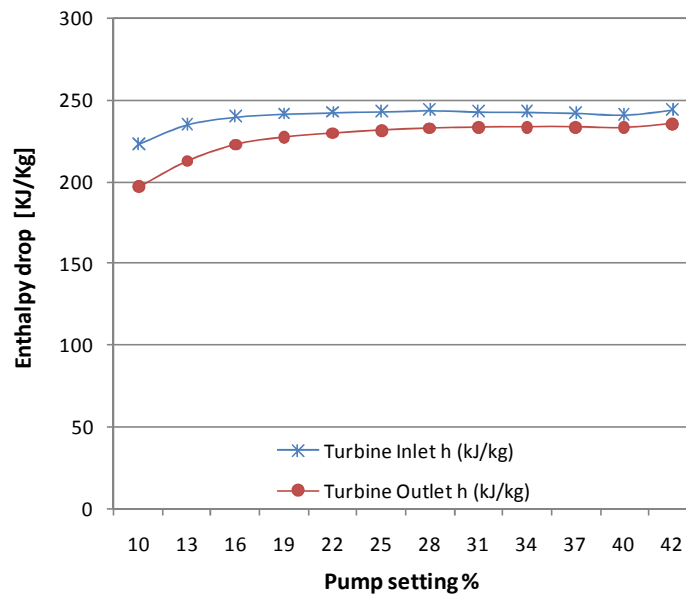
Figure 6.33 Expander enthalpy drop vs. pump setting
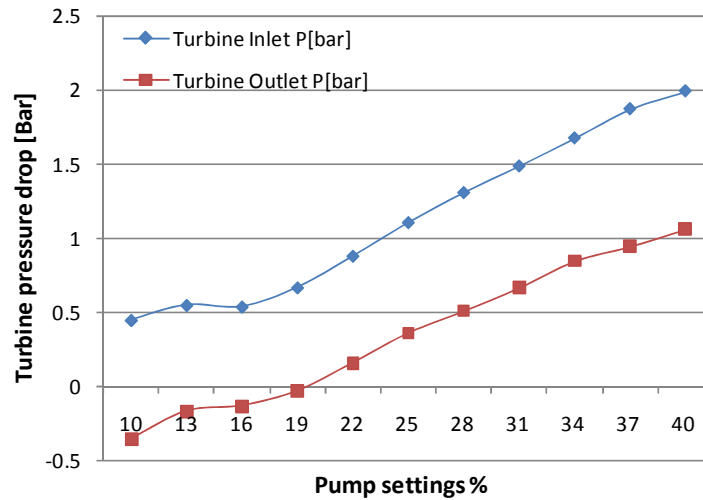
Figure 6.34 Expander pressure drop vs. pump setting

with respect to the electric boiler performance is quiet low and was a major constraint affecting the system performance. The heat demand at higher flow rates and pressure could not be met by the boiler as temperature drops at higher pressures. The consequence is a drop in expander rpm despite increasing the flow rate. This makes it obvious that expander rpm drops with the heat input and temperature as indicated in Figure 6.30. This performance characteristic, points to the fact that the boiler heat output cannot support further heat demand by the system. This is a laboratory limitation resulting from the maximum output of the boiler and therefore system optimization was effected to extract the maximum heat from the boiler. Figure 6.33 and Figure 6.34 shows the margins in both enthalpy and pressure drop respectively when viewed against the rpm in Figure 6.32. The pressure drop appears to have a resounding effect on the expander rpm as the enthalpy drop though significant has a slim differential margin. The energy balance of the system is indicated in Figure

6.35 while the characteristics of the heat output in various components are shown against the working fluid flow rate in Figure 6.36. In both cases, the
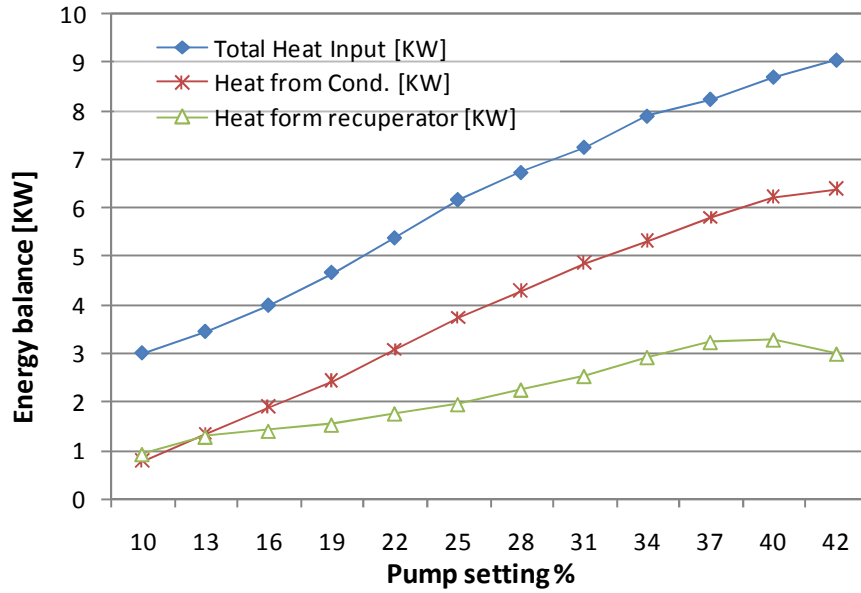
Figure 6.35 Cycle energy balance vs. pump setting
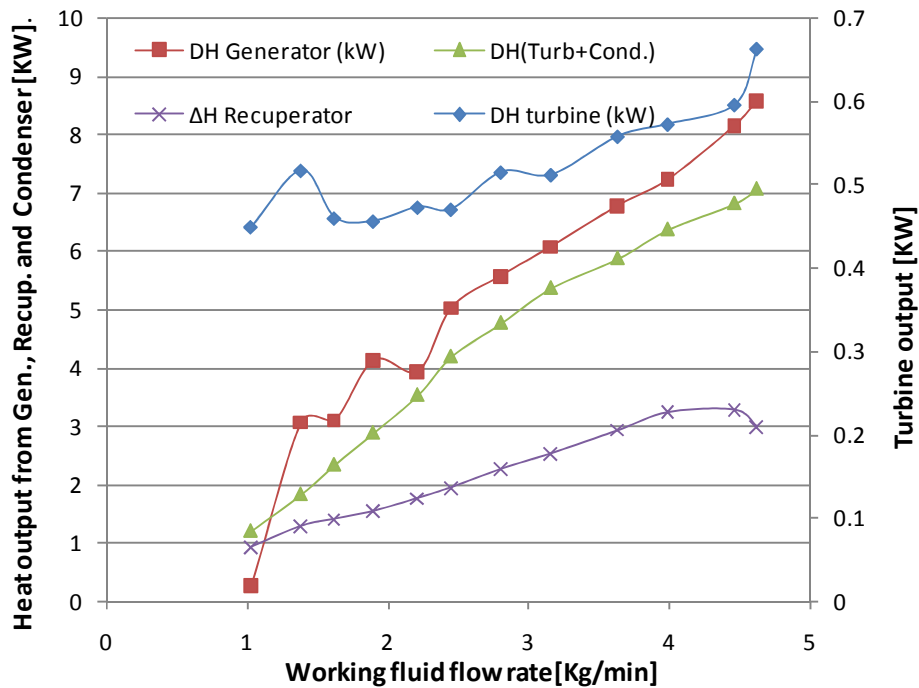
Figure 6.36 Heat output and heat rejection in various components vs. working fluid flow rate

output is in kW and indicates that heat output or heat rejection is influenced by the flow rate. The EES modelling for an ideal system is indicated in Table 6.13 while the actual cycle performance analysis is indicated in Table 6.14 which due to irreversibility in the various components making up the cycle is much lower than the ideal.

Table 6.13 Ideal Performance parameters of system output (Test 3)

Parameter	Nomenclature	value	unit
Boiler heat rate	Q_{in}	8.70	kW
Condenser heat sink	Q_{out}	6.21	kW
Pump power output	W_p	0.0396	kJ/kg
Turbine power output	W_t	12.50	kJ/kg
Power required to operate pump	τ_p	0.00317	[-]
Net power output	W_{net}	12.46	kJ/kg
Carnot efficiency	η_{Carnot}	17.25	%
Cycle efficiency	η_{ideal}	10.38	%
Working fluid mass flow rate	$\dot{m}_{HFE7100}$	0.0744	kg/s
Hot water flow rate	$\dot{m}_{water}$	0.250	kg/s

Table 6.14 Actual performance parameters against pump setting

Pump setting	W_t	W_{net}	Q_{in}	$\eta_{actual,thermal}$
%	(kW)	(kW)	(kW)	[%]
10	0.380	0.360	3.010	11.98
13	0.440	0.430	3.450	10.10
16	0.390	0.370	3.990	8.50
19	0.380	0.356	4.670	6.20
22	0.400	0.335	5.380	5.73
25	0.400	0.309	6.170	4.30
28	0.430	0.319	6.730	3.90
31	0.430	0.298	7.250	3.30
34	0.480	0.325	7.890	3.20
37	0.485	0.311	8.240	2.80
40	0.500	0.311	8.700	2.60

6.2.7: Experimental Test of the ORC system involving the use of HFE 7000 with electric boiler as heat source.

6.2.7.1 Background

The HFE 7000 as working fluid became necessary because of the limitation imposed by the electric boiler maximum operating temperature at 115°C and the boiler output capacity is 9kW. The boiling point of HFE 7000 is 34°C when compared to HFE 7100, which has a boiling point of 61°C. The saturation temperature at different operating pressures derived from the EES software is indicated in Figure 6.37 and normally considered with respect to irreversibilities within the components of the CHP system.
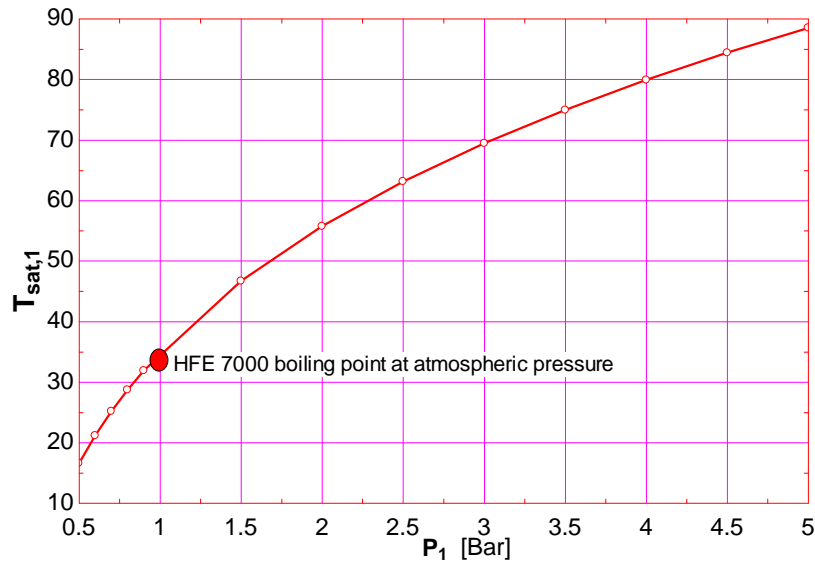
Figure 6.37: T_sat vs. P of HFE 7000 showing the boiling point at atmospheric pressure

Table 6.15: Properties of HFE 7000

Properties of HFE 7000

Chemical Name	Molecular formula	Molecular weight	Critical pressure	Critical temp.	Critical density	*Heat of Vaporization
Methoxy-heptafluoropropane	$C_3F_7OCH_3$	200g/mol	2.48MPa	165.3^{o}C	553kg/m^3	142kJ/kg

*HFE 7000 liquid density@ 25°C – 1400kg/m^3; Boilingpoint–34°C @1atmos; Vapour pressure ~ 64.6 kPa.

This novel heat transfer fluid is environmentally friendly with low global warming potential (GWP) and has advantages as a direct expansion fluid. It has good thermal stability and is non-flammable. The chemical name of HFE 7000 is methoxyfluoropropane and the property at one atmosphere is as indicated in Table 6.15. HFE 7000 and HFE 7100 are highly wetting liquids with low contact angles and surface tension on most surfaces. This created some problems during sealing at joints and pipe couplings and usually brazed or welded joints and compressed fittings are preferable to pipe threads [130]. If pipe threads are used as applicable in this work, epoxy, leak lock, locktite or some other compatible sealant must be used

as suggested by Tuma et al [130]. Teflon tapes sometimes do not always produce desired results and some TFE-based sealants often dissolve in HFE-fluids. Tuma et al, [130] enumerated basic considerations when using the HFE fluids in a heat transfer system as follows;

- ❖ caution in the use of valves with "packed" shaft seals as those designed for water service are prone to leakage and to be avoided; ceramic shaft seals performs better with proper design but magnetically coupled pumps or canned pumps are preferable;

- ❖ With the use of hoses, HFE fluids can extract plasticizers from elastomeric hoses, the reason being that the mass of hose in a system is generally large and thereby becoming a source of contaminant, which can result in systemic problems and ;

- ❖ for low temperature applications, TFE or corrugated stainless hoses can be considered for use;

- ❖ vacuum break valve that opens at a prescribed vacuum level is desirable when sealing the system as the air that enters a system through such a valve can be significant;

- ❖ leaked HFEs evaporates quickly and leaves no residue and ordinary halogen detectors can detect HFE leaks that might otherwise be hard to find when investigating leaks in a conventional way;

- ❖ evaporative fluid loss mechanism can result in high fluid losses over many thermal cycles [131] and can be avoided by employing a valve designed to maintain positive pressure.

6.2.8 Test Conditions and measured data for Test - 3

The test condition for the experimental test - 3 using HFE 7000 is given in

Table 6.16. The use of this novel fluid is an improvement to earlier sets of

tests and parameters. The pump flow rate had increased to 52% but it is

noticed that there is a drop in both rpm and pressure despite increase in

flow rate and this is due to flow resistance resulting in slight drop in

Table 6.16: Experimental Test Parameters

HFE700 flow ratio %	Time [h:m:s]	Turbine RPM	Gauge pressure @ turbine inlet(bar)	HFE7000 flow rate(l/min)	Vapour quality in sight glass
10	10:11:30	0	0	26	Clear
13	10:22:00	564	0.40	27	Clear
16	10:32:20	700	0.50	35	Clear
19	10:40:30	730	0.77	47	Clear
22	10:55:30	818	1.00	53	Clear
25	11:04:40	885	1.15	59	Clear
28	11:13:40	930	1.34	67	Clear
31	11:23:40	966	1.50	76	Clear
34	11:34:20	986	1.70	80	Clear
37	11:49:40	1019	1.85	92	Clear
40	12:00:20	1044	2.00	98	Clear
43	12:12:10	1058	2.15	107	Clear
46	12:23:10	1072	2.25	110	Clear
49	12:34:10	1082	2.40	116	Clear
52	12:45:10	1073	2.32	122	Clear

pressure and expander rpm. This trend is common in most of the tests

carried out but for the experiments performed with HFE 7100, a mixture of

liquid and vapour is observed at higher flow rate because of the same
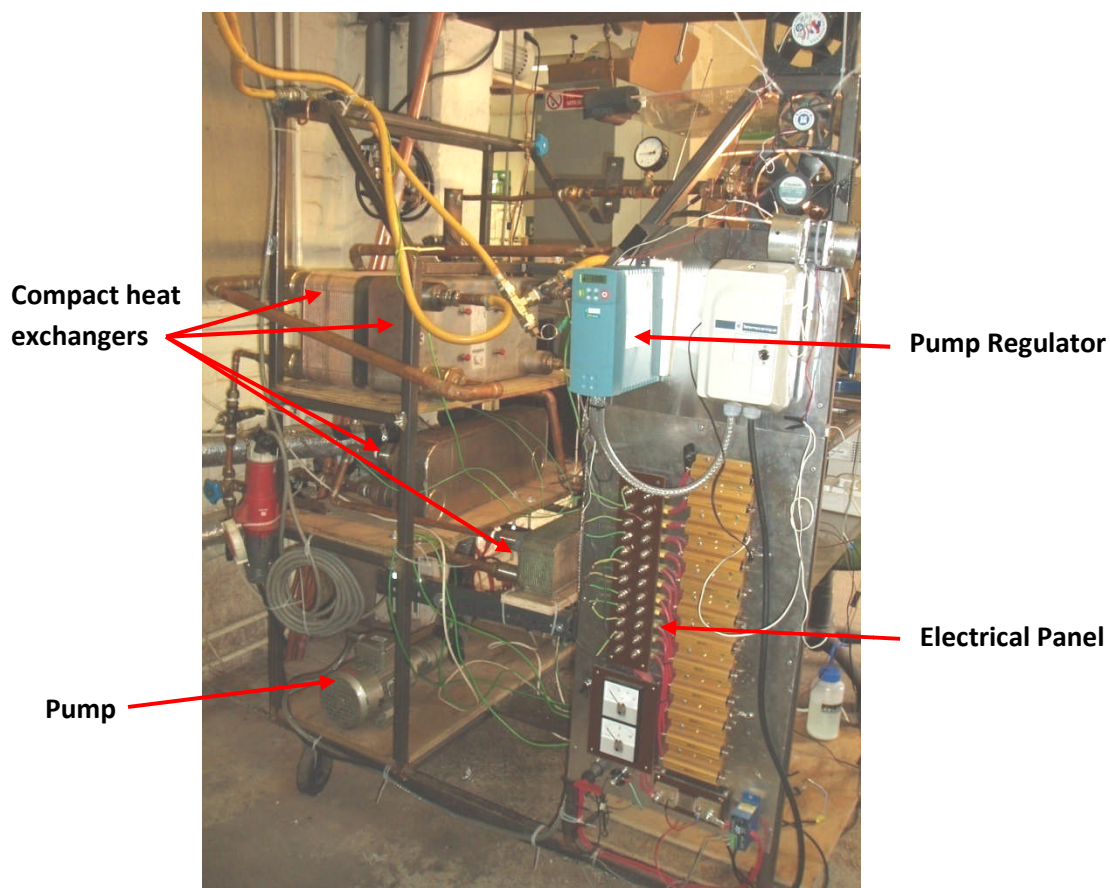
Figure 6.38: Left view of Experimental Test Rig
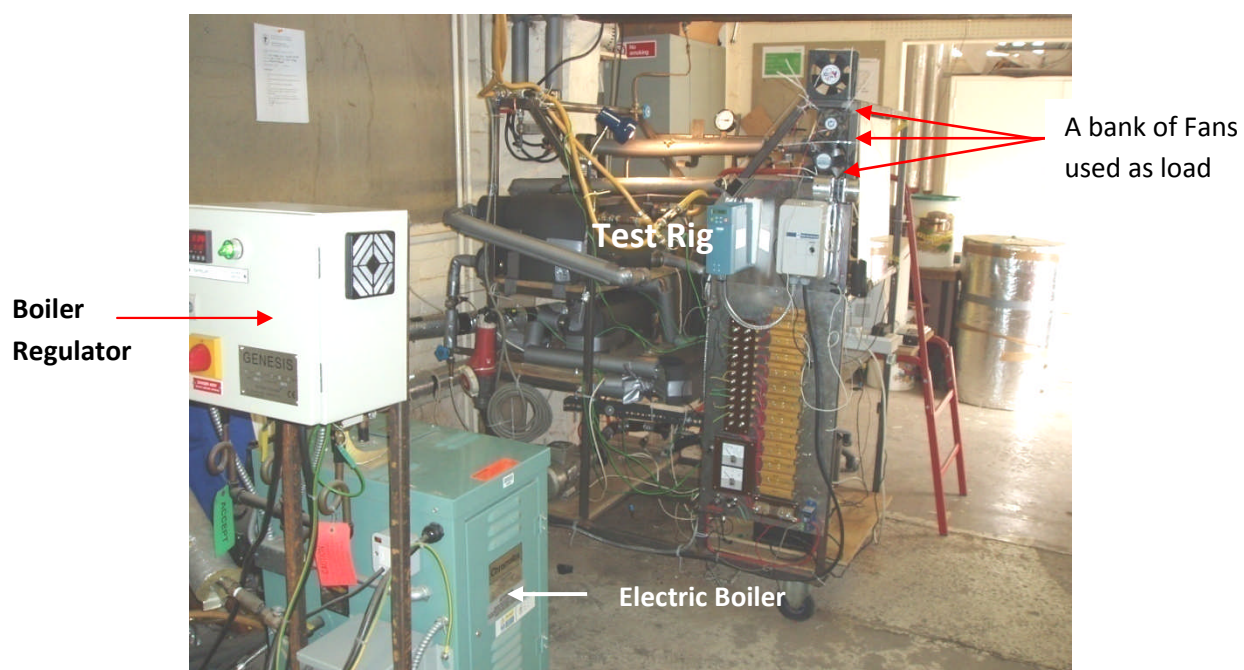
Figure 6.39: Left view of Test Rig showing Electric Boiler and Boiler

Figure 6.40: Right view of Test Rig showing Computer unit and Electric boiler in the background
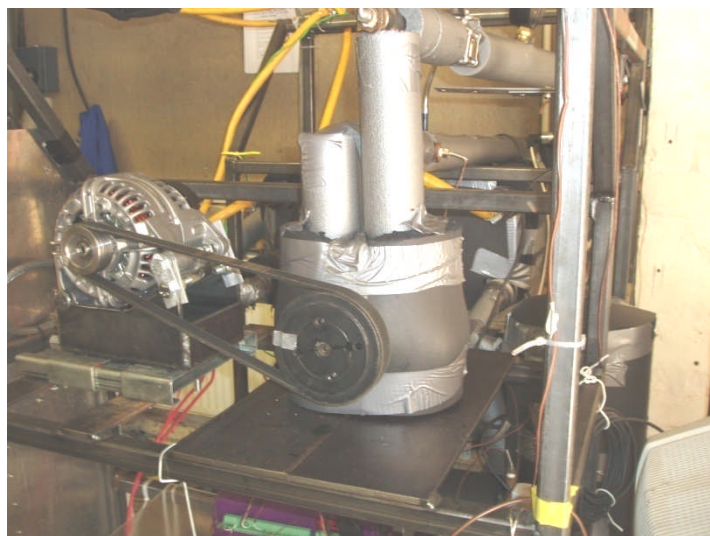
Figure 6.41: Close-up view of insulated Expander and the automotive Alternator used as electric generator

reasons and also because HFE 7100 has a higher boiling point than HFE 7000. In cases where heat demand exceeds supply, there is pressure drop and a deceleration of the expander or turbine rpm. Figure 6.38 to Figure 6.41 show different views and details of the Test Rig without further change in configuration and Figure 6.41 in particular shows the insulated expander a measure aimed at improving system performance. This test performed over a period of five hours has the temperature performance characteristics indicated in Figure 6.42 and pressure performance characteristics shown in Figure 6.43. The data in the Table 6.17 show system performance data and some calculated outcome such as heat addition and rejection.
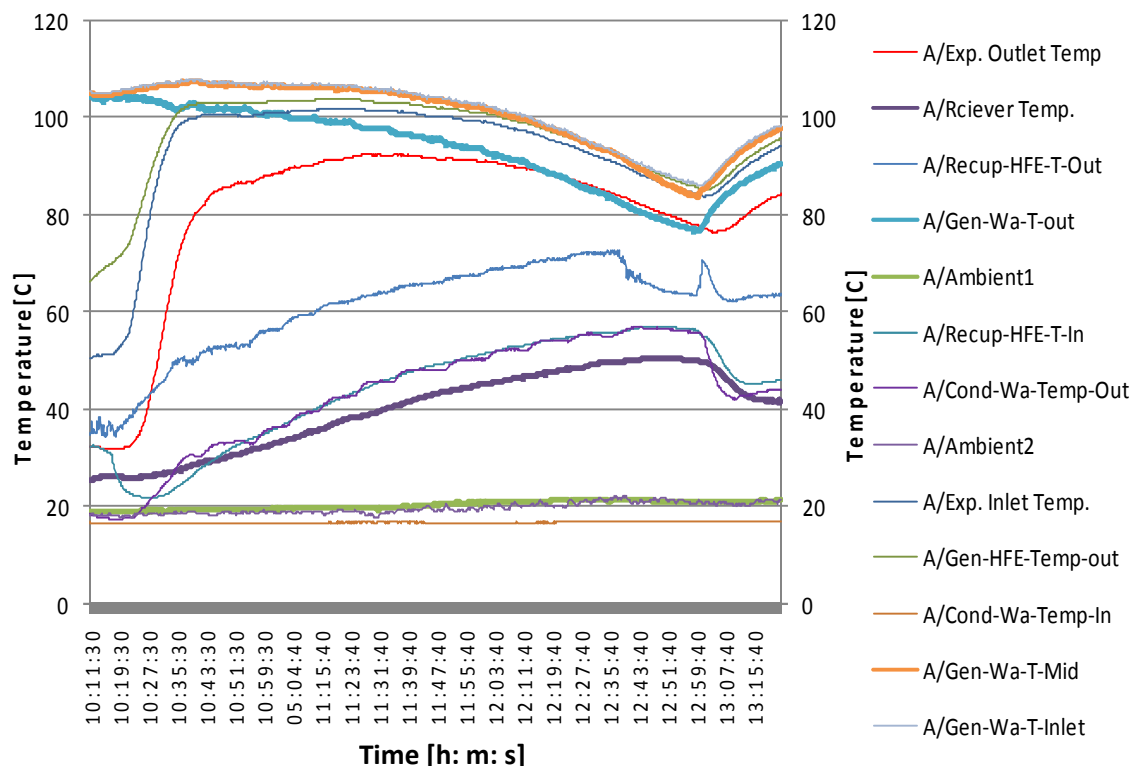
Figure 6.42: Inlet and outlet Temperature of various components vs.Time
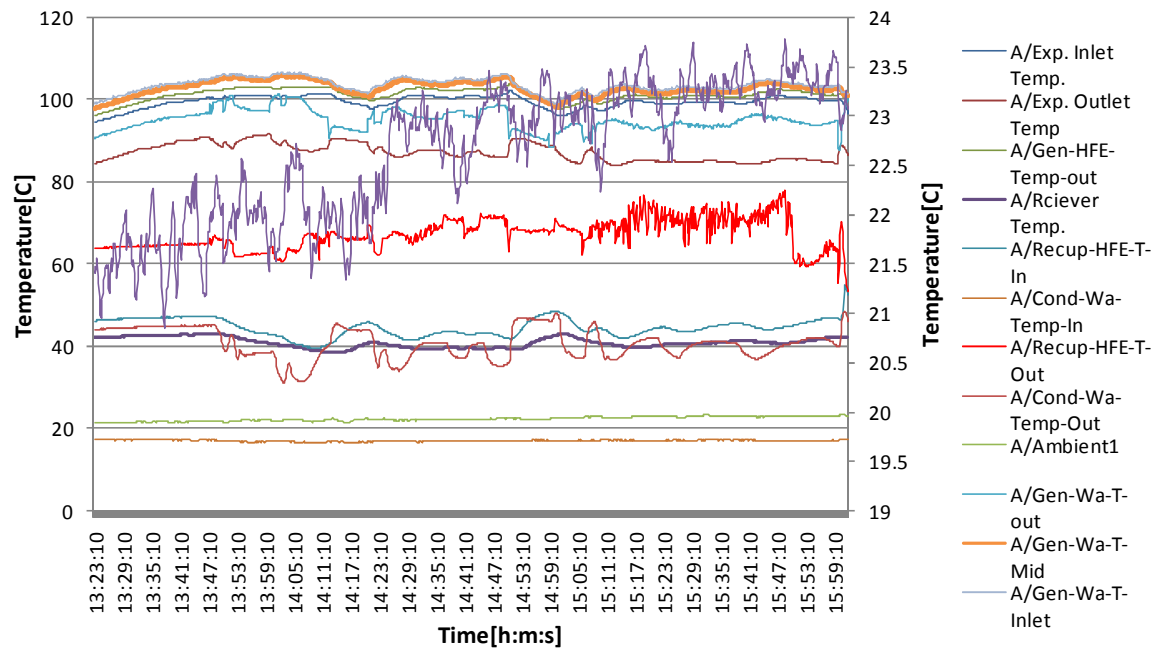
Figure 6.42: Inlet and outlet Temperature vs. time (contd.)

This shows a build up in temperature at the turbine inlet and as the pumping rate increases the temperature starts dropping slightly as it approaches the 49% pumping ratio mark.Though the turbine inlet pressure in Table 7.4 increases progressively, the temperature shows a downward gradient and does not follow the pressure curve. This is as a result of limitation imposed by the heat carrier as temperature thermodynamically responds to the operating pressure of the system. The temperature and pressure charts are based on pump flowrate increments over time. The pumping setting is started at 10% and increased by three percentage point margin per-duration and continued to a maximum allowable flow rate of the system which varies depending on the type of working fluid and operating temperature. The initial flow rate of 10% is usually very uncertain in terms of the data acquisition because the start up condition is unstable and with a lot of stream resistance but nonetheless important in

195

understanding the system performance when compared with higher flow rate conditions.
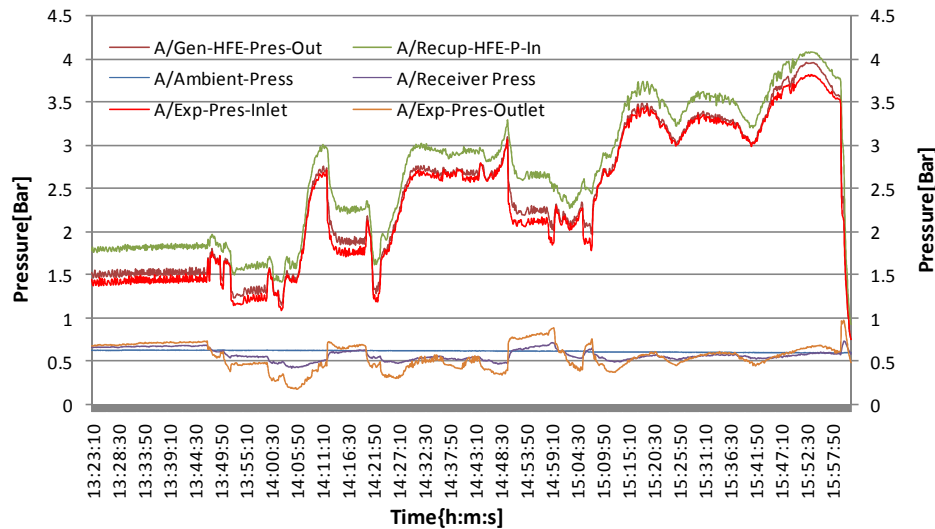
Figure 6.43: Inlet and outlet Pressure vs. time

The expander rpm responds to the flow rate, the stream flow and pressure. Others are expander inlet pressure and temperature as well as the enthalpies at the inlet and exit of the expander (turbine) shown in Figure 6.45 and the pressure drop in Figure 6.46. The pumping rate and the expander rpm are shown in Figure 6.44. The expander output and rpm are very crucial factors in the electrical test because of the peculiar characteristics of the electric generator, an automotive alternator already discussed in chapter three; section 3.4.

Table 6.17: Experimental data from Test - 3 of the ORC system using the electric boiler as heat source

Pump	Turbine							ΔH turbine	Generator		Recuperator		Total Heat Input	Heat from Cond.	Working fluid
setting %	inlet T[C]	Outlet T [C]	Inlet P[bar]	Outlet P[bar]	Inlet h (kJ/kg)	Outlet h (kJ/kg)	rpm[-]	[kW]	Refr. Outlet T[C]	Refri. inlet T[C]	inlet T[C]	outlet T[C]	[kW]	[kW]	Flowrate(kg/s)
10	51.82	32.39	-0.036	-0.279	234	217	0	-0.47	69.81	26.49	29.49	36.35	1.269	0.406	0.02
13	74.7	41.72	0.232	-0.265	254.9	225.4	564	10.91	85.51	26.59	22.42	42.43	2.999	1.355	0.02
16	97.73	71.49	0.547	-0.102	276.9	252.4	700	32.92	100.99	27.99	24.72	49.46	5.481	3.297	0.02
19	100.51	84.85	0.724	0.109	279.4	264.9	730	44.84	109.39	30.3	30.88	52.65	5.635	4.294	0.03
22	100.83	88.01	0.909	0.266	279.5	267.7	818	56.81	109.43	32.74	35.39	55.86	6.305	4.77	0.03
25	101.56	90.76	1.166	0.495	279.8	270.1	885	75.11	108.92	36.09	40.32	60.38	7.494	5.77	0.04
28	101.55	90.74	1.163	0.492	279.8	270	990	79.30	109.91	36.05	40.26	60.34	7.48	5.76	0.04
31	101.57	92.44	1.455	0.719	279.4	271.4	966	96.15	109.7	39.41	44.94	63.48	8.48	6.69	0.05
34	100.8	92.16	1.634	0.971	279.4	270.9	986	106.27	102.87	42.36	49.29	65.67	9.05	7.22	0.05
37	99.67	91.49	1.8	1.008	277	270	1019	117.10	101.73	44.66	50.71	67.43	9.65	7.66	0.06
40	99.28	90.61	1.945	1.127	275.3	268.9	1044	126.77	100.27	46.23	52.63	69.08	10.03	8.06	0.06
43	95.99	88.91	2.086	1.235	272.8	267	1059	135.05	97.92	47.76	54.31	70.68	10.27	8.44	0.07
46	99.09	86.57	2.178	1.307	269.01	264.6	1072	141.68	94.91	49.19	55.59	72.02	10.38	8.7	0.07
49	89.93	83.74	2.25	1.408	266.4	261.6	1082	144.59	91.68	50.26	56.43	69.78	10.42	8.76	0.08

197
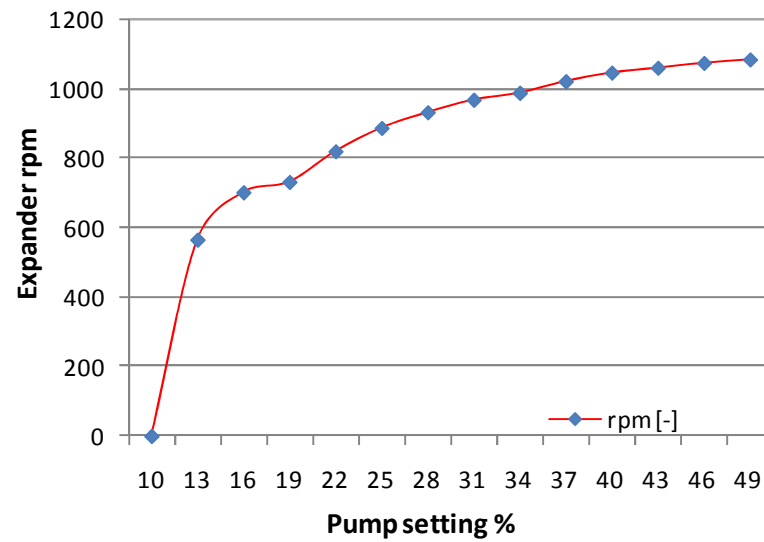
Figure 6.44: Expander rpm vs. pump setting
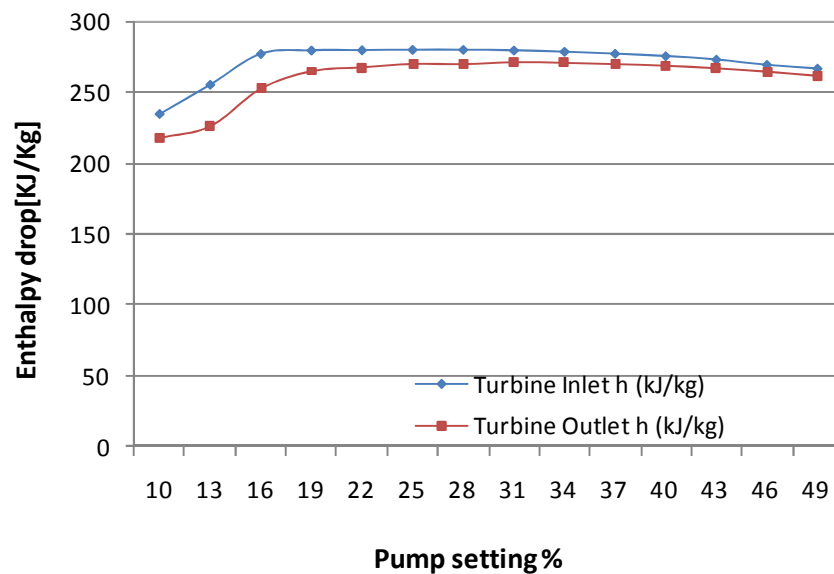
Figure 6.45: Expander enthalpy drop vs. pump setting
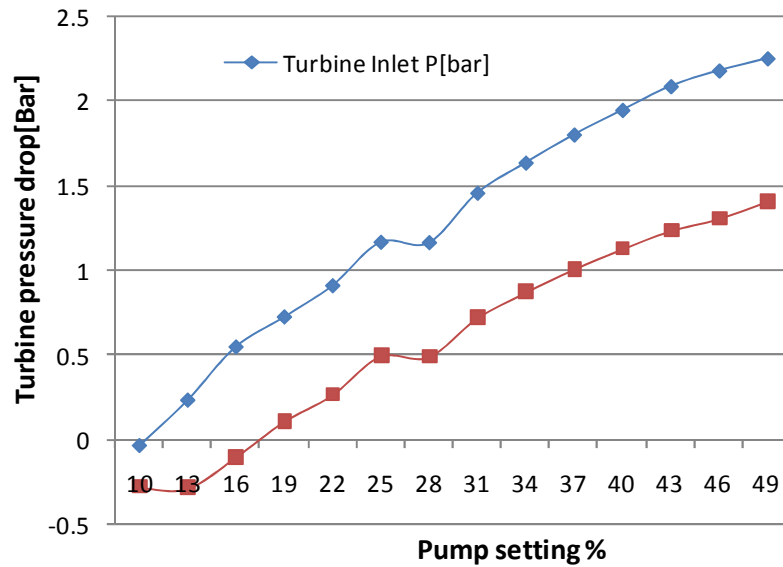
Figure 6.46: Expander pressure drop vs. pump setting

The alternator ignition point or cut-in, that is the output range at which the alternator switches on. This is at about 800 revolutions per minute(rpm) for most of the alternators used . The alternator will not generate power at rpm significantly lower than the 800rpm mark. However, it is important to note that for the system to be productive, the turbine output and rpm must be raised to generate enough torque to drive the electric generator and overcome the imposed mechanical and electrical loads produced during the process. This is normally dependent on the heat source and operating pressure of the system especially with respect to heat addition to the working fluid and the pressure and temperature difference across the expansion phase. Figure 6.47 and Figure 6.48 show the energy performance characteristics of the system with respect to three major components; the evaporator, the recuperator and the condenser against pumping rate responsible for heat addition and rejection process of the system
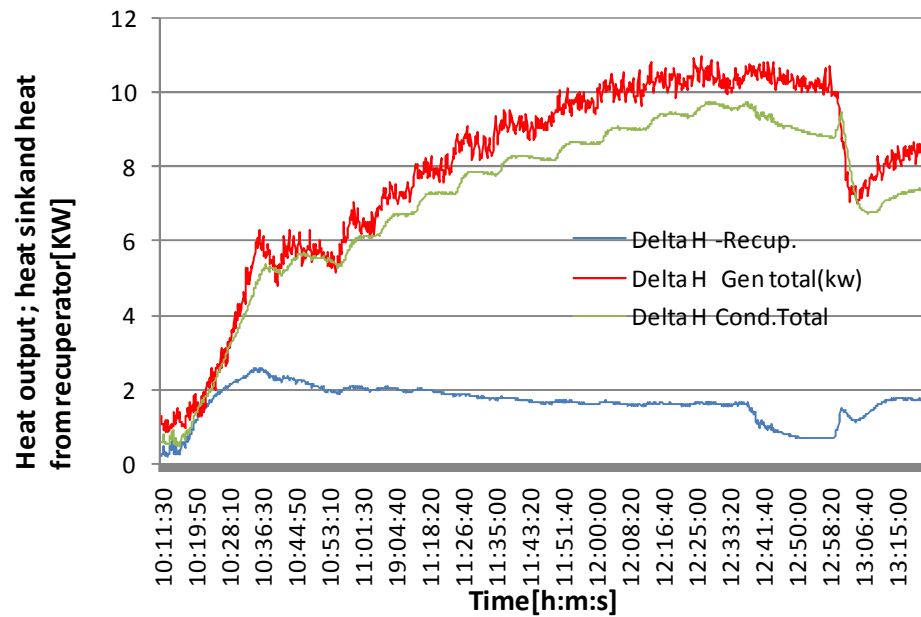
Figure 6.47: Heat output and heat sink of evaporator and condenser vs. time
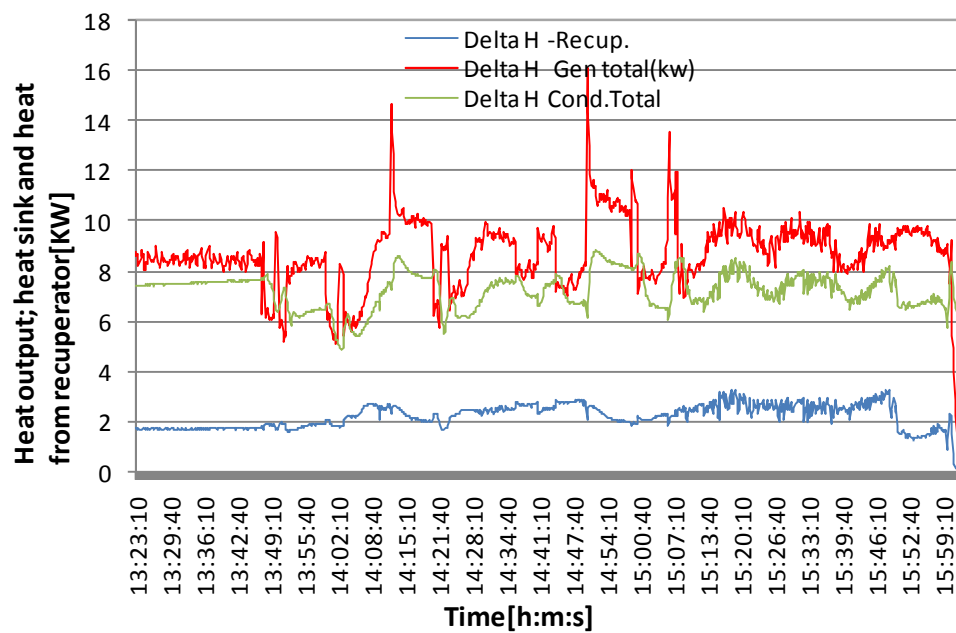
Figure 6.47: Heat output and heat sink of evaporator and condenser vs. time (contd.)
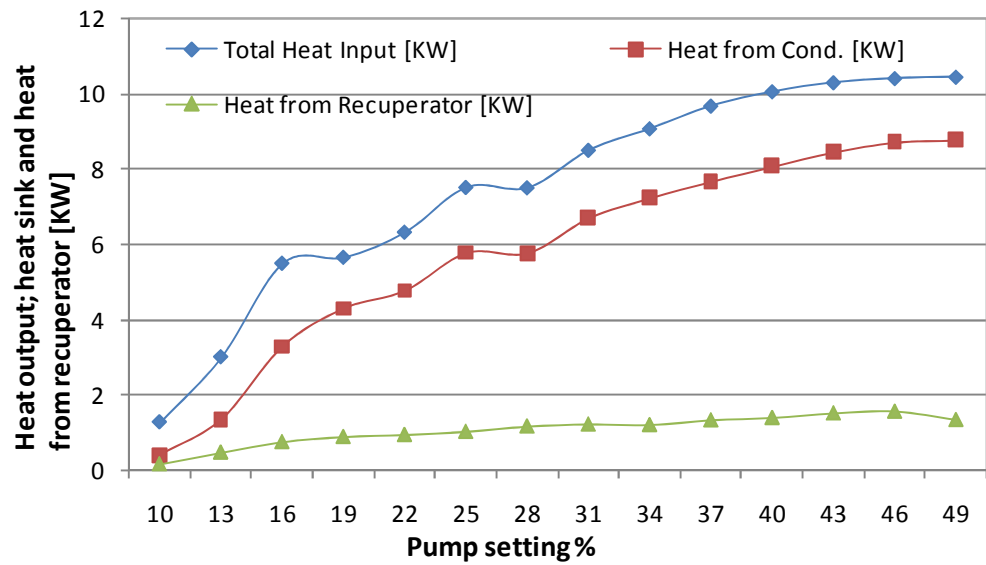
Figure 6.48 Heat output and heat sink of evaporator and condenser vs. pump setting

The electrical test is included in chapter seven having analysed the various test performances based on the expander output and system efficiency. This is preparatory to performing an electrical output test of the system. While the expander depends on the input pressure, temperature, and enthalpy, the electric generator depends on the mechanical energy generated by the expanders rotating shaft which is simultaneously converted into electricity.

The EES software is used to derive the table of parametric values at different state points for an ideal cycle as indicated in Table 6.18 and some of the performance parameters are shown in Table 6.17 and there is a big contrast between the ideal cycle performed within the 49% pump setting mark when viewed against the actual cycle in Table 6.19.

Table 6.18: Ideal Performance parameters of system output (Test 4)

Parameter	Nomenclature	value	unit
Boiler heat rate	Q_{in}	10.42	kW
Condenser heat sink	Q_{out}	8.76	kW
Pump power output	W_p	0.00004	kW
Turbine power output	W_t	1.437	kW
Power required to operate pump	T_p	0.00025	[-]
Net power output	W_{net}	1.436	kW
Carnot efficiency	η_{Carnot}	16.69	%
Cycle efficiency	η_{ideal}	12.82	%
Working fluid mass flow rate	$\dot{m}_{HFE7000}$	0.07625	kg/s
Hot water flow rate	$\dot{m}_{water}$	0.250	kg/s

Table 6.19: Actual performance parameters against pump setting

Pump setting	W_t	W_{net}	Q_{in}	$\eta_{actual,thermal}$
%	(kW)	(kW)	(kW)	[%]
22	0.350	0.295	6.305	4.67
25	0.320	0.243	7.498	3.24
28	0.366	0.291	7.480	3.89
31	0.339	0.240	8.480	2.83
34	0.335	0.220	9.050	2.43
37	0.360	0.231	9.650	2.40
40	0.361	0.218	10.03	2.17
43	0.347	0.218	10.27	2.12
46	0.314	0.197	10.27	1.94
49	0.311	0.195	10.42	1.87

The actual cycle thermal efficiency drops as the flow rate increases and this is due to irreversibility in the cycle or cycle components. The
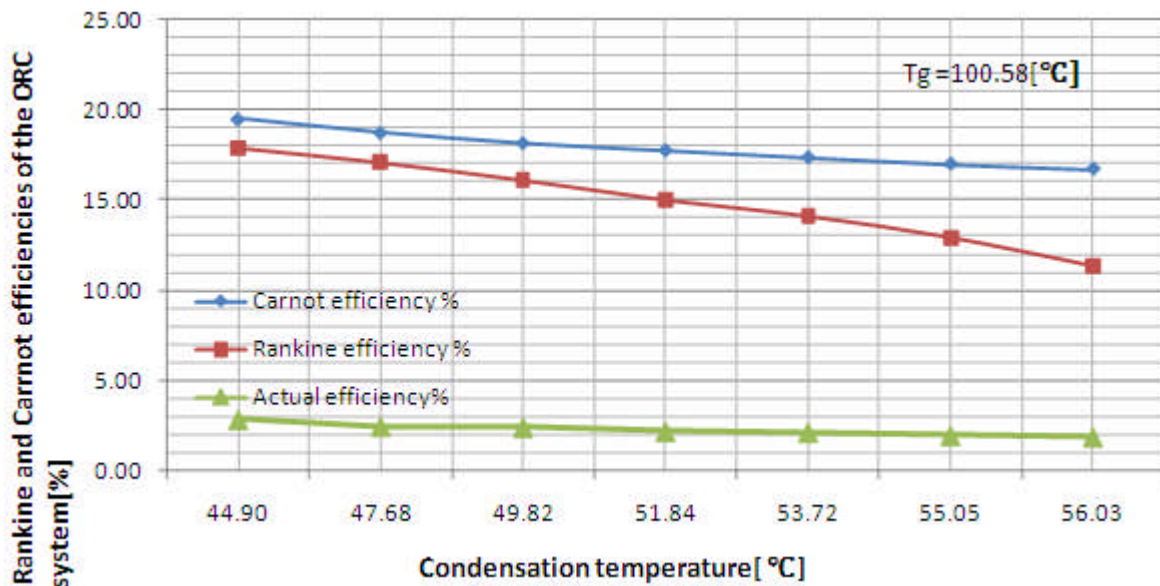
Figure 6.49: ORC efficiencies including the actual vs. condensation temperature

efficiencies recorded at both 10% and 13% pump setting are not considered because it is at a stage where the system is still stabilizing and might involve an uncertainty factor but beyond this range the system stabilizes. However the performance still shows a downward trend in the cycle efficiency as shown in Table 6.19 and Figure 6.49.

6.3 Summary

The experiments carried out and described in this chapter is after a careful study and analysis had been undertaken considering the various component parts of the Organic Rankine cycle system. Preliminary tests using compressed air to check the proper functioning of the prime mover was carried out observing specifically stipulated test procedures and precautions. This includes the starting procedure before any test commences and the outcome reported. The series of experimental tests

involving the use of the electric boiler as the heat source followed after the preliminary tests involving heat addition and the use of an environmentally friendly working fluid HFE 7100 and HFE 7000. These series of tests also had to go through operational checks before the commencement of any test and the results of the experimental test involving the use of HFE 7100 are reported in this chapter including the performance parameters and efficiencies. The various tests are categorised into three major spectrums, with Test 1 under a steady state condition. The Test 2 and Test 3 involved the introduction of a recuperator at the exhaust of the prime mover. This had some positive variations of the expander rpm. This has to do with effect of the recuperator and the increment of the average heat addition temperature and pressure at the inlet of the expander. The use of vacuum pump for system evacuation enabled the lowering of the temperature at which the working fluid is vaporised while the recuperator increased the average temperature at which heat is transferred to the the working fluid. The differences in temperature between Test 1, Test 2 and Test 3 showed 87.93^{o}C for Test 1 and 100.7^{o}C - 102.42^{o}C, for Tests 2 and 3 respectively allowing for pressure differentials in each case and directly influencing the increase in rpm of the expander. These improvements are shown in graphs in this chapter indicating also the test parameters. However, further system optimization was necessary because of the limited heat output at the maximum temperature of 115°C from the electric boiler which was an unavoidable laboratory constraint. A working fluid HFE 7000 with a lower boiling point than HFE 7100 was introduced to improve performance

and the outcome are indicated in the next chapter involving the use of

biomass boiler as the heat source.

Chapter 7: Biomass ORC Experimentation

7.1 Background

The use of biomass fuel in this work points to the concept of exploiting non-fossils in an ORC micro-CHP production and averting a single fuel dependency, as well as delivering on carbon savings as a carbon neutral fuel. The Biomass boiler used like most biomass power plants today is a direct-fired system and it is a 25kW Model Green-Tec boiler manufactured by Ashwell engineering services limited U.K, with dimensions of 1270 x 1500 x 785 mm. It weighs 350kg empty and also has an integral hopper. The biomass boiler is a high efficiency automatically controlled boiler with self cleaning underfeeds stoker and latest in burning technology. The fire bed is a small but efficiently burns the right amount of fuel to keep the water in the boiler at the desired temperature and the biomass fuel used in this experiment is the wood pellet. Combustion is virtually smokeless and the appliance complies with EN303/5 for efficiency testing and emissions with an overall net efficiency in excess of 85%. Some of the operating mechanisms include;

1/. A dual thermostat incorporating two setting dials for temperature control and the other for higher safety limit control.

2/. Control panel with proportional firing rate timer and purge cycle timer for the F/D fan.

The boiler details are shown in Figure 7.1 - Figure 7.6 with very simple working mechanisms including the heat retarding cleaning chains that

keeps the channels through the heat exchanger free from sooth and by

manipulating the cleaning chain operating rod the heat exchanger is kept
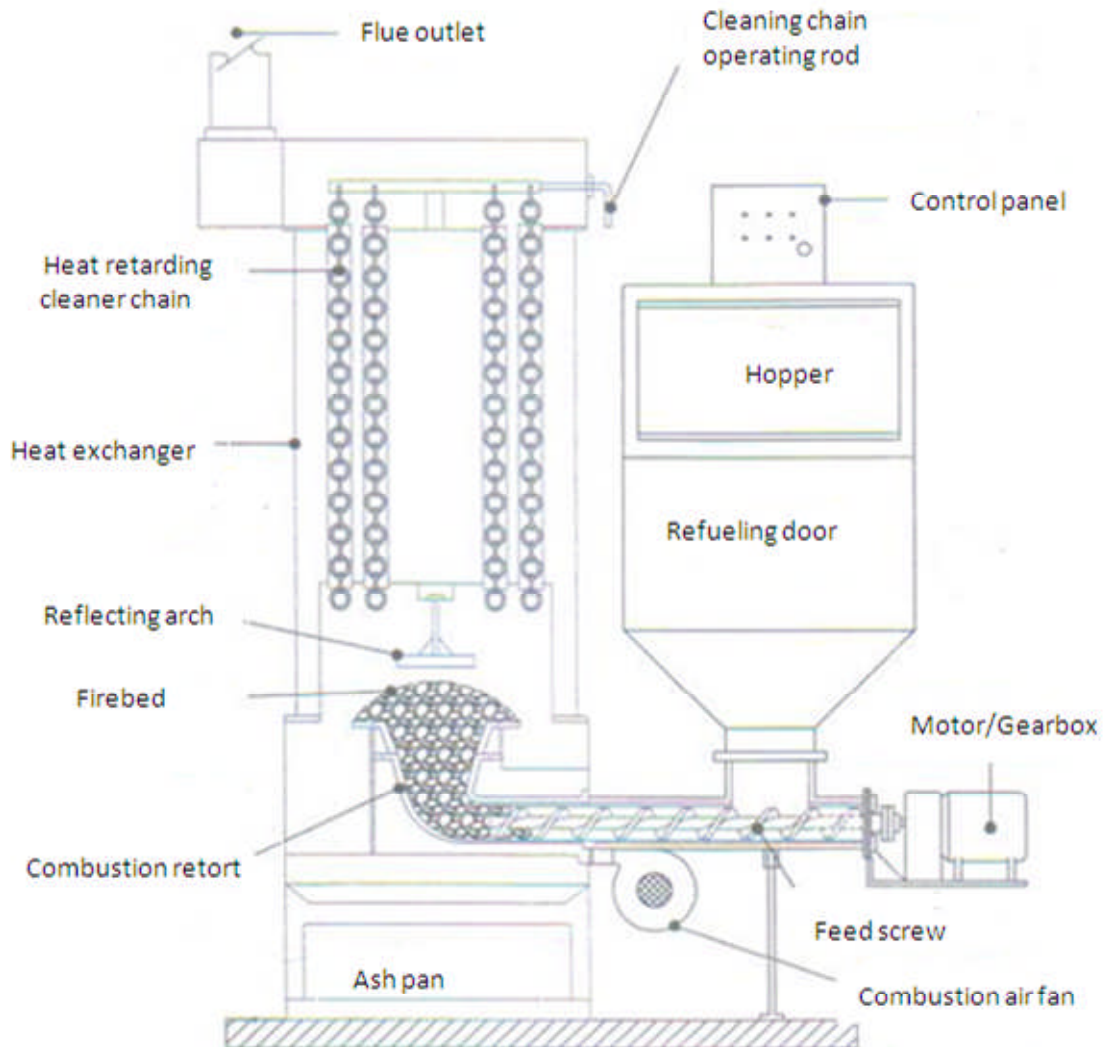
Figure 7.1: Biomass 25kW underfed Boiler/Stoker
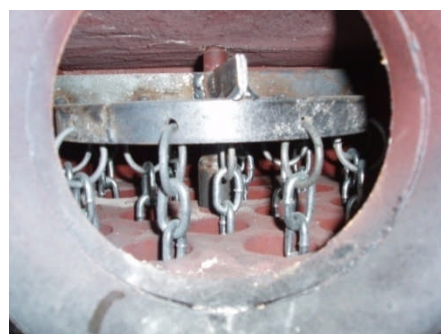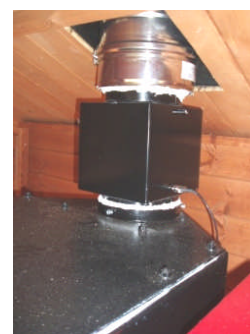
A – Cleaner chain   **B- Flue outlet**

Figure 7.2: Heat retarding cleaner chain and Flue outlet

207

from clogging while burnt out ash is collected in the ash pan and requires emptying at least once a week. The boiler operational procedure is not as different from that described earlier in this chapter involving the electric boiler. The process involves;

1/. Filling in water into the boiler through a water supply hose connected to the mains water outlet.

2/. Putting of biomass fuel into the hopper and with the stoker supplying the pellet based fuel to the combustion chamber by mean of a screw feed device driven by a gear attached to an onboard electric motor.

3/. The boiler is switched on by means of the start button on the control panel and the ignition is automatic and air is supplied by a combustion air fan and enough ventilation is allowed within the boiler housing when the boiler is active allowing the availability of enough oxygen for combustion.

4/.The boiler is allowed to attain the maximum temperature before the actual experiment commences by switching on the test rig and following the procedure described with the electric boiler tests.

The average pellet consumption is given as;

1 kg pellet = 5kW/hr @ 25kW – 5kg of fuel / hr of running

If the boiler burns for 6 hrs/day – 30 kgs/day

30kgs * 7days = 210kgs/wk

4 months (16 weeks) @ 210 kgs/week = 3,360kgs

4 months @ 50% of winter month's consumption

for summer   = 1,680kgs

Total per year is 5,040kgs or 5.040 tonnes for $25kW_{boiler}$

This comes to about 201kg per kW per year.

Figure 7.3: Photograph of Biomass boiler as installed for experiment

A -Typical combustion retort   **B - Biomass pellet fuel**

Figure 7.4: Photograph of combustion retort and biomass pellets

A-Photograph of combustion chamber
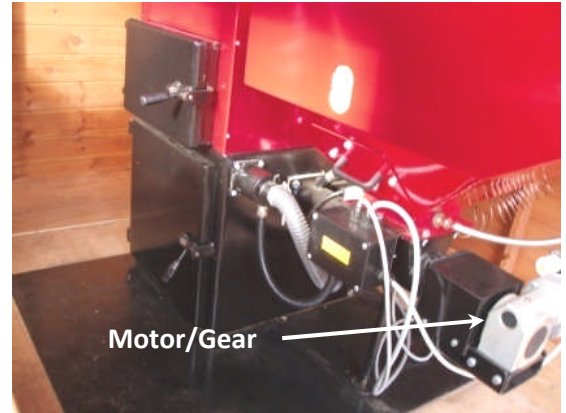
B- Stoker motor/gear

Figure 7.5: Details of Biomass boiler

A-Biomass boiler housing connection and connecting pipes
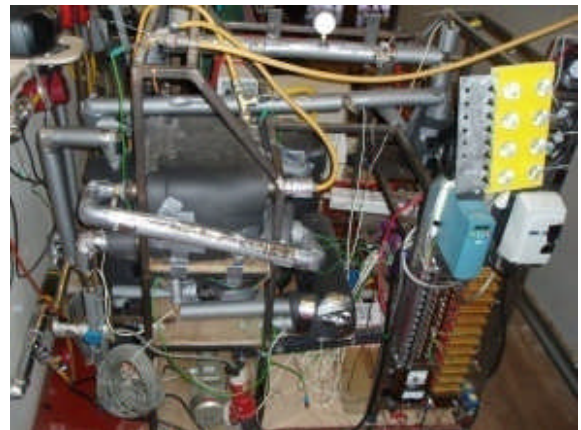
B-Photo of Test rig and piping to boiler

Figure 7.6 Connection of hot water supply pipes to Test rig

The schematic diagram of the biomass experimentation is shown in Figure

7.7 indicating the various components that make up the system.
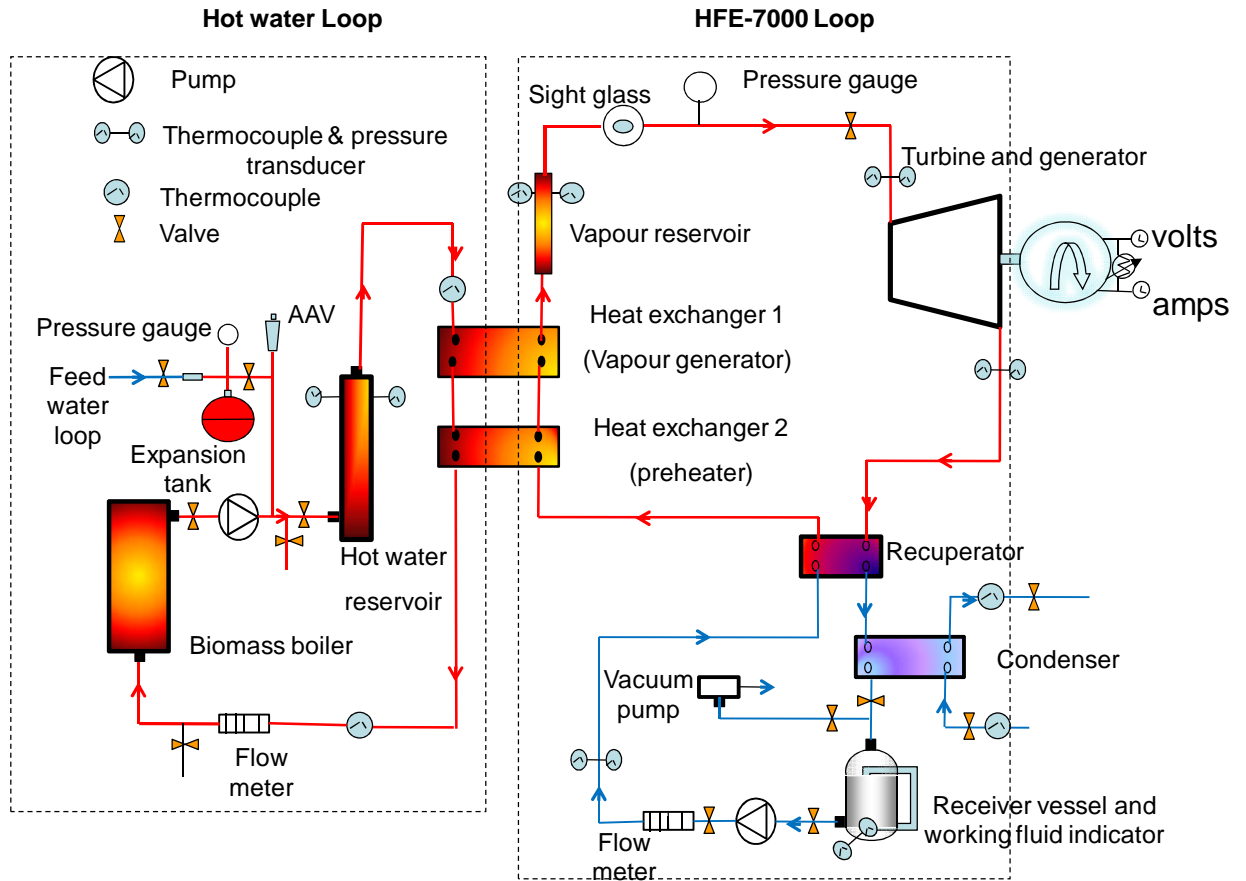
Figure 7.7 Schematic diagram of the Biomass boiler test

The design pragmatism makes it possible to change from one heat source

to another with minimal adjustments to the system and it was easy to

change from the electric boiler to the biomass boiler and the system is

also designed as a mobile unit which can be moved to different locations

7.2 Test conditions and measured data – Test 4

The test conditions are as specified in Table 7.1 indicating the working fluid pump flow rate and other governing parameters including the turbine rpm over time. The 0 rpm is an indication that the turbine has not become active even though the system is operational. This sometimes occurs because of high operational torque or enough working has not been vaporised to drive the mechanism which sometimes takes a couple of minutes to achieve.

Table 7.1: Experimental Test Parameters

HFE7000 flow ratio %	Time [h:m:s]	Turbine RPM	Gauge pressure @ turbine inlet(bar)	HFE 7000 flow rate(l/min)	Vapour quality in sight glass
10	11:10:00	0	0.4	16	clear
13	11:28:40	0	0.4	15	clear
16	11:39:50	820	0.35	38	clear
19	11:54:30	1020	0.45	46	clear
22	12:25:00	1233	0.65	53	clear
25	12:36:00	1437	0.80	60	clear
28	12:48:00	1550	0.85	67	clear
31	13:01:00	1660	0.92	75	clear
34	13:13:50	1720	1.03	83	clear
37	13:25:00	1820	1.25	95	clear
40	13:39:20	1887	1.30	104	clear
43	14:05:30	1911	1.40	112	clear
46	14:15:30	1984	1.55	122	clear
49	14:25:00	2015	1.64	132	clear

The measured data are shown in Table 7.2 indicating the temperature and pressure data with input and output at various points in the cycle as well as other cycle parameters.

Table 7.2: Experimental data from Test - 4 of the ORC system using biomass boiler as heat source

Pump					Turbine				Generator		Recuperator		Total Heat Input	Heat from Cond.
setting %	inlet T[C]	Outlet T[C]	Inlet P[bar]	Outlet P[bar]	Inlet h (kJ/Kg)	Outlet h (kJ/Kg)	ΔH turbine [kW]	rpm [-]	Refr. Outlet T[C]	Refr. inlet T[C]	inlet T[C]	outlet T[C]	[kW]	[kW]
10	59.37	31.99	0.448	-0.183	240	216.5	0.266	0	65.08	15.7	15.7	40.35	2.64	1.01
13	78.17	47.79	0.69	-0.27	257.4	230.8	0.282	0	86.1	15.61	15.61	47.21	2.35	0.74
16	86.77	64.32	0.63	-0.23	265.9	245.9	0.537	820	91.52	15.03	15.03	45.95	4.24	2.43
19	85.3	71.8	0.62	-0.14	264.5	252.8	0.380	1020	88.52	13.87	13.87	41.06	2.06	1.35
22	85.58	72.72	0.75	-0.11	264.6	253.6	0.412	1233	88.38	13.76	13.76	42.62	6.61	4.41
25	86.27	75.06	0.844	-0.12	265.1	255.8	0.394	1437	89.12	14.18	14.18	46.54	7.07	5.12
28	87.48	76.65	0.95	-0.1	266.1	257.3	0.417	1550	89.98	14.4	14.4	48.49	7.91	5.74
31	87.42	77.52	1.89	-0.06	264.5	258.1	0.339	1660	89.78	14.16	14.16	49.64	8.87	6.46
34	86.99	77.85	2.22	0.003	263.4	258.3	0.299	1720	89.23	14.57	14.57	49.52	9.84	7.21
37	87.76	78.98	2.74	0.08	263.3	259.2	0.275	1820	90.01	15.57	15.57	49.69	10.47	7.94
40	87.85	79.24	2.72	0.17	263.4	259.3	0.301	1887	89.99	17.75	17.75	51.29	11.01	8.68
43	88.49	79.13	3.01	0.25	263.5	259	0.356	1911	90.58	19.14	19.14	52.47	11.62	8.68
46	88.24	79.74	3.46	0.34	262.4	259.5	0.250	1994	90.29	20.42	20.42	53.19	12.58	9.66
49	87.3	79.52	3.49	0.43	261.4	259.2	0.205	2015	89.39	22.2	22.2	56.33	12.93	10.18

The enthalpies are derived through calculations using the EES software based on the measured data. The heat input from the heat source and the heat sink are then determined by further calculation also accomplished by means of the software.

The graphical representation of the measured data in Figure 7.8 indicate the characteristics of the inlet and outlet temperature due to heat flow and heat transfer in the cycle especially at the expanders inlet and exhaust port. The temperatures at the water side of the heat source over the duration of the experiment are also shown. It is seen that the temperature of the heat source when compared to the electric boiler is lower even at the turbine inlet temperature. The biomass average temperature is 93.5^{o}C at the water side and 84.5^{o}C at the turbine inlet temperature after heat
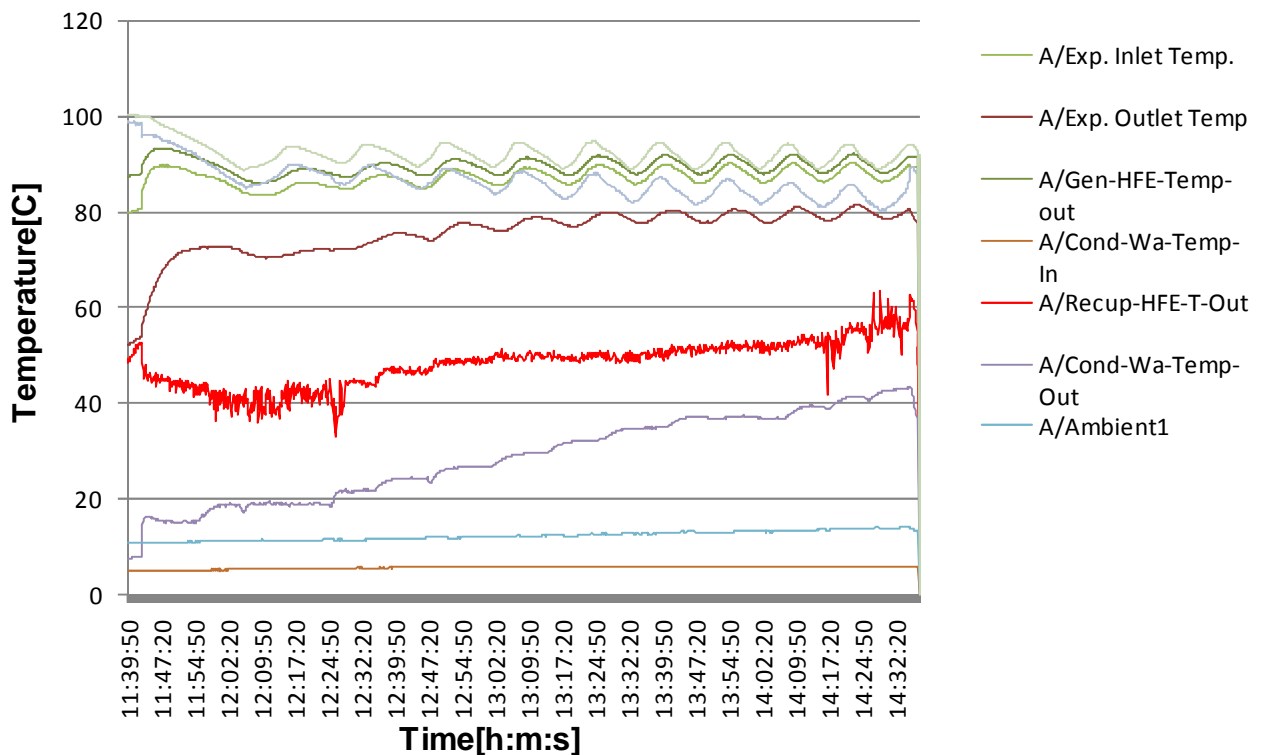
Figure 7.8: Working fluid inlet and outlet temperature at different points in the ORC cycle vs. time
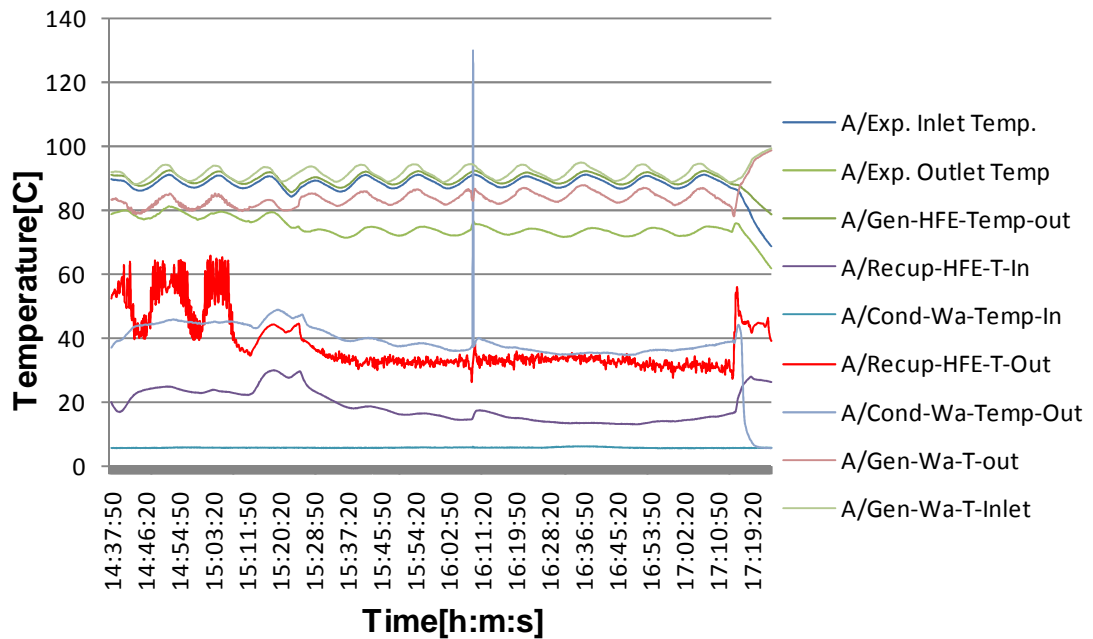
Figure 7.8: Working fluid inlet and outlet temperature at different points in the ORC cycle vs. time (contd.)

transfer while the electric boiler heat supply temperature averaged 110.96^oC and the turbine inlet temperature after heat transfer is $93,4^o$C.The variation in temperature between the 9kW electric boiler and the 25kW biomass boiler is in their operating pressures. The electric boiler maximum operating pressure is 6 bars while the biomass boiler is 3 bars. This is a limitation experienced in the course of the experiment as both the electric boiler and the biomass boiler had imposed limitations; while the electric boiler is limited in output, the biomass boiler has limitation due to operating pressure restrictions. Therefore temperature could not be raised beyond the allowable limits as temperature increases responds to the operating pressure.

215

Figure 7.9 shows the characteristics of the temperature pattern with respect to the pumping rate.
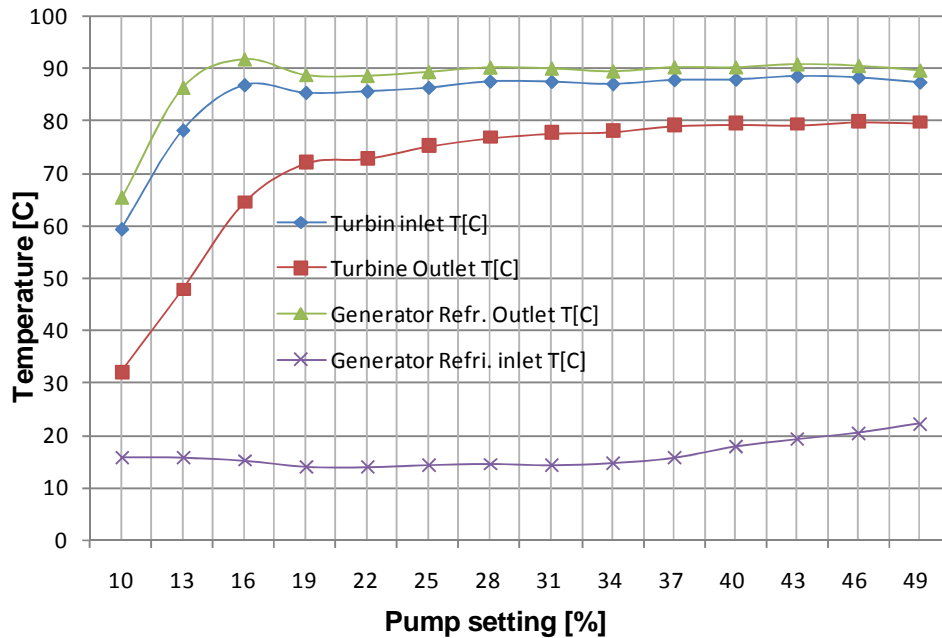
Figure 7.9: Working fluid inlet and outlet temperature at different points in the ORC cycle vs. pump setting

Figure 7.10 is the pressure characteristics of the cycle vs. time while Figure 7.11 indicates the pressure drop in the expander which is very significant compared to the expander pressure drop while using the electric boiler shown in Figure 6.46. The improvement also resulted in higher expander rpm as seen in Table 7.1 and the reason for the improvement being the lowering of the average temperature of the heat sink in the condenser and thus improving performance and this is in the range of 16.2^{o}C for biomass boiler and 39.6^{o}C for the electric boiler. The condenser sink temperature has to be kept high so that the available heat generated in the electric boiler will be adequate to raise water temperature required in the heat transfer process to the working fluid in the vapour generator. Lower heat sink temperature will require extra energy to raise

the desired temperature for the working fluid which the boiler cannot supply.
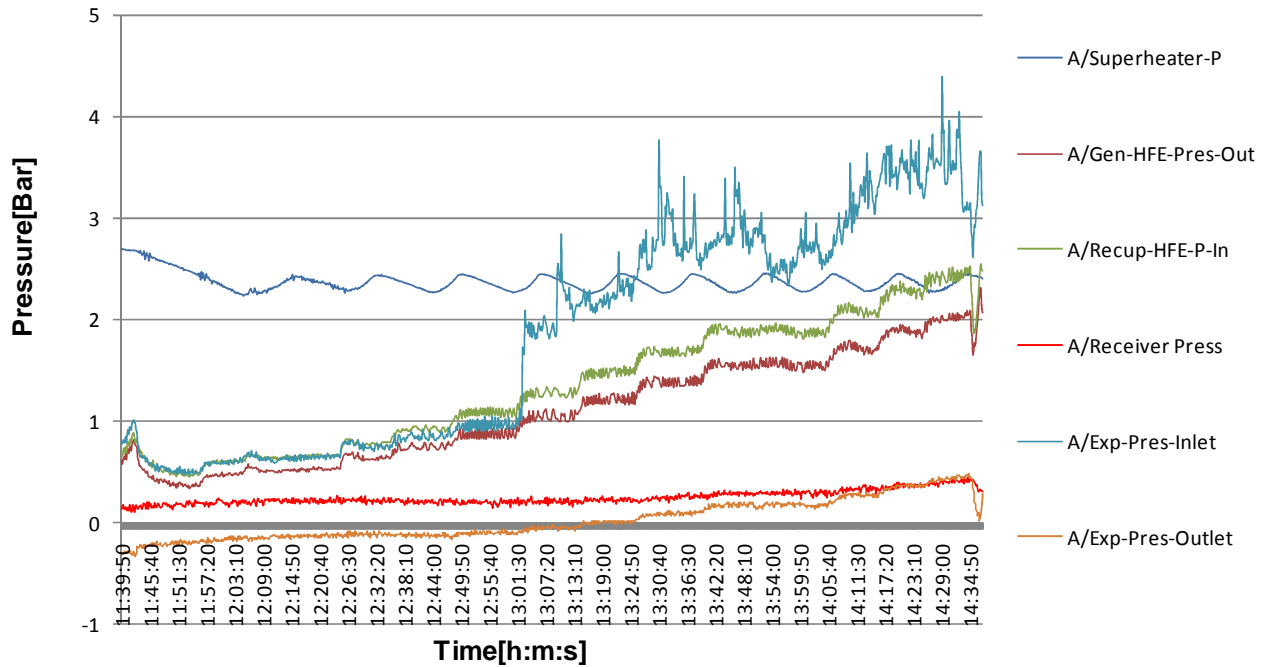
Figure 7.10: Inlet and outlet pressure of the ORC cycle vs. time
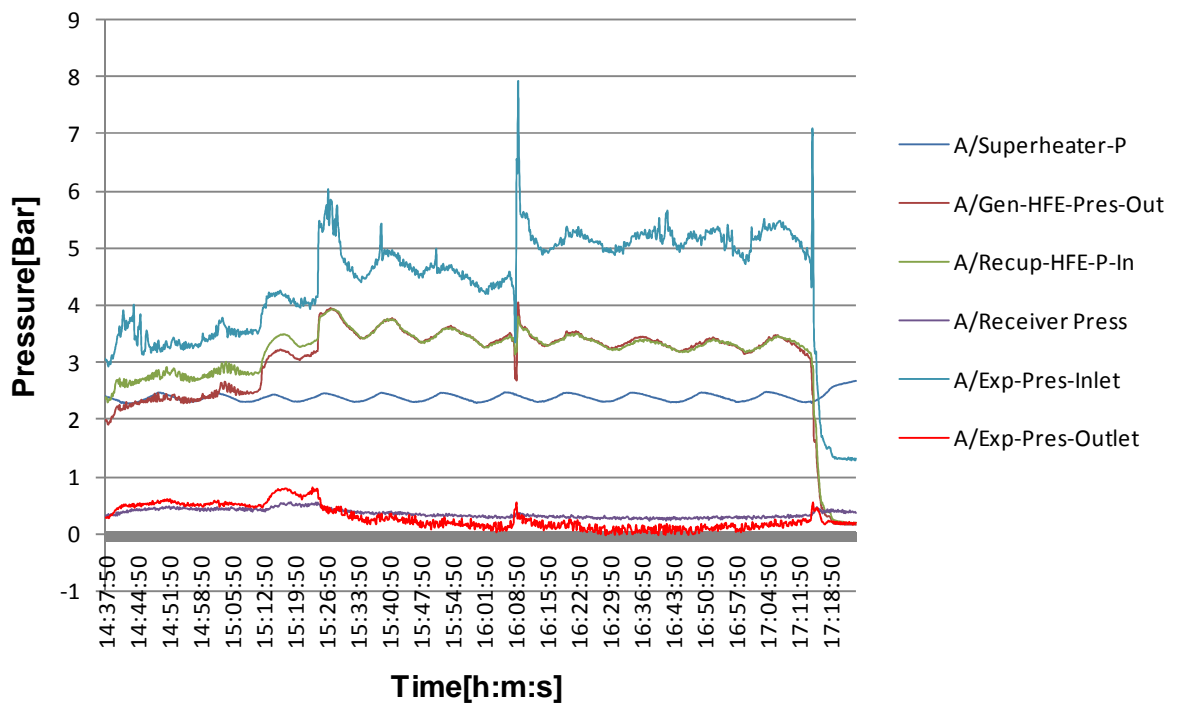
Figure 7.10: Inlet and outlet pressure of the ORC cycle vs. time (Contd.)

The heat balance is also brought into focus as an essential aspect of the heat supply process indicated graphically against pump setting and time.
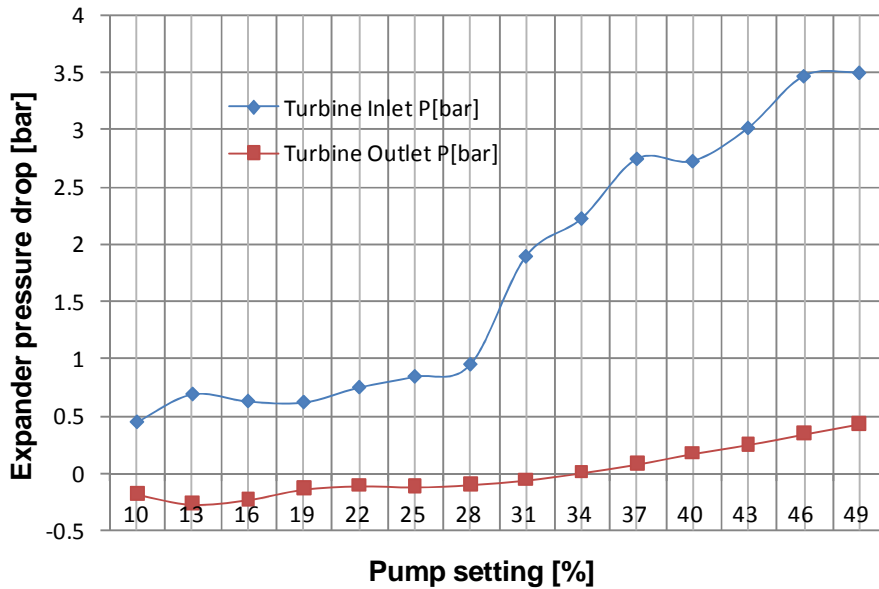
Figure 7.11: Turbine (Expander) pressure drop vs. pump setting

The energy balance of the cycle is assessed in Figure 7.12 and Figure 7.13 showing the heat input and heat sink of the vapour generator and the condenser in kW.
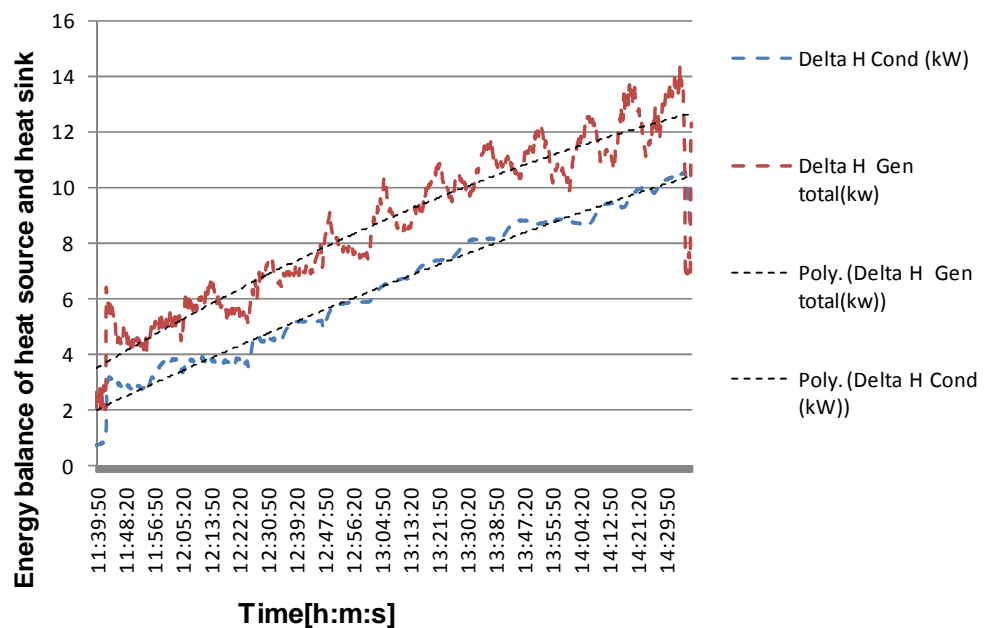
Figure 7.12: Energy balance of cycle vs. time
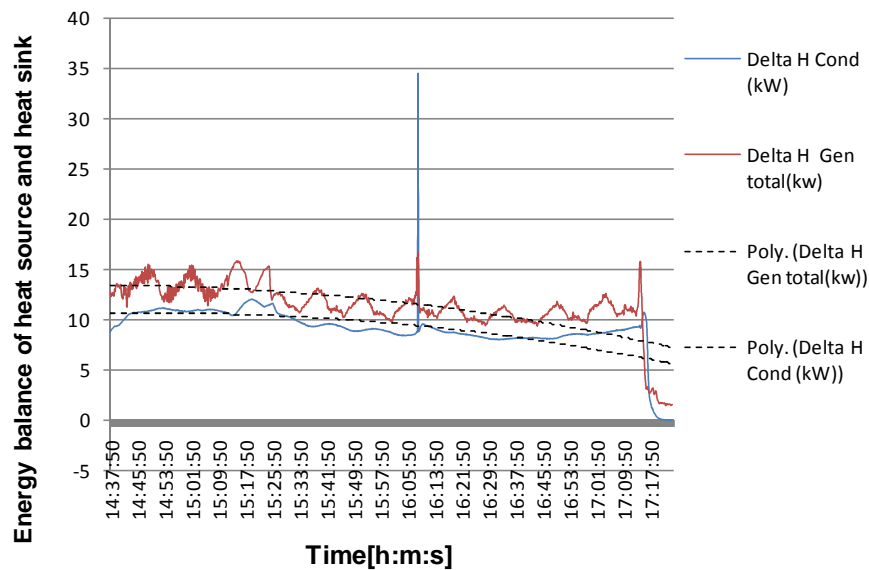
Figure 7.12: Energy balance of cycle vs. time (contd.)
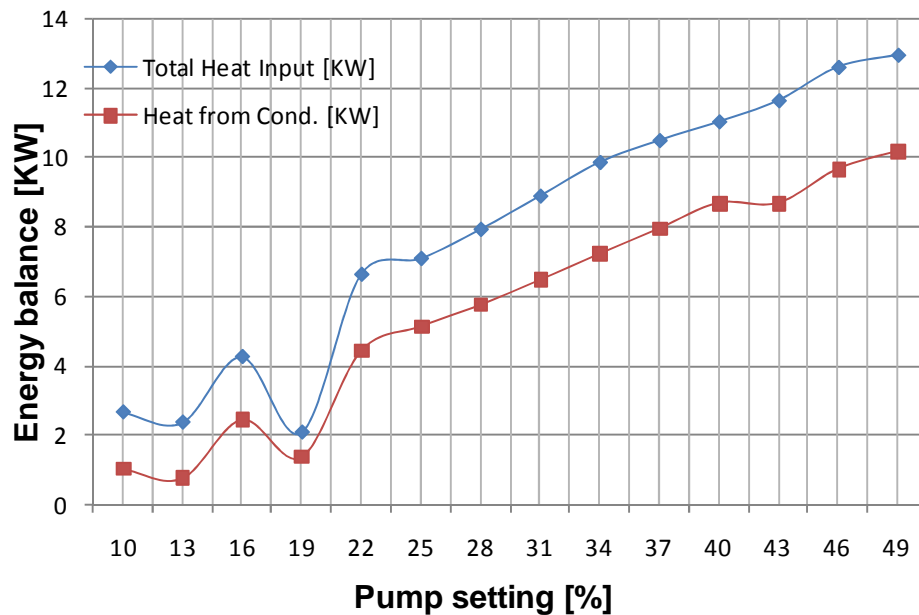
Figure 7.13: Energy balance of cycle vs. pump setting

Figure 7.12 is a representation of the energy balance against the pumping

rate and the performance characteristics of the heat flow process. The 10

- 16% mark show initial instability in the flow stream but soon normalises

as pumping rate increases. The EES software is used to derive to

determine the efficiency of the ideal and the Carnot cycle. This forms a

comparative basis between the practical test and the ideal cycle. The contrast between the practical test and the ideal or Carnot cycle is seen in the drop in efficiency of the actual test which is lower than the Carnot efficiency due to irreversibility in the cycle or cycle components. The ideal cycle analysis indicated in Table 7.3 shows the parameters considered including the water flow rate and the working fluid flow rate.

Table 7.3: Ideal Performance parameters of system output (Test 4)

Parameter	Nomenclature	value	unit
Boiler heat rate	Q_{in}	12.93	kW
Condenser heat sink	Q_{out}	10.18	kW
Pump power output	W_p	0.021	kW
Turbine power output	W_t	3.33	kW
Power required to operate pump	τ_p	0.0063	[-]
Net power output	W_{net}	3.31	kW
Carnot efficiency	η_{Carnot}	24.10	%
Cycle efficiency	η_{ideal}	17.25	%
Working fluid mass flow rate	$\dot{m}_{HFE7000}$	0.117	kg/s
Hot water flow rate	$\dot{m}_{water}$	0.35	kg/s

The actual or practical cycle efficiencies are shown in Table 7.4 with respect to the pump settings starting from 10% pumping rate to the 49% mark in approximately 3% incremental. The values have been derived by calculation applying the equation of state and using the EES software to derive the thermodynamic properties of the working fluid, HFE 7000. The expander output had been calculated by using two known variables in writing procedures in the software equation window and solving for the unknown values.

Table 7.4: Actual performance parameters against pump setting

Pump setting	W_t	W_{net}	Q_{in}	$\eta_{actual,thermal}$
%	(kW)	(kW)	(kW)	[%]
22	0.390	0.372	6.61	5.60
25	0.370	0.339	7.07	4.80
28	0.347	0.347	7.91	4.40
31	0.323	0.274	8.87	3.10
34	0.284	0.238	9.84	2.40
37	0.261	0.215	10.47	2.05
40	0.255	0.210	11.01	1.91
43	0.238	0.205	11.62	1.80
46	0.237	0.181	12.58	1.40
49	0.195	0.125	12.93	1.01

From Table 7.4 and Figure 7.14 it is seen that the efficiency of the practical process is lower than in an ideal cycle and the turbine output W_t is low and turbines are known to be irreversible due to high degree of turbulence and scrubbing of fluid or fluid friction.
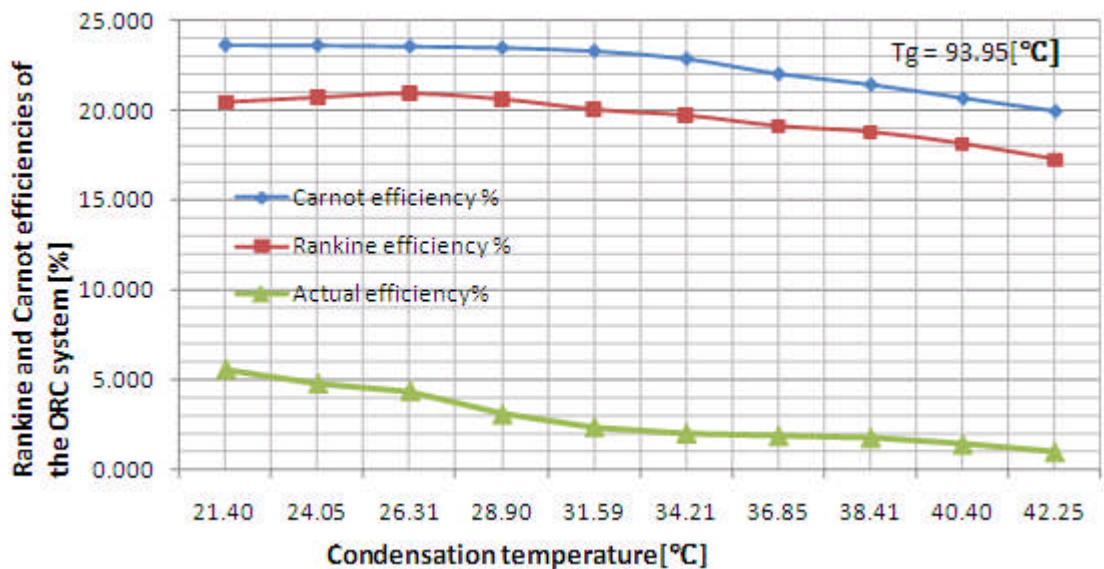
Figure 7.14: ORC efficiencies including the actual vs. condensation temperature

However Table 7.1 registered higher turbine rpm than any other test because of bigger pressure drop which means that despite the a lower turbine inlet temperature, the biomass test showed good performance in the power test. The lower exhaust temperature in the condenser however improved the performance of the system, the reason being the enhanced pressure drop.

The biomass boiler had some obvious limitation because the maximum operating pressure is fixed at 3 bars and therefore temperature was only 95°C regulated and the heat input averaged 12.93 kW at a flow rate of 21 Kg/min. This output can be increased but by increasing the flow rate the stream pressure will also increase. This will result in the flow stream pressure rising above the allowable operating pressures and put the system at risk. The experiment was run on the safe mode and within the tolerable output but performance will be higher with boiler optimization.

The electrical power test has been performed involving the use of the electric boiler and the biomass boiler and using HFE 7000. The electrical power test using HFE 7100 which has a higher boiling point than HFE 7000 did not progress further because when the substance at the dry saturated vapour line looses heat slightly or experience a sudden drop in temperature due to inadequate heat supply, droplets of liquid will begin to form resulting in wet vapour or a mixture at the inlet port of the turbine. This slows down the turbine because of the presence and bombardment of liquid molecules which can affect the vanes and damage the device.

7.3 Electrical Power output Test

The experimental tests performed in Chapter six considered turbine (expander) performance and enabling parameters, however the electricity power test involved the imposition of electrical load on the system which also generates a mechanical load. This slows the speed of the expander even as electrical power is generated by the alternator. The amount of electricity generated depends on a number of factors which include, the heat input and temperature at the expander inlet, the inlet pressure and pressure drop, the expander rpm and the imposed load on the system. Normal electricity production by traditional means cited in literature has efficiency of 30-40%, but the organic Rankine production has a much lower efficiency and Donghong Wei et al [132], puts the value at between 8 - 12%. It is also known that 1kW of power generates 2kW of usable heat energy [133]. However, this system though successful in electricity generation produces less heat due to laboratory limitations with the prospects of further improvements. This is because the boiler output is fixed and various optimization strategies were carried out to extract most of the available heat in the supply stream.

7.3.1 Measurement of electrical output

The electrical measurement is by means of a network of electrical components and measurement devices shown in Figure 7.14, such as the
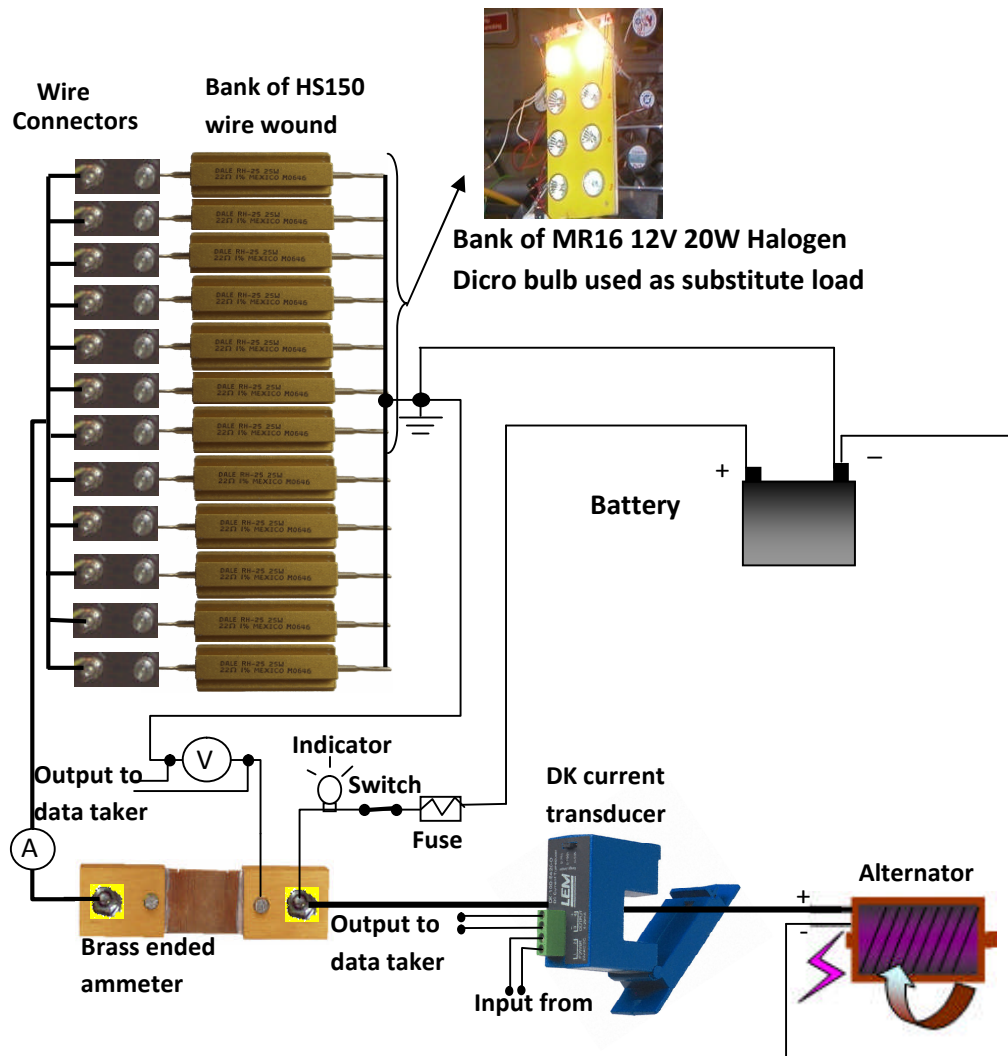
Figure 7.14: Electrical circuit and measurement devices

DK current transducer that transmits the readings to the data logger so that the readings can be stored in the computer. A bank of HS150 wound wire resistors and wire connectors including a bank of MR16 20W halogen Dicro bulbs are also used as load. Also used as load is a series of RW207S 12V; 5W auto bulbs shown in Figure 7.16, and normally measurements are verified by multiplying the recorded voltage and the current readings. The load points are connected in parallel and gradually increased to the bearable output of the system. Both the bulbs and the
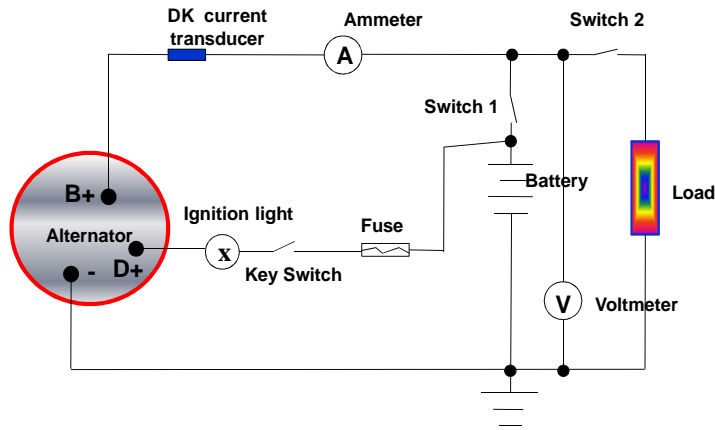
Figure 7.15: Alternator Circuit diagram with variable load of dc fans, 20W Bulbs, and HS150 wire wound resistors

wire wound resistors, including a series of dc fans are used differently for the load tests as indicated in Figure 7.17. The 12 volts battery is used to excite the alternator and the battery gets charged when the system becomes fully operational in addition to power production. If the ignition light is on when the system is operational, it basically means that the alternator output is lower than the battery voltage an indication that charging is not occurring. The alternator wiring diagram in Figure 7.15 shows the configuration and operating process of the electrical system with reference to the automotive alternator. The electrical system is operated by three main switches, the key switch, switch 1 and switch 2. The sequence is to turn on switch 1, followed by key switch and then switch 2. Switch 1 isolates or links up the battery when required especially

A: RW 207S, 12V; 5W Bulb   **B:** Dichro MR16; 12V, 20W halogen bulb
Figure 7.16: Photo of bulbs employed as load during testing

12V DC
Fans

Pump Regulator

Electrical Panel

Series of HS150
Resistors

DK current
transducer
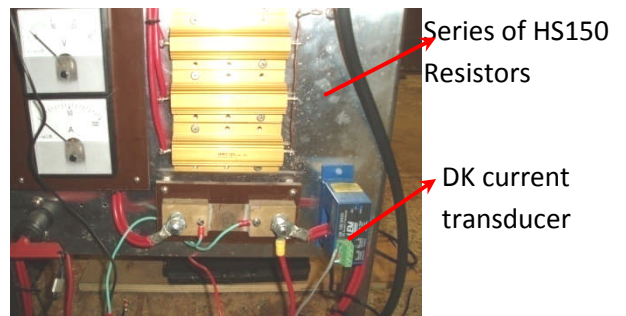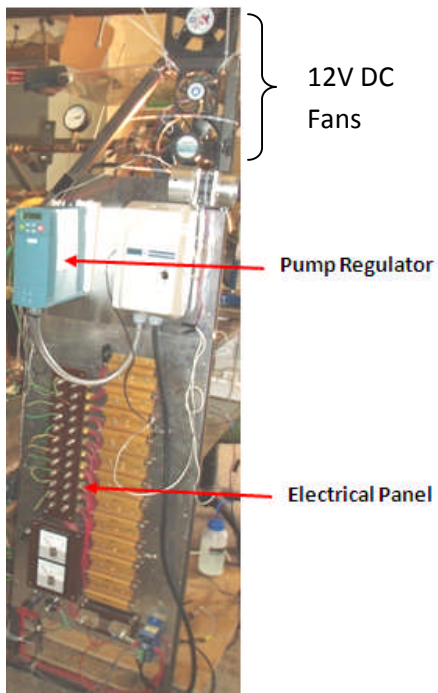
B: Voltmeter and Ammeter
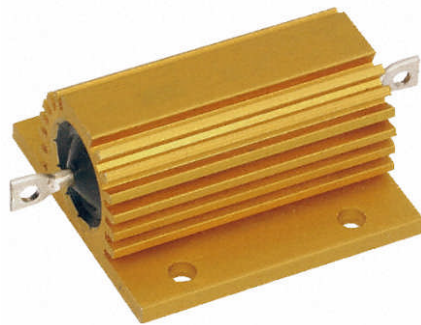
A: Electrical Panel   **C:** HS150 watts resistor
Figure 7.17: Details of Electrical panel and HS150 Resistor

when charging the battery and the key switch when turned on causes the

alternator to enter the excite mode or switch-on mode ready to produce

power. When switch 2 is turned on, switch 1 is turned off to power the

loads which might be any of the three mentioned earlier i.e. the bulbs or

the dc fans and or the HS150 wire wound resistors. To both charge the battery and power the load switch 1 and 2 must be switched on at the same time so that both processes are operational. Figure 7.16 show the two different kinds of bulb used in the load tests but Figure 7.17 indicates the electrical panel, and detail views of the panel and the HS150 resistor shown in alphabetical order of A, B and C respectively. The HS150 resistor dissipates the electrical energy as heat when used as the load.

Table 7.5 and Figure7.18 show both table and chart of the performance characteristics of HFE 7000 with respect to the electric boiler as heat

Table 7.5: Electric boiler performance data using HFE 7000

Pump setting %	Boiler pressure [Bar]	Boiler Temperature [℃]	Turbine rpm [-]
10	5.1	115	0
13	5.1	115	564
16	5.1	115	700
19	5	115	730
22	4.95	115	818
25	4.9	115	885
28	4.87	115	930
31	4.85	114.5	966
34	4.75	113	986
37	4.65	112	1019
40	4.55	110	1044
43	4.4	107	1058
46	4.3	104	1072
49	4.2	101	1082
52	4.1	98	1073
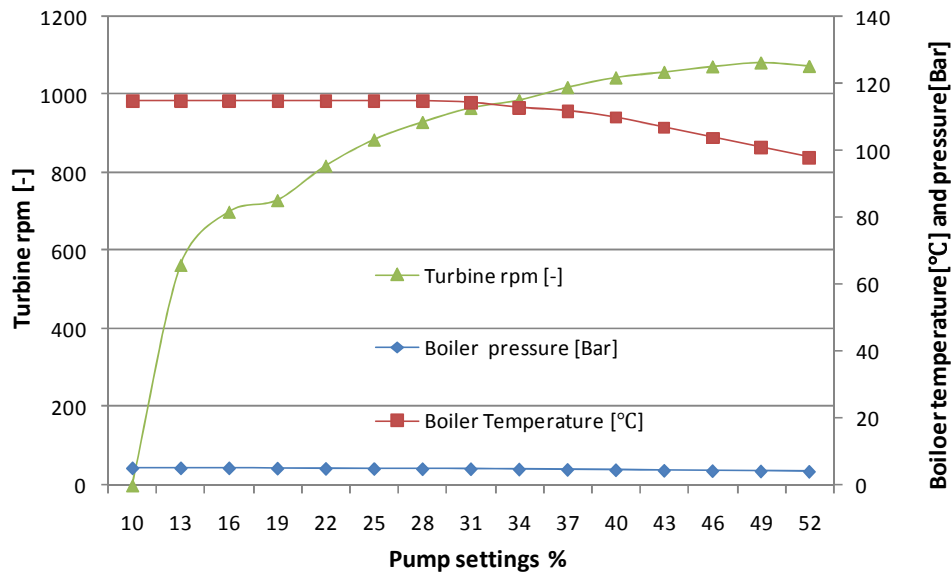
Figure 7.18: HFE 7000 performance chart

source with temperature and boiler pressure beginning to drop at higher flow rates. The rpm starts dropping as temperature reduces to 98°C and the reason for the reduction being the boiler inability to supply enough heat at higher flow rate because of its limited capacity. Also the boiler pressure decreases as flow rate increases and temperature remains fairly stable initially but starts decreasing with increases in flow rate. It is seen that pressure increases with increase in flow rate since each flow setting is run at constant pressure. However when temperature starts dropping, the system performance is affected.

Table 7.6 and Figure 7.19 is the measured data from the biomass ORC test using HFE 7000 in which same trends are observed but this time with an increase in turbine rpm mainly due to big pressure drop in the expander. Though the biomass boiler temperature remained lower than that of the electric boiler, the impressive pressure drop improved expander performance from a maximum of 1082 derived from the electric boiler test

to 2015 revolutions per minute (rpm) in this test. The turbine rpm is an essential part of electricity generation as the alternator must be sustained above the cut-in speed. The alternator cut-in rpm or ignition point is the rotational speed at which it starts producing power. This is ensured by maintaining a high turbine speed as the device slows down under electrical load. The alternator must be driven at speeds above 800rpm under load in order to produce any form of power. This is helped by sizing the turbine to alternator pulley by a ratio of 2:1 to increase alternator rpm.

Table 7.6: Biomass boiler performance data using HFE 7000

Pump setting %	Biomass boiler pressure[bar]	Biomass boiler temperature[C]	rpm [-]
10	3	100	0
13	2.9	100.2	0
16	2.7	95.2	820
19	2.5	92.3	1020
22	2.6	96.1	1233
25	2.5	91	1437
28	2.5	90.1	1550
31	2.5	92	1660
34	2.6	94.2	1720
37	2.6	94.4	1820
40	2.6	94	1887
43	2.5	93.5	1911
46	2.55	93.8	1984
49	2.56	94.4	2015
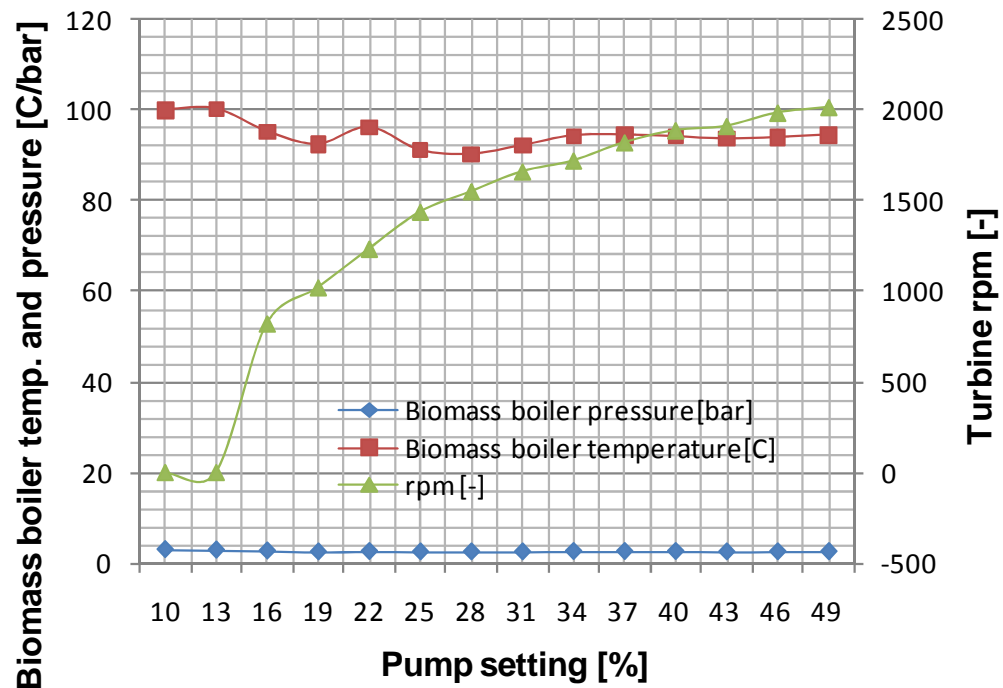
Figure 7.19: Biomass boiler temperature, pressure and turbine rpm vs. Pump settings

The turbine to alternator conversion efficiency of between is 40 - 65 % [112]. Figure 7.20 and Figure 7.21 indicate test performance based on the output voltage and current as well as the power output in watts; a product of the voltage and the current over time. The figures mentioned above indicate power output derived by using 20 watts halogen bulbs connected in parallel as resistance load and increasing the number of bulbs involved in the electrical load test. Subsequent test included the use of HS150 watts wire wound resistors which are connected in parallel and also systematically increased in numerical terms as resistance load. The system is allowed to run for a prolonged length of time to ensure that there is stability in output at the different load points. This is reflected in the power output chart in Figure 7.21 showing the some consistency in output

which means that the system performance is successful despite the limitations imposed by the boilers' low heat output.

The systems consistency is further tested with a confirmatory test shown in Figure 7.22 and Figure 7.23. HFE 7000 did better because of its low boiling point. Having performed the power test using the electric boiler as heat source, the biomass ORC power test was carried out and the measured data from the biomass test is shown in Figure 7.24 showing voltage and current output and Figure 7.25 is the power output. The average power output from the electric boiler experiment and the biomass boiler test is 90.39W and 113.31W respectively. The maximum power output is the tolerable output for the energy input and any further loading at this point will result in alternator rpm being lower than the cut-in speed.
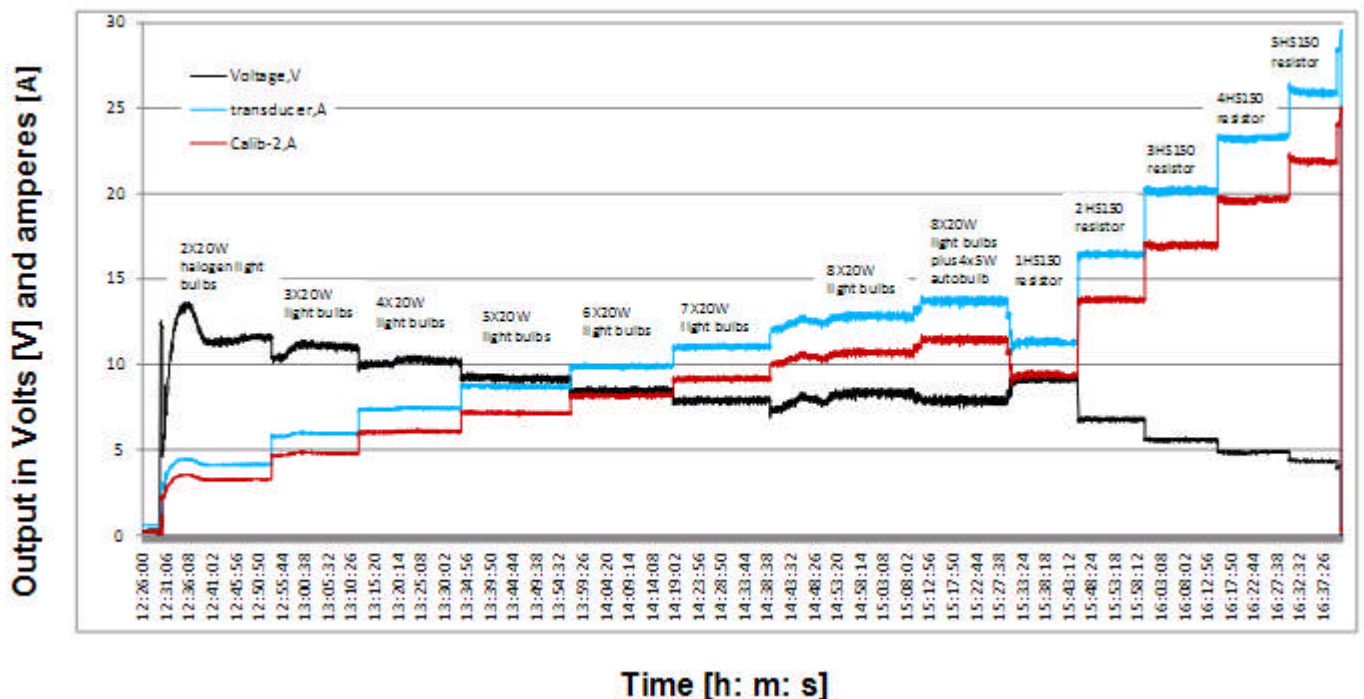
Figure 7.20: Voltage and current output vs. time (Electric boiler)
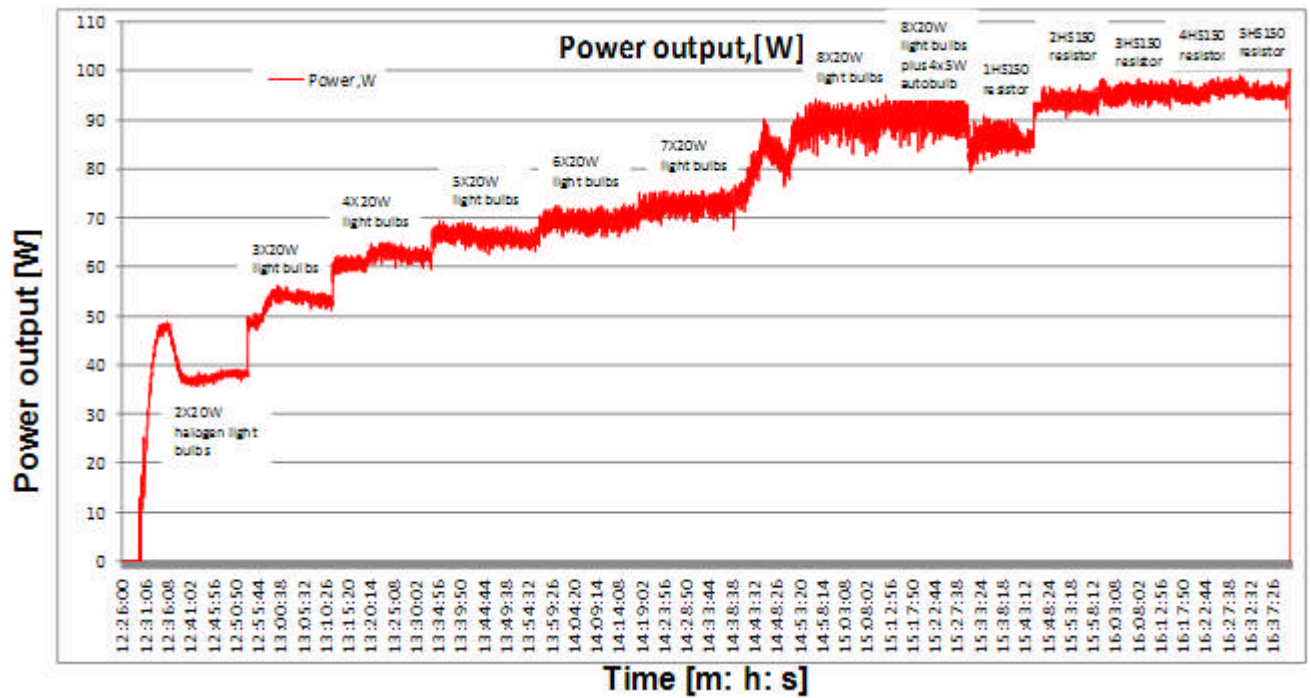
Figure 7.21: Electrical output vs. time (Electric boiler)
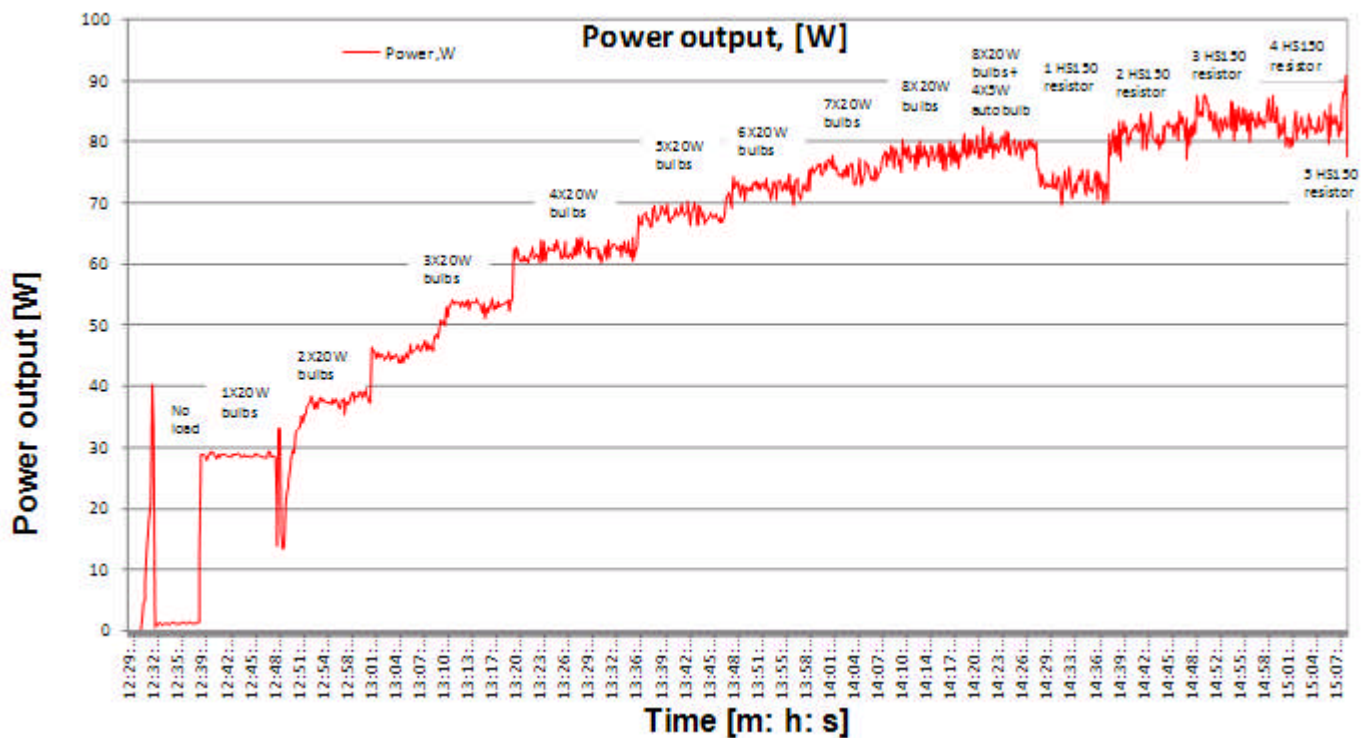
Figure 7.22: Confirmatory voltage and current output vs. time (Electric boiler)
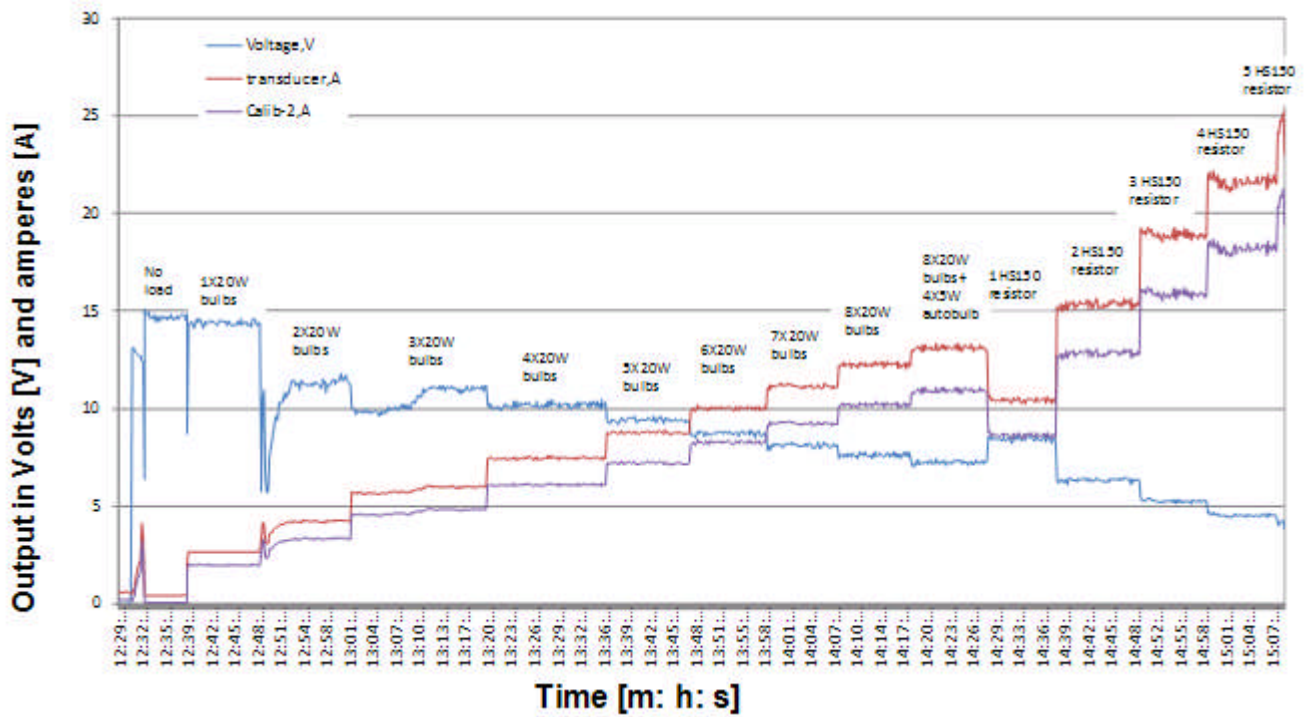
Figure 7.23: Confirmatory electrical output test vs. time (Elec. boiler)
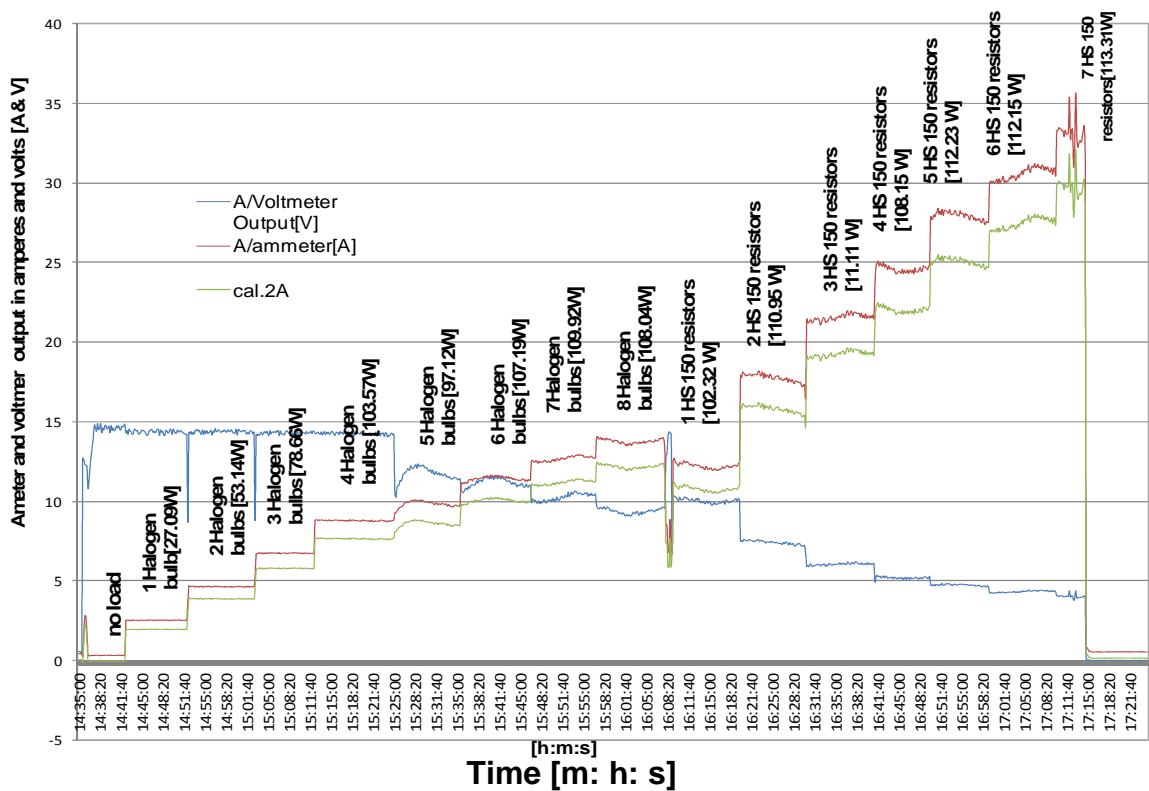
Figure 7.24: Voltage and current output vs. time (Biomass)
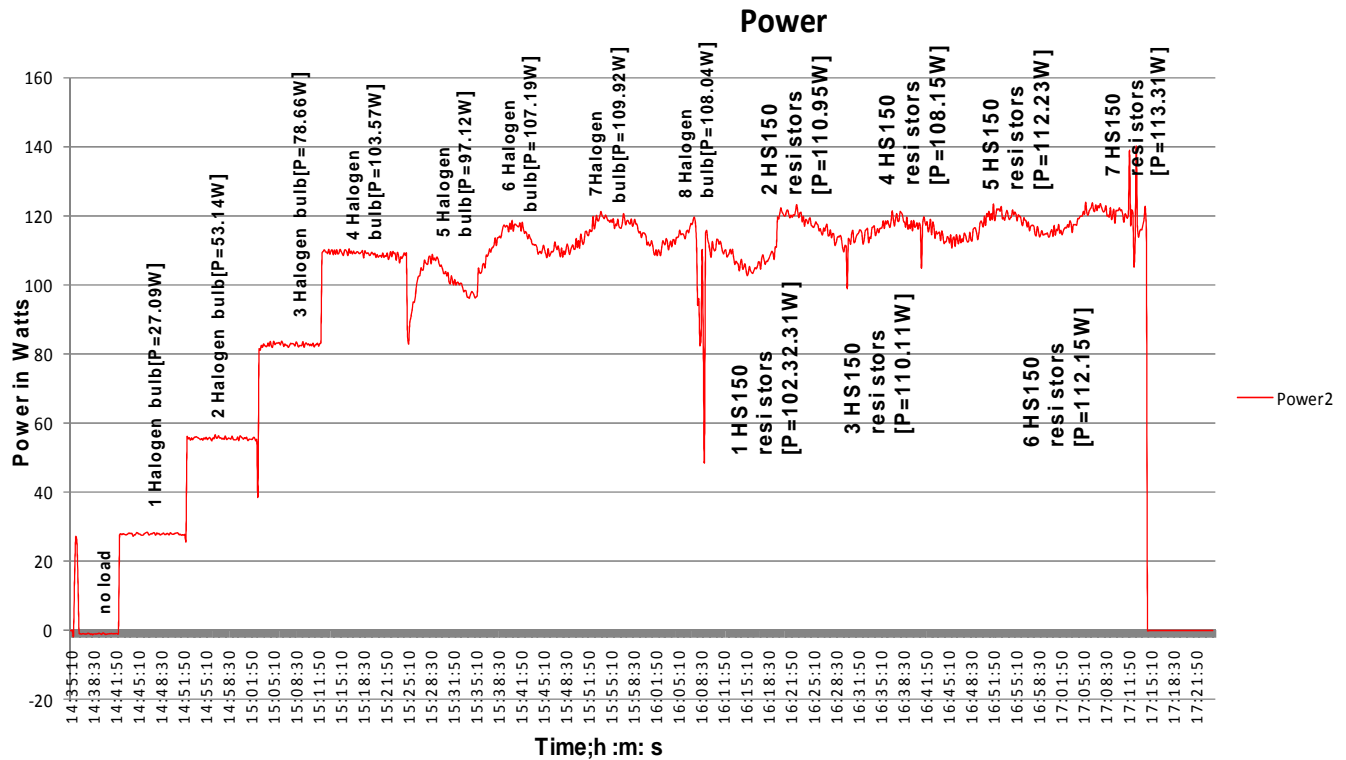
Figure 7.25: Electrical output vs. time (Biomass)

The electrical output tests are sequentially represented in Figure 7.26 and Figure 7.27 respectively showing a gradual increase in resistance load starting with two 12V; 20 watts halogen bulbs and increasing the number to 12 bulbs, the last four bulbs being a 12V; 5watts automotive bulbs.

The corresponding power output is indicated in each Figure. However, Figure 7.26 load sequence is alphabetically represented by letters A-D while Figure 7.27 is represented by letters E - H respectively and electrical outputs are accordingly indicated against each alphabet. This is basically a demonstration of system performance and indeed a positive indicator of the potency of the system.
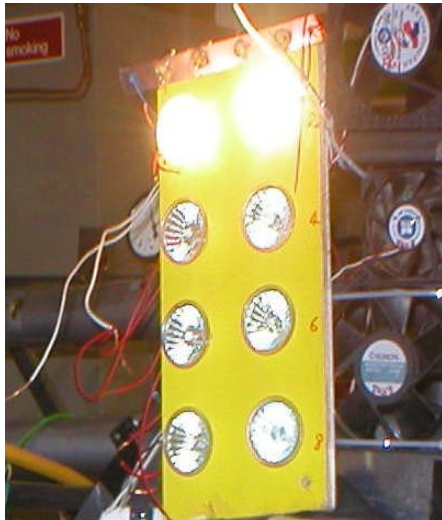
A: 2 halogen bulbs connected in

Parallel as load-output = 37.63W
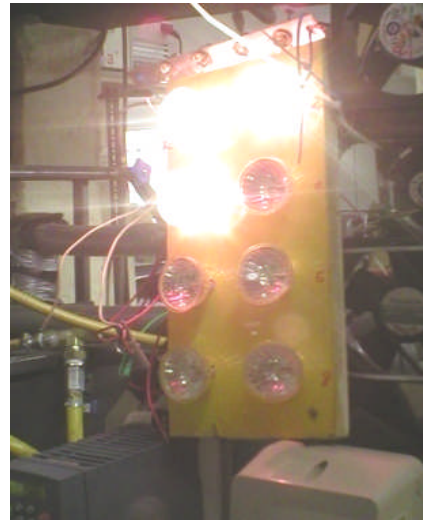
B: 3 halogen bulbs connected in

parallel as load- output = 53.76W
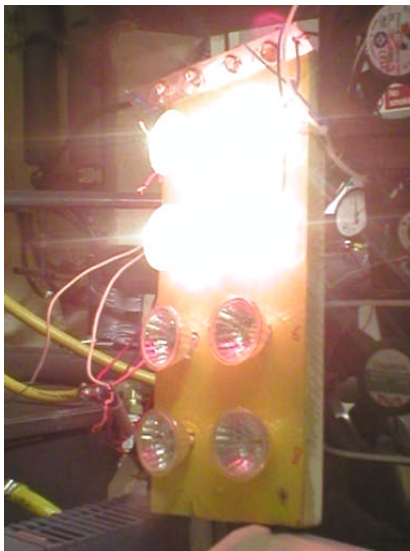
C: 4 halogen bulbs connected in
Parallel as load-output = 62.65W
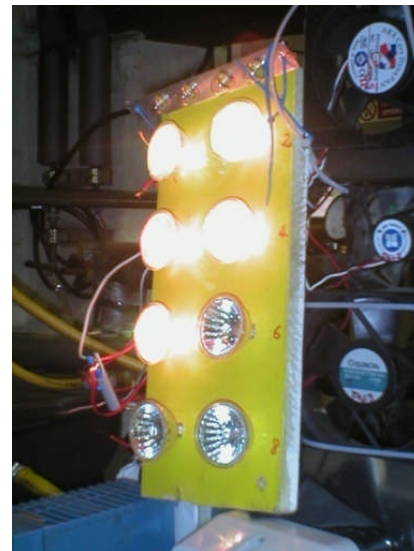
D: 5 halogen bulbs connected in
parallel as load –output= 65.76W

Figure 7.26 Electrical output tests involving up to a maximum of five halogen bulbs commencing from an initial two number
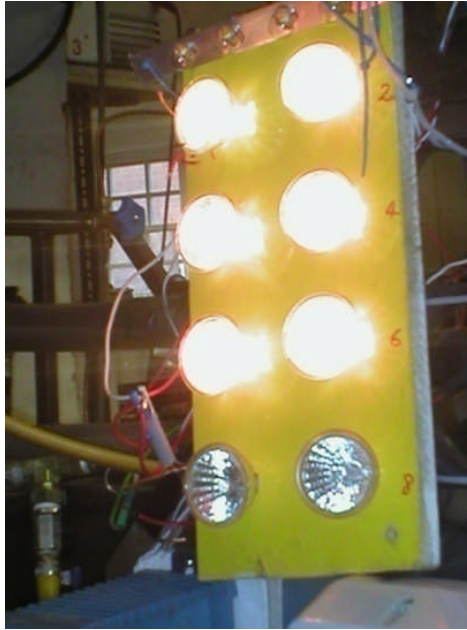
E: 6 halogen bulbs connected in Parallel as load-output = 69.75W
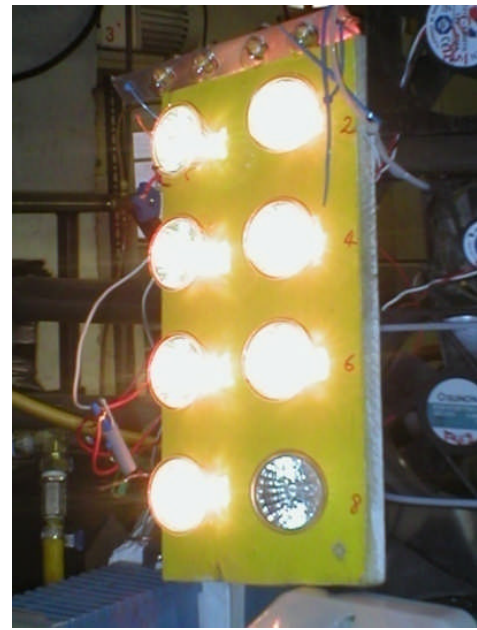
F: 7 halogen bulbs connected in parallel as load –output= 72.56W
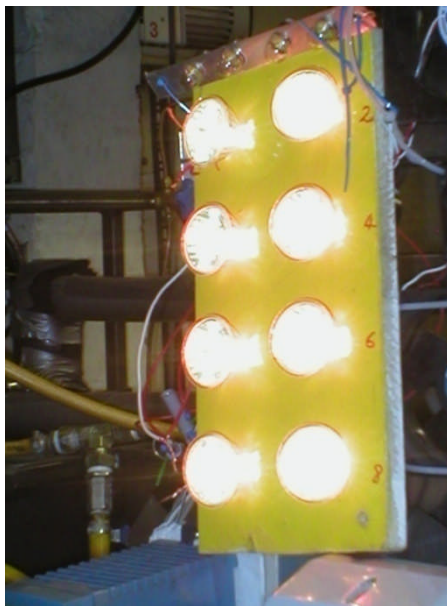
G: 8 halogen bulbs connected in Parallel as load-output = 89.51W
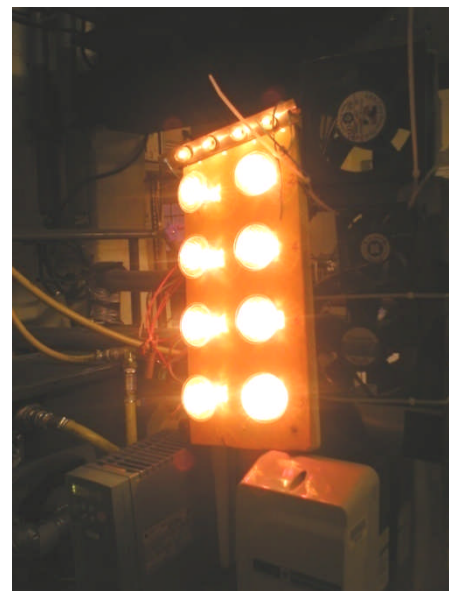
H: 8 halogen bulbs connected in parallel + 4-12V; 5W auto bulbs employed as load-output= 90.39W

Figure 7.27 Electrical output tests involving up to a maximum of eight halogen bulbs and 4 auto bulbs continuing from 6 bulbs
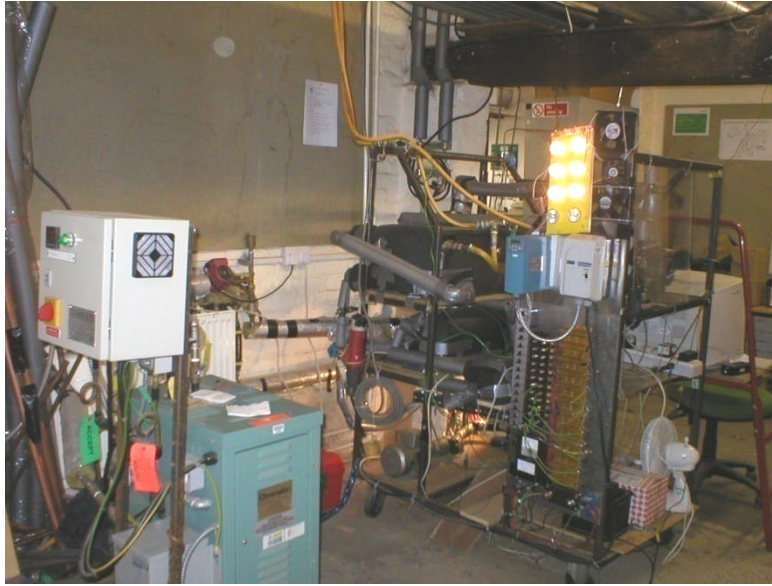
Figure 7.28 Power output from system shown against the background of test rig and electric boiler
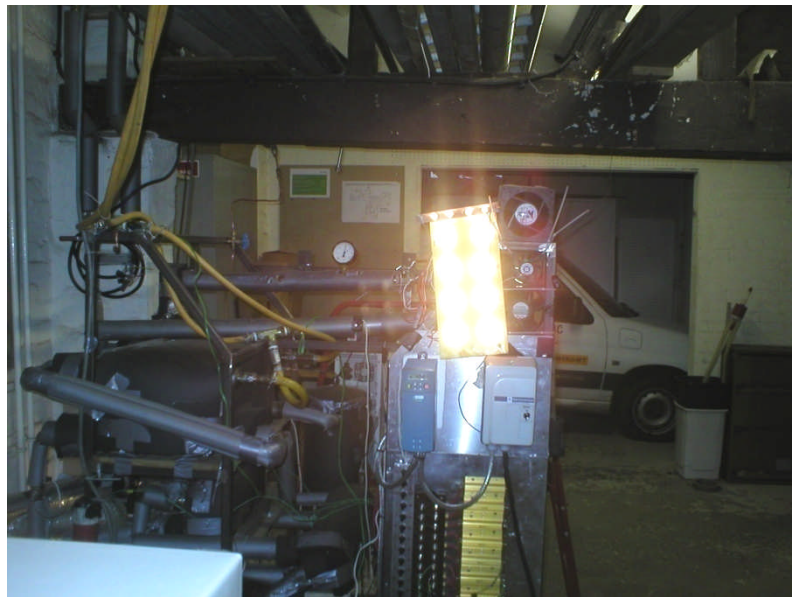
Figure 7.29 Fully lit arrays of test bulbs at maximum electrical output against the backdrop of test rig and in total, 12 bulbs are used as test load.

Figure 7.28 and Figure 7.29 show the rig setup and the power production

process being demonstrated, which is the key concept of using energy

stored both in biomass fuel and in the organic fluid to generate mechanical

energy via the expander and then converting it to electricity using the

alternator. The electrical efficiency though low is a positive way forward for CO2 mitigation using biomass fuel; a carbon neutral source of renewable energy. The predicted electrical efficiency using the electric boiler is 16.6 – 21.6% and 11.6-15% for the biomass boiler as calculated. The actual electrical efficiency based on the achieved output of 113W is 1.25% for the electric boiler and 0.9% for the biomass boiler respectively. The former is based on 9kW capacity for the electric boiler and 12.93kW for the biomass boiler.

Table 7.7: Performance output and Efficiencies of the biomass ORC experiment

Performance Description of biomass test	Theoretical assumptions [%]	Actual [%]	Remarks
Carnot efficiency	24.10	/	Theoretical efficiency only
Rankine efficiency	17.25	3.20	Lower actual efficiency
Alternator efficiency	40 - 65	55	Conversion efficiency
Electricity efficiency	6 - 7.8	0.44-0.9	Actual is low due to optimal operating conditions
Boiler efficiency	85	52	Actual is less due to regulated boiler heat output
Electricity output	2kWe	0.113kWe	maximum system output
Energy balance of ORC at 49% Pumping rate	/	78.7	input/output energy ratio
CHP efficiency		53	Due to boiler operational limit

However higher electrical efficiency can be realised but for the limitations imposed by the biomass boiler operating conditions limiting the operating temperature to 95°C when compared to HFE 7000 Critical temperature of 165.3^{o}C.

The comparism between the electric boiler and the biomass boiler is not necessarily to match output but the former was used to investigate and

determined the best operating conditions for the biomass ORC experiment. Table 7.7 is a summary of the biomass CHP system performance showing theoretical assumptions and the actual efficiencies. The actual performance is due to deviations in system expected output. The boiler is a 25kW biomass boiler but the maximum operating pressure is restricted to 3 bars and the maximum temperature as a result is 95°C and temperature could not be raised higher during the experiment. The biomass boiler useful energy was 12,93kW at 52% efficiency instead of the nameplate efficiency of 85%. However, if the flow rate was increased from 21 litres per minute used to 40 litres per minute by simple calculation using the product of the flow rate (kg/s), specific heat capacity of water (kJ/kg.K) and change in temperature (^{o}C) the maximum energy output from the biomass boiler can be achieved. This will increase the operating pressure above the specified limit. A reconfiguration involving some upgrading and retrofitting of the biomass boiler will address the problem but that process is outside the scope of this research work. This apparent fact also affected the performance of the Rankine engine because Rankine engine efficiency increases with increase in maximum operating temperature. The introduction of a recuperator in the cycle was to harness exhaust turbine heat to preheat the working fluid pumped to the vapour generator to increase the average temperature at which heat is transferred to the working fluid as an optimization strategy though with micro effect on the efficency.

7.4 Biomass CHP production

The system as a CHP produces low temperature hot water that is suitable for domestic washing but can be heated further for space heating and the system CHP efficiency is 53%. The low grade quality of the hot water is because of the recuperator at the exhaust of the turbine and the optimal operating conditions. To improve heat supply, a more robust source needs to be introduced that could yield temperatures between 120°C and 200°C or the existing ones retrofitted to perform the task. This option was not followed through being outside the scope and budget of this work and therefore a subject worth considering in perspective in a future research opportunity. The significance of raising the temperature at the turbine inlet is because of the critical temperature of both HFE 7100 and HFE 7000 is 195.3^{o}C and 165.3^{o}C respectively and fluids with higher critical temperature allows for a higher boiling temperature. The average temperature raised for both working fluids remained below 100°C because of the limited output of available facilities, especially the boilers. To be able to raise both the temperature and pressure to near the critical point, there is the need for a more robust heat source required to boost outputs.

7.5 Summary

Despite the fact that the biomass ORC has low efficiency of upto 53%, there is however some advantages as the system and most of the components work without maintenanace and this will result in low personnel and repairs costs. The Rankine engine is light weight, very low maintenance and cheap when compared with conventional turbines. In

this chapter, two major experiments are performed, on the one hand the electric boiler is employed as heat source and HFE 7000 as working fluid and on the other hand the biomass boiler is the heat source and the same working fluid is used. The electricity test is performed based on the best operating conditions and the resultant output of 113W though low because of limitations imposed by the boiler optimal operating conditions remains a vital demonstration of the potency of generating power by this process. The electrical efficiency is 0.9 - 1.25 %. In the previous chapter are experiments that measured turbine performance and identified the conditions that produced the highest rpm at about 49% pump setting crucial for driving the electric generator. The tests in this chapter are performed with inference to the previous results. As a CHP, the heat production was low grade heat at an average temperature of upto 30 - 40°C. This is because the recuperator extracted heat at the exhaust of the prime mover to preheat the working fluid pumped into the vapour generator and this reduced the amount and quality of heat available for use. The general low performance is sequel to the limitations imposed by the operational specifications and resultant output capacity of the biomass boiler.

Chapter 8: Conclusions and Further Work

8.1: Conclusions

This research work can be viewed in two broad spectrums; one is an appraisal of different aspects and reviews that form the basis for conceptualization of the work and another being the design and experimentation to demonstrate the key concept of the novel micro-CHP ORC process. Two novel working fluids, HFE 7100 and HFE 7000 are used as working fluid while a multivane expander is used as the micro turbine.

In all, four series of experimental investigations were carried out with acceptable results demonstrating the practicability of the novel micro-biomass ORC system. Each of the four tests numbered 1 - 4 is an outcome of a series of many other tests which were performed and aimed at system optimization and overcoming initial difficulties of articulating the system. Two heat sources were used; a 9kW electric boiler was used for preliminary tests and a 25kW biomass boiler was used for the final test. Each test is an improvement on the previous experiment. Both boilers had operational restrictions which must be accommodated in terms of the exit temperature. While the electric boiler is limited by its output capacity, the biomass boiler was limited by operating pressure of not more than 3 bars which puts the final average temperature slightly below a $100^{o}C$.

The first test i.e. tests - 1 had more insulation added and a vacuum pump is used to evacuate the system having sorted the sealing off all leaks in the system. The turbine was the most difficult to seal as the original seal was inadequate, prompting the use of external sealing with epoxy sealants

which stopped all leaking, resulting in an improvement of both the pumping process as rpm improved to 1336 rpm. However a mixture of liquid and vapour was present in the flow stream as the flow rate increased beyond the 30% mark due to limited heat supply from the boiler and because of HFE 7100 boiling point at 61°C. Further testing is discouraged if wet vapour is found in the flow stream.

In the second test i.e. Test - 2 further modifications had to be accommodated by the introduction of a recuperator in the cycle immediately after the turbine exhaust port which is a heat recovery measure and an improvement on Test - 1. The measure will ensure that the working fluid being pumped into the vapour generator is preheated by the heat from the turbine exhaust in the recuperator. This measure did improve the average heat transfer and temperature at the inlet of the turbine from 88.79^{o}C in Test - 1 to 98.39^{o}C but turbine rpm was seen to be less than Test – 1 at 940 rpm because of additional length of pipes and a couple of new bends to connect the recuperator but the improvement in heat transfer proved to be a useful in subsequent experiments especially involving the second working fluid HFE 7000 with electric boiler as heat source and in the biomass ORC test.

Test – 3 was performed using the electric boiler as heat source but without further modification to the test rig and HFE 7000 is used as working fluid to take advantage of lower boiling point which is less than HFE 7100. The result is that turbine rpm stepped up to 1082 rpm and the average temperature improved slightly at 98.45^{o}C. This is a strong indication that with the electric boiler, turbine inlet temperature stagnates within this

range. System performance is therefore a direct response to the limited input temperature.

The biomass boiler ORC test is the Test - 4 having same configurations as Test - 3 except for the biomass boiler connection to the test rig as heat source. The result show great potential for the biomass option though the boiler operating pressure is fixed at 3 bars and cannot in the circumstance be exceeded as turbine inlet temperature hinged at an average of 84.5^{o}C and the boiler exit temperature averaged 93.5^{o}C at the waterside. However despite this limited output, the expander rpm attained a speed of 2015 rpm made possible by the significant pressure drop in the expander. The electrical output test for both test - 3 and Test – 4 are similar but the biomass can in future be optimized by increasing the operating pressure in order to exploit its full potentials including changing the working fluid pump which long history of use. The biomass boiler was run at a water flow rate of up to 21 litres per minute yielding 12.93 kW of hot water against the nameplate output of 25kW. The tests and measurements in this research thesis are satisfactory based on the best case scenario. However this is a key demonstration of the concept of producing heat and power by using an environmentally friendly working fluid as the energy recoverable from the pressure difference is transformed into useful work in the micro turbine and the other portion is converted into heat. The electrical efficiency is between 0.9 - 1.25% and the overall system efficiency stands at 53%.

8.2: Further Work

8.2.1: Biomass ORC system

The anticipated 2kWe electrical output of the Biomass fired combined heat and power (CHP) ORC system will require further optimization and or retrofitting of the heat source to raise the necessary temperature in order to realise the expected electrical output. With enhanced turbine inlet temperature, turbine inlet pressure can be increased to drive the device at rpm that generates enough torque to overcome the resistance induced by the electrical load in the alternator. Rankine efficiency can be increased by altering two main properties; pressure and temperature of the boiler. It is also pertinent to suggest aspects, components, materials and devices that might be subject of further work, including systemic optimization and these are;

8.2.2: Working fluid

  The critical temperature of the working fluid must be key in setting new range for boiler temperature either by procurement or retrofitting to boost boiler output which must be capable of raising temperature of up to 200°C. This is predicated on the fact that the critical temperature of HFE 7100 is 195.3^{o}C and that of HFE 7000 is 165.3^{o}C respectively and that the boiler must be capable of sustaining temperature within this range across the heat transfer boundaries but not exceed the rated value as that might lead to substance decomposition or deterioration. This will enable pressures to be sufficiently raised to overcome the resistance generated in the alternator due to resistant load and to improve rpm and by implication the

electrical output of the alternator. The alternator depends on higher rpm to enhance power production.

8.2.3; The Automotive Alternator

The alternator employed in the test performed within the limits of available input to generate an electrical output. However, the turbine rpm must be raised sufficiently above the alternator cut-in rpm to improve performance. The suggestion is that of boosting heat input at the heat source as earlier proposed as current temperature peaked under a 100°C. In this work operating pressure could not be raised as temperature is relative to pressure, therefore performance was minimal but with positive indication that system can perform better than the present status and the heavy duty alternator required to produce 2kWe can be employed as the current output could not drive it when tested because of high operating torque, see Figure 8.1.

Figure 8.1: End and front view of heavy duty Prestolite alternator

8.2.4: Micro Turbine

The non-conventional micro turbine or expander is the Gast Air Motor, an air compressor reconfigured to operate thus. The critical aspects that need further investigation are the leaks from the expander seals as temperature and pressure increases over a period of time. Heat resistant seals are

suggested to replace the existing ones and possibly using the external sealants which proved to be effective during the current tests. Both strategies involving the combination of the two methods can be adopted for an excellent and enduring performance.
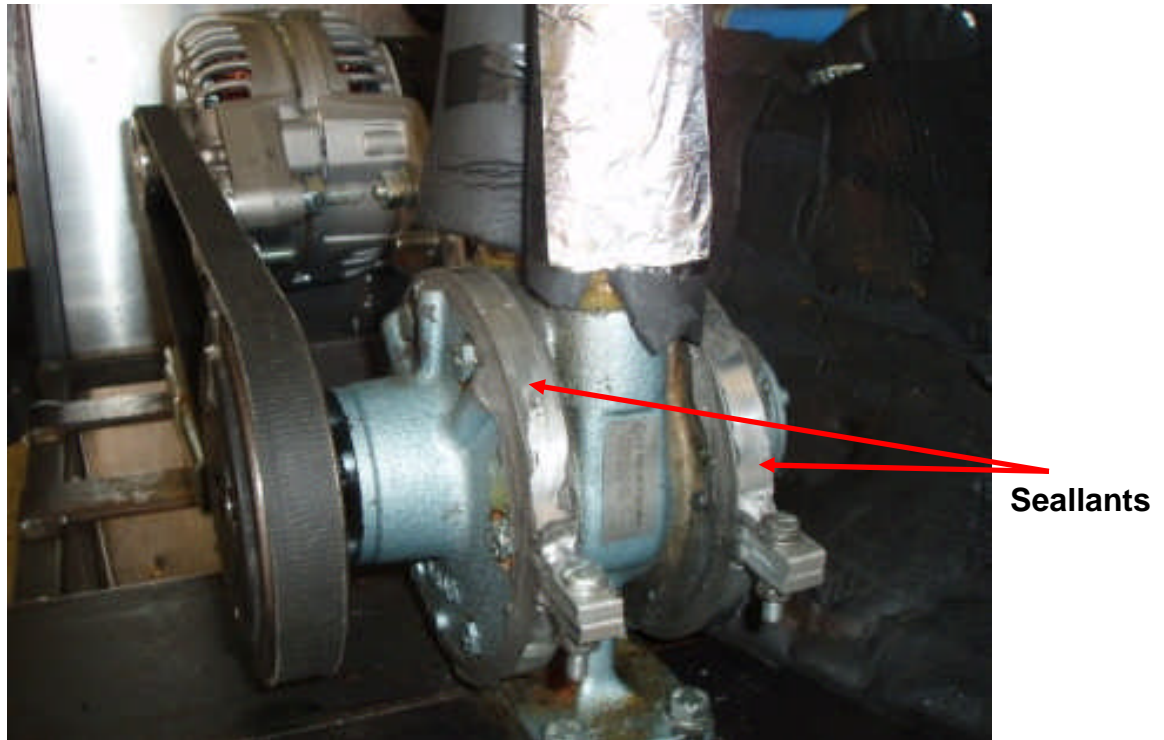
Seallants

Figure 8.2: Turbine showing epoxy seallants

8.2.5 Components, Materials and the System:

A more surgical and concise approach need to be adopted in further investigation of the biomass system including components re-evaluation. Investigation should involve specially designed heat exchangers and connection strategies between pipes and other components making up the system and these needs to be considered in further work. The highlights that need to come to a sharp focus as key optimization strategy will include;

❖ Assessment of the performance of HFE (hydroflouroether) at boiling point and under superheated conditions to properly assess its transport properties at varying heat transfer conditions.

❖ A design strategy that reduces excessive bends in the pipe work and also ensures leak free coupling and sealing of pipes and joints.

❖ Reducing cost and energy requirements by adopting control strategies that make the system stand alone.

❖ Demonstration of a robust state of art system that is mobile and can be deployed quickly in remote or isolated locations to function as a stand alone system.

❖ Broaden the technological knowledge by encouraging transfer to engineers, manufacturers, allied consultants and designers.

❖ Develop cost effective strategies and efficient system utilizing different forms of renewable energy resource from the biomass stock and other sources as; waste heat, geothermal and solar thermal energy.

The scope of the work will be futher broadened to include the economic analysis of the initial and operating costs as well as technological innovations looking at;

a/. A hybrid system that combines biomass and solar energy as energy source for CHP production.

b/. Solar desalination system that is driven by ORC will be used to desalination of sea water to produce drinking water for coastal population as scientist are predicting global water shortages predicated on the

anticipated effect of global warming and climate change on a massive scale.

c/. Improvement of the turbine as well as using the srew expander in place of vane expander.

References

1. Pablo Fernandez Ruiz et al, Report/ Executive Summary to the EU Commission, 2005.

2. BP-Statistical Review of World Energy, 2007.

3. http://www.exxonmobil.com

4. Riffat, S.B., Zhao, X, A novel hybrid heat pipe solar collector/CHP system- Part 1: system design and construction, Renewable Energy. vol.29, issue 12. March; 2004: 40.2

5. EU directive 2004/8/EC; http://energy.eu/directives/1_0522004022/en00500060.pdf; the official journal of the European Union, 2004.

6. Wikipedia, Oil Prices 1861-2006, http://en.wikipedia/wiki/Image:Oil Prices1861-2006.jpg. 2009.

7. TCS, Texas Citizens for Science, Texas Energy Planning Council, available online http://www.texscience.org/energy.php,2007.

8. R. E. Niggeman, W. J. Greenlee, P. Lacey, Fluid Selection and Optimization of an Organic Rankine Cycle waste heat power conversion system, ASME 78-WA;Jan.,1978.

9. Eckard, S.E., Multi-Vane expander as the prime mover in low temperature solar or waste heat applications, Proc. 1975 IECEC, AUG., 1975, No. 759204 pp1399-405.

10. Cheng Eng Cong, Sanjayan Velauthan, Amer Nordin Darus Sustainable power; solar thermal Driven ORC. International Conference on Recent Advances in Mechanical & Materials Engineering. (ICRAMME), Khala Lumper, Malaysia, May 2005; 91.

11. Curran, H.M., Use of organic working fluids in Rankine Engines, 15th Intersociety Energy Conversion Engineering Conference, Seattle, Wash, .Aug, 1980; 80-9194.

12. Barber, R and D. Prigmore, "Solar Powered Heat Engines", Solar Energy Handbook, J. F. Kreider and F. Kreith eds.McGraw-Hill,New York,1991.

13. http://www.zebu.uoregon.edu; 1998.

14. Stern N. stern; "The economics of climate change, the Stern review", Cambridge University Press, Cambridge, 2006.

15. M. L. Parry et al, Impacts, Vulnerabilities and Adaptation in developing Countries, IPCC, Cambridge University Press, Cambridge, UK; 2007,pp 687-716.

16. An Assessment of the Intergovernmental panel on Climate change (IPCC; Valencia, Spain, November, 2007.

17. BP Statistical review of World Energy, 2007.

18. http://europa.eu.int/comm/environment/climate/pdf/c.2004_130 eu commission trading scheme, 2005.

19. European Union Emission Trading scheme; http://www.defra.gov.uk/climatechange/trading/eu/what

20. Meehle G.A. et al, IPCC Fourth Assessment Report of the Intergovernmental Panel on Climate Change, IPCC, 2007.

21. http://upload.wikimedia.org/wikipedia/commons/9/94/ShrinkingLake Chad-1973-1997-EO.jpg

22. Oludasu et al, Nigerian's household energy sector; Issues and supply/demand frontiers, 1994, Butterworth-Heinemann Limited.

23. United Nation Environment Programme; 2000, Industry and Environment Review.

24. http://www.wasteonline.org.uk/resources/InformationSheets/vehicle.htm

25. J. Karl, Decentralised Energy systems, New Technologies in Liberalised Energy Market; Oldenburg Vela, Munched, 2004, Germany

26. http://www.sinauer.com

27. Koren, Herman, Michael S. Bisesi, Handbook of Environmental Health: Pollutants Interaction in Air; 2003 (T&E).

28. Dr.S.Schuck; http://www.users.bigpond.com/SteveSchuck/ABT

29. *EUROPA, European Commission,*

   (*http://europa.eu.int/comm/research/energy/nn/nn_rt/nn_rt_bm/article_1 111_en.*)

30. IEA Bioenergy, Biomass Combustion and Co-firing: An Overview.

31. Twidell, J."Biomass Energy", Renewable Energy World, 1998.vol.1, no3, pp38-39.

32. EUBIA - European Biomass Industry Association; Biomass Characteristics; http://www.eubia.org/115.0html.

33. Svoboda k. ,Poharely M., Martinec J., Baxter D., Hunter Ch., Integration of biomass drying with Combustion/Gasification technologies and minimization of organic compounds, 32nd International Conference of SSCHE, Slovakia, May, 2005.

34. http://www.eubia.com

35. EU Biomass-Green energy for Europe, EUR.21350, 2005

36. http://www.mo.nrcs.usda.gov.

37. What is gasification, Frontline Bio Energy, Inc; http://www.frontlinebioenergy.com/id17.html

38. http://www.irishphotnews.com

39. Turkenberg et al, Renewable energy technologies, in (eds. J Goldenberg et al); World Energy Assessment: Energy and the Challenge of Sustainability. UN Development Programme, New York, 2000.

40. Faaij, A., I. Steetskamp, A. van Wijk, *Exploration of the land potential for the production of biomass for energy in the Netherlands.* Biomass and Bioenergy, Vol 14.No. 5/6. Pp.439-456, 1998

41. Loo, van, S., J. Koppjan (eds.), *Handbook Biomass Combustion and Co-firing*, Twente University Press, Enschede, the Netherlands, 2002.

42. http://www.reuk.co.uk

43. K Braber, *Anaerobic digestion of municipal solid waste: A modern waste disposal option on the verge of breakthrough* Biomass and Bioenergy, Volume 9, Issues 1-5, 1995, Pages 365-376

44. http://www.habmigern2003.info/biogas/Pyrolysis .htm

45. Bridgewater, A.V. *The status of fast pyrolysis of biomass in Europe.* Proceedings of the 10th European Biomass Conference and Technology Exhibition, Wurzburg, Germany, (1998), pp 268-271.

46. Naber, J.E., F. Goudriaan, A.S. Louter, *Further development and commercialisation of the small scale Hydro-Thermal Upgrading Process for Biomass Liquefaction.* In: Proceedings of the Third Biomass Conference of the America's, Montreal, 1997.

47. http://www.desipower.com/technology/tech_main.htm

48. US Departmentof Energy (DOE), NREL, 1998;
http://www.puco.ohio.gov/PUCO/IndustryTopics.cfm?id=4400.

49. DETR, UK climate change draft programme, 1998.

50. Pilavachi PA, ''Mini and micr-gas turbine for combined heat and power''
Applied Thermal Engineering, 2002

51. Fairchild PD, Labinor SD, Zaltash A, Rizy DT, Experimental and
theoreticalstudy of micro turbine based BCHP system, ASME
International Congress, 2001, NY, USA

52. Gomes E, do Nascimento M, Lora E, Pilidis P, Haslam A, Performance
evaluation and case studies of microturbine fuelled with natural gas and
diesel. Part A: Journal of Power and Energy, 2004; 599-607.

53. Bruno JC, Massagues LI, Coronas A, Stand – alone and grid connected
performance analysis of regenerative micro turbine cogeneration plant.
Part A: Journal of Power and Energy 2004, 218: 15-22.

54. J.M.Piers, D. Reynaerts, F. Verplaetsen, M. Poeson, P. Renier, A
Microturbine for Electric Power generation, Proc. MME'02,
Sinaia,Romania; pp 275-278.

55. McDonald, C.F. Low-cost compact primary surface recuperator concept
for micro turbines; Applied Thermal Engineering, 2002, 20:471-497.

56. Fuel cells basics;
www.energysolutionscentre.org/distgen/AppGuide/Chapters/Chap4/4-
4Fuel_C...12/05/2009.

57. http://americanhistory.si.edu/fuelcells/basics.htm..12/05/2009

58. Florschuetz, L.W. Extension of the Hottel-Whillier model to the analysis
of combined photovoltaic/thermal flat-plate collectors; Solar Energy
1979, 22(4):361-366.

59. Zondag, H.A, D.W. de Vries, W.G.J. van Helden, R.J. C. van Zolingen
and A.A. van Steenhoren; The yield of different combined PV-thermal
collector design, 2003, Solar Energy 74(3): 253-269.

60. Huang, B.J., T.H. Lin, W.C.Hung, and F.S.Sun; Performance evaluation
of solar photovoltaic/thermal systems 2001. Solar Energy 70(5):443-
448.

61. He Wei, Tin-Tai Chow, Ju Ji, Jianping Lu, Gang Pei, and Lok-Shun Chan; Hybrid photovoltaic and thermal solat collector designed for natural circulation of water 2006, Applied Energy 83(30):199-210.

62. A .Ibrahim, K. Sopian, M.Y.Othman; Simulation of building integrated photovaoltaic solar collector (BIPVT); EM^{3}ARC, 2007.

63. J.Hanson, H.Sorenson; PV/Thermal Solar System, www.iea-shc.org/task35.

64. http://www.pvtsolar.com/how.html

65. Badr, O., S. Naik, and P. W. O'Callaghan, 1991, "Expansion Machine for a Low Power-Output Steam Rankine-Cycle Engine," *Applied Energy*, 39, pp. 93-116.

66. Yamamoto, T., T. Furuhata, N. Arai, and K. Mori, 2001, "Design and Testing of the Organic Rankine Cycle," *Energy,* 26(3), pp. 239-251.

67. Kane, M., D. Larrain, D. Favrat, and Y. Allani, 2003, "Small Hybrid Solar Power System," *Energy*, 28, pp. 1427-1443.

68. Larjola, J, 1995, "Electricity from Industrial Waste Heat Using High-Speed Organic Rankine Cycle (ORC)," *International Journal of Production Economics*, 41, pp. 227-235.

69. Smith, T. C. B., "Low Cost Organic Rankine Cycles for Grid Connected Power Generation," *Proceedings of the ISES Solar World Congress*, 2003, Göteborg, Sweden, International Solar Energy Society, 8 p.

70. Wells, D. N., "Scroll Expansion Machines for Solar Power and Cooling Systems." 2000, *Proceedings of Solar 2000*, Madison, WI, American Society of Mechanical Engineers, 7p.

71. http://www.eren.doe.gov/biopower

72. A .Schuster, S. Karellas, E.Kakaras, H. Spliethoff, Energetic and economic investigation of Organic Rankine Cycle applications,Appplied Thermal Engineering, Aug;2008

73. Ingwald Obernberger et al, Basic iformation regarding decentralized CHP plants based on biomass combustion in selected IEA partner countries final report, Graz, Austria; Feb; 2004.

74. Small Scale Electricity Production from Biomass; http://www.turboden.it/en/applications_detail.asp?titolo=Biomass

75. Auckland, D.W., Green, A., Luff, A.C., and Shuttleworth, R.: 'The feasibility of kilowatt combined heat and power systems for domestic use'. Proceedings of Universities Power Engineering Conference, 1991, pp. 285-288

76. Government statistical service: "Digest of United Kingdom energy Statistics"; 1994, HMSO, London, 1995

77. Electricity generation in the home: evaluation of single-house domestic combined heat and power; Pearce, J.M.; Al Zahawi, B.A.T.; Auckland, D.W.; Starr, F. Science, Measurement and Technology, IEE Proceedings - Volume 143, Issue 6, Nov 1996 Page(s):345 – 350

78. Everett, R., Horton, A., Doggart, J., and Willoughby, J.: 'Linford low energy houses'. Report ETSUS- 1025, Energy Technology Support Unit, Harwell, 1985

79. V. M. Nguyen et al; March, 2000, "Development of a prototype low-temperature Rankine cycle electricity generation system", Applied thermal Engineering 21(2001) 169-181.

80. Takahisa Yamamoto et al; Design and testing of the Organic Rankine Cycle, ScienceDirect- Energy: vol26. Issue 3, March 2001, pp 239-251

81. Badr O, Probert SD, et al, Performance of multi-vane expanders;Appl Energ 1985;20(4):253-85,

82. Donghong Wei et al;Dynamic modelling and simulation of an Organic Rankine Cycle (ORC) system for waste heat recovery ; Applied Thermal Engineering 28 (2008) 1216–1224

83. Badr O, Probert SD, O'Callaghan PW. Selecting a working fluid for a Rankine cycle engine. Appl Energ 1985; 21:1–42.

84. Badr O, O'Callaghan PW, et al. Thermodynamic and thermophysical properties of organic working fluids for Rankine cycle engines. Appl. Energ 1985; 19(1):1–40.

85. Badr O, Probert SD, et al. Multi-vane expanders: vane dynamics and friction losses. Appl Energ 1985; 20(4):253–85.

86. Badr O, O'Callaghan PW, et al. Multi-vane expanders as prime movers for low-grade organic Rankine cycle engines. Appl Energ1984; 16(2):129–46.

87. Badr O, O'Callaghan PW, et al. Multi-vane expanders: geometry and vane kinematics. Appl Energ 1985; 19(3):159–82.

88. Fréchette, L.G, Lee C., Arslan S., Liu Y.C., "Design of a Micro fabricated Rankine Cycle Steam Turbine for power Generation", *Proc. ASME Int'l/Mech. Eng. Cong. & Expo.*,

89. Takeo S.Saitoh, Akira Hoshi; Proposed solar Rankine cycle system with phase change steam accumulator and CPC solar collector, IECEC 2002 paper, no.20150.

90. Cheng Eng Cong, Sanjayan Velautham, Amer Nordin Doris; Solar thermal driven ORC, Proceedings of the International conference of recent advances in Mechanical and Maaterial engineering, 2005, Kuala Lampur, Malaysia.

91. R.B.Peterson, H. Wang, T.Henon; Performance of a small-scale regenerative Rankine power cycle employing a scroll expander. Proc, IMechE, vol.222. PA: Journal of Power and Energy, 2008.

92. http://en.wikipedia.org/wiki/Carnot_cycle

93. http://www.angelfire.com/ultra/omshome/powercycles.htm##Rankine Cycle, Jan., 2009.

94. http://www.mhtl.uwaterloo.ca/courses/me354/lectures/pdffiles/c5.pdf

95. Donghong Wei et al, Performance analysis and optimization of Organic Rankine cycle (ORC) for waste heat recovery; Oct., 2006.
Wash., D.C., Nov. 16-21, 2003.

96. K. M. Lee and M.L. Chien et al., Parameters analysis on Organic Rankine Cycle energy recovery system, Energ Convers Manage 28(2) (1988), pp.129-136.Abstract.

97. T. C. Hung, Shai, S. K. Wang; A review of Organic Rankine Cycle (ORCs) for the recovery of low-grade waste heat, Energy (2297) (1997)661-667.

98. J. Larjola, P. Sarkomaa, Suistoranta; 'New technology ORC-plant for heat recovery of diesel engines, in 17th International Congress on Combustion Engines(CIMAC 1978)', June 8-11,1987,Paper D-12, Warsaw

99. C. Somayaji, P. Mago, L.M. Chamra, 'Second law analysis and optimization of Organic Rankine Cycles in; ASME Power Conference, Paper no. PWR 2006-88061, Atlanta GA, M AY 2-4, 2006.

100. S. Quoilin, Experimental Study and Modelling of a low Temperature Rankine Cycle for small scale Cogeneration; Thesis, Faculty of Applied Sciences, University of Liege; May, 2007.

101. Status Report on Solar Thermal Power Plants, Pilkington Solar International GmbH; Colonge, Germany, 1996.

102. S. Canada, Parabolic Trough Organic Rankine cycle Solar Power Plant, presented at the 2004 DOE Solar Energy Technologies Program review meeting; October, 2004, Denver, Colorado.

103. The effect of temperature and pressure on Rankine cycle efficiency, http://www.angelfire.com/ultra/omshome/powercycles.htm

104. AICS ;(http://www.nicnas.gov.au)

105. NOHSC (2004) Approved criteria for classifying hazardous substances, 3rd edition [NOHSC: 1008(2004)]. National Occupational Health and Safety Commission.

106. FORS (Federal Office of Road Safety), Australian Code for the Transport of Dangerous Goods by Road and Rail, (1998) 6th ediion. Canberra, AGPS.

107. European Commission "Technical Guidance Document on Risk Assessment in support of Commission Directive 93/67/EEC on risk assessment for new notified substances"; (2003).

108. Derelanko M.J "Toxicologist's Pocket Handbook"; (2000) Boca Raton, CRC Press.

109. NICNAS, July, 1990.
(http://www.nicnas.gov.au/Publications/chemical Gazette.asp)

110. DT500;
(http://www.datataker.com/Datalogger_Manual/Construction), 2003; Datataker Users' manual, series 3.

111. http://www.answers.com/library/Britannica Concise Encyclopedia-cid-2362

112. D. M. Whaley et al, 'Extracting More Power from the Lundell Car Alternator'; Australian Universities Power Conference (AUPEC, 2004), Brisbane Australia.

113. D. J. Perreault and V. Caliskan, "A new design for automotive alternators". In IEEE/SAE International Congress on Transportation Electronics (Convergence), SAE paper 2000-1-C084, 2000.

114. http://www.prestolite.com/literature/alts/PP1097_bld_12v.pdf

115. http://www.datataker.com/Datalogger_Manual/Construction%20of%20the%20dataTaker%20500%20600.htm

116. http://www.nktechnologies.com/content/download/DT_Series.pdf

117. http://www.coleparmer.co.uk/catalog/product_view.asp?sku=08500

118. http://www.wikipedia.org/wiki/LMTD

119. http://www.alfalaval.com/solution-finder/products/cb/Documents/CB%20Series%20-%20CB14-77.pdf

120. Air Conditioning and Refrigeration Journal, The magazine of the Indian Society of Heating, Refrigerating and Air Conditioning Engineers 7th Oct, 2008. 10.49am.
http://www.hvcindia.org.in/journal/2001.apr./articlehttp://www.hvacindia.org.in/journal 2001.apr)

121. Royce n. Brown, 'Compressors; Selection and Sizing, third edition, pp.126; Published by Elsevier, 2005.

122. G. F. Robertson and C. H. Wolgemuth, Analysis and test apparatus for a vane expander using steam. Proc. 1975, IECEC, Aug,.1975, No 75925, pp1406-10.

123. G. F. Robertson and C. H. Wolgemuth, Experimental and Analytical Study of friction, leakage and heat transfer in a vane expander,Proc.1978,IECEC, Aug.,1978, No.789521, pp1430-41.

124. Thomas A. Davidson et al, Design and Analysis of a 1KW Rankine cycle, employing a multi-vane expander for use with a low temperature Solar collector, Thesis; Massachusetts Institute of Technology, US, May, 1997.

125. Professor Vladimir Chumsky, Reciprocating and Rotary Compressors, Compressor and Refrigeration Department, Technical University of Prague .pp275-86, SNTL 1965.

126. Ertesvåg, I. S., 1998, "Kjell Vading's engine principle – Thermodynamic analysis and functional analysis" (in Norwegian). Report No. TR F4708, Sintef Energy Research, Trondheim, Norway.

127. http://www.jotek-eng.com/documentation/Brochure%20-%20RotoVane%20General%20-%20JoTEK.pdf

128. http://ristretto.ecn.purdue.edu/class/me200/files/me200_notes_f08_week12-14.pdf

129. http://www.answers.com/topic/globe-valve

130. Tuma, P.E "Segregated Hydrofluoroethers: Long term Alternative Heat Transfer Liquids." Proceedings of the 2000 Earth Technologies Forum, Oct.; 2000, Washington, D.C., PP.266-75.

131. Tuma, P.E. and Touseignant, L. "Modelling Vapour Leak Rate and System Pressure for Single-Phase Heat Transfer Systems that Utilize Fluorinated Heat Transfer Liquids, 2000.

132. Donghong Wei, Xueshang Lu, Zhen Lu, Jiaming Gu; "Dynamic modelling and simulation of Organic Rankine Cylce(ORC) System for waste heat recovery system; Applied thermal Engineering 28(2008)1216-1224.

133. http//www.ecpower.co.uk/princip.jsp., Nov., 2008. EC Power UK. Ltd.

Appendices

Appendix I: Characteristics and Properties of HFEs
    Table1_1: Physical properties of HFE 7000 and HFE 7100

Property	Low Temperature					
	HFE HFE-7000[1] $C_3F_7OCH_3$	Fluorinert FC-87[1]	HFE HFE-7100[1] $C_4F_8OCH_3$	Fluorinert FC-72[1]	HFE HFE-7200[1] $C_4F_8OC_2H_5$	Galden HT-70[2]
Atmospheric Lifetime [yrs]	4.7	N/A	4.1	N/A	0.8	N/A
GWP (100 year ITH)	400	N/A	320	N/A	55	N/A
Boiling Point [°C]	34	N/A	61	-	76	N/A
Pour Point [°C]	-122.5	N/A	-138	-	-135	-
Useful low Temperature [°C][4]	-122.5	N/A	-106	-	-106	-
Density [kg/m3]	1400	N/A	1420	-	1510	-
Coefficient of Expansion [1/°C]	0.00219	N/A	0.0016	-	0.0018	-
Specific Heat [J/kg-K]	1300	N/A	1220		1180	-
Viscosity [cSt] at 25°C at -40°C	0.32 0.78	N/A	0.37 1.1	N/A	0.44 1.26	N/A
Dielectric Strength [kV, 0.1 inch gap]	~40	N/A	~40	N/A	~40	N/A
Dielectric Constant	7.4	N/A	7.3	N/A	7.4	N/A
Electrical Resistivity [ohm-cm]	1.E+08	N/A	1.E+08	N/A	1.E+08	N/A

N/A – Not applicable

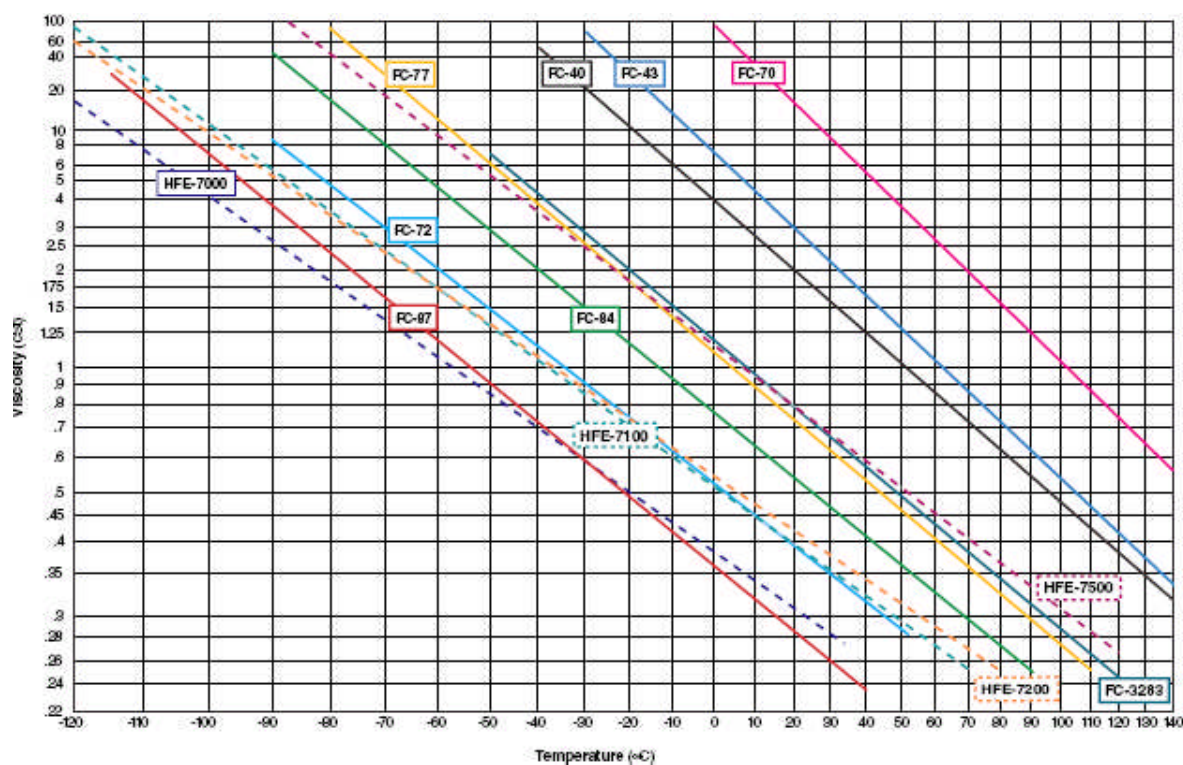Source: http://multimedia.3m.com/mws/mediawebserver

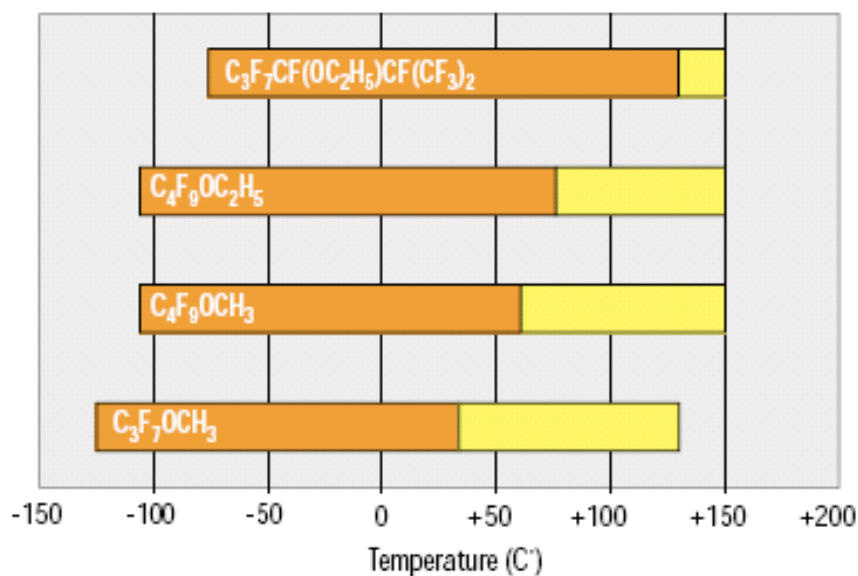**Figure1_1; Viscosity vs. Temperature of HFE 7000 and HFE 7100**

Figure 1_2: Useful temperature range of four segregated HFEs. Yellow bars show the liquid range. Orange bars show the pumpable range, as dictated by thermal stability.

Source: http://multimedia.3m.com/mws/mediawebserver

261

Table1_2: Compatibility with HFEs

Metals		
Copper	Iron	Zinc
Stainless steel	Titanium	Aluminum

Hard polymers		
Polyethylene	Polypropylene	Phenolic
ABS	Nylon	Ryton
Polyvinlychloride (PVC)	Polycarbonate (Lexan)	Polyetheretherketone (PEEK)
Acrylic (Plexiglas)	Rulon	Thermoplastics
PTFE (Teflon)	Polysulfone	Epoxies

Elastomers[1]		
Nitrile	Silicone	Ethylene propylene (EP or EPDM)
Butyl	Fluorocarbon	Stillman SR721-80
Stilllman SR634-70	Stillman TH1387	Parker EPR 540-80
Bay Seal Co. B0612-70	Natural rubber	Jackson Flex. Prods. EPR E3450-80
Fluorosilicone	Polysulfide	Parker EPR E515-80
Chloroprene	Polyurethane	Newman EPDM 2107
Polyacrylate	Styrene butadiene	International Seal E480

Hoses		
Tygon C-544-A I.B. polyurethane		TFE
Tygon 3370 I.B. silicone		Parker Parflex 550
Flexfab 5521 silicone		Aeroquip FC373
Nalgene 290 PUR polyurethane		TFE, PFA

[1]Compatibility depends upon the specific formulation. The specific compounds shown have performed well in extraction studies.
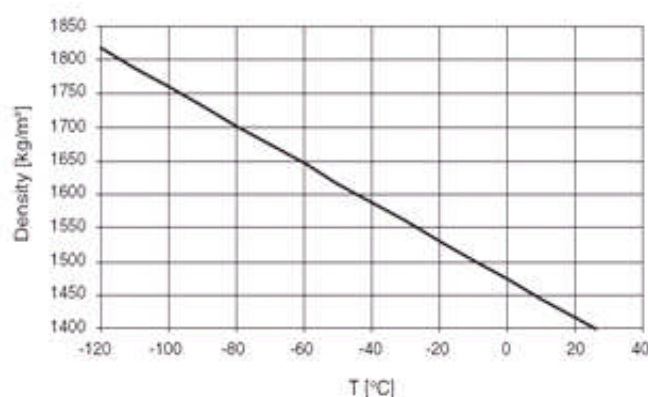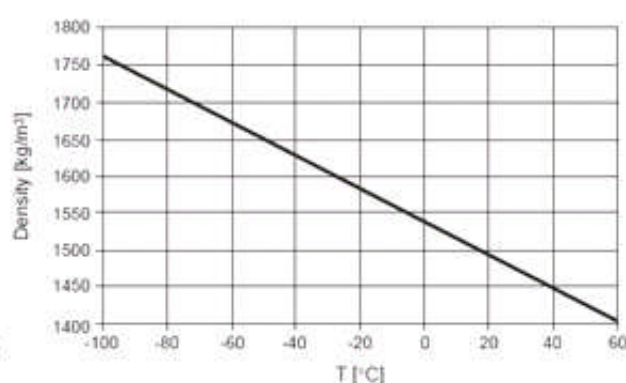
A - HFE 7000 liquid density   **B - HFE 7100 liquid density**

Figure 1_3; Liquid densities of HFE 7000 and HFE7100

Source: http://multimedia.3m.com/mws/mediawebserver

Appendix II: Eurotherm 650 speed Control

Figure II_1; Eurotherm 650 series HFEs pump speed control

Table II_1: Control key Definitions

| Key	Operation	Description
(E)	Escape	*Navigation* – Displays the previous level's menu *Parameter* – Returns to the parameter list *Trip Display*– Removes Trip or Error message from display allowing investigation of parameters
(M)	Menu	*Navigation* – Displays the next menu level, or the first parameter of the current Menu *Parameter* – Moves cursor to the left when the parameter is adjustable
▲	Increment	*Navigation* – Move upwards through the menu system *Parameter* – Increase value of the displayed parameter *Local Mode* – Increase value of the local setpoint
▼	Decrement	*Navigation* – Move down through the menu system *Parameter* – Decrease value of the displayed parameter *Local Mode* – Decrease value of the local setpoint
(I)	Run	*Local Mode* – Run the drive *Trip Reset* – Resets trip condition allowing drive to resume operation
(O)	Stop	*Local Mode* – Stops the drive. Trip Reset in all modes *Navigation* – Press and hold to toggle between Local and Remote Control modes (refer to page 5.4) *Trip Reset* – Resets trip condition allowing drive to resume operation

From; http://www.acpd.co.uk/sei/s/1488/f165.pdf

The pump speed control in Figure II_1 is used to regulate the pumping rate so that the flow rate can be regulated. This made it easy for different flow rates to be operated during the experiments and control the pump incrementally in percentage ratings and the control key definitions is shown in Table II.1.

Appendix III: Scroll Expander

A Scroll expander is a scroll compressor operating in a reverse direction. It is compact and light weight in design with no complex internal suction and discharge valves. The scroll expander is a rotating displacement device with a fixed spiral within the element housing and an eccentric movable
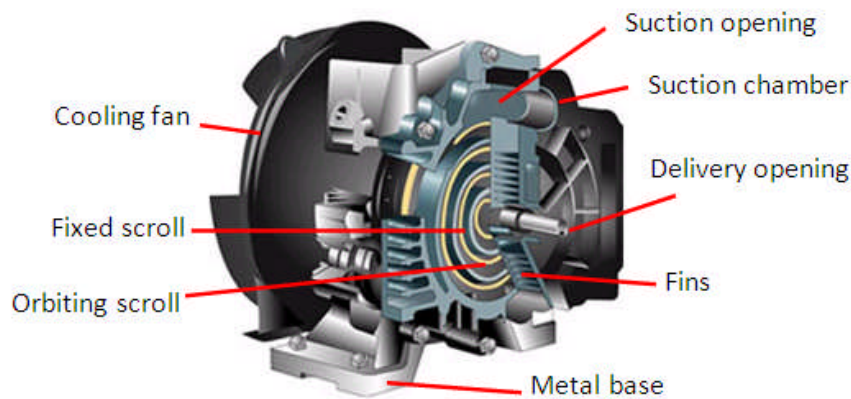
A. Isometric diagram of a scroll expander (www.compressorworld.com.au)
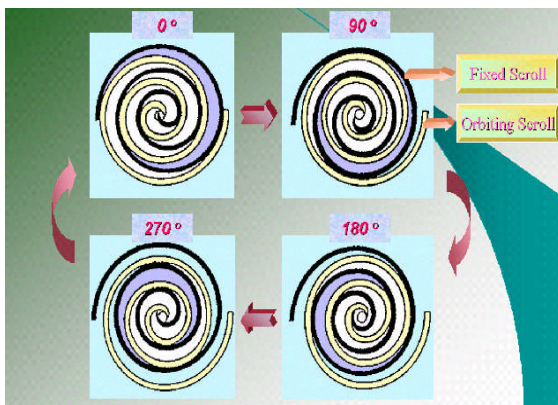
A. Operational sequence   C. Sectional view of a scroll expander
of scroll expander(http://me.kaist.ac.kr)   (http://images.google.co.uk/images?)
Figure III: Detail diagram of a typical scroll expander.

spiral that runs eccentrically around the center of the fixed spiral. During each orbit, several pockets of the working fluid are either compressed or expanded down simultaneously so that operation is virtually continous.

264
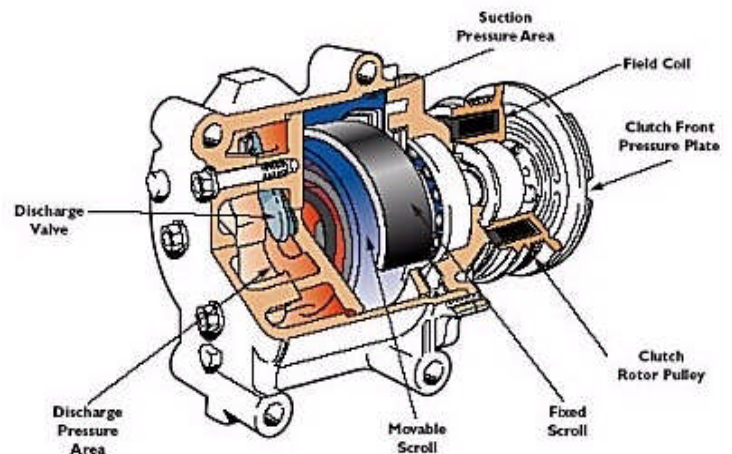
Appendix IV: Connection of Sensors to 500 range Datataker Daterlogger
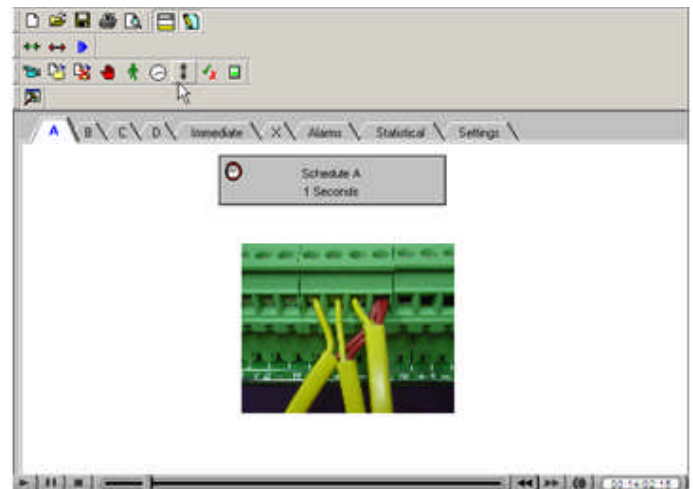
A – DATATAKER DT-500   B – Thermocouple wire Connection

Figure IV_1: Datataker and Sensor connection
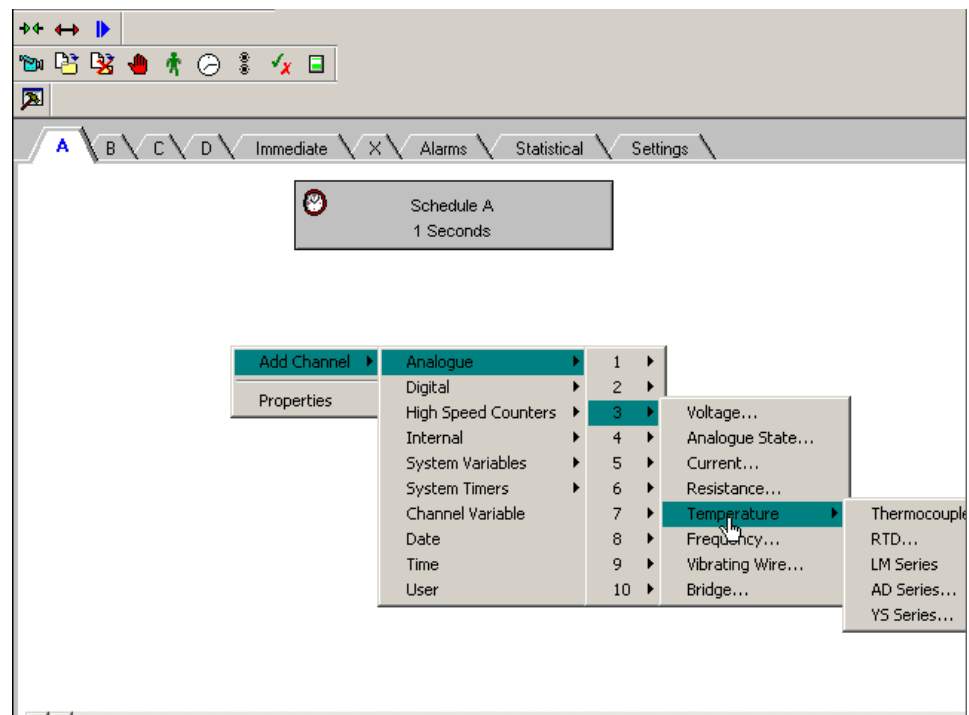
Step 1

Figure IV_1 shows a DT Series Datalogger and Thermocouple wire

connections to a channel displaying sensor connection procedure.

Step 1 – Right click on the blank programming window of the logger and select; Add channel > Analogue > channel 3 > Temperature > Thermocouple
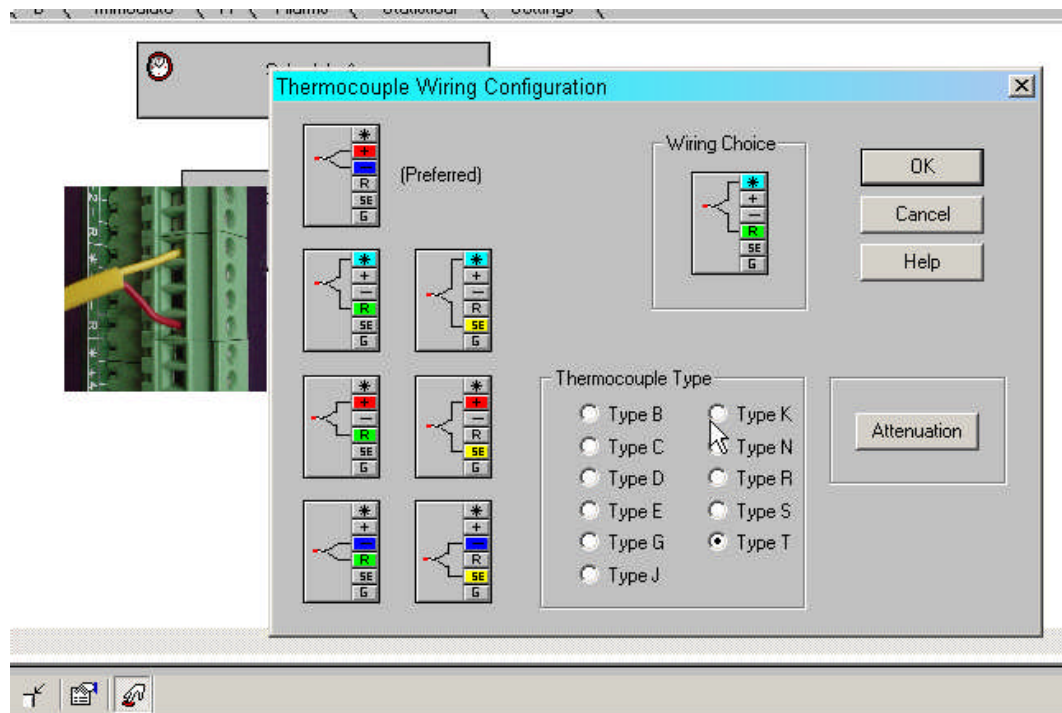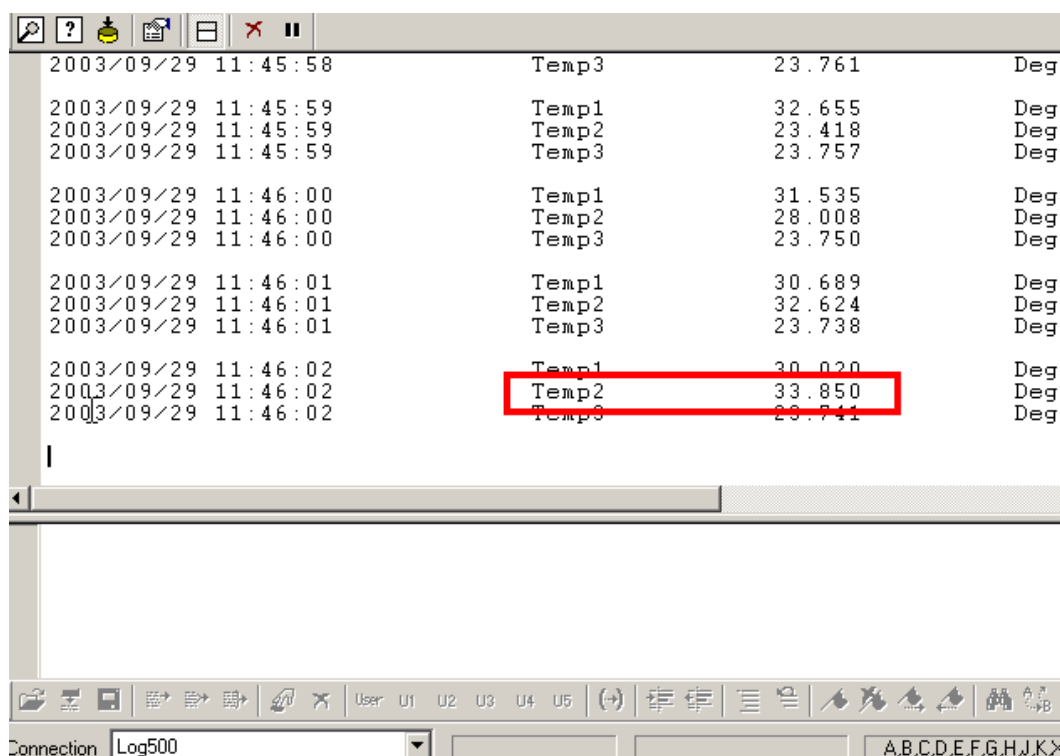
Step 2 – Select the Thermocouple wiring configuration, in this instance, R and +, see the wiring choice confirming the selection, click the radio button to select Type T and click OK. Then connect wire accordingly to the datalogger. Normally the negative terminal is connected to R and up to three wires per channel and the three positive wires are to be connected to the –ve, +ve, and the *.

Step 3 - Involves labelling; and by right clicking on the wiring choice, the channel label dialogue box appears. Type in the label and click OK and it will be displayed beside each channel.
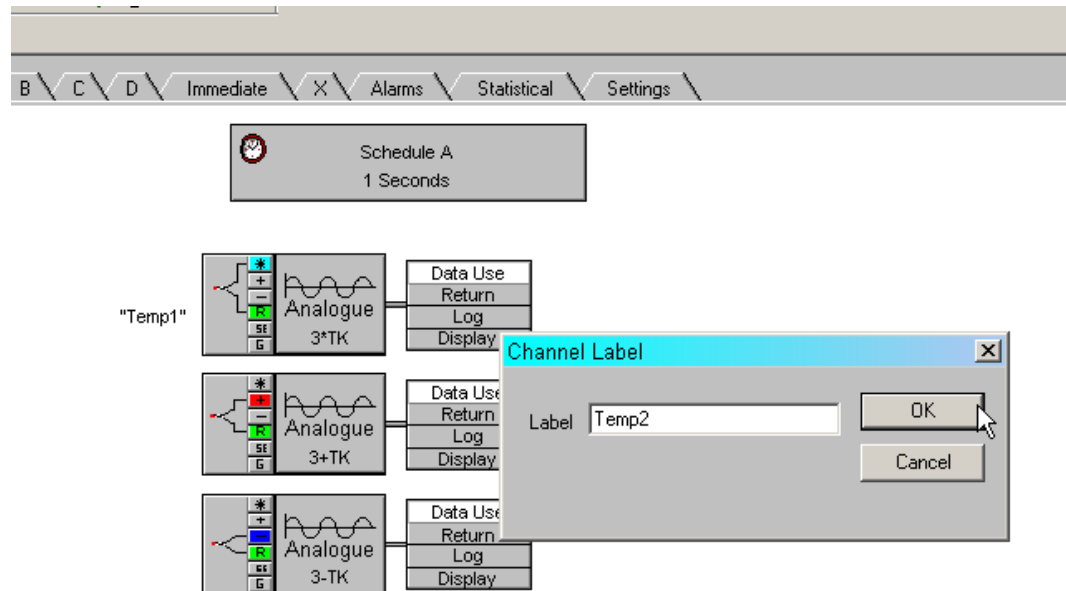
Step 3

This is repeated for each sensor to be used for the experiment. The label can be interchanged if there is a change in the positioning of a particular sensor or a swap of sensors by reviewing the process again. The label makes it possible for recorded data to be matched with the sensor from which they are emanating.

STEP – 4 Select - programme and select - send to connection; choose

text and real time data will be displayed
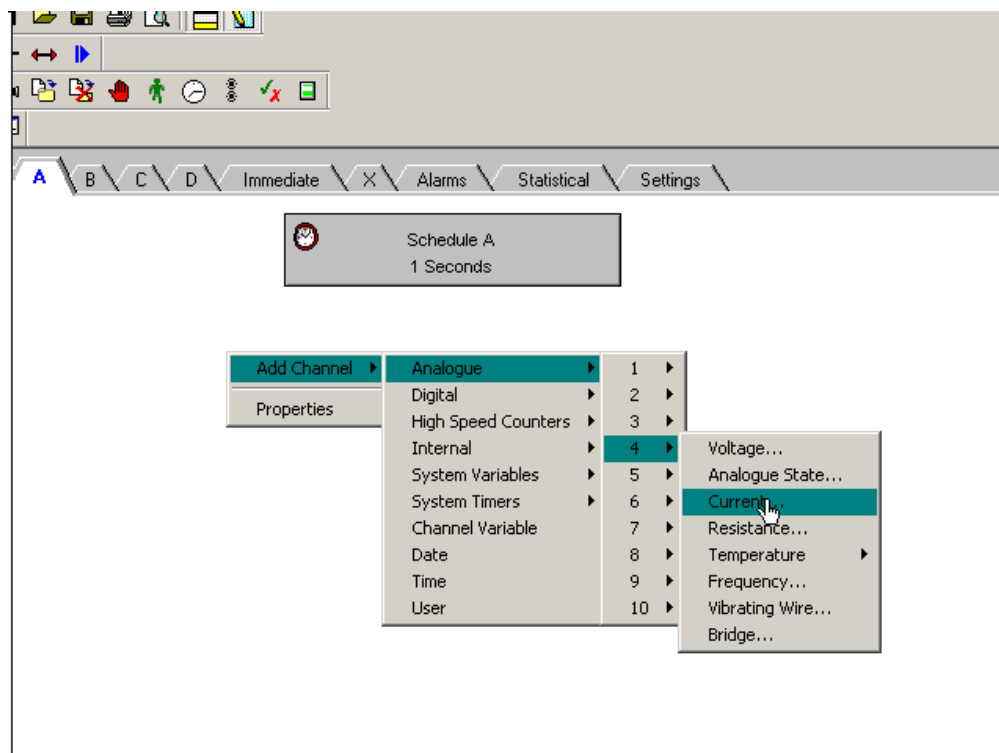
Step 5 – The process is repeated for current
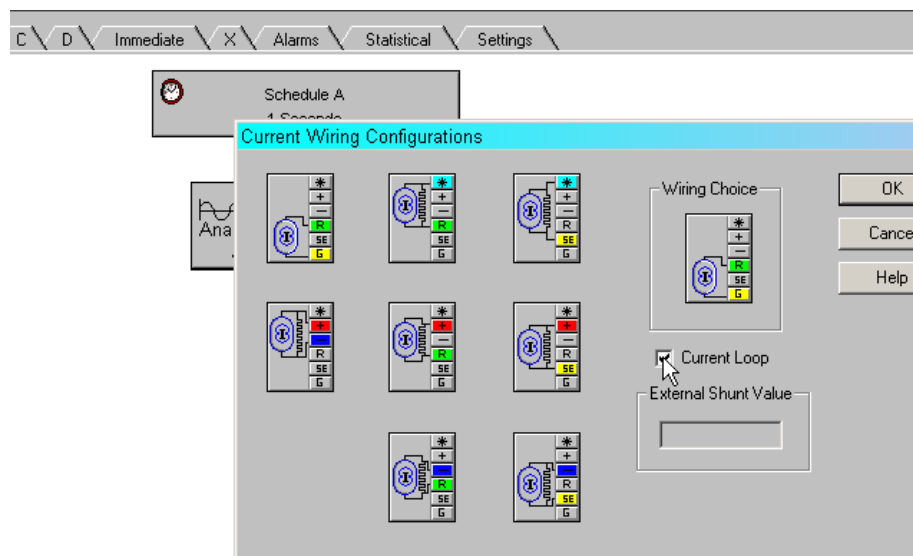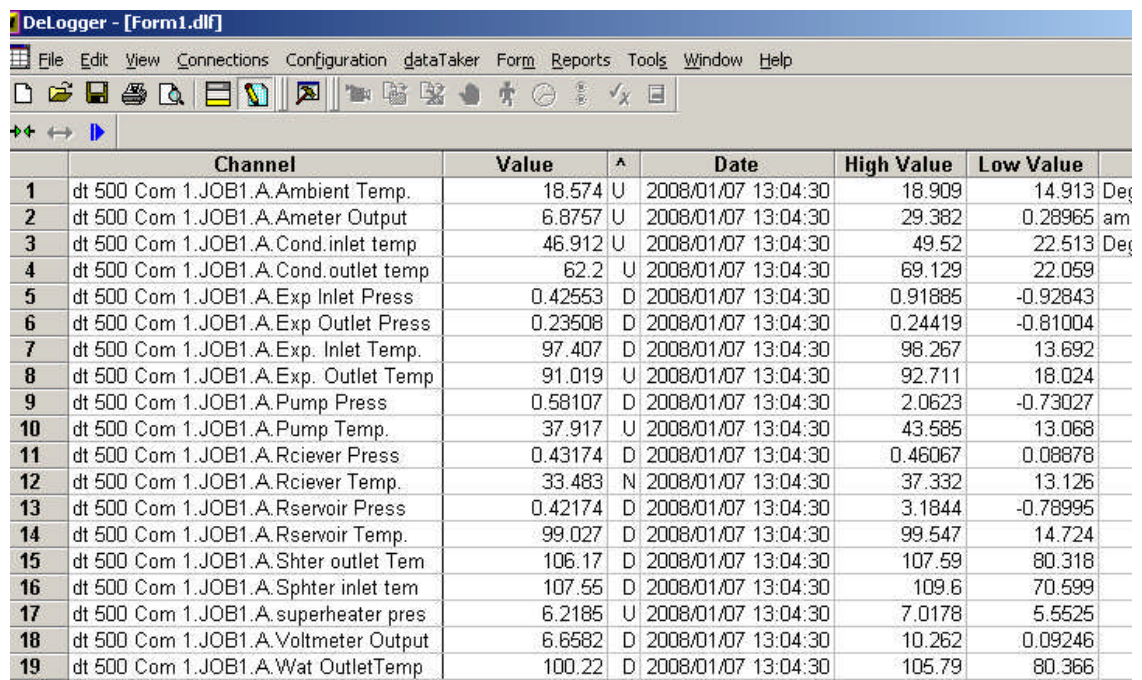
Step 6 – Select the channel, click the radio button to select current loop and click OK.
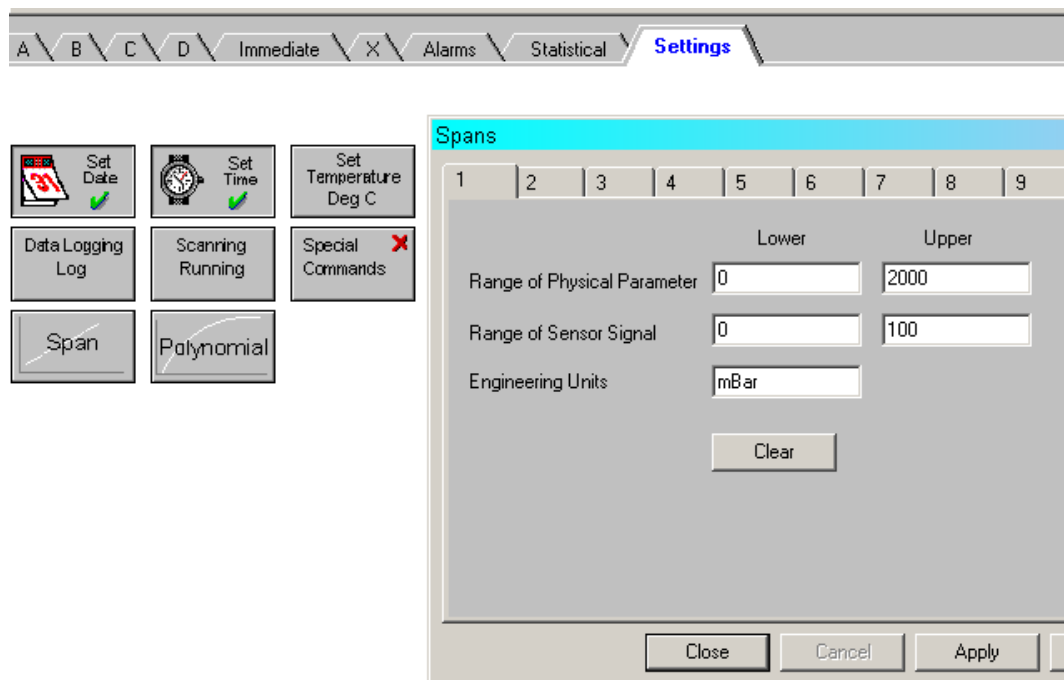
Step 7 – Set the transducer span by choosing setting on the program window, select span and then complete the range and click apply to finish and send to connection to get real time data returned.

The datalogging process is a very crucial phase of the experiment and precaution must be taken tp protect the datalogger from damage. Some of the risk involved water spilling on the logger or wires are allowed to bridge. This will crash the datalogger. Another danger to the logger is overloading; resistors can be used to set signals within the range of the datalogger. Figure IV_2 is a sample data from actual experiment indicating how data is returned in real time showing the channels, the value and date and time.

	Channel	Value	^	Date	High Value	Low Value	
1	dt 500 Com 1.JOB1.A.Ambient Temp.	18.574	U	2008/01/07 13:04:30	18.909	14.913	Deg
2	dt 500 Com 1.JOB1.A.Ameter Output	6.8757	U	2008/01/07 13:04:30	29.382	0.28965	am
3	dt 500 Com 1.JOB1.A.Cond.inlet temp	46.912	U	2008/01/07 13:04:30	49.52	22.513	Deg
4	dt 500 Com 1.JOB1.A.Cond.outlet temp	62.2	U	2008/01/07 13:04:30	69.129	22.059	
5	dt 500 Com 1.JOB1.A.Exp Inlet Press	0.42553	D	2008/01/07 13:04:30	0.91885	-0.92843	
6	dt 500 Com 1.JOB1.A.Exp Outlet Press	0.23508	D	2008/01/07 13:04:30	0.24419	-0.81004	
7	dt 500 Com 1.JOB1.A.Exp. Inlet Temp.	97.407	D	2008/01/07 13:04:30	98.267	13.692	
8	dt 500 Com 1.JOB1.A.Exp. Outlet Temp	91.019	U	2008/01/07 13:04:30	92.711	18.024	
9	dt 500 Com 1.JOB1.A.Pump Press	0.58107	D	2008/01/07 13:04:30	2.0623	-0.73027	
10	dt 500 Com 1.JOB1.A.Pump Temp.	37.917	U	2008/01/07 13:04:30	43.585	13.068	
11	dt 500 Com 1.JOB1.A.Rciever Press	0.43174	D	2008/01/07 13:04:30	0.46067	0.08878	
12	dt 500 Com 1.JOB1.A.Rciever Temp.	33.483	N	2008/01/07 13:04:30	37.332	13.126	
13	dt 500 Com 1.JOB1.A.Rservoir Press	0.42174	D	2008/01/07 13:04:30	3.1844	-0.78995	
14	dt 500 Com 1.JOB1.A.Rservoir Temp.	99.027	D	2008/01/07 13:04:30	99.547	14.724	
15	dt 500 Com 1.JOB1.A.Shter outlet Tem	106.17	D	2008/01/07 13:04:30	107.59	80.318	
16	dt 500 Com 1.JOB1.A.Sphter inlet tem	107.55	D	2008/01/07 13:04:30	109.6	70.599	
17	dt 500 Com 1.JOB1.A.superheater pres	6.2185	U	2008/01/07 13:04:30	7.0178	5.5525	
18	dt 500 Com 1.JOB1.A.Voltmeter Output	6.6582	D	2008/01/07 13:04:30	10.262	0.09246	
19	dt 500 Com 1.JOB1.A.Wat OutletTemp	100.22	D	2008/01/07 13:04:30	105.79	80.366	

Figure IV_2: Sample Data returned in real time during actual test

Appendix V: Sample data

Table V_1: Sample of Raw results from the data logger

Time	A/Exp. Inlet Temp.	A/Exp. Outlet Temp	A/Gen-HFE-Temp-out	A/Rciever Temp.
09:30:50	12.65	8.3487	20.617	9.6637
09:31:00	12.66	8.3946	20.662	9.7094
09:31:10	12.668	8.402	20.601	9.7168
09:31:20	12.607	8.3761	20.541	9.6552
09:31:30	12.616	8.4207	20.584	9.7354
09:31:40	12.624	8.3576	20.489	9.6372
09:31:50	12.668	8.4021	20.498	9.6812
09:32:00	12.677	8.4468	20.472	9.7257
09:32:10	12.652	8.4209	20.482	9.7356
09:32:20	12.659	8.4283	20.455	9.743
09:32:30	12.597	8.4372	20.394	9.7519
09:32:40	12.571	8.4101	20.334	9.7248
09:32:50	12.615	8.4906	20.377	9.734
09:33:00	12.553	8.4275	20.317	9.7423
09:33:10	12.562	8.508	20.326	9.7868
09:33:20	12.571	8.4809	20.3	9.7955
09:33:30	12.543	8.4529	20.273	9.7676
09:33:40	12.481	8.4612	20.177	9.7405
09:33:50	12.525	8.5058	20.152	9.785
09:34:00	12.499	8.5145	20.126	9.7583
09:34:10	12.506	8.522	20.099	9.8011
09:34:20	12.479	8.5307	20.108	9.7744
09:34:30	12.453	8.5394	20.082	9.7831
09:34:40	12.462	8.5481	20.09	9.7918
09:34:50	12.435	8.5568	20.064	9.8005
09:35:00	12.409	8.5655	20.004	9.8092
09:35:10	12.417	8.5387	19.978	9.8178
09:35:20	12.353	8.509	19.914	9.7882
09:35:30	12.326	8.5177	19.888	9.7611
09:35:40	12.298	8.5252	19.896	9.7686
09:35:50	12.307	8.5339	19.87	9.7772
09:36:00	12.28	8.5426	19.844	9.8216

Appendix VI: EES Modelling Equations using Procedures

Figure VI_1: Biomass (ORC) Organic Rankine cycle

FigureVI_2: T-S chat of the biomass ORC system

5_1: Biomass ORC Regenrative system"
"!Purpose To find the optimal operating parameters particularly pressure and temperature, in [KPa] and [C] "

P[5]=454.95[kpa]
P[3]=302.96[KPa]
P[6]=144.89[KPa]
T[1]=21.49[C]
T[2]=22.20[C]
x[5]=1   "1 saturated or supersaturated vapour"

"!Refrigerant Pump analysis"
P[1]=P[6]   " neglect pressure in the condenser"
P[2]=P[3]
x[1]=0   " 0 indicates saturated liquid"
Eta_p=0.65
h[1]=Enthalpy(HFE7000,P=P[1],x=x[1])
s[1]=Entropy(HFE7000,P=P[1],x=x[1])
V[1]=volume(HFE7000,P=P[1],x=x[1])
W_p_s=v[1]*(P[2]-P[1])
W_p=W_p_s/Eta_p
h[2]=W_p+h[1]   "energy balance of adiabatic pump"
v[2]=volume(HFE7000,P=P[2],h=h[2])
s[2]=Entropy(HFE7000,P=P[2],h=h[2])

"! Recuperator analysis"
T[3]=56.33[C]
dt=34.13[C]
m=0.117[Kg/s]
cp=1.30[KJ/Kg.K]
h[3]=Enthalpy(HFE7000,T=T[3],x=x[5])
DeltaH_recp=m*cp*dt
s[3]=Entropy(HFE7000,T=T[3],x=x[5])
v[3]=volume(HFE7000,T=T[3],x=x[5])

"!Boiler analysis"
T[4]=89.39[C]   " Generator exit temperature before turbine inlet"
h[4]=Enthalpy(HFE7000,T=T[4],x=x[5])
Q_in=h[4]-h[2]
s[4]=Entropy(HFE7000,T=T[4],x=x[5])
v[4]=volume(HFE7000,T=T[4],x=x[5])

"!Turbine inlet analysis"
T[5]=87.30[C]   "actual turbine inlet temperature"
h[5]=Enthalpy(HFE7000,T=T[5],x=x[5])
s[5]=entropy(HFE7000,T=T[5],x=x[5])
v[5]=volume(HFE7000,T=T[5],x=x[5])
W_t1_s=(h[5]-h_g[6])
W_t1=W_t1_s*Eta_t   "energy balance of adiabatic Turbine"
Eta_t=0.85
W_net=W_t1-W_p
Eta_thermal=W_net/Q_in
Eta_thermal_carnot=1-(T[1]+273)/(115+273)

"!Turbine exit analysis"
T[6]=79.52[C]
h[6]=Enthalpy(HFE7000,P=P[6],x=x[1])
h_f[6]=Enthalpy(HFE7000,P=P[6],x=x[1])
h_g[6]=Enthalpy(HFE7000,P=P[6],x=x[5])
h_fg[6]=h_g[6]-h_f[6]
s_s[6]=s[5]
s_f[6]=Entropy(HFE7000,P=P[6],x=x[1])
s_g[6]=Entropy(HFE7000,P=P[6],x=x[5])
s_fg[6]=s_g[6]-s_f[6]
x_s[6]=s[5]-s_f[6]/s_fg[6]
h_s[6]=h_f[6]+x_s[6]*h_fg[6]
T_s[6]=Temperature(HFE7000,P=P[6],x=x[1])

The software has an inbuilt capability to generate the residual table that summarises all the input and variables as well as displaying the enabling equations in the residual table shown in Table 5.2.

Table 5.3 indicate all the values solved as displayed in the solution window as a result of all the specified input data within the range or similar to data from the actual experiment in implementing the ideal Rankine cycle. The software will also indicate if there were any unit problems encountered during the iterations and the time it takes to conclude the calculation is also indicated.

Table 5_1: Residual table generated with EES software

There are a total of 53 equations in 5 blocks in the Main program.

Block	Rel. Res.	Abs. Res.	Units	Calls	Equations
0	0.000E+00	0.000E+00	OK	1	**P[5]**=454.95[kpa]
0	0.000E+00	0.000E+00	OK	1	**P[3]**=302.96[KPa]
0	0.000E+00	0.000E+00	OK	1	**P[6]**=144.89[KPa]
0	0.000E+00	0.000E+00	OK	1	**T[1]**=21.49[C]
0	0.000E+00	0.000E+00	OK	1	**T[2]**=22.20[C]
0	0.000E+00	0.000E+00	OK	1	**x[5]**=1
0	0.000E+00	0.000E+00	OK	1	**x[1]**=0
0	0.000E+00	0.000E+00	OK	1	**Eta_p**=0.65
0	0.000E+00	0.000E+00	OK	1	**T[3]**=56.33[C]
0	0.000E+00	0.000E+00	OK	1	**dt**=34.13[C]
0	0.000E+00	0.000E+00	OK	1	**m**=0.117[Kg/s]
0	0.000E+00	0.000E+00	?	1	**cp**=1.30[KJ/Kg.K]
0	0.000E+00	0.000E+00	OK	1	**T[4]**=89.39[C]
0	0.000E+00	0.000E+00	OK	1	**T[5]**=87.30[C]
0	0.000E+00	0.000E+00	OK	1	**Eta_t**=0.85
0	0.000E+00	0.000E+00	OK	1	**T[6]**=79.52[C]
0	0.000E+00	0.000E+00	OK	4	**P[1]**=P[6]
0	0.000E+00	0.000E+00	OK	4	**P[2]**=P[3]
0	0.000E+00	0.000E+00	OK	4	**h[1]**=Enthalpy(HFE7000,P=P[1],x=x[1])
0	0.000E+00	0.000E+00	OK	4	**s[1]**=Entropy(HFE7000,P=P[1],x=x[1])
0	0.000E+00	0.000E+00	OK	4	**V[1]**=volume(HFE7000,P=P[1],x=x[1])
0	0.000E+00	0.000E+00	OK	4	**W_p_s**=v[1]*(P[2]-P[1])
0	0.000E+00	0.000E+00	OK	4	**W_p**=W_p_s/Eta_p
0	0.000E+00	0.000E+00	OK	4	**h[2]**=W_p+h[1]
0	0.000E+00	0.000E+00	OK	4	**v[2]**=volume(HFE7000,P=P[2],h=h[2])
0	0.000E+00	0.000E+00	OK	4	**s[2]**=Entropy(HFE7000,P=P[2],h=h[2])
0	0.000E+00	0.000E+00	OK	4	**h[3]**=Enthalpy(HFE7000,T=T[3],x=x[5])
0	0.000E+00	0.000E+00	?	4	**DeltaH_recp**=m*cp*dt
0	0.000E+00	0.000E+00	OK	4	**s[3]**=Entropy(HFE7000,T=T[3],x=x[5])
0	0.000E+00	0.000E+00	OK	4	**v[3]**=volume(HFE7000,T=T[3],x=x[5])
0	0.000E+00	0.000E+00	OK	4	**h[4]**=Enthalpy(HFE7000,T=T[4],x=x[5])
0	0.000E+00	0.000E+00	OK	4	**Q_in**=h[4]-h[2]
0	0.000E+00	0.000E+00	OK	4	**s[4]**=Entropy(HFE7000,T=T[4],x=x[5])
0	0.000E+00	0.000E+00	OK	4	**v[4]**=volume(HFE7000,T=T[4],x=x[5])
0	0.000E+00	0.000E+00	OK	4	**h[5]**=Enthalpy(HFE7000,T=T[5],x=x[5])
0	0.000E+00	0.000E+00	OK	4	**s[5]**=entropy(HFE7000,T=T[5],x=x[5])
0	0.000E+00	0.000E+00	OK	4	**v[5]**=volume(HFE7000,T=T[5],x=x[5])
0	0.000E+00	0.000E+00	?	4	**Eta_thermal_carnot**=1-(T[1]+273)/(115+273)
0	0.000E+00	0.000E+00	OK	4	**h[6]**=Enthalpy(HFE7000,P=P[6],x=x[1])
0	0.000E+00	0.000E+00	OK	4	**h_f[6]**=Enthalpy(HFE7000,P=P[6],x=x[1])
0	0.000E+00	0.000E+00	OK	4	**h_g[6]**=Enthalpy(HFE7000,P=P[6],x=x[5])
0	0.000E+00	0.000E+00	OK	4	**h_fg[6]**=h_g[6]-h_f[6]
0	0.000E+00	0.000E+00	OK	4	**s_s[6]**=s[5]
0	0.000E+00	0.000E+00	OK	4	**s_f[6]**=Entropy(HFE7000,P=P[6],x=x[1])
0	0.000E+00	0.000E+00	OK	4	**s_g[6]**=Entropy(HFE7000,P=P[6],x=x[5])
0	0.000E+00	0.000E+00	OK	4	**s_fg[6]**=s_g[6]-s_f[6]
0	0.000E+00	0.000E+00	?	4	**x_s[6]**=s[5]-s_f[6]/s_fg[6]
0	0.000E+00	0.000E+00	OK	4	**h_s[6]**=h_f[6]+x_s[6]*h_fg[6]

0	0.000E+00	0.000E+00	OK	4	

T_s[6]=Temperature(HFE7000,P=P[6],x=x[1])

0	0.000E+00	0.000E+00	OK	4	**W_t1_s**=(h[5]-h_g[6])
0	0.000E+00	0.000E+00	OK	4	**W_t1**=W_t1_s*Eta_t
0	0.000E+00	0.000E+00	OK	4	**W_net**=W_t1-W_p
0	0.000E+00	0.000E+00	OK	4	**Eta_thermal**=W_net/Q_in

Variables shown in bold font are determined by the equation(s) in each block.

Table 5_3: Table of values derived from the solution window of EES software for HFE7100

Unit Settings: [kJ]/[C]/[kPa]/[kg]/[degrees]

$c_p = 1.3 \ [KJ/Kg.K]$

$\eta_p = 0.65 \ [-]$

$\eta_{thermal,carnot} = 0.241 \ [-]$

$W_{net} = 28.32 \ [kJ/kg]$

$W_{t1} = 28.5 \ [kJ/kg]$

$\delta H_{recp} = 5.191 \ [kW]$

$\eta_t = 0.85 \ [-]$

$m = 0.117 \ [Kg/s]$

$W_p = 0.1796 \ [kJ/kg]$

$W_{t1 \ s} = 33.52 \ [kJ/kg]$

$dt = 34.13 \ [C]$

$\eta_{thermal} = 0.1725 \ [-]$

$Q_{in} = 164.2 \ [kJ/kg]$

$W_{p,s} = 0.1167 \ [kJ/kg]$

No unit problems were detected.
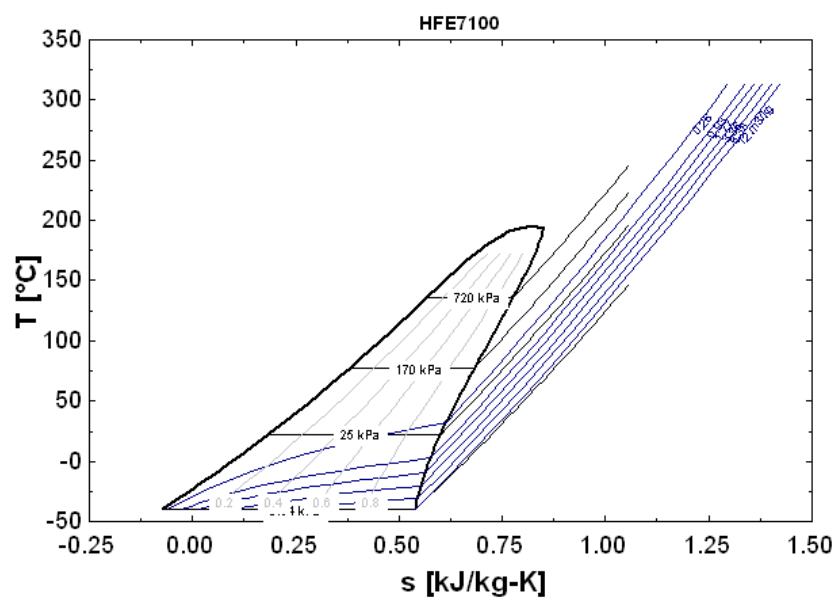
Calculation time = .0 sec.

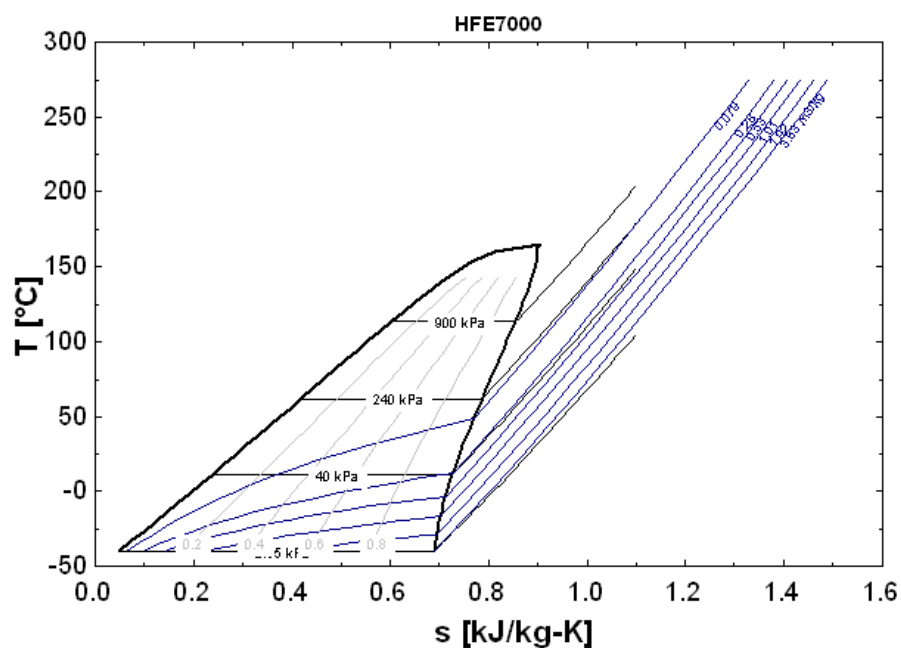**Figure V_3: Property plot for HFE 7100 using EES Software**

Figure V_4: Property plot for HFE 7000 using EES Software